Nevada Department of Transportation

Report No. 608-17-803

Lateral Analysis Guidelines for Drilled Shafts in Nevada Based on LRFD Framework

July 2022

Disclaimer

This work was sponsored by the Nevada Department of Transportation. The contents of this report reflect the views of the authors, who are responsible for the facts and the accuracy of the data presented herein. The contents do not necessarily reflect the official views or policies of the State of Nevada at the time of publication. This report does not constitute a standard, specification, or regulation.

TECHNICAL REPORT DOCUMENTATION PAGE

1. Report No. 608-17-803	2. Government Accession No.	3. Recipient's Catalog No.
4. Title and Subtitle Lateral Analysis Guidelines for Drilled Shafts in Nevada Based on LRFD Framework		5. Report Date July 2022
		6. Performing Organization Code
7. Author(s) Ramin Motamed; Raj Siddharthan; David Sanders; Fahim M. Bhuiyan		8. Performing Organization Report No.
9. Performing Organization Name and Address Department of Civil and Environmental Engineering University of Nevada, Reno 1664 N. Virginia Street Reno, NV 89557-0258		10. Work Unit No.
		11. Contract or Grant No. P608-17-803
12. Sponsoring Agency Name and Address Nevada Department of Transportation 1263 South Stewart Street Carson City, NV 89712		13. Type of Report and Period Covered Final Report December 2017 to July 2022
		14. Sponsoring Agency Code
15. Supplementary Notes		

16. Abstract

The major goal of this research is to improve the conventional p-y analysis in the context of larger diameter drilled shafts. The conservative lateral response due to the absence of lateral resistance components in p-y analysis for larger diameter shafts has been termed as 'diameter effect' in past research. To apply and evaluate the proposed unified p-y analysis, a MATLAB-based, finite-difference program, NVShaft, has been developed. During the initial development stage, NVShaft was verified by comparing the predicted responses with classical p-y solutions and responses obtained from available commercial programs. To evaluate NVShaft, and the unified p-y method, available literature on lateral load tests on larger diameter shafts was explored. The following load test programs were considered to validate the numerical p-y analysis in NVShaft: 1) Las Vegas load test program, 2) Incheon Bridge cyclic lateral load test, 3) PISA load test program, 4) University of California, San Diego load test, 5) University of Florida centrifuge test and 6) Raiders Stadium load test. To perform these validation exercises, the p-y soil models were computed based on interpreted soil characteristics from relevant load test reports. No calibrations of the p-y models were attempted in this regard. It was found that shorter embedment depth and larger axial load significantly increase the tip resistances in the p-y model. A user manual for NVShaft and the outline of the three methods to perform lateral stability analysis in NVShaft have been included in this report as well.

17. Key Words Drilled shafts; lateral analysis; MATLAB; NVShaft; LRFD; diameter effect; load test; soil characteristics; foundations; cementation	18. Distribution Statement No restrictions. This document is available through the: National Technical Information Services Springfield, VA 22161 www.ntis.gov

19. Security Classif (of this report) Unclassified	20. Security Classif (of this page) Unclassified	21. No. of Pages 254	22. Price n/a

Lateral Analysis Guidelines for Drilled Shafts in Nevada Based on LRFD Framework

Prepared for

The Nevada Department of Transportation

Prepared by

Ramin Motamed (PI), Ph.D., P.E.
Associate Professor
Email: motamed@unr.edu
Tel: 775-784-6960,

and

Raj Siddharthan, Ph.D., P.E.
Professor
Email: siddhart@unr.edu

and

David Sanders, Ph.D.
Professor
Email: sandersd@iastate.edu

and

Fahim M. Bhuiyan
Graduate Research Assistant
Email: fbhuiyan@nevada.unr.edu

Department of Civil and Environmental Engineering
University of Nevada
1664 N. Virginia St.
Reno, NV 89557-0258

July 31, 2022

University of Nevada, Reno

ABSTRACT

The major goal of this research is to improve the conventional *p-y* analysis in the context of larger diameter drilled shafts. The conservative lateral response due to the absence of lateral resistance components in *p-y* analysis for larger diameter shafts has been termed as 'diameter effect' in past research. In this study, a unified *p-y* analysis is proposed, by including the resisting moment due to side shear, tip shear, and tip moment resistances in the conventional BNWF model. A simplified tip moment resistance model applicable for any type of soil material, and to be used as part of the unified *p-y* spring model is also proposed. To apply and evaluate the proposed unified *p-y* analysis, a MATLAB-based, finite-difference program, NVShaft, has been developed. During the initial development stage, NVShaft was verified by comparing the predicted responses with classical *p-y* solutions and responses obtained from available commercial programs. To evaluate NVShaft, and the unified *p-y* method, available literature on lateral load tests on larger diameter shafts was explored. The following load test programs were considered to validate the numerical *p-y* analysis in NVShaft: 1) Las Vegas load test program, 2) Incheon Bridge cyclic lateral load test, 3) PISA load test program, 4) University of California, San Diego load test, 5) University of Florida centrifuge test and 6) Raiders Stadium load test. To perform these validation exercises, the *p-y* soil models were computed based on interpreted soil characteristics from relevant load test reports. No calibrations of the *p-y* models were attempted in this regard.

To understand the effect of soil strength parameters, embedment depths, and axial load on different additional lateral resistance components with increasing shaft diameter, further investigation was done in the form of a parametric study. The numerical models constructed from original test conditions in the sandy and clayey sites from the PISA load test program were used as reference models in this context.

The diameter effect seems to be more apparent in the clayey soil, compared to the sandy soil from the PISA load test program. It was found that shorter embedment depth and larger axial load significantly increase the tip resistances in the *p-y* model.

NVShaft is also capable of performing numerical axial load (*t-z*) analysis, along with a unique feature to simulate bi-directional axial load test. The validation example of the *t-z* capability of NVShaft is presented by simulating axial load tests from projects in Las Vegas. The use of *t-z* models for soft rock and Florida limestone to model the axial resistance of caliche material is also presented in this context.

NVShaft also has the feature to carry out lateral stability analysis to obtain critical shaft length following two existing methods practiced in Nevada DOT and Arizona DOT and a new method proposed by the authors. A user manual for NVShaft and the outline of the three methods to perform lateral stability analysis in NVShaft have been included in this report as well.

ACKNOWLEDGEMENTS

This research was funded by the Nevada Department of Transportation (NDOT) through agreement no. P608-17-803. The discussion with Michael Taylor, P.E. on the development of the finite-difference program, NVShaft is greatly appreciated.

The authors would like to express their thanks to Dr. Zia Zafir from Kleinfelder, Abbas Bafghi, and Dr. Gary Norris for the constructive discussions about the I-15/US 95 load test program in Las Vegas. We also thank Peter Faust and Eleazar Sotelo of Malcolm Drilling Company, Inc., for providing us with the load test reports from the Raiders Stadium project in Las Vegas. The discussion with Diane Fiorelli from Langan about the Raider Stadium load tests is also appreciated.

The authors appreciate the help from the former graduate student, Dr. Seyed-Farzan Kazemi, in implementing the advanced MATLAB programming to develop NVShaft. We also thank the graduate student, Rami Skaff for his support regarding the output generation feature of NVShaft. Our special thanks to the former graduate student, Dr. Joseph Toth, for his assistance in collecting and interpreting load test reports.

DISCLAIMER

The opinions, findings, and conclusions expressed in this publication are those of the authors and not necessarily those of the Nevada Department of Transportation or University of Nevada, Reno. Alternative accessible formats of this document will be provided upon request. Persons with disabilities who need an alternative accessible format of this information, or who require some other reasonable accommodation to participate, should contact Dr. Ramin Motamed, Associate Professor, Department of Civil and Environmental Engineering, University of Nevada, Reno. Tel: (775) 784-6960; Email: motamed@unr.edu.

TABLE OF CONTENTS

LIST OF TABLES

LIST OF FIGURES

CHAPTER 1

STATEMENT OF RESEARCH

1.1 Introduction

The use of drilled shaft foundations has increased substantially around the globe in major engineering projects. Drilled shafts are known for their capability to transmit large structural loads from offshore wind turbines, bridge piers, and abutments. The ability to resist seismic load due to high flexural strength, small footprint, and ease of construction in different soil and groundwater conditions are some of the major advantages of drilled shaft foundation. A single drilled shaft foundation in many cases is considered an alternative to several smaller diameter monopiles, and recent trends indicate the use of larger diameter drilled shafts in engineering projects. In Europe, some of the thousands of offshore wind turbines are supported by drilled shafts with a diameter (D) as high as 6 m, and there is a possibility of drilled shafts having a diameter of 10 m in near future (Byrne et al., 2015).

A major part of this research has been done in the context of Nevada's local subsurface condition. The presence of intermittent hard, competent caliche layers in the cemented soil condition of Las Vegas Valley makes the use of drilled shaft as a deep foundation system a sustainable and economical solution to support infrastructures in the region (Rinne et al., 1996; Zafir and Vanderpool, 1998; Fiorelli et al., 2018). Caliche is a type of sedimentary rock material formed by cementation of calcium carbonate between fine and coarse-grained particles in the presence of ground moisture content (Werle and Luke, 2007). Caliche is typically classified as Intermediate Geomaterial (IGM) for engineering purposes (Brown et al., 2010; Motamed et al., 2016). The cemented rock-like soil deposits are known for their

erratic existence as discontinuous lenses and pose major challenges to site characterization. Due to its stiff nature and variation in the degree of cementation, sampling cannot be done without resorting to expensive drilling and coring, and obtaining intact cored samples is often not possible for weakly cemented material (Werle and Luke, 2007; Stanton et al., 2017). Lack of material properties from laboratory tests on caliche is a major limitation recognized by the engineers in the region, and performing standard penetration tests also results in refusal SPT-N values in many cases (Rinne et al., 1996; Stanton et al., 2017). The degree of cementation of caliche layers can be quantified by unconfined compressive strength (q_u) values, and previous studies suggest q_u may vary between 30 psi to 20,000 psi (Cibor, 1983; Saint-Pierre, 2018).

The design of drilled shaft typically involves performing field axial and lateral load tests, which is a reliable means to validate the load-carrying capacity of the foundation in local soil conditions. The study emphasizes numerical lateral load analysis of drilled shafts, which is popularly known as Beam on nonlinear Winkler foundation (BNWF) model, Winkler's spring model, or the *p-y* method. The *p-y* method offers a simple and elegant solution to model complex soil-shaft interaction in lateral load analysis and is a recommended tool by design codes such as American Petroleum Institute (API, 2014) and AASHTO (2020). The simplified method was first introduced by Hetényi and Hetbenyi (1946) and assumes the lateral resistance of soil as a series of uncoupled *p-y* springs, while the shaft is modeled as Euler's idealized beam (McClelland and Focht, 1956; Matlock and Reese, 1960). The complex nature of soil material in contact with laterally loaded drilled shaft led to the development of several nonlinear *p-y* models, based on lateral load tests conducted on slender piles of diameter in the range of 1 ft to 2 ft (Matlock, 1970; Reese et al., 1974; Reese and Welch, 1975; O'Neill and Gazioglu,

1984; Reese and Nyman, 1978). The following fourth-order differential equation is solved numerically using computer programs [i.e., LPILE (Reese et al., 2000)] while performing the *p*-*y* analysis,

$$EI\frac{d^4y}{dx^4} + Q_z\frac{d^2y}{dx^2} - p - w = 0 \tag{1.1}$$

Where E = elastic modulus of drilled shaft section, I = moment of inertia, y = deflection at depth x, Q_z = axial load in the shaft, p = soil reaction per unit length, and w = applied distributed load per unit length.

Similar to *p*-*y* analysis, the numerical axial load analysis i.e., *t*-*z* method is a simplified design tool to perform preliminary investigation for axial loading conditions. Brown et al. (2010) argues that the *t*-*z* method often fails to characterize sensitive parameters relating to shaft construction and site-specific soil condition, and suggests relying on field load test results to verify the numerical predictions. Nevertheless, the *t*-*z* method is widely used to perform preliminary design calculations for axial loading. In the *t*-*z* analysis, the vertical side resistance developed around the circumference of the shaft, and the end bearing resistance at the shaft tip is represented by a series of *t*-*z* springs, and an end bearing *q*-*z* spring, respectively. The following differential equation is solved numerically, using computer programs such as TZ-PILE (Ensoft, 2014),

$$-EI\frac{d^2z}{dx^2} + tC = 0 \tag{1.2}$$

where, E = elastic modulus of shaft section, A = shaft cross-sectional area at depth x, z = vertical shaft movement at depth x, t = soil side resistance at depth x,

and C = circumference of shaft segment at depth x. The mobilized axial force (Q) in the shaft at depth x due to axial deformation is given by,

$$Q(x) = -EI\frac{dz}{dx} \tag{1.3}$$

The focus of this study is the improvement of numerical axial and lateral load analysis of large diameter drilled shafts and the evaluation of a developed numerical tool in the context of the local soil condition of Nevada. A MATLAB-based, comprehensive load analysis program, NVShaft has been developed, which is capable of performing both *p-y* and *t-z* analysis by following the finite-difference approach. NVShaft has a unique feature that allows the user to perform axial load analysis of bi-directional static load tests. The numerical capabilities of NVShaft have been verified based on comparisons with predicted responses obtained from available commercial programs such as LPILE and TZ-PILE. The validation of NVShaft was carried out based on simulations of numerous field load tests in different subsurface conditions. One of the major goals of this study is to incorporate additional lateral resistance mechanisms in numerical lateral load analysis, which is generally not captured in larger diameter shafts (Ashour and Helal, 2014; Taghavi et al., 2020; McVay and Niraula, 2004). A unified *p-y* analysis is proposed in this study, which can include the resisting moment per unit length due to side shear (m_r), tip shear (v_b), and tip moment resistances (m_b). The absence of these lateral resistances often results in inaccuracy in numerical responses, which is termed the "pile diameter effect" (Finn and Dowling, 2015). The capability to perform unified *p-y* analysis is presented, with a major focus on the simulations of lateral load tests conducted on large diameter shafts in Nevada's cemented soil conditions. A parametric study to investigate the effects of different soil-shaft parameters on additional lateral

resistance components is also presented.

1.2 Motivation and Background

Previous research addresses the limitations of conventional *p-y* analysis in the context of large diameter drilled shafts, which can be attributed to the following two factors:

1. The *p-y* models to simulate lateral resistance of soil fail to comply with site-specific material characteristics.
2. The conventional Winkler's spring model fails to include additional lateral resistance mechanisms.

1.2.1 Development of Site-Specific *p-y* Models

Previous studies suggest the API (2014) recommended classical *p-y* models often yield unreliable response for larger-diameter drilled shafts (Bhushan and Scheyhing, 2002; McVay and Niraula, 2004; Ashour and Helal, 2014; Li et al., 2017). For example, Bhushan and Scheyhing (2002) performed *p-y* analyses to simulate lateral load tests conducted on dense sandy soil in the San Diego area and reported that the finite-difference program LPILE requires p-multipliers between 2 to 8 to accurately predict lateral response. Li et al. (2017) performed *p-y* analysis on two open-ended steel pipe piles embedded in overconsolidated dense sand, with an outer diameter of 0.34 m, embedded length of 2.2 m, and slenderness ratio of 6.5. It was observed that, for overconsolidated dense sand, the use of API *p-y* curve overestimates initial

stiffness at a deeper depth and underestimates ultimate soil resistance at shallow depth.

To improve the accuracy of lateral soil-shaft interaction during *p-y* analysis, site-specific *p-y* models have been proposed in many recent studies. Brown et al. (1994) proposed a method to calibrate site-specific *p-y* model parameters from inclinometer data using a least-squares regression analysis. In this case, soil strength and stiffness parameters are used as fitting variables which are made functions of pile deflection. Juirnarongrit and Ashford (2004) conducted full-scale lateral load tests on cast-in-drilled-hole (CIDH) piles with diameter ranging from 0.4 m to 1.2 m. The back-calculated *p-y* curves exhibited increased resistance with depth. Due to cementation, the soil appeared to be more cohesive in nature and non-zero soil resistance was recorded near the ground surface. The back-calculated curves were used to develop a *p-y* model for weakly cemented sand. In an effort to improve the *p-y* analysis in the context of clayey soil condition in China, Fu et al. (2020) proposed a more site-specific *p-y* model, and observed significant deviation from actual response when the API *p-y* model is implemented in the finite-element (FE) analysis. Li and Yang (2017) proposed a site-specific *p-y* model for frozen silt which is capable of producing 50 to 170 times of lateral soil resistance from *p-y* model for sand by Reese et al. (1974). Jeong et al. (2011) derived experimental *p-y* model for marine clay based on four field load tests conducted at Incheon Bridge site. Lateral load tests were performed on three driven steel piles (LTP-1, LTP-2, LTP-3) with 1.016 m of outer diameter, 25.6 m of depth, 16 mm of wall thickness, and pile head of 1 m above ground surface; and on a drilled shaft (LTP-4) with 2.4 m of diameter, 45 m of depth and pile head of 9.1 m above the ground surface. Proposed *p-y* model for marine clay was compared with O'Neill and Gazioglu (1984) and Matlock (1970) *p-y* models using finite-difference Computer Program, FB-Pier (Hoit et al.,

2001). Beyond initial loading steps, larger displacements and bending moments were obtained from existing models than the proposed *p-y* model for marine clay. This difference in displacement and bending moment seemed more apparent in flexible piles compared to the rigid pile, which has been validated by conducting a parametric study on pile-soil rigidity. In another study, Suryasentana and Lehane (2014) numerically generated Cone Penetration Test (CPT) profiles in sandy soil by performing Cavity Expansion Simulation proposed by Yu and Mitchell (1998) and developed a CPT-based *p-y* model for piles in sand. In a similar study, Li et al. (2014) also proposed a more robust CPT-based *p-y* model for siliceous sand, based on six lateral load tests performed on open-ended steel pipe piles. Park et al. (2017) developed a *p-y* model based on field lateral load tests and empirical formula for basalt at Jeju Island in South Korea. A hyperbolic relationship for rock *p-y* curve was used in regression analysis to develop the proposed *p-y* model. Zhang and Andersen (2017) proposed a simple framework to construct site-specific *p-y* curves for clay from laboratory shear stress-strain data. The framework is based on a simple observation that the shape of the *p-y* curve resembles the shape of the shear stress-strain curve. So, the stress-strain curve from the laboratory can be scaled to obtain a site-specific *p-y* model for clay.

1.2.2 Past Investigations on Diameter Effect

The limitation of *p-y* analysis due to larger diameter is often termed as "diameter effect". Finn and Dowling (2015) performed *p-y* analysis for drilled shafts with diameter ranging from 0.2 m to 2 m using LPILE and the FE program, VERSAT-P3D (Wu, 2006). Conservative response was observed based on LPILE analyses on larger diameter (D > 1.25 m) shafts when lateral deflection exceeded 60 mm.

To quantify the diameter effect, Finn and Dowling (2015) established an empirical relationship between pile diameter and load level at a given head displacement based on VERSAT analyses. From the study by Janoyan et al. (2006), it was reported that a 1.8 diameter pile has 60% more capacity compared to the predicted response from using the API *p-y* curve. Ismael (2007) conducted a series of load tests on piles with increasing diameter and found that by increasing the pile diameter by 66%, the lateral load capacity increases 60%. Yang et al. (2016) performed a series of numerical modeling using both FE and *p-y* method to investigate the diameter effect. FE modeling of the laterally loaded pile was done using Abaqus (Abaqus, 2011) which is validated by examining a field lateral load test conducted at Blessington, Ireland. The lateral test involved an open-ended steel pipe pile embedded in the sand, with 0.34 m of diameter, 14 mm of wall thickness, and 4.35 m of embedded length. The response predicted by Abaqus was compared with the response obtained from using the API *p-y* model. Yang et al. (2016) reported that the API method over-estimated the pile's capacity when $D \geq 2$ m. It was observed that the over-estimation of lateral resistance by *p-y* method is proportional to pile diameter, and the FE model generates higher lateral displacement at deeper depth compared to *p-y* model. Based on the parametric study, an empirical coefficient is proposed to adjust the lateral load capacity estimated by API/DNV *p-y* model based on the pile diameter effect.

1.2.3 Improvements to Numerical Lateral Load Analysis

Previous studies adopted different approaches to address the diameter effect in numerical lateral load analysis. Vallabhan and Alikhanlou (1982) developed a simple, discrete model for short circular rigid pier in clay, with several components

of lateral soil resistances, including m_r, v_b and m_b. For the proposed model, a rigid pier undergoing very small displacement and rotation is assumed. A set of spring systems have been used to categorize stiffness properties of different resistance components. A stiffness equation has been developed, based on Minimum Total Potential Energy Theorem (Langhaar, 2016), for linear soil properties. The non-linearity of the spring system can be included by following the iterative solution process at each incremental load. Vallabhan and Alikhanlou (1982) assessed the influence of different springs and observed significant improvement when v_b and m_r springs were added to the model. McVay et al. (2008) developed tip shear and tip moment resistance models for Florida limestone based on centrifuge lateral load tests conducted on drilled shafts with 6 ft and 9 ft diameters. Based on a previous study to formulate *p-y* model for Florida limestone (McVay and Niraula, 2004), it has been observed that not considering side shear in back-calculated *p-y* curves may cause errors as high as 26% for a 12 ft diameter shaft. Fuentes et al. (2021) also developed a tip shear resistance model based on Coulomb theory, for cohesionless soil considering offshore monopiles with diameters between 5 m to 7 m and embedment lengths between 20 m to 30 m.

Ashour and Helal (2014) calculated m_r as a function of vertical side shear resistance due to axial load, the vertical component of lateral deflection, and flexural deformation of shaft. To improve the *p-y* analysis, Ashour and Helal (2014) integrated m_r into the strain wedge model (Norris, 1986; Ashour and Norris, 2000). An iterative process is developed at a small strain value to solve the modified *p-y* equation. It was assumed that mobilization of side shear resistance in stiff clay and weak rock only occurs on the passive side, due to the gap area during lateral loading on the active side. Ashour and Helal (2014) assumed the distribution of mobilized side shear reaches peak values at the extremities and decreases at the

sides following a cosine function. FE analysis was conducted considering a drilled shaft of 1.22 m diameter and 5 m length in stiff clay to investigate the effects of clay and pile properties on the development of mobilized side shear resistance. From the investigation, Ashour and Helal (2014) observed a 31% increase in the shaft head lateral stiffness at L/D = 4, which reduces to 7% at L/D = 7, indicating more additional lateral resistance due to mobilized side shear for a shorter pile. In another study, Taghavi et al. (2020) proposed an improved *p-y* method by integrating the moment-rotational (m_r-θ) relationship in BNWF model as a result of coupling of axial and lateral resistances. The contribution of shaft diameter, length, boundary conditions, and soil/rock strength properties in the coupling was also investigated. The proposed *p-y* method was validated based on four case studies, including a centrifuge (D = 1.38 m) and full scale (D = 2.74 m) lateral load test on Florida Limestone. Compared to conventional *p-y* method, performing coupled *p-y* analysis reduced computed maximum bending moment and deflection up to 12% and 19%, respectively. Increasing shaft diameter from 1.22 m to 2.74 m in coupled analysis based on Bhushan et al. (1979) load test resulted in a double amount of increase in lateral resistance (Taghavi et al., 2020).

To overcome the limitations of site-specific lateral resistance models and the absence of additional springs in the conventional lateral load analysis, Byrne et al. (2015) suggested an advanced numerical-based design method, involving calibration between sophisticated 3D FE analysis and field lateral load test. The new design method has been showcased in 15 lateral load tests on piles with diameters ranging from 0.273 m to 2 m, in two different sites: 1) stiff to very stiff overconsolidated, ductile, Quaternary clay located in Cowden, North-East England; and 2) dense to very dense marine Pleistocene sand located in Dunkirk, Northern France. Two design methods for the laterally loaded shaft are introduced (Byrne et al., 2019). In

the proposed 'Rule-Based Method', a pre-defined mathematical function obtained from optimization and calibration is used. Byrne et al. (2019) suggests using this method in the initial feasibility design of drilled shafts. The 'Numerical based method' includes detailed 3D FE analyses along with high-level site investigation and testing. This method is more sophisticated and accurate, and can be updated with the improvement of numerical modeling and also consecutive updates on lateral pile response on particular soil types. According to this method, first, a set of calibrations in 3D FE analysis should be conducted spanning a range of design parameters. Soil reaction curves should be extracted from numerical analysis and comply with normalized parameters given by Kelly et al. (2006) and LeBlanc et al. (2010). These curves are then incorporated into a simple 1-D FE model, which uses a more robust Timoshenko Beam Theory.

In a more recent study, Wang et al. (2020) proposed a unified two-spring model for normally consolidated soft clay, considering different L/D ratios. The method suggests a *p-y* model combining hyperbolic tangent function and bearing capacity factor formulation proposed by Jeanjean (2009). A moment-rotation (M_R-θ_R) model developed for soft clay is applied at the rotation point, which is defined at the depth where pure rotation and zero deflection occur. According to Wang et al. (2020), the rotation point of laterally loaded monopiles in soft clay is typically observed at the depth of $0.8L$. The proposed M_R-θ_R model can combine the effect from base shear and base moment resistances, and automatically adjust to flexible shaft response by returning zero values. It has been found that, for flexible piles ($10 < L/D \leq 30$), mobilized vertical side shear contributes to 1% of lateral capacity, while for semi-rigid and rigid piles, vertical side shear contributes up to 6% of lateral capacity.

In a study by Fu et al. (2020), a multi-spring model for clayey soil condition in China is proposed, including three soil spring components: 1) lateral soil resistance (*p-y*) spring; 2) tip base shear spring; and 3) moment-rotation spring due to the mobilized side shear along shaft length. All the lateral spring components of the model have been derived from soil shear stress-strain response. The *p-y* spring for clay was derived based on the scaling methodology by Zhang and Andersen (2017) and the ultimate bearing capacity calculation proposed by Zhang et al. (2016). The base shear spring for clay was derived following the scaling of the stress-strain curve proposed by Zhang and Andersen (2019). A scaling relation between moment-rotation spring and stress-strain response, applicable for clay material has been proposed. The validation of the proposed model was done by conducting FE analysis using Abaqus, considering a 6 m diameter monopile with L/D ratios ranging from 3 to 10. The results were compared with results obtained from back-analysis (B-A) using the proposed model. The difference between FE analysis and B-A results, particularly for $L/D = 3$, was observed when both base shear and moment-rotation springs were neglected. The use of API *p-y* spring instead of the selected *p-y* model for soft clay also caused considerable deviations from the FE analysis results.

1.3 Research Objectives

The major goal of this study is to develop a verified and validated numerical tool capable of performing lateral load analysis based on an improve *p-y* method. The study focuses on mitigating the diameter effect in *p-y* analysis, which becomes more apparent for larger diameter drilled shafts, as discussed in the previous section. A unified *p-y* method is proposed in this regard, which can incorporate mobilization

of side shear resistance calculated from the defined *t-z* models, along with the inclusion of tip shear and tip moment resistance models. A modified *p-y* equation for circular shaft section is proposed, with an additional term for resisting moment per unit length due to mobilized side shear resistance (m_r),

$$EI\frac{d^4y}{dz^4} + Q_z\frac{d^2y}{dz^2} - \frac{D^3}{4}(C_{ma} + C_{mp})\frac{d^2y}{dz^2} - p - w = 0 \tag{1.4}$$

where, C_{ma} and C_{mp}, corresponding to active and passive side of the laterally loaded shaft, are simplified terms containing the integrals of secant slope obtained from the mobilized *t-z* curve. These can be related to resisting moments developed at the active (m_a) and passive (m_p) sides of the drilled shafts as shown in the following equation,

$$m_r = m_{rp} + m_{ra} = \frac{D^3}{4}(C_{ma} + C_{mp})\frac{dy}{dz} \tag{1.5}$$

A MATLAB-based, finite-difference program, NVShaft has been developed, which is capable of performing the proposed unified *p-y* analysis. The program features a collection of built-in axial and lateral resistance models from available literature, including a simplified tip moment resistance model proposed in this study. NVShaft can also perform numerical *t-z* analysis, with a unique feature to simulate bi-directional axial load tests, making NVShaft a comprehensive load analysis tool. An overview of various objectives followed through the development of NVShaft is summarized below:

- Collection and compilation of lateral load test data particularly for large diameter shafts.

- Verification of *p-y* and *t-z* analysis and related features (i.e., included *p-y* and *t-z* models) based on outputs obtained from available commercial programs.
- Validation of NVShaft to perform conventional *p-y* analysis based on simulations of field lateral load tests, with emphasis on cemented soil condition in Las Vegas Valley.
- Validation of NVShaft to perform *t-z* analysis, including bi-directional static load test simulations based on available axial field load tests in cemented soil conditions.
- Evaluation of the proposed unified *p-y* analysis using NVShaft, by simulating lateral load tests on smaller and larger diameter shafts in different subsurface conditions.
- Parametric study to investigate the effect of soil strength parameters, shaft embedment depth, applied axial load, etc. on additional lateral resistance mechanisms to cause diameter effect.

Summary of selected lateral and axial load tests used for validation in NVShaft is shown in Table 1.1 and Table 1.2 below,

The research aims to improve the accuracy of lateral load analysis of drilled shafts and to provide an efficient numerical tool to help obtain more realistic design outcomes for engineers. The proposed unified *p-y* method presents a simple way to make major improvements to lateral load analysis in the context of large diameter drilled shafts. The developed finite-difference program, NVShaft can be used as a research tool to further explore the mechanism of diameter effect in the context of more recently developed resistance models.

Table 1.1: List of lateral load tests used for validation in NVShaft.

No.	Load Test Program	Site Location	Reference	Drilled Shaft/Pile Specification
1	Las Vegas Load Test Program	Las Vegas, NV	Rinne et al. (1996)	2 ft diameter shaft with L = 35.7 ft & 8 ft diameter shaft with L = 32 ft
2	Incheon Bridge Cyclic Lateral Load Test	Incheon Bridge site, South Korea	Jeong et al. (2007)	3 ft diameter steel pile with L = 87 ft & 8 ft diameter shaft with L = 175 ft
3	PISA Load Test Program	Cowden, England & Dunkirk, France	Byrne et al. (2015)	6.5 ft diameter shaft with L = 68 ft
4	University of California, San Diego Load Test	University of California, San Diego	Juirnarongrit and Ashford (2004)	2 ft diameter pile with L = 44 ft & 4 ft diameter pile with L = 43 ft
5	University of Florida Centrifuge Test	University of Florida	McVay and Niraula (2004)	6 ft diameter prototype scale shaft with L = 25 ft
6	Raiders Stadium Load Test	Las Vegas, NV	Fiorelli et al. (2018)	Four 2 ft diameter test piles with approx. L = 25 ft

1.4 Organization of the Report

This report is comprised of six chapters and is based on two journals and three peer-reviewed conference papers. The title and publication status of each paper has been attached at the end of this section.

In the first chapter, some background on the applicability and design of drilled shaft foundation in terms of numerical axial and lateral load analysis is discussed. Since the validation of the developed numerical program, NVShaft, was carried out in the context of cemented soil condition of Las Vegas, a brief discussion on caliche

Table 1.2: List of axial load tests used for validation in NVShaft.

No.	Load Test Program	Site Location	Reference	Drilled Shaft Specification
1	Las Vegas Load Test Program	Las Vegas, NV	Rinne et al. (1996)	2 ft diameter shaft with L = 35.7 ft & 8 ft diameter shaft with L = 32 ft
2	Las Vegas City Center Load Test	Las Vegas, NV	LOADTEST (2005)	4 ft diameter shaft with L = 116.8 ft
3	University of Florida Centrifuge Test	University of Florida	McVay and Niraula (2004)	6 ft diameter prototype scale shaft with L = 25 ft

material properties and engineering challenges encountered in caliche dominant sites are included. The literature review includes the limitations of the conventional *p-y* method, past research on diameter effect, recently developed site-specific *p-y* models, and recent improvements to numerical lateral load analysis. Finally, the research objectives and organization of this report are explained.

In the second chapter, the developed MATLAB-based, finite-difference program, NVShaft, is introduced. Different capabilities of NVShaft regarding numerical lateral load analysis are highlighted in this chapter, along with one verification example. The evaluation of the new *p-y* analysis tool based on the I-15/US 95 load test program (Rinne et al., 1996) in cemented soil conditions in Las Vegas valley is presented.

In the third chapter, the capability of NVShaft to perform numerical *t-z* analysis is presented. The evaluation of two available rock *t-z* models by simulating axial load tests from the I-15/US 95 project and Las Vegas City Center project (LOADTEST, 2005) is discussed. This chapter highlights NVShaft's unique ability to perform

numerical simulation of the bi-directional static load test.

In the fourth chapter, a unified *p-y* method, along with a simplified tip moment resistance model applicable for any kind of soil material is presented. This chapter presents the evaluation of the unified *p-y* analysis based on simulations of large diameter shafts from I-15/US 95 and PISA load test programs Byrne et al. (2015). The chapter concludes with a diameter effect study in the context of the mentioned load test programs.

The fifth chapter presents a more elaborate parametric investigation of the effect of different soil and shaft properties on the diameter effect. This has been done based on numerical simulations at two different sites from the PISA load test program. The chapter briefly presents a unified *p-y* analysis performed in the context of the Incheon load test program (Jeong et al., 2011) conducted in marine clay, and lateral load tests in weakly cemented sand (Juirnarongrit and Ashford, 2004) conducted at the University of California, San Diego.

The sixth and final chapter summarizes the major findings and improvements on numerical *p-y* analysis, and provide recommendations for future studies.

Chapter 2

Title: Evaluation of a New *p-y* Analysis Tool for Lateral Analysis of Drilled Shafts using Load Tests in Nevada

Publication status: Published in the DFI 45th Annual Conference on Deep Foundations (peer-reviewed conference paper)

Citation: Bhuiyan, F. M., Siddharthan, R. V., Motamed, R., and Sanders, D. H. (2020). Evaluation of a new *p-y* analysis tool for lateral analysis of drilled shafts using load tests in Nevada. In *DFI 45th Annual Conference on Deep Foundations*, pages 303–312.

October 13-16

Chapter 3

Title: Evaluation of Existing *t-z* Models for Caliche Based on Numerical Analysis of Bi-Directional Load Tests using NVShaft

Publication status: Published in the DFI 46th Annual Conference on Deep Foundations (peer-reviewed conference paper)

Citation: Bhuiyan, F. M., Toth, J., Siddharthan, R. V., and Motamed, R. (2021). Evaluation of existing *t-z* models for caliche based on numerical analysis of bi-directional load tests using NVShaft. In *DFI 46th Annual Conference on Deep Foundations*, pages 21–31, Las Vegas, Nevada. October 12-15

Chapter 4

Title: Evaluation of a Unified *p-y* Method for Lateral Analysis of Large-Diameter Drilled Shafts using NVShaft

Publication status: Accepted in the Elsevier Journal of Transportation Geotechnics

Citation: Bhuiyan, F. M., Motamed, R., Siddharthan, R. V., and Sanders, D. H. (2022b). Evaluation of a unified *p-y* method for lateral analysis of large-diameter drilled shafts using NVShaft. *Transportation Geotechnics*. Accepted

Chapter 5

Title: Numerical Investigation of Diameter Effect on Lateral Response of Deep Foundation: Parametric Study Based on Field Load Tests

Publication status: Under preparation for submission to the Elsevier Journal of Transportation Geotechnics

Citation: Bhuiyan, F. M., Motamed, R., and Siddharthan, R. V. (2022a). Numerical investigation of diameter effect on lateral response of deep foundation: Parametric study based on field load tests. *Transportation Geotechnics*. Under preparation

1.5 References

AASHTO (2020). *AASHTO LRFD Bridge Design Specifications*. AASHTO, Washington, D.C.

Abaqus, G. (2011). Abaqus 6.11. *Dassault Systemes Simulia Corporation, Providence, RI, USA*.

API (2014). *API Recommended Practice 2A-WSD - Planning, Designing, and Constructing Fixed Offshore Platforms – Working Stress Design*. API.

Ashour, M. and Helal, A. (2014). Contribution of vertical skin friction to the lateral resistance of large-diameter shafts. *Journal of Bridge Engineering*, 19(2):289–302.

Ashour, M. and Norris, G. (2000). Modeling lateral soil-pile response based on soil-pile interaction. *Journal of Geotechnical and Geoenvironmental Engineering*, 126(5):420–428.

Bhuiyan, F. M., Motamed, R., and Siddharthan, R. V. (2022a). Numerical investigation of diameter effect on lateral response of deep foundation: Parametric study based on field load tests. *Transportation Geotechnics*. Under preparation.

Bhuiyan, F. M., Motamed, R., Siddharthan, R. V., and Sanders, D. H. (2022b). Evaluation of a unified *p-y* method for lateral analysis of large-diameter drilled shafts using NVShaft. *Transportation Geotechnics*. Accepted.

Bhuiyan, F. M., Siddharthan, R. V., Motamed, R., and Sanders, D. H. (2020). Evaluation of a new *p-y* analysis tool for lateral analysis of drilled shafts using load tests in Nevada. In *DFI 45th Annual Conference on Deep Foundations*, pages 303–312. October 13-16.

Bhuiyan, F. M., Toth, J., Siddharthan, R. V., and Motamed, R. (2021). Evaluation of existing *t-z* models for caliche based on numerical analysis of bi-directional load tests using NVShaft. In *DFI 46th Annual Conference on Deep Foundations*, pages 21–31, Las Vegas, Nevada. October 12-15.

Bhushan, K., Fong, P. T., and Haley, S. C. (1979). Lateral load tests on drilled piers in stiff clays. *Journal of the Geotechnical Engineering Division*, 105(8):969–985.

Bhushan, K. and Scheyhing, C. (2002). Lateral load tests on drilled piers in San Diego area residual and formational soils. In *Proceedings 27th annual conference on deep foundations, San Diego, CA*.

Brown, D. A., Hidden, S. A., and Zhang, S. (1994). Determination of py curves using inclinometer data. *Geotechnical Testing Journal*, 17(2):150–158.

Brown, D. A., Turner, J. P., Castelli, R. J., and Americas, P. (2010). Drilled shafts: Construction procedures and lrfd design methods. Technical Report FHWA-NHI-10-016, United States. Federal Highway Administration.

Byrne, B., McAdam, R., Burd, H., Houlsby, G., Martin, C., Zdravkovic, L., Taborda, D., Potts, D., Jardine, R., Sideri, M., et al. (2015). New design methods for large diameter piles under lateral loading for offshore wind applications. In *3rd International Symposium on Frontiers in Offshore Geotechnics (ISFOG 2015), Oslo, Norway, June*, pages 10–12.

Byrne, B. W., Burd, H. J., Zdravkovic, L., Abadie, C. N., Houlsby, G. T., Jardine, R. J., Martin, C. M., McAdam, R. A., Pacheco Andrade, M., Pedro, A. M., et al. (2019). Pisa design methods for offshore wind turbine monopiles. In *Offshore Technology Conference*. OnePetro.

Cibor, J. M. (1983). Geotechnical considerations of las vegas valley. In *Geological environmental and soil properties*, pages 351–373. ASCE.

Ensoft (2014). *Analysis of load versus settlement for an axially-loaded deep foundation*. Ensoft, Inc., Austin, TX.

Finn, W. L. and Dowling, J. (2015). Modelling effects of pile diameter. *Canadian Geotechnical Journal*, 53(1):173–178.

Fiorelli, D., Zorne, J., Siegel, T., and Faust, P. (2018). Value engineering – design risk and reward at major sport arena projects. In *DFI 43rd Annual Conference on Deep Foundations*, page 3, Anaheim, California.

Fu, D., Zhang, Y., Aamodt, K. K., and Yan, Y. (2020). A multi-spring model for monopile analysis in soft clays. *Marine Structures*, 72:102768.

Fuentes, W., Gil, M., and Rivillas, G. (2021). A p–y model for large diameter monopiles in sands subjected to lateral loading under static and long-term cyclic conditions. *Journal of Geotechnical and Geoenvironmental Engineering*, 147(2):04020164.

Hetényi, M. and Hetbenyi, M. I. (1946). *Beams on elastic foundation: theory with applications in the fields of civil and mechanical engineering*, volume 16. University of Michigan press Ann Arbor, MI.

Hoit, M., Hays, C., McVay, M., and Williams, M. (2001). Fb-pier users guide and manual for the analysis of group pile foundations. *Florida Department of Transportation and the Federal Highway Administration, Tallahassee, Fla, Contract# DTF61–95–00157*.

Ismael, N. F. (2007). Lateral load tests on bored piles and pile groups in sand. In *7th FMGM 2007: Field Measurements in Geomechanics*, pages 1–11.

Janoyan, K. D., Wallace, J. W., and Stewart, J. P. (2006). Full-scale cyclic lateral load test of reinforced concrete pier-column. *ACI structural journal*, 103(2):178.

Jeanjean, P. (2009). Re-assessment of py curves for soft clays from centrifuge testing and finite element modeling. In *Offshore Technology Conference*. OnePetro.

Jeong, S., Kim, Y., and Kim, J. (2011). Influence on lateral rigidity of offshore piles using proposed p–y curves. *Ocean engineering*, 38(2-3):397–408.

Jeong, S., Kim, Y., Kim, J., and Shin, S. (2007). Cyclic lateral load tests of offshore large diameter piles of incheon bridge in marine clay. In *The Seventeenth International Offshore and Polar Engineering Conference*. OnePetro.

Juirnarongrit, T. and Ashford, S. A. (2004). Lateral load behavior of cast-in-drilled-hole piles in weakly cemented sand. *Transportation research record*, 1868(1):190–198.

Kelly, R., Houlsby, G., and Byrne, B. (2006). A comparison of field and laboratory tests of caisson foundations in sand and clay. *Géotechnique*, 56(9):617–626.

Langhaar, H. L. (2016). *Energy methods in applied mechanics*. Courier Dover Publications.

LeBlanc, C., Houlsby, G., and Byrne, B. (2010). Response of stiff piles in sand to long-term cyclic lateral loading. *Géotechnique*, 60(2):79–90.

Li, Q. and Yang, Z. (2017). P–Y approach for laterally loaded piles in frozen silt. *Journal of geotechnical and geoenvironmental engineering*, 143(5):04017001.

Li, W., Igoe, D., and Gavin, K. (2014). Evaluation of cpt-based p–y models for laterally loaded piles in siliceous sand. *Géotechnique Letters*, 4(2):110–117.

Li, W., Zhu, B., and Yang, M. (2017). Static response of monopile to lateral load in overconsolidated dense sand. *Journal of Geotechnical and Geoenvironmental Engineering*, 143(7).

LOADTEST (2005). Report on drilled shaft load testing (Osterberg method), City Center - test shaft 1, Las Vegas, NV. Project No. LT-9160-1, LOADTEST, Inc.

Matlock, H. (1970). Correlations for design of laterally loaded piles in soft clay. *Offshore technology in civil engineering's hall of fame papers from the early years*, pages 77–94.

Matlock, H. and Reese, L. C. (1960). Generalized solutions for laterally loaded piles. *Journal of the Soil Mechanics and foundations Division*, 86(5):63–92.

McClelland, B. and Focht, J. (1956). Soil modulus for laterally loaded piles. *Journal of the Soil Mechanics and Foundations division*, 82(4):1081–1.

McVay, M. and Niraula, L. (2004). Development of PY curves for large diameter piles/drilled shafts in limestone for FBPIER. Technical Report Final Report.

McVay, M. C. et al. (2008). Distribution of end bearing, tip shear and rotation on drilled shafts with combined loading in Florida limestone. Technical Report Final Report.

Motamed, R., Elfass, S., Stanton, K., et al. (2016). LRFD resistance factor calibration for axially loaded drilled shafts in the las vegas valley. Technical report, Nevada. Dept. of Transportation.

Norris, G. (1986). Theoretically based bef laterally loaded pile analysis. In *Proceedings of the 3rd international conference on numerical methods in offshore piling*, pages 361–386. Navtes.

O'Neill, M. and Gazioglu, S. (1984). Integrated formulation of py relationships in clays. *A Report to the American Petroleum Institute, Report PRAC-82-41-2, University of Houston*.

Park, J. J., Yang, K. H., and Huh, J. C. (2017). Analysis of py curve of drilled shafts socketed into basalt at jeju island. *International Journal of Offshore and Polar Engineering*, 27(04):374–382.

Reese, L. and Nyman, K. (1978). Field load tests of instrumented drilled shafts at Islamorada, Florida. *Report to the Girdler Foundation and Exploration Corporation, Clearwater, FL, February*.

Reese, L. C., Cox, W. R., and Koop, F. D. (1974). Analysis of laterally loaded piles in sand. *Offshore technology in civil engineering hall of fame papers from the early years*, pages pp. 95–105.

Reese, L. C., Wang, S. T., Isenhower, W. M., Arrellaga, J. A., and Hendrix, J. (2000). A program for the analysis of piles and drilled shafts under lateral loads. *Ensoft, Inc., Austin, TX*.

Reese, L. C. and Welch, R. C. (1975). Lateral loading of deep foundations in stiff clay. *Journal of the Geotechnical engineering division*, 101(7):pp. 633–649.

Rinne, E., Thompson, J., and Vanderpool, W. (1996). *I-15/US 95 load test program, Las Vegas, Nevada*. Kleinfelder, Inc., Las Vegas, Nevada.

Saint-Pierre, E. (2018). The development of a material model for engineering behavior characteristics of cemented soils for the las vegas valley. Master's thesis, University of Nevada, Reno, Reno, Nevada.

Stanton, K., Motamed, R., and Elfass, S. (2017). Robust LRFD resistance factor

calibration for axially loaded drilled shafts in las vegas. *Journal of Geotechnical and Geoenvironmental Engineering*, 143(6):06017004.

Suryasentana, S. K. and Lehane, B. M. (2014). Numerical derivation of cpt-based p–y curves for piles in sand. *Géotechnique*, 64(3):186–194.

Taghavi, A., McVay, M., Niraula, L., Davidson, M., and Patil, A. (2020). Axial and lateral resistance coupling in the analysis of large-diameter drilled shafts. *Engineering Structures*, 206:110160.

Vallabhan, C. G. and Alikhanlou, F. (1982). Short rigid piers in clays. *Journal of the Geotechnical Engineering Division*, 108(10):1255–1272.

Wang, L., Lai, Y., Hong, Y., and Mašín, D. (2020). A unified lateral soil reaction model for monopiles in soft clay considering various length-to-diameter (l/d) ratios. *Ocean Engineering*, 212:107492.

Werle, J. and Luke, B. (2007). Engineering with heavily cemented soils in Las Vegas, Nevada. In *Problematic soils and rocks and in situ characterization*, pages 1–9.

Wu, G. (2006). VERSAT-P3D: A computer program for dynamic 3-dimensional finite element analysis of single piles and pile groups. *Wutec Geotechnical International, Vancouver, Canada*.

Yang, M., Ge, B., Li, W., and Zhu, B. (2016). Dimension effect on py model used for design of laterally loaded piles. *Procedia engineering*, 143:598–606.

Yu, H. and Mitchell, J. (1998). Analysis of cone resistance: review of methods. *Journal of geotechnical and geoenvironmental engineering*, 124(2):140–149.

Zafir, Z. and Vanderpool, W. (1998). Lateral response of large diameter drilled shafts:

I-15/US 95 load test program. In *Proc., 33rd Engineering Geology and Geotechnical Engineering Symp*, pages 161–176.

Zhang, Y. and Andersen, K. H. (2017). Scaling of lateral pile py response in clay from laboratory stress-strain curves. *Marine Structures*, 53:124–135.

Zhang, Y. and Andersen, K. H. (2019). Soil reaction curves for monopiles in clay. *Marine Structures*, 65:94–113.

Zhang, Y., Andersen, K. H., and Tedesco, G. (2016). Ultimate bearing capacity of laterally loaded piles in clay–some practical considerations. *Marine Structures*, 50:260–275.

CHAPTER 2

EVALUATION OF A NEW *P-Y* ANALYSIS TOOL FOR LATERAL ANALYSIS OF DRILLED SHAFTS USING LOAD TESTS IN NEVADA

Abstract

Large-diameter drilled shafts (DS) are a critical part of a seismic-resistant system, and therefore it is important to be able to accurately model lateral resistance. To undertake the lateral load analysis of large-diameter DS, a finite-difference *p-y* analysis program, NVShaft, is being developed at the University of Nevada Reno. Validation of the new program involved numerous *p-y* analyses using commercially available programs. Subsequent comparisons suggested the program's ability to yield reasonable predictions for typical diameter DS. Based on the I-15/US 95 load test program carried out in Las Vegas, NV, this study presents the evaluation of NVShaft in Nevada's subsurface condition. Lateral load analyses of a 2 ft and an 8 ft diameter DS were attempted using NVShaft. The location of the applied lateral loads and the presence of cemented soil-layers were incorporated in the modeling. A good agreement between NVShaft prediction and the measured response was found for the 2 ft diameter DS. For the 8 ft diameter DS, a stiffer response was predicted. The inspections of the moment-curvature characteristics at different load levels suggested cracked response of the concrete due to prior axial load testing may be one of the reasons behind the deviation.

2.1 Intoduction

The Ability to transmit large loads in a variety of soil and rock profiles within a small footprint and high flexural strength to counter seismic loads are some of the advantages of drilled shafts (DS) compared to other types of deep foundations. The use of large diameter DS has increased substantially both in the US and Europe in recent years, as a suitable foundation system to support offshore wind turbines, bridge piers, tall buildings, and bridge abutments. Some of the thousands of offshore wind turbines installed in Europe are supported by DS with the diameter as high as 6m (Byrne et al., 2015). Design codes (e.g. API 2014) recommend using beam on nonlinear Winkler foundation (BNWF) models, commonly known as the *p-y* method to perform lateral load analysis. In the *p-y* method, localized soil's lateral resistance is represented using nonlinear *p-y* models. The DS is assumed to behave like an Euler's idealized beam and commonly the finite difference numerical computation is done by discretizing such beam in several nodes (McClelland and Focht, 1956; Reese et al., 1974). The nonlinear *p-y* relations that characterize the soil resistance are derived based on correlations with instrumented field tests undertaken using slender piles of diameter in the range of 1 ft to 2ft. Despite being adopted in numerous computer software packages for its simplicity and reliability, the *p-y* method appears to yield very conservative responses for large diameter DS (Ashour and Helal, 2014; McVay and Niraula, 2004). For dense sandy soil in the San Diego area, Bhushan and Scheyhing (2002) found that LPILE requires p-multipliers between 2 to 8 to accurately predict the load-deflection response based on measured data. The problem originates from the inherent inability of the *p-y* model itself to capture the characteristics of soil resistance associated with large diameter DS. Also, lack of *p-y* curves to represent untested soil types, layered soil conditions, the direct

use of *p-y* curves obtained based on field lateral load test conducted on the slender piles (Matlock, 1970; Welch and Reese, 1972; Reese et al., 1974) add to the constraints. To address these limitations, more appropriate *p-y* curves have been proposed based on lateral load tests on large diameter DS with advanced instrumentation, or new design methodology has been recommended. Finn and Dowling (2015) conducted a parametric study using LPILE (Reese et al., 2000) and VERSAT-P3D (Wu, 2006) to obtain load-deflection curves for different pile diameters ranging from 0.2 m to 2 m. While LPILE uses the finite difference method, VERSAT-P3D is a 3D finite element (FE) based program. A Significant diameter effect was observed only when lateral deflection exceeded 60 mm, particularly for large diameter DS. Based on VERSAT analysis, the relationship between pile diameter and load level at a given head displacement was developed. Byrne et al. (2015) proposed a 'Numerical-Based Design Method' involving more detailed site investigation, testing, and in-depth 3D FE analysis to proceed with the design of large diameter DS.

In this paper, a MATLAB based finite difference software, NVShaft is introduced, which is currently being developed in the University of Nevada, Reno to address some of the limitations in the *p-y* method. NVShaft is proved to be capable of conducting conventional *p-y* analysis based on comparison with numerous analyses conducted in LPILE, as well as field load tests and centrifuge data. One such example of comparison with multiple different soil layers and the nonlinear DS response is presented in this paper. Nonlinear stiffness properties of the DS can be incorporated in NVShaft in the form of user-input moment-curvature relationships. Any location for application of the lateral load as boundary condition can also be specified. Users can model tapered DS, specify p-multipliers in soil properties, define five different types of boundary conditions at the top and shear resistance model at DS tip. For layered soil media, NVShaft can perform layering correction

(Georgiadis, 1983) and perform *p-y* analysis using any of 19 *p-y* curve models included in the program. Some of these features of NVShaft were utilized in order to assess its ability to evaluate lateral DS response in local soil conditions in Nevada.

The load test program performed as part of the Interstate I-15/US 95 Interchange project was chosen for this purpose (Rinne et al., 1996). Lateral tests on 2 ft diameter and 8 ft diameter DS in site No. 1 were intentionally chosen to observe the diameter effect when using the conventional *p-y* analysis. Axial load tests were conducted in both of these test shafts prior to the lateral load test, which made a significant impact on lateral response. Two boring logs from the site indicated the presence of caliche, partially cemented dense sandy clay and plastic silty sand layers at various locations of the soil profiles. Results from NVShaft analysis were compared with a COM624P prediction reported by Zafir and Vanderpool (1998) and field measurements. It was found that the difference between predicted and measured curvatures can be attributed to the deviation in the lateral load responses.

2.2 I-15/US 95 Load Test Program

An extensive load test program as a part of geotechnical investigation associated with Interstate 1-15/US 95 reconstruction project was carried out in Las Vegas, Nevada in 1995 (Rinne et al., 1996). The goal was to get a better understanding of the response of DS under axial and lateral loading in Nevada's soil conditions. The outcome of the project was to ascertain axial and lateral design capacities and to help to develop the geotechnical design criteria of the DS. A total of 13 DS were constructed that included 2 ft, 8 ft diameter single DS, and four DS groups comprising of 2 ft diameter DS within 11 ft diameter cap. In total, five lateral and

ten axial load tests were conducted in four different locations, about a one-half mile west of downtown Las Vegas. A primary motivation for the load tests was to use the response from the tests to develop side shear and end bearing capacity relative to the role of partially cemented soil and caliche layers. The Las Vegas area is known to experience some minor shaking from underground blasting and earthquakes. The load tests can also provide better insight into the lateral behavior of DS in such scenarios. In this study, 2 ft diameter and 8 ft diameter DS from site No. 1 were chosen for lateral load analysis using NVShaft.

2.2.1 Subsurface Exploration and Soil Conditions

Five borings were made using truck-mounted drilled rigs and continuous flight, hollow stem auger. In site No. 1, two boring logs in close proximity, boring B-1, and B-5 were made. Hard to very hard cemented cores were obtained by using Nx size coring equipment. Standard penetration tests using a Central Mining Equipment (CME) auto hammer was carried out in all boring locations. Some of the major laboratory tests included grain size distribution, Atterberg Limits, direct shear strength, unconfined compression strength, and triaxial shear strength tests. The unconfined test was conducted on four caliche core samples, resulting in unconfined compressive strength value (q_u) ranging from 4060 psi to 9320 psi.

The upper 2.5 to 3.5 ft of the surface layer at site No. 1 consisted of low plastic to non-plastic silty sand, followed by a stiff, low to high plastic sandy clay up to 14 ft depth. Some remnants of alluvial and sheet wash soil from the original construction of interchange were also present near-surface. The first caliche layer was encountered from 14 to 13.5 ft depths and existed up to 18.5 to 21 ft depth in

borings B-1 and B-5, respectively. Groundwater was at 13 ft and 10 ft depth after drilling as reported in logs for B-1 and B-5 respectively. The first caliche layer was followed by several layers of partially cemented, medium to very dense clayey and silty sand strata up to 32 ft depth. A 1 ft thick caliche layers were found at 32 ft depth in boring B-1, while in B-5 a clayey gravel layer was found at the same location. Another 2 ft thick caliche layer at 35 ft depth was preceded and followed by stiff sandy clay and dense to very dense clayey sand.

Information from the soil exploration program was used to develop soil profiles for numerical analysis in this study, which is summarized in Tables 2.1 and 2.2. The selected *p-y* curves for NVShaft analysis and required material properties, such as unit weight (γ), angle of friction (ϕ), cohesive strength (c_u), uniaxial compressive strength (q_u), soil modulus (E_s) and strain factor i.e. strain at 50% strain level (ϵ_{50}) values depending on soil types are shown. Several empirical formulas and correlations from FHWA (Brown et al., 2010) and Caltrans (2019) manual were used to obtain other needed soil parameters. For the first caliche layer in boring B-1, the *p-y* curve back-calculated from the triaxial test result was utilized as a user-input model. For other caliche layers, the *p-y* curve for vuggy limestone (Reese and Nyman, 1978) was adopted. A *p-y* curve incorporating a wide range of soil ductility and relative soil-shaft stiffness given by the Integrated Clay Method (O'Neill and Gazioglu, 1984) was used for the stiff clay layers.

2.2.2 Details of Test Shafts and Lateral Load Test Configuration

For 2 ft diameter DS, 21" diameter O-Cell with hydraulic ram was placed 32.2 ft below grade. Longitudinal bars consisted of eight bundled groups of three #9 bars

Table 2.1: Representative soil profile for 2 ft diameter DS in I-15/US 95 load test program, Las Vegas.

Depth (ft)	*p-y* Curve Used	SPT-N	γ (pcf)	ϕ (Degree)	c_u (psf)	q_u (psi)	E_s (ksf)	ϵ_{50}
0 - 3.5	Sand	26	91	37	-	-	-	-
3.5 - 6.5	Integrated Clay	31	113.1	-	4400*	-	1160	0.0043
6.5 - 10	Integrated Clay	50	120	-	4136	-	1036	0.0043
10 - 14	Integrated Clay	15	113.1	-	2369	-	914	0.0045
14 - 18.5	User-input *p-y*	50	136	-	-	-	-	-
18.5 - 24	Sand	50	133	37	-	-	-	-
24 - 28	Sand	49	133	32*	-	-	-	-
28 - 31.5	Sand	39	133	37	-	-	-	-
31.5 - 33	Vuggy Limestone	50	136	-	-	7819*	-	-
33 - 35	Sand	40	130	37	-	-	-	-
35 - 38	Vuggy Limestone	50	136	-	-	7778*	-	-

∗ Measured from in-situ/laboratory

Table 2.2: Representative soil profile for 8 ft diameter DS in I-15/US 95 load test program, Las Vegas.

Depth (ft)	*p-y* Curve Used	SPT-N	γ (pcf)	ϕ (Degree)	c_u (psf)	q_u (psi)	E_s (ksf)	ϵ_{50}
0 - 2.5	Sand	26	91	37	-	-	-	-
2.5 - 5.5	Integrated Clay	13	108	-	2215	-	726	0.0047
5.5 - 7.5	Integrated Clay	42	109	-	5277	-	1216	0.0045
7.5 - 12	Integrated Clay	16	125	-	2640	-	580	0.0052
12 - 13.5	Sand	13	120	33	-	-	-	-
13.5 - 21	Vuggy Limestone	-	136	-	-	9583*	-	-
21 - 26	Sand	50	138	40	-	-	-	-
26 - 32	Sand	50	133	40	-	-	-	-

∗ Measured from in-situ/laboratory

that were evenly spaced around 18″ spiral-tied cage. The pitch of the tie bar was 3″ up to the depth of 14 ft and 9″ from that depth, continuing up to the location of O-Cell.

The 8 ft diameter DS was designed to carry 2000 kips of maximum lateral load.

The reinforcement cage consisted of 24 2-bar bundles of #11 longitudinal bars tied within 84″ diameter spiral cage. Tie bars consisted of continuous # 5 bar at a three-inch pitch. The schematic of 2 ft and 8 ft diameter DS along with the generalized soil profiles are shown in Fig. 2.1.

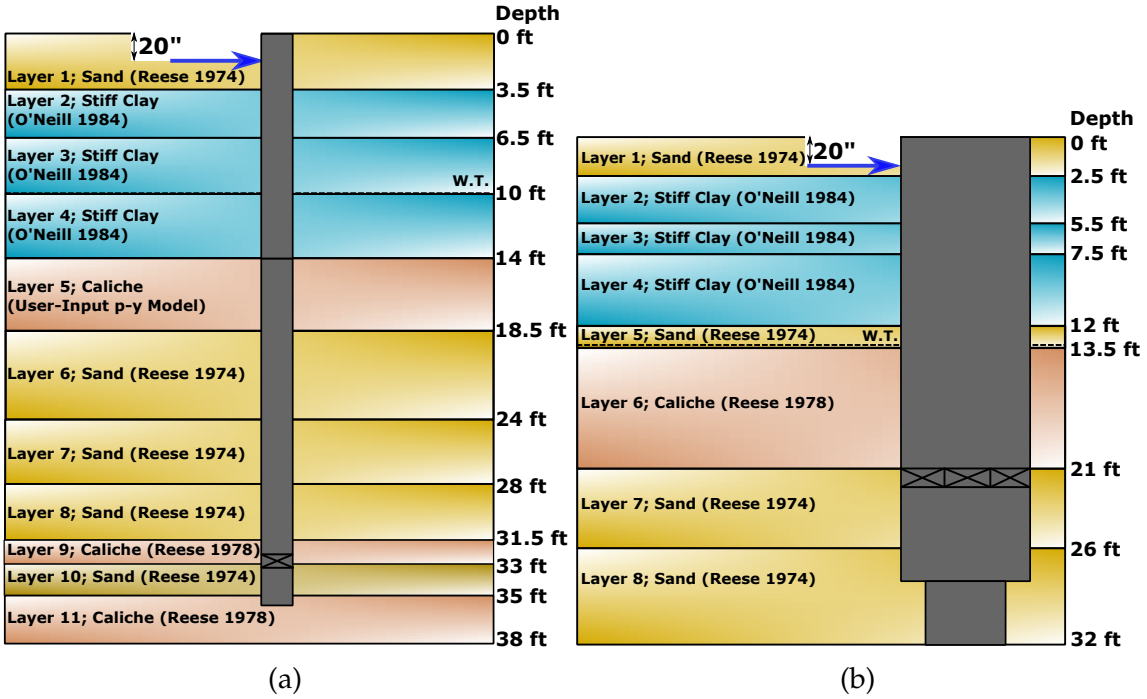

Figure 2.1: Schematics of DS details and generalized soil profile for 2 ft diameter (left) and 8 ft diameter (right) test shafts in I-15/US 95 load test program, Las Vegas.

For both test shafts, the lateral load was applied using hydraulic jack (with the capacity of 600 kips and 2000 kips for 2 ft and 8 ft diameter DS respectively) about 20″ below ground level. The 2 ft diameter DS was subjected to 228 kips of maximum test load, in 12 kips increments, and maximum horizontal deflection was 3.198″. For 8 ft diameter DS, in 100 kips increments, the maximum applied load was 1578 kips. The maximum recorded groundline lateral deflection was 1.37″.

2.2.3 Field Observations During Axial Load Tests and Related Uncertainties

During axial load tests, which were conducted prior to lateral load tests, 366 kips and 3914 kips of maximum axial loads were applied via O-Cells placed in the middle depth of 2 ft and 8 ft diameter DS respectively. For the 8 ft diameter DS, vertical displacements of top and bottom portions were 1.351" and 0.807", respectively at the maximum axial load level. Loads were applied in three cycles on the 8 ft diameter DS, which caused the formation of cracks and upward heave at the nearby ground surface. At the level of 2228 kips of axial load, an average upward heave from DS edge up to the radial distance of 5 ft was reported to be around 0.53". Also, the tensile strain reported in the strain profile diagram near O-Cells location indicated a possible crushing of concrete. For the 2 ft diameter DS, the deformation in the axial load test was comparatively lower (0.041" of upward and 0.807" of downward movement of the DS at maximum axial load).

From the field observations during the axial load test response, it is clear that the lateral load test conducted on the 8 ft diameter DS could have been significantly affected by the prior severe soil-shaft response. The presence of cementation in soil layers is another major factor to add to the complication. As stated by Brown et al. (2010), cementation in the sand may deteriorate during drilling and sampling, which may cause the sample to appear to be uncemented. Lack of reported soil properties led to the use of multiple empirical formulas, which also adds to the uncertainties in the prediction of DS response in the lateral load analysis.

2.3 Development of NVShaft

A MATLAB based, finite difference program NVShaft is being developed as part of a Nevada of Department of Transportation (NDOT) funded research project aiming to improve the lateral load analysis in the context of Nevada soil conditions. A total of 19 different *p-y* curves, based on different soil/rock conditions, have been included in the program's library at this time in the project. Some of the recently developed *p-y* curves (e.g. O'Neill and Gazioglu 1984) claim to provide a better representation of lateral resistance. A list of the *p-y* models available in the current version of the program is shown in Table 2.3.

Table 2.3: Summary of *p-y* curve models included in NVShaft.

Soil Type	Clay	Sand	Rock	Special/Other Type
Number of *p-y* Models	6	4	4	5

While performing the *p-y* analysis, NVShaft solves for DS displacement, slope, moment and shear force using the fourth-order differential equation in eq. 2.1,

$$EI\frac{d^4y}{dx^4} + P_x\frac{d^2y}{dx^2} - p - w = 0 \tag{2.1}$$

Where E = elastic modulus of DS section, I = moment of inertia of DS section, y = deflection at depth x, P_x = vertical load on head, p = soil reaction per unit length, and w = applied distributed load per unit length.

NVShaft can perform *p-y* analysis on the DS with multiple sections including nonlinear properties using user-defined moment-curvature relationships. The program can implement the layering correction method proposed by Georgiadis (1983) for layered soil profiles. In this method, the effect of stiffness characteristics

of upper soil layers to the lower ones is defined in the form of equivalent depths. Tapered DS can be modeled by assigning different values for the diameter at the head and the tip. Similar to the current state of practice, p-multipliers can also be specified for specific *p-y* curves. Users can specify five different types of boundary conditions at the top, and also shear resistance model at the tip of the DS. The location of boundary conditions, such as shear force can also be set as an input. NVShaft also has additional features like calculating the critical length of DS based on analysis with multiple loading conditions.

Each of these features and *p-y* models was verified by comparing the responses from identical models made in popular commercial *p-y* program and NVShaft. One such example of validation by comparing the outputs with LPILE in terms of deflection and bending moment profiles is shown in Fig. 2.2. The model includes a nonlinear DS with 3 ft diameter and 50 ft in length, embedded in 8 different types of soils. The soil parameters and nonlinear DS properties were retrieved from examples 23 and 15 respectively from LPILE's user manual (Isenhower et al., 2017). The analyses were carried out after applying the layering correction, which ended up producing almost identical responses. Relative to LPILE response, the difference in maximum deflections and bending moments were 2.66% and 1.24% respectively. This small deviation in outputs mostly stems from different numerical integration schemes adopted by these two programs while performing layering correction for soil layers.

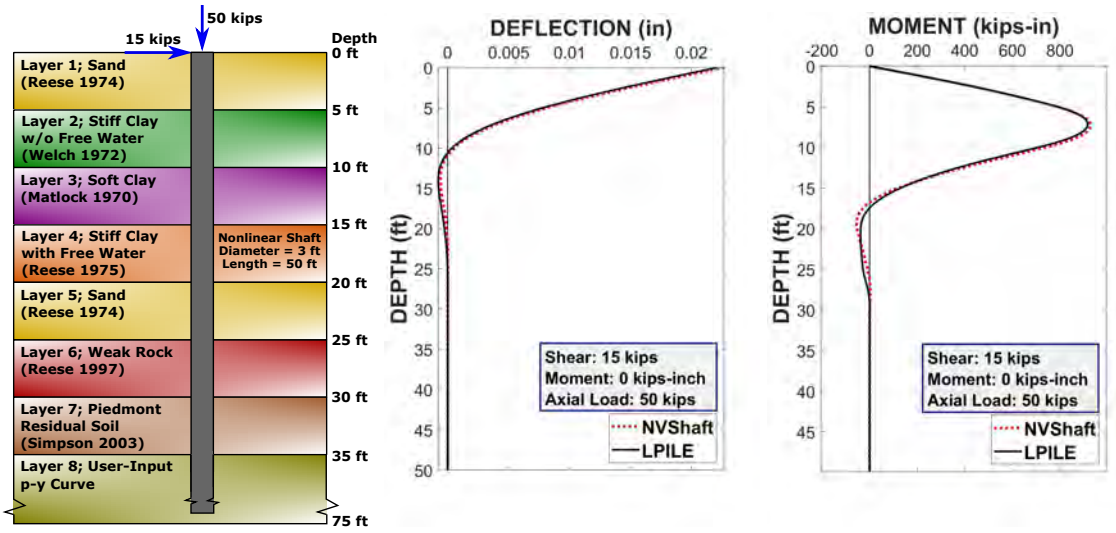

(a) (b) (c)

Figure 2.2: Numerical model and outputs from identical *p-y* analyses performed for comparison between NVShaft and LPILE.

2.4 Prediction of I-15/US 95 Load Test by NVShaft

Numerical *p-y* analyses were carried out using the NVShaft program, to evaluate the program's capabilities to predict the response of the large-diameter DS based on the I-15/US 95 load test program. To investigate the diameter effect, analyses were conducted for 2 ft and 8 ft diameter DS from site No. 1. Zero bending moment and multiple shear forces applied at 20" from DS head were specified as boundary conditions. While calibrating the model, it was observed that the location of the applied lateral load caused a significant impact on the results. Moment-curvature relationships for the DS were generated in CSiBridge (Wilson, 2016) program, which is shown in Fig. 2.3.

The deflection profile and load-deflection plot for 2 ft diameter DS obtained from NVShaft analysis are presented in Fig. 2.4. The Corresponding measured DS and COM624P (currently LPILE) predicted response by Zafir and Vanderpool

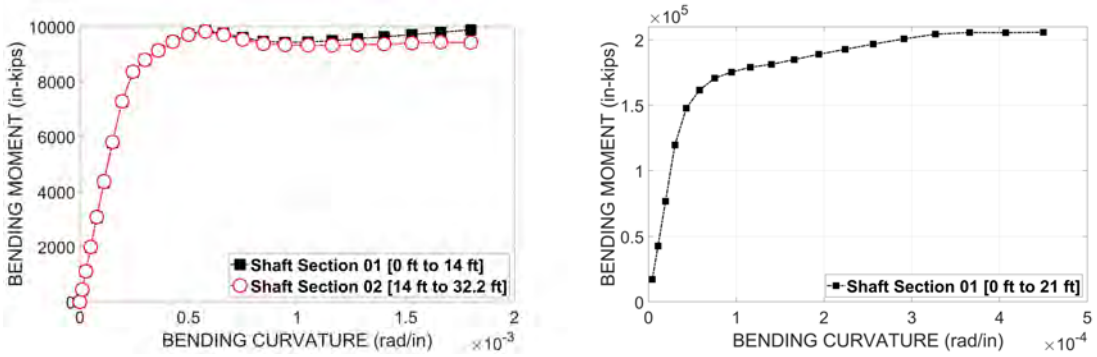

(a) (b)

Figure 2.3: CSiBridge generated moment-curvature curves for 2 ft diameter (left) and 8 ft diameter (right) DS.

(1998) are also included in the plots for comparison. A similar type of comparison plots is shown in Fig. 2.5 for 8 ft diameter DS. A very good match between NVShaft predicted response and measured data at smaller load levels can be observed for both of these DS. Compared to NVShaft, the measured response is slightly stiffer at these load levels for 8 ft diameter DS, indicating possible diameter effects in the *p-y* analysis. The head deflections predicted by NVShaft at corresponding maximum lateral loads are 3.39″ and 1″, for 2 ft and 8 ft diameter DS respectively. Predictions yielded by COM624P are softer compared to other types of responses, as seen in load-deflection plots.

At higher load levels, particularly for the case of 8 ft diameter DS, the response obtained from NVShaft is significantly stiffer compared to measured data. This deviation can be explained by comparing the maximum curvatures at different load levels based on the numerical and measured response as shown in Fig. 2.6. Based on CSiBridge simulated nonlinear flexural model used in the analysis, predicted maximum curvature closely follows the measured one for 2 ft diameter DS, at small to medium load levels. This indicates the ability of NVShaft to make a reasonable prediction in terms of curvature response for 2 ft diameter DS.

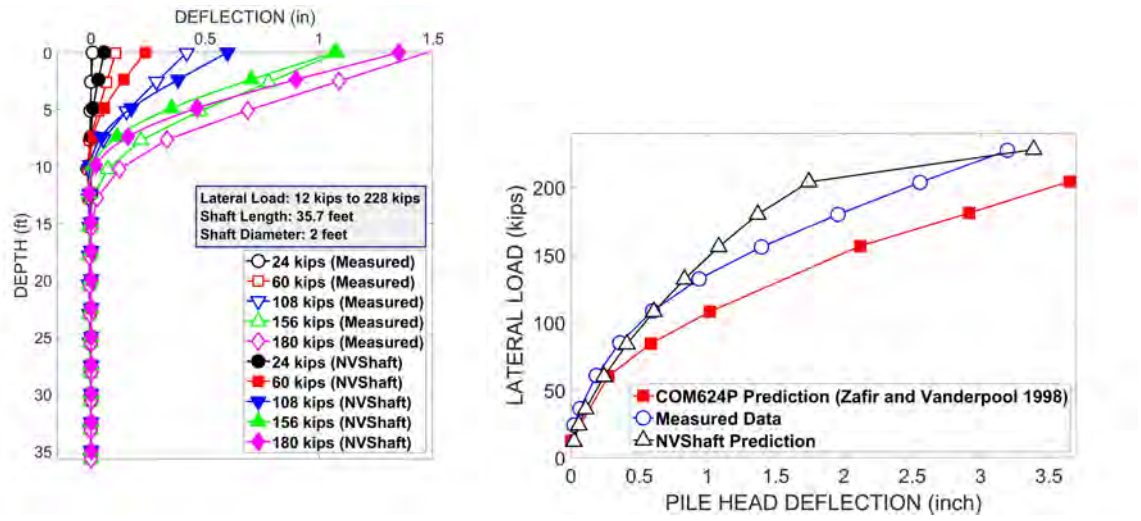

(a) (b)

Figure 2.4: The response of 2 ft diameter DS based on numerical calculation (NVShaft and COM624P) and measured data.

A similar type of investigation done for 8 ft diameter DS shows significantly higher maximum curvature predicted by NVShaft. One of the possible reasons is the cracked response of concrete originating from the prior crushing during the axial load test. The rigid movement of the cracked upper portion of the DS that follows at higher applied lateral loads explains the softer measured DS response. Observed excessive upward heave and crack formation in the soil during axial load tests prior to the lateral load tests make the continuum-based *p-y* analysis somewhat challenging. The Presence of cemented soil layers, higher stiffness at O-Cell locations, and the use of empirical formulas to obtain soil properties also add to the complication.

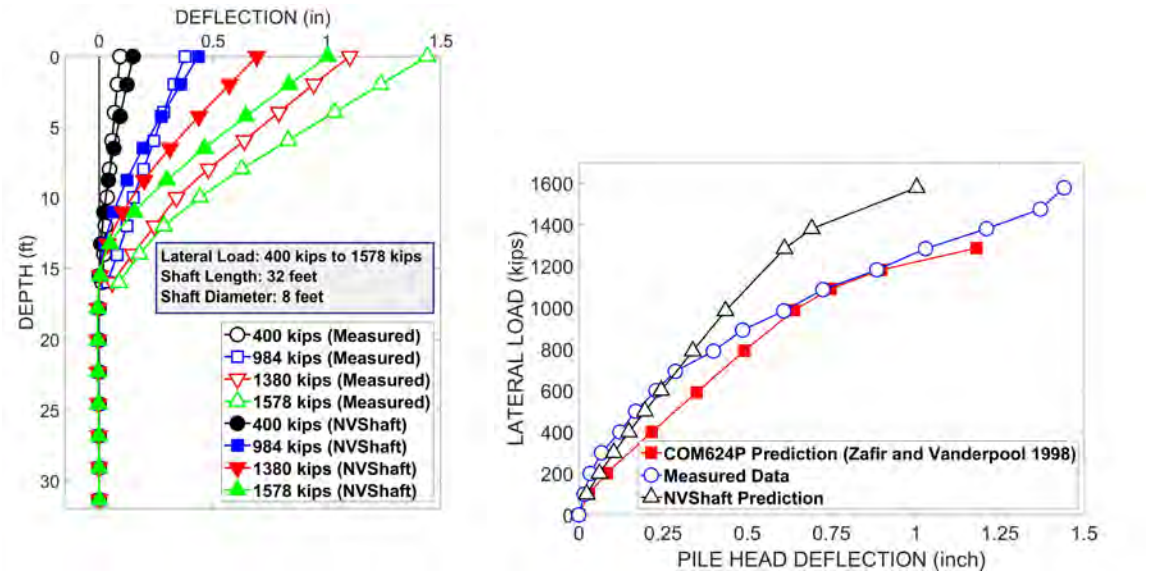

(a) (b)

Figure 2.5: The response of 8 ft diameter DS based on numerical calculation (NVShaft and COM624P) and measured data.

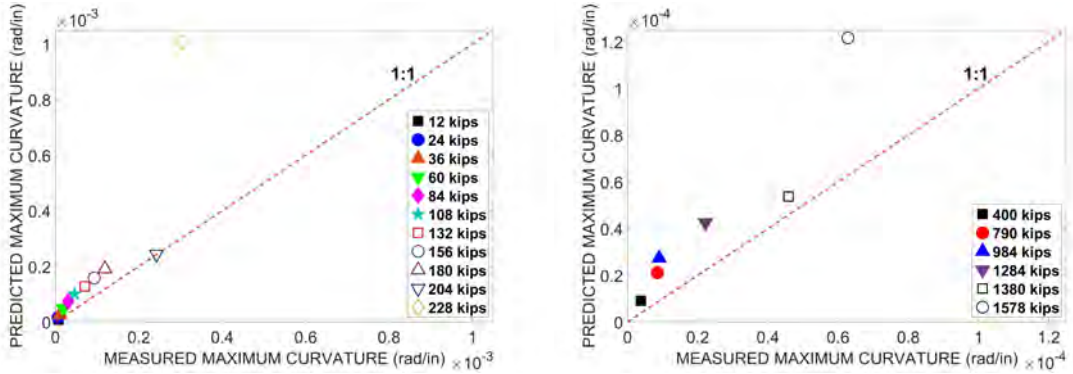

(a) (b)

Figure 2.6: Predicted vs measured maximum curvature for 2 ft diameter (left) and 8 ft diameter (right) DS.

2.5 Summary and Conclusions

To improve the overall *p-y* method of lateral load analysis on large diameter shafts, a MATLAB based numerical, finite difference program, NVShaft, is currently being developed at the University of Nevada, Reno. As of now, a total of 19 *p-y* models

have been included in the program's library. Users can specify p-multipliers, different types of boundary conditions, the location of applied lateral load, and relevant tip shear resistance in the model. Each of these features has been validated based on comparison from many analyses done in similar programs used in current practice. One such example is presented to compare the response obtained by NVShaft and LPILE from *p-y* analysis on a nonlinear DS embedded in layered soil medium. Differences of 2.66% and 1.24% in maximum deflection and bending moment, respectively, from separate, identical analyses indicate the new program's capability to perform conventional *p-y* analysis.

To verify NVShaft in a more practical perspective, I-15/US 95 load test program in Las Vegas, Nevada was used as a reference. Lateral load tests on a 2 ft diameter (35.7 ft in length) and an 8 ft diameter (32 ft in length) DS from site No. 1 were modeled in NVShaft to study the diameter effect. Two adjacent boreholes near test shafts revealed the presence of partially cemented soil, mostly in the form of stiff sandy clay and dense silty sand layers. Starting from 13.5 ft of depth, fully cemented caliche layers at several depths were encountered. The *p-y* model for vuggy limestone and the user-input model back-calculated from triaxial test results were used to attenuate the unpredictability of the caliche layers. In both test shafts, lateral loads were applied 20″ below grade level from the hydraulic jack. The maximum measured horizontal deflection of the 2 ft diameter DS was 3.198″ at a maximum lateral load of 228 kips. For the 8 ft diameter DS, the maximum recorded horizontal deflection was 1.37″ at a maximum lateral load of 1578 kips.

A very good match with measured response was obtained in both cases from NVShaft analyses at small load levels. The maximum head deflections captured in numerical analysis at corresponding final lateral loads were 3.39″ and 1″, for

the 2 ft and 8 ft diameter DS respectively. For the 8 ft diameter DS, the measured response was relatively stiffer than the predicted response at lower load levels, indicating possible diameter effects in play. At higher lateral loads, measured responses were softer in comparison, particularly for the 8 ft diameter DS. The record of the axial load test performed beforehand indicates severe crushing of concrete, the upward heave of soil, and crack formation along with the radial distance from the 8 ft diameter DS location. This extreme response of the soil-shaft system adds to the complexity in the nonlinear flexural behavior and the overall lateral load test. An inspection of the maximum measured and predicted bending curvature also points out the cracked response of concrete during the lateral test on the 8 ft diameter DS. On the other hand, for the 2 ft diameter DS, the maximum predicted curvatures at small to medium load levels complied well with the measured response. This particular observation reinforces NVShaft's capability to reasonably capture the nonlinear DS response during *p-y* analysis. Beyond the scope of this study, NVShaft also showed promise based on comparison with several other field load and centrifuge load test responses.

2.6 References

API (2014). *API Recommended Practice 2A-WSD - Planning, Designing, and Constructing Fixed Offshore Platforms – Working Stress Design*. API.

Ashour, M. and Helal, A. (2014). Contribution of vertical skin friction to the lateral resistance of large-diameter shafts. *Journal of Bridge Engineering*, 19(2):289–302.

Bhushan, K. and Scheyhing, C. (2002). Lateral load tests on drilled piers in San

Diego area residual and formational soils. In *Proceedings 27th annual conference on deep foundations, San Diego, CA*.

Brown, D. A., Turner, J. P., Castelli, R. J., and Americas, P. (2010). Drilled shafts: Construction procedures and lrfd design methods. Technical Report FHWA-NHI-10-016, United States. Federal Highway Administration.

Byrne, B., McAdam, R., Burd, H., Houlsby, G., Martin, C., Zdravkovic, L., Taborda, D., Potts, D., Jardine, R., Sideri, M., et al. (2015). New design methods for large diameter piles under lateral loading for offshore wind applications. In *3rd International Symposium on Frontiers in Offshore Geotechnics (ISFOG 2015), Oslo, Norway, June*, pages 10–12.

Caltrans (2019). *Caltrans geotechnical manual*.

Finn, W. L. and Dowling, J. (2015). Modelling effects of pile diameter. *Canadian Geotechnical Journal*, 53(1):173–178.

Georgiadis, M. (1983). Development of py curves for layered soils. In *Geotechnical practice in offshore engineering*, pages 536–545. ASCE.

Isenhower, W. M., Wang, S.-T., and Vasquez, L. G. (2017). *User's manual for LPile 2018*. Ensoft, Austin, TX.

Matlock, H. (1970). Correlations for design of laterally loaded piles in soft clay. *Offshore technology in civil engineering's hall of fame papers from the early years*, pages 77–94.

McClelland, B. and Focht, J. (1956). Soil modulus for laterally loaded piles. *Journal of the Soil Mechanics and Foundations division*, 82(4):1081–1.

McVay, M. and Niraula, L. (2004). Development of PY curves for large diameter piles/drilled shafts in limestone for FBPIER. Technical Report Final Report, University of Florida.

O'Neill, M. and Gazioglu, S. (1984). Integrated formulation of py relationships in clays. *A Report to the American Petroleum Institute, Report PRAC-82-41-2, University of Houston*.

Reese, L. and Nyman, K. (1978). Field load tests of instrumented drilled shafts at Islamorada, Florida. *Report to the Girdler Foundation and Exploration Corporation, Clearwater, FL, February*.

Reese, L. C., Cox, W. R., and Koop, F. D. (1974). Analysis of laterally loaded piles in sand. *Offshore technology in civil engineering hall of fame papers from the early years*, pages 95–105.

Reese, L. C., Wang, S. T., Isenhower, W. M., Arrellaga, J. A., and Hendrix, J. (2000). A program for the analysis of piles and drilled shafts under lateral loads. *Ensoft, Inc., Austin, TX*.

Rinne, E., Thompson, J., and Vanderpool, W. (1996). *I-15/US 95 load test program, Las Vegas, Nevada*. Kleinfelder, Inc., Las Vegas, Nevada.

Welch, R. C. and Reese, L. C. (1972). Laterally loaded behavior of drilled shafts. Research Report 3-5-65-89, Center for Highway Research, The University of Texas at Austin.

Wilson, E. L. (2016). CSI analysis reference manual for SAP2000, ETABS, SAFE and CSIBridge. *Berkeley: Computer & Structures Inc*.

Wu, G. (2006). VERSAT-P3D: A computer program for dynamic 3-dimensional finite

element analysis of single piles and pile groups. *Wutec Geotechnical International, Vancouver, Canada*.

Zafir, Z. and Vanderpool, W. (1998). Lateral response of large diameter drilled shafts: I-15/US 95 load test program. In *Proc., 33rd Engineering Geology and Geotechnical Engineering Symp*, pages 161–176.

CHAPTER 3

EVALUATION OF EXISTING *T-Z* MODELS FOR CALICHE BASED ON NUMERICAL ANALYSIS OF BI-DIRECTIONAL LOAD TESTS USING NVSHAFT

Abstract

The difficulty in material characterization and the erratic response of cemented soil layers, such as caliche in the Las Vegas valley, creates challenges for practicing engineers to reliably predict the response of deep foundations. The focus of this paper is the numerical prediction of axial response in drilled shaft foundations, which are commonly used in infrastructure projects (i.e., bridges and tall buildings) in Las Vegas, NV. The prevalence of hard caliche layers with variation in the degree of cementation add to the complication in numerical modeling. In this study, the applicability of two existing *t-z* models, developed for Florida limestone and soft rock, was evaluated based on numerical simulations of three bi-directional load tests conducted at caliche-dominant sites. The corresponding top-down load tests were also simulated for further assessment. A MATLAB-based finite-difference program, NVShaft, has been used to implement the mentioned *t-z* models in axial load analysis. Complexity originating from drilled shaft construction and the interaction with caliche during one axial load test resulted in a stiffer predicted response compared to measure data. For the other two load tests, both *t-z* models produced comparable load-displacement responses. It was observed that the *t-z* model for Florida limestone predicted relatively stiffer responses and higher drilled shaft capacity.

3.1 Introduction

Numerical simulation of axial load-deformation response of deep foundations, known as *t-z* method is often used as a simplified design tool. In this method, the interactive soil-shaft response under axial loading is characterized through linear or nonlinear *t-z* (i.e., side resistance) and *q-z* (i.e., end bearing) models. The *t-z* analysis can be performed using commercially available programs such as TZ-PILE (Ensoft, 2014). Although the method offers a simple solution to perform trial design, Brown et al. (2010) advised to rely on multiple field load tests to verify the numerical predictions, as the derived load transfer (i.e., *t-z* and *q-z*) curves often fail to capture sensitive parameters relating to construction technique and subsurface materials. To address this issue, Stanton et al. (2015) implemented a semi-empirical procedure to calculate load transfer models in the computer program CGI-DFSAP and reported improved accuracy in numerical *t-z* prediction.

Caliche is a rock-like, calcium carbonate cemented material (Werle and Luke, 2007) typically classified as an Intermediate Geomaterial (IGM) for engineering purposes (Brown et al., 2010; Motamed et al., 2016). Caliche is known to exist intermittently as discontinuous lenses across the Las Vegas valley, which poses significant challenges in site characterization. The unconfined compressive strength (q_u) of caliche may vary between 3,000 psi to 10,000 psi (Cibor, 1983; Saint-Pierre, 2018). There have been reports of sudden changes in cementation of caliche within very small depth (Rinne et al., 1996). Performing axial load tests (conventional top-down and bi-directional) on drilled shafts embedded in cemented soils introduces additional complexity for design consideration. Karakouzian et al. (2015) observed monolithic behavior at the interface between the concrete of a drilled shaft and the encompassing caliche layer. This monolithic behavior failed to result in minimal

displacement (about 0.2-0.3 inches) required to mobilize ultimate skin friction during axial load testing (Karakouzian et al., 2015). In a recent study, Afsharhasani et al. (2020) investigated the effect of the proximity of bi-directional cell relative to the caliche layer. The study concluded that placing bi-directional cells near the most competent caliche layer ensured adequate mobilization of material which produced reliable shaft resistance.

The focus of this paper is to evaluate two existing *t-z* models developed for Florida Limestone (McVay and Niraula, 2004) and weak rock (Asem and Gardoni, 2019), to simulate side resistance of caliche in numerical *t-z* analysis. A MATLAB-based finite-difference program, NVShaft is implemented to simulate axial load tests in caliche dominant soils throughout Las Vegas. Unlike most available finite-difference *t-z* analysis programs, NVShaft allows the users to specify the location of applied axial load and enables one to simulate both conventional top-loaded and bi-directional static load tests. NVShaft's capability to produce reliable axial load response is highlighted by producing identical outputs, by analyzing an example problem from the TZ-PILE user manual. Two bi-directional load tests from the I-15/US 95 reconstruction project (Rinne et al., 1996) and a bi-directional test from the Las Vegas City Center project (LOADTEST, 2005) were used in developing the finite-difference model. The predicted responses from NVShaft analyses were compared with their respective measured shaft responses to assess the applicability of the mentioned *t-z* models, for both static top-down and bi-directional load test simulations. The top-down axial responses obtained from NVShaft predictions were compared against calculated equivalent top load-settlement curves. The relative locations of the bi-directional cells along the shaft length were taken into consideration following recommendations by Afsharhasani et al. (2020) to interpret the results.

3.2 Numerical Axial Load Analysis in NVShaft

NVShaft is a MATLAB based, finite-difference program currently under development at University of Nevada, Reno. The program was originally developed as part of an NDOT funded research project to improve numerical lateral load analysis in Nevada's local soil condition (Bhuiyan et al., 2020). The capabilities of NVShaft have been extended to perform numerical axial load (t-z) analysis, where the drilled shaft is modeled as a linear elastic and perfectly plastic axially loaded beam similar to other commercial programs such as RSPile (Rocscience, 2018). The complex soil-shaft interaction is simplied by replacing the encompassing soil with a series of t-z springs along the length of the shaft, to characterize side resistance and a q-z spring at shaft tip location, to characterize end bearing (Mosher and Dawkins, 2000). The numerical representation of side resistance and end bearing resistance mobilization in axially loaded drilled shafts for conventional top-down and bi-directional static tests for a given applied load Q_a is shown in Fig. 3.1. In a bi-directional static load test, the axial load is applied via bi-directional cell. The cell assembly is embedded within the shaft concrete, typically at a depth intended to achieve equal mobilization above and below the cell (Brown et al., 2010). To obtain the axial load response, the following differential equation can be solved using a finite-difference approach (Rocscience, 2018),

$$-EI\frac{d^2z}{dx^2} + tC = 0 \tag{3.1}$$

where, E = elastic modulus of shaft section, A = shaft cross-sectional area at depth x, z = vertical shaft movement at depth x, t = soil side resistance at depth x, and C = circumference of shaft segment at depth x. The mobilized axial force (Q) in

the shaft at depth x due to axial deformation is given by,

$$Q(x) = -EI\frac{dz}{dx} \tag{3.2}$$

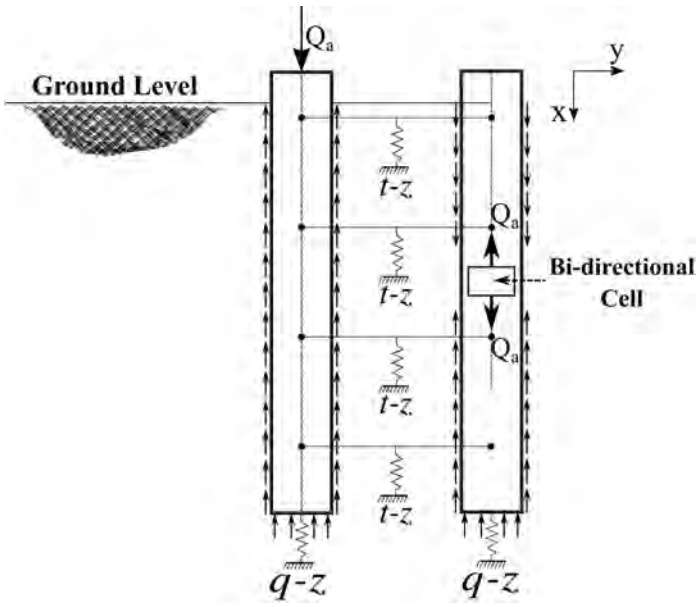

Figure 3.1: Numerical load transfer mechanism for axially loaded drilled shaft for conventional top-down and bi-directional static load test.

While performing numerical *t-z* analysis, NVShaft solves Eq. 3.1 by implementing relevant boundary conditions depending on the type of axial load test simulation. For a top-down static load test, the boundary condition is the applied load at the shaft head, and end bearing resistance at the shaft tip obtained from *q-z* model. Shaft tip displacement can be also be specified as a boundary condition instead of applied load. To simulate bi-directional static load test, the user can specify the location of the applied axial load (i.e., bi-directional cell), which is used as an internal boundary condition in the finite-difference domain. Zero axial load at the shaft head and end bearing resistance at the shaft tip are also applied as boundary conditions in this case. Using Eq. 3.2, NVShaft computes mobilized axial load along shaft length. Users can select suitable *t-z* and *q-z* curves from the

NVShaft library to model side resistance and end bearing resistance for different material types. A summary of such available models included in NVShaft to date is shown in Table 3.1. Users can also specify their *t*-*z* and *q*-*z* models as user-defined inputs.

Table 3.1: Summary of *t*-*z* and *q*-*z* models included in NVShaft.

Material Type	Model Name	Author	Model Type
Sand	API Sand	API (2014)	*t*-*z* and *q*-*z*
	Mosher Sand	Mosher (1984)	*t*-*z* and *q*-*z*
Clay	API Clay	API (2014)	*t*-*z* and *q*-*z*
	Coyle Reese Clay	Coyle and Reese (1966)	*t*-*z* and *q*-*z*
Rock	Florida Limestone	McVay and Niraula (2004)	*t*-*z*
	Soft Rock	Asem and Gardoni (2019)	*t*-*z*

The capability of NVShaft to produce reasonable outputs after performing numerical *t*-*z* analysis was verified by comparing the outputs generated from TZ-PILE analysis. Example problem 1 from the TZ-PILE user manual (Ensoft, 2014) describes a 131.2 ft (40 m) long open-ended steel pipe pile with an outside diameter of 3.3 ft (1 m) with wall thickness of 0.8 in (20 mm). Other relevant input parameters such as the *t*-*z* models at the top and bottom of the steel pile and the *q*-*z* model at the tip location can be obtained from the example description. The NVShaft and TZ-PILE predicted mobilized axial load profiles for three different levels of tip displacement; and a load-settlement comparison plot up to 1.2 inches (30 mm) of maximum tip displacement is shown in Fig. 3.2. A good match between NVShaft and TZ-PILE generated axial load response can be observed. Relative to TZ-PILE response, NVShaft predicted shaft head settlement resulted in a maximum of 2.88% deviation. Similar observations were made based on a series of additional examples.

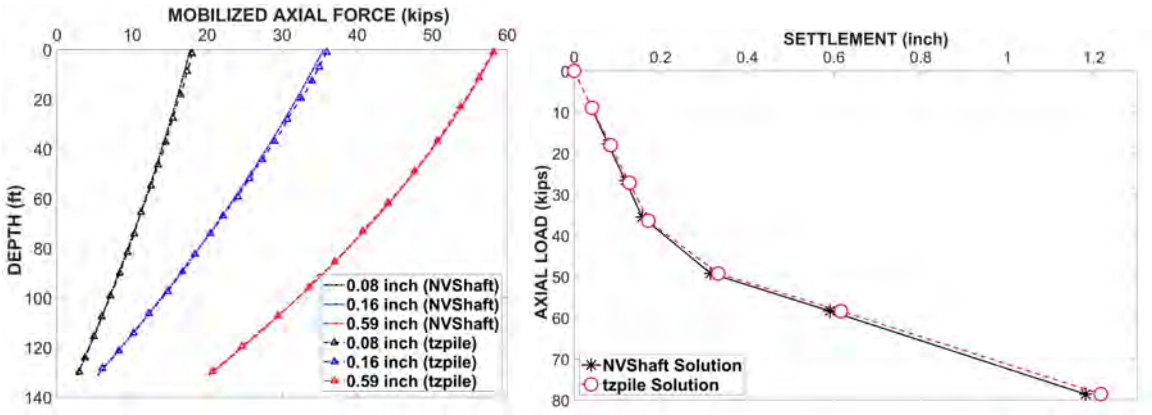

(a) (b)

Figure 3.2: Comparison between NVShaft and TZ-PILE predicted responses for verification: mobilized axial force profiles at specified shaft tip displacements (left) and load-settlement plot (right).

3.3 Modeling Side Resistance of Caliche

Numerical modeling of bi-directional static load tests in cemented soil was attempted in NVShaft, to evaluate the capability of two existing *t-z* models to represent side resistance of caliche dominant soils. Looking at the soil exploration reports of the considered load test programs, limited information was obtained from the caliche deposits. This makes the characterization of caliche in numerical models challenging. In many cases, the SPT-N values are inconclusive and also represent the surrounding weak soil material due to small thickness. As the sampling of caliche is difficult, obtaining laboratory-measured q_u at multiple depths is often not possible.

Based on laboratory shear wave velocity measurements and unconfined compressive strength tests, Saint-Pierre (2018) proposed the following empirical formula for caliche,

$$q_u = 4 * 10^{-9} * V_s^{3.0724} \tag{3.3}$$

where, q_u is in units of psi. V_s is the shear wave velocity and is in units of ft/s. In the same study, empirical correlations between shear wave velocity, unit weight, and Young's Modulus were also proposed. These relationships, if properly utilized, can make reasonable estimates of the strength and deformation properties of caliche. The obtained material properties of caliche were implemented to generate two existing *t-z* models of rock material in numerical simulations. A brief description of these models is discussed below.

3.3.1 Side Resistance (*t-z*) Model for Florida Limestone

A *t-z* model for Florida limestone was formulated based on multiple instrumented axial centrifuge tests, all performed on 6 ft (1.83 m) diameter shafts with 18 ft (5.5m) of embedment depth (McVay and Niraula, 2004). The test shafts were founded in synthetic limestone with unconfined compressive strengths of 20 ksf, 40 ksf, and 80 ksf. The obtained side resistance (t) was normalized with ultimate side resistance (t_u) and the displacement (u) was normalized with shaft diameter (D). The following *t-z* model for Florida limestone was developed based on the normalized measured centrifuge data,

$$\frac{t}{t_u} = 0.96 * R^{0.33}, \quad 0 \leq R \leq 0.5 \tag{3.4}$$

$$\frac{t}{t_u} = 0.86 * R^{0.16}, \quad 0.5 < R \leq 3.0 \tag{3.5}$$

$$\frac{t}{t_u} = 1.0, \quad R > 3.0 \tag{3.6}$$

Where, $R = z/D * 100$. The ultimate side resistance can be approximated based on the FDOT design equation given in McVay et al. (1992).

3.3.2 Side Resistance (*t-z*) Model for Soft Rock

A *t-z* model for drilled shafts socketed in soft rock material was proposed by Asem and Gardoni (2019). The parameters affecting the side resistance mobilization (i.e., initial shear stiffness, peak side resistance) were identified based on an axial load test database. An empirical framework was developed based on the compiled database to obtain necessary rock mass engineering properties to develop the *t-z* model. Following the approach taken by Duncan and Chang (1970), Gupta (2012), and others, the following hyperbolic equation was proposed up to the mobilization of peak side resistance,

$$t = \frac{z}{1/K_{si} + z * R_f/t_{sp}} \tag{3.7}$$

where, K_{si} = initial shear stiffness, R_f = Fitting Ratio and t_{sp}= peak side resistance. Based on the assumption that the side resistance of soft rock decreases with post-peak displacement, the latter part of the proposed model is defined by introducing a brittleness index (I_B), which is used to obtain the reduction in side resistance at the post-peak displacement of 0.59 inch (15 mm). Based on the observation made by Saint-Pierre (2018), for caliche, I_B may range between 0.67 to 0.89. The proposed *t-z* model is formulated based on rock material properties such as mass rock modulus

(E_m), geologicial strengh index (GSI), material constant (m_i) and drained rock mass friction angle (ϕ_m). For carbonate rock sediments, the m_i ranges between 8 to 12 (Brown et al., 2010). Due to this small variation, the m_i for caliche was assumed to be 10 to calculate the soft rock *t-z* model in all the load test simulations discussed in this paper.

3.4 Details of Axial Load Tests in Caliche

Two load tests from the I-15/US 95 reconstruction project (Rinne et al., 1996) and one from the Las Vegas City Center project (LOADTEST, 2005) were modeled in NVShaft. The drilled shafts from the load test programs had diameters ranging from 2 ft to 8 ft, and embedded depths ranging from 32 ft to 116.8 ft. Table 3.2 summarizes the drilled shaft properties, location of the bi-directional cells, upper and lower depths, and strengths of the caliche layers. In all the load tests, the bi-directional cells were installed below the caliche layers. The 8 ft diameter shaft from the I-15/US 95 project had bi-directional cells located right below the caliche layer. The same can be said about the 2 ft diameter shaft, which also had a caliche layer below the bi-directional cell. The details on the mentioned load test programs are briefly described below.

3.4.1 I-15/ US 95 Load Test Program

A large-scale load test program carried out as part of the I-15/US 95 interchange upgrade at Las Vegas, Nevada consisted of a total of five lateral and ten bi-directional static load tests in four different locations (Rinne et al., 1996; Bhuiyan et al., 2020).

Table 3.2: Drilled shaft configuration; location, and strength of caliche layers from the mentioned load test programs.

Load Test Program	Shaft Diameter (ft)	Shaft Embedment Depth (ft)	Depth of Bi-Directional Cell(s) (ft)	Upper and Lower Depths of Caliche Layers (ft)	Unconfined Compressive Strength of Caliche (psi)
I-15/US 95	8	32	21	13.5 - 21	9,583
	2	82.5	39.1	14 - 17	6,000
				30.5 - 37.5	6,000
				43 - 44	6,000
City Center, LV	4	116.8	60	16.5 - 19	2,354
				32.5 - 36	2,354

The responses from the axial load tests were utilized to assess the side resistance and end bearing capacity of the drilled shaft in cemented soil conditions. Site characterization comprised standard penetration tests at five boring locations and several laboratory tests. The majority of the soil profiles consisted of partially-cemented dense clayey and silty sand with some intermittent hard to very hard caliche layers. Hard cemented soil and caliche were sampled using Nx size coring equipment. Based on unconfined and triaxial compressive strength tests performed on caliche samples, the unconfined compressive strength value ranged from 4,060 psi to 10,645 psi. For both 8 ft and 2 ft diameter test shafts, strain gages were installed at seven levels from top of shafts to bi-directional cell depths.

The 8 ft diameter shaft was designed to carry a maximum of 18,000 kips of axial load. A maximum of 3,914 kips of axial load was applied in 200 psi increments, resulting in 1.351 inches of upward shaft head movement and 0.807 inches of downward bi-directional cell movement. It was concluded that the shaft failed simultaneously in side resistance and end bearing. The load was applied in two more cycles, which caused some degree of radial upward heave of soil and crack formation. At 2,228 kips of test load, the reported soil upward heave varied from

0.75 inches at shaft edge to 0.37 inches at a radial distance of 5 ft. The reported axial strain profile indicated tensile strain at the first strain gage level at 5.7 ft depth and also around the upper depth of the existing caliche layer at higher load levels. As stated by Karakouzian et al. (2015), strong bonding between the competent caliche layer and the shaft concrete often results in a monolithic response at the interface with an inadequate amount of slippage. The monolithic soil-shaft response is a possible reason for the upward movement of the ground surface in this case. As explained by Sinnreich (2012), the development of tensile strain is the indication of possible micro-fracturing of the shaft concrete material. The very stiff cemented soil or caliche may have restricted the elastic compression of shaft material during the curing process. When the internal stress within the shaft concrete exceeds the tensile limit, micro-fractures are formed (Sinnreich, 2012). Crushing of concrete material resulting in the damage to the bi-directional cells was also observed (A. Bafghi, personal communication, October 24, 2019), which explains the tensile strain value near the bi-directional cells location. These special observations regarding this test shaft will be crucial in comparing the measured response with NVShaft predictions.

In the first axial load tests conducted on the 2 ft diameter shaft, a maximum of 978 kips of the axial load was applied in 200 psi pressure increments. The maximum upward movement of shaft top and downward bi-directional cell movements were 0.012 inches and 0.221 inches, respectively. The test was terminated as inadequate strength of shaft concrete was observed from the concrete cylinder strength test.

3.4.2 Las Vegas City Center Load Test Program

A bi-directional static load test conducted on a 4 ft diameter, 116.8 ft long shaft as part of the Las Vegas City Center project (LOADTEST, 2005) was considered in this study. The shaft head and tip were located 5.2 ft and 122 ft below the ground surface, respectively. Pair of strain gages were installed at three levels each, both above and below the bi-directional cell assembly. To measure elastic compression between shaft top and bi-directional cell, steel pipes along with telltales were used. Subsurface investigation at the test shaft location revealed the presence of clayey sand, gravel, sandy clay, and caliche. Two caliche layers with 2.5 ft and 3.5 ft thickness were identified above the bi-directional cell located at 60 ft. No laboratory test results regarding the caliche layers were mentioned in the available load test report, and only the SPT-N value at the bottom of the second caliche layer was reported. A maximum of 4,720 kips of axial load was applied, resulting in 0.32 inches and 1.29 inches of the upward top of and downward bottom of bi-directional cells movements, respectively. It was mentioned that the shaft movement exceeded the approximated creep limit, particularly in side resistance below the bi-directional cell. Crushing of concrete near the cell location is reported to be the possible reason. The equivalent top load-settlement curve was back-calculated, indicating 0.25 inches of shaft settlement with 0.18 inches of elastic compression corresponding to 3,350 kips of maximum axial load.

3.5 Axial Load Tests Simulations in NVShaft

The mentioned load test programs were modeled in NVShaft, to simulate both conventional top-down and bi-directional static tests through numerical *t-z* analysis.

The side resistance and end bearing of sand and clay material were generated using the API Sand and API Clay *t*-*z* and *q*-*z* models (API, 2014). The relevant soil material properties to use as input parameters were either obtained from their respective load test reports or calculated from several empirical correlations from FHWA (Brown et al., 2010) and Caltrans (2021) manual. Separate NVShaft simulations were carried out after implementing the Florida limestone (McVay and Niraula, 2004) and soft rock *t*-*z* models (Asem and Gardoni, 2019) for all the caliche layers. The empirical formula proposed by Saint-Pierre (2018), as shown in Eq. 3.3, was used to obtain the unconfined compressive strength of caliche material in cases where laboratory measured data were not available. It should be noted that using such formula adds to the uncertainty of the numerical models.

3.5.1 Numerical Predictions of I-15/ US 95 Load Test Program

The NVShaft predicted and field-measured axial load responses for both conventional top-down and bi-directional static load test simulations of 8 ft diameter shaft are presented in Fig. 3.3. The single caliche layer encountered in this particular load test was modeled using the side resistance (*t*-*z*) models given for Florida limestone (McVay and Niraula, 2004) and soft rock (Asem and Gardoni, 2019). The results of the analyses including the corresponding NVShaft predicted responses are shown in Fig. 3.3. The constructed equivalent top-down rigid curve based on field load test data, considering both scenarios of rigid and elastic compression is also presented. For both types of load test simulations, the measured field responses were significantly softer compared to the NVShaft predicted responses. This discrepancy can be attributed to the deficiency in drilled shaft construction i.e., the possibility of micro-fracturing of concrete, leading to highly nonlinear shaft stiffness (Sinnreich,

2012). The severe monolithic soil-shaft response due to the strong bonding between caliche and shaft concrete (Karakouzian et al., 2015) is another possible reason behind the softer response in the field. Since there was no caliche layer below the bi-directional cells assembly, identical downward movement was predicted in both bi-directional load test analyses using both *t-z* models.

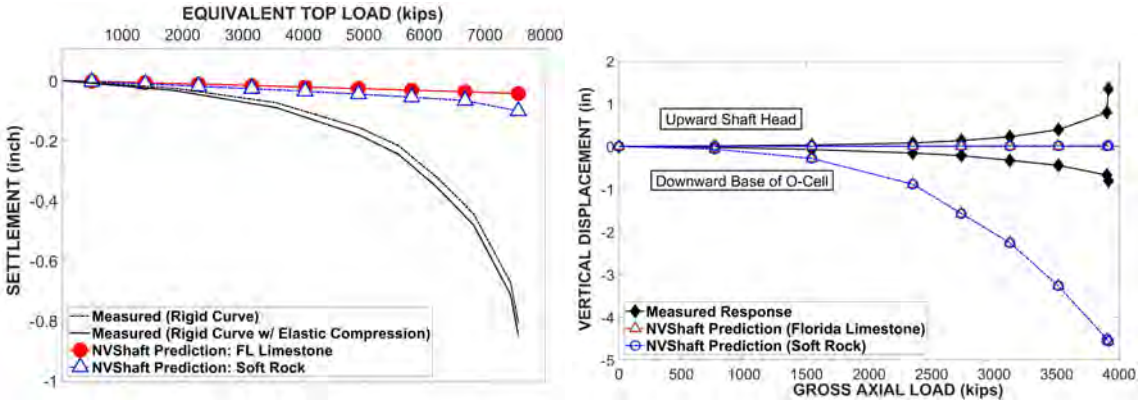

(a) (b)

Figure 3.3: NVShaft predicted responses of 8 ft diameter shaft (I-15/US 95 project) from conventional top-down (left) and bi-directional static (right) load test simulations, along with measured data.

The 2 ft diameter shaft had two caliche layers above and one below the bi-directional cell location. As shown in Fig. 3.4, using both *t-z* models resulted in fair agreements between NVShaft predicted and measured responses, in both types of load test simulations. Unlike the previous case, the presence of a caliche layer below the bi-directional cell location resulted in a difference in predicted downward movement of the shaft, when different *t-z* models were implemented in that location. As seen in Fig. 3.4, the axial load response of this particular drilled shaft up to the maximum applied axial load is really small, indicating insufficient mobilization of side resistance. Limited displacement between the shaft and surrounding caliche layer during bi-directional load tests often results in partial mobilization of side resistance (Fellenius and Ann, 2010; Karakouzian et al., 2015). These types of

outcomes from the axial load test present challenges in achieving the necessary accuracy in drilled shaft design and reducing costs of construction (Paikowsky and Tolosko, 1999). One benefit of performing *t*-*z* analysis is that higher axial loads can be assigned to the models to achieve hypothetical failure conditions. For this particular test shaft, further numerical simulations using the *t*-*z* model developed for Florida limestone predicted significantly higher axial load capacity (around 12,000 kips) compared to the *t*-*z* model for soft rock (around 3,000 kips). The *t*-*z* model for soft rock also resulted in softer axial load response in all the axial load test simulations mentioned in this study.

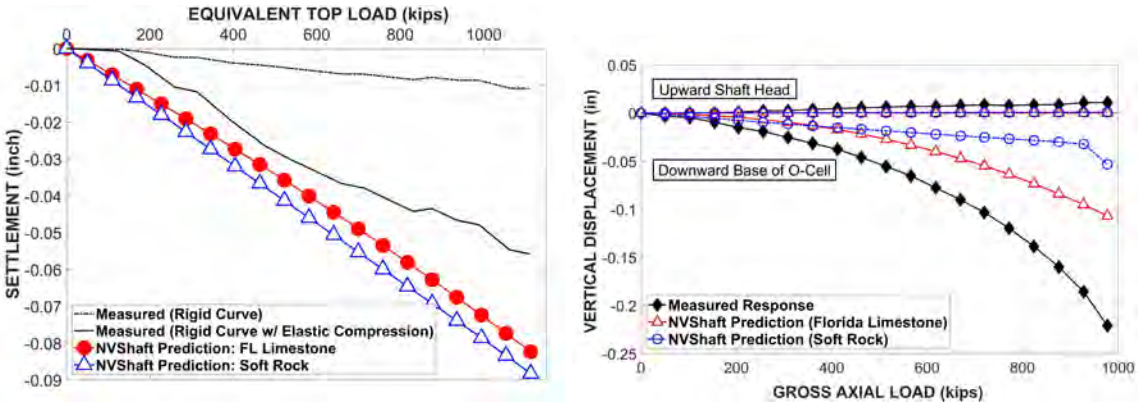

(a) (b)

Figure 3.4: NVShaft predicted responses of 2 ft diameter shaft (I-15/US 95 project) from conventional top-down (left) and bi-directional static (right) load test simulations, along with measured data.

3.5.2 Numerical Predictions of Las Vegas City Center Load Test Program

Similar to the previous two analyses, the 4 ft diameter shaft from the Las Vegas City Center project was modeled and analyzed in NVShaft. The load-displacement plots shown in Fig. 3.5, suggest reasonable agreement between the measured and

predicted responses for both of the considered *t*-*z* models. The equivalent top load-settlement curve with elastic compression based on measured bi-directional axial load response was softer, compared to the NVShaft predicted top-down load responses. As explained by Afsharhasani et al. (2020), the mobilization of side resistance in caliche is less in this case during the bi-directional test, compared to the case when the axial load is applied at the top. The bi-directional cell was installed 24 ft below the nearest caliche layer, which caused the applied load to be transferred in weaker soil layers before reaching caliche, compared to the top-down case scenario. Also, the *t*-*z* model for soft rock failed to predict the shaft response at maximum test load (4720 kips), indicating lower axial load capacity in side resistance in numerical analysis (Fig. 3.5). A comparison between measured and predicted mobilized gross axial load profiles at three different loads, along with generalized soil profile is presented in Fig. 3.6. The sharp decreases in mobilized loads can be observed at the locations of caliche layers, which contradicts the relatively gradual change in mobilize load based on measured data. The existing *t*-*z* and *q*-*z* models failed to capture the exact load transfer mechanism in both side resistance (along shaft length) and end bearing (at shaft tip) resistances in this case.

3.6 Summary and Conclusions

Two existing *t*-*z* models, formulated for Florida Limestone and weak rock, to simulate side resistance for caliche were evaluated based on numerical axial load analysis. Three bi-directional static load tests performed in caliche dominant sites from I-15/US 95 and Las Vegas City Center projects were considered. A MATLAB-based, finite-difference program, NVShaft was used to perform *t*-*z* analyses, which is capable of simulating both conventional top-down and bi-directional static load

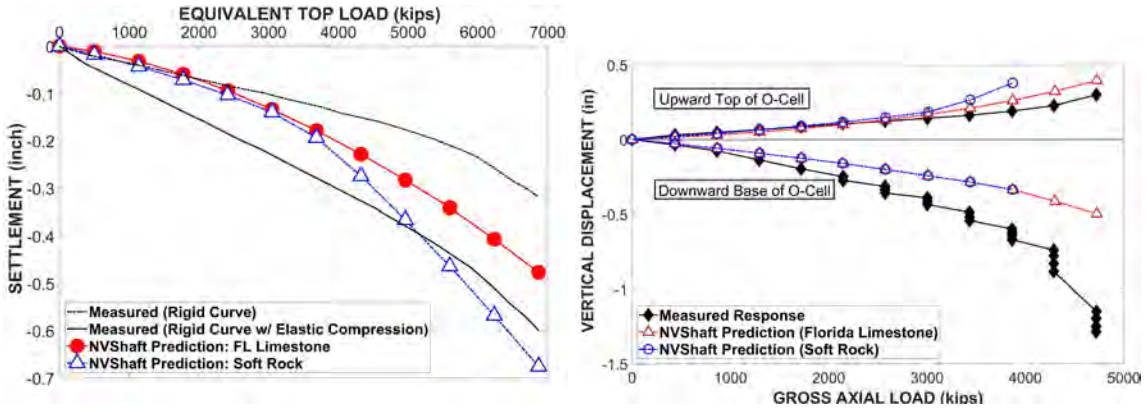

(a) (b)

Figure 3.5: NVShaft predicted responses of 4 ft diameter Shaft (Las Vegas City Center Project) from conventional top-down (left) and bi-directional static (right) load test simulations, along with measured data.

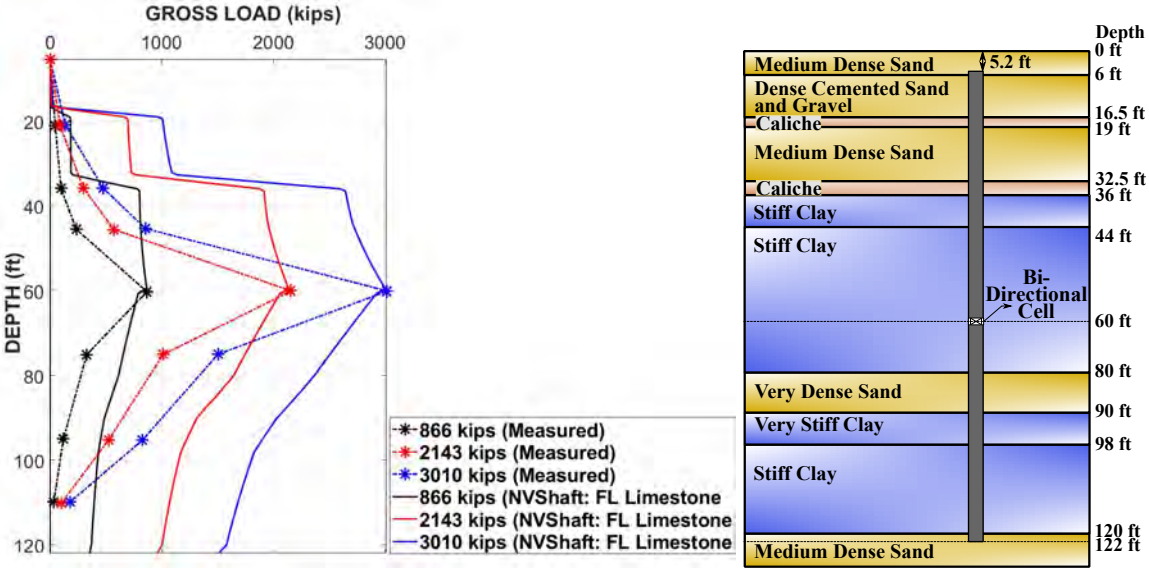

(a) (b)

Figure 3.6: Comparison between measured and predicted mobilized axial gross load at three different load levels (left) and schematics of the generalized soil profile (right) for 4 ft diameter shaft (Las Vegas City Center Project).

tests. The side resistance characteristics of the caliche layers reported from site investigations were generated using the mentioned *t-z* models.

From the I-15/US 95 project, drilled shafts with 8 ft and 2 ft diameters were

modeled. For the 8 ft diameter shaft, the deficiency in drilled shaft construction leading to the possible formation of micro-fractures in shaft concrete resulted in highly nonlinear stiffness. Upward soil heave and radial crack formation due to possible monolithic soil-shaft response were also reported. Both of these facts attribute to the softer measured axial shaft response compared to NVShaft predicted ones for the 8 ft diameter shaft. For the 2 ft diameter shaft, NVshaft analysis produced a reasonably good predicted response compared to measured data. In this case, the measured response was small at the maximum applied bi-directional load, and similar to many axial load tests conducted in caliche, the axial load capacity of the shaft was inconclusive. By exploiting NVShaft's capability to simulate response at higher axial load, it was observed that using the *t-z* model for Florida limestone resulted in higher capacity, and stiffer response compared to the *t-z* model for soft rock. A similar observation was made based on axial load test simulations of all the test shafts mentioned in this study.

A reasonable match between measured data and NVShaft predicted top-down and bi-directional static axial load response for the 4 ft diameter shaft from the Las Vegas, City Center project was obtained, after applying both *t-z* models. The equivalent top load-settlement curve obtained from measured bi-directional cell movement indicated a softer response, compared to the top-down predicted response. This observation substantiates the findings by Afsharhasani et al. (2020), and emphasize the location of bi-directional cell relative to caliche in interpreting the measured load test results.

3.7 References

Afsharhasani, R., Karakouzian, M., and Farhangi, V. (2020). Effect of competent caliche layers on measuring the capacity of axially loaded drilled shafts using the osterberg test. *Applied Sciences*, 10(18):6169.

API (2014). *API Recommended Practice 2A-WSD - Planning, Designing, and Constructing Fixed Offshore Platforms – Working Stress Design*. API.

Asem, P. and Gardoni, P. (2019). A load-transfer function for the side resistance of drilled shafts in soft rock. *Soils and Foundations*, 59(5):1241–1259.

Bhuiyan, F. M., Siddharthan, R. V., Motamed, R., and Sanders, D. H. (2020). Evaluation of a new *p-y* analysis tool for lateral analysis of drilled shafts using load tests in Nevada. In *DFI 45th Annual Conference on Deep Foundations*, pages 303–312. October 13-16.

Brown, D. A., Turner, J. P., Castelli, R. J., and Americas, P. (2010). Drilled shafts: Construction procedures and lrfd design methods. Technical Report FHWA-NHI-10-016, United States. Federal Highway Administration.

Caltrans (2021). *Caltrans geotechnical manual*.

Cibor, J. M. (1983). Geotechnical considerations of las vegas valley. In *Geological environmental and soil properties*, pages 351–373. ASCE.

Coyle, H. M. and Reese, L. C. (1966). Load transfer for axially loaded piles in clay. *Journal of the soil mechanics and foundations division*, 92(2):1–26.

Duncan, J. M. and Chang, C.-Y. (1970). Nonlinear analysis of stress and strain in soils. *Journal of the soil mechanics and foundations division*, 96(5):1629–1653.

Ensoft (2014). *Analysis of load versus settlement for an axially-loaded deep foundation*. Ensoft, Inc., Austin, TX.

Fellenius, B. H. and Ann, T. S. (2010). Combination of o-cell test and conventional head-down test. In *Art of Foundation Engineering Practice*, pages 240–259.

Gupta, R. C. (2012). Hyperbolic model for load tests on instrumented drilled shafts in intermediate geomaterials and rock. *Journal of Geotechnical and Geoenvironmental Engineering*, 138(11):1407–1414.

Karakouzian, M., Afsharhasani, R., and Kluzniak, B. (2015). Elastic analysis of drilled shaft foundations in soil profiles with intermediate caliche layers. In *IFCEE 2015*, pages 922–928.

LOADTEST (2005). Report on drilled shaft load testing (Osterberg method), City Center - test shaft 1, Las Vegas, NV. Project No. LT-9160-1, LOADTEST, Inc.

McVay, M. and Niraula, L. (2004). Development of PY curves for large diameter piles/drilled shafts in limestone for FBPIER. Technical Report Final Report, University of Florida.

McVay, M., Townsend, F., and Williams, R. (1992). Design of socketed drilled shafts in limestone. *Journal of geotechnical engineering*, 118(10):1626–1637.

Mosher, R. and Dawkins, W. (2000). Theoretical manual for pile foundations. Report No. ERDTC/ITL TR-00-5, US Army Corps of Engineers, Washington, Washington, DC.

Mosher, R. L. (1984). Load transfer criteria for numerical analysis of axially loaded piles in sand. Technical report, U. S. Army Waterways Experiment Station, Automatic Data Processing Center, Vicksburg, Mississippi.

Motamed, R., Elfass, S., Stanton, K., et al. (2016). LRFD resistance factor calibration for axially loaded drilled shafts in the las vegas valley. Technical report, Nevada. Dept. of Transportation.

Paikowsky, S. G. and Tolosko, T. A. (1999). Extrapolation of pile capacity from non-failed load tests. Publication No. FHWA-RD-99-170, U.S. Department of Transportation, Washington, DC.

Rinne, E., Thompson, J., and Vanderpool, W. (1996). *I-15/US 95 load test program, Las Vegas, Nevada*. Kleinfelder, Inc., Las Vegas, Nevada.

Rocscience (2018). *Axially loaded piles*. Rocscience, Inc., Toronto, Canada.

Saint-Pierre, E. (2018). The development of a material model for engineering behavior characteristics of cemented soils for the las vegas valley. Master's thesis, University of Nevada, Reno, Reno, Nevada.

Sinnreich, J. (2012). Strain gage analysis for nonlinear pile stiffness. *Geotechnical Testing Journal*, 35(2):367–374.

Stanton, K., Motamed, R., Elfass, S., and Ellison, K. (2015). An evaluation of tz analysis methods. In *DFI 40th Annual Conference on Deep Foundations*, pages 27–36, Oakland, CA.

Werle, J. and Luke, B. (2007). Engineering with heavily cemented soils in Las Vegas, Nevada. In *Problematic soils and rocks and in situ characterization*, pages 1–9.

CHAPTER 4

EVALUATION OF A UNIFIED *P-Y* METHOD FOR LATERAL ANALYSIS OF LARGE-DIAMETER DRILLED SHAFTS USING NVSHAFT

Abstract

Lateral load analyses of large-diameter drilled shafts based on the conventional *p-y* method tend to result in unreliable responses. The paper highlights a unified *p-y* analysis that incorporates vertical side shear-induced moment and tip resistances, which becomes significant in laterally-loaded large-diameter drilled shafts. A simplified tip moment resistance model applicable to any well-defined soil or rock material is also proposed. To perform unified *p-y* analysis, a finite-difference-based comprehensive load analysis program, NVShaft, has been developed. The lateral shaft response using NVShaft was evaluated using two field load tests from Las Vegas in cemented soil, and two field load tests in sand and clay dominant sites from the PISA project in Europe. Comparison between measured responses and numerical predictions signifies the relative importance of added resistance components in the unified *p-y* analysis in different subsurface materials. Further investigation on diameter effects in the context of mentioned load test programs indicates that additional lateral resistance in large-diameter shaft comes mostly from side shear-induced resisting moment, followed by tip shear resistance.

4.1 Introduction

For its simplicity and ease of analysis, the beam on nonlinear Winkler foundation (BNWF) model, more commonly known as the *p-y* method, is routinely used by practicing engineers to perform lateral load analysis of deep foundations. As referenced in the design codes, such as American Petroleum Institute (API, 2014) and AASHTO (2020), the *p-y* method is an efficient numerical tool to design deep foundations for lateral loading. Such analysis is typically performed using commercially available numerical programs, such as LPILE (Reese et al., 2000). In conventional *p-y* analysis, the soil-shaft interaction is modeled by a series of nonlinear *p-y* lateral resistance springs along the shaft length, which is appropriate for smaller-diameter drilled shafts (¡0.61 m). The *p-y* soil models commonly used for sand and clay materials (i.e. Matlock (1970), Reese et al. (1974), Reese and Welch (1975)) were obtained from lateral load tests conducted on smaller diameter piles, ranging from 0.32 m to around 0.61 m. However, large-diameter drilled shafts are becoming more common in both the U.S. and Europe, due to both recent advances in construction technologies, and their ability to resist seismic loads. Some of the recently installed drilled shafts supporting offshore wind turbines have a typical diameter of 6 m, and the current trend indicates the possibility of shaft diameter being 10 m or more in the near future (Byrne et al., 2015). Researchers have reported that when aforementioned *p-y* soil models are used on a laterally-loaded large-diameter drilled shafts, unreliable load-displacement responses are obtained (Bhushan and Scheyhing, 2002; McVay and Niraula, 2004; Li et al., 2017; Finn and Dowling, 2015). The limitations of conventional *p-y* analysis for considering large-diameter drilled shafts is termed "pile diameter effect." To address the issue of softer numerical prediction due to this diameter effect, Lam et al. (1998) recommended that a scaling

factor equal to the ratio of the shaft diameter to 0.61 m should be applied either to the subgrade modulus or to the *p-y* resistance values. Finn and Dowling (2015) observed significant diameter effects when lateral deflection exceeded 0.06 m for piles with diameters ranging from 0.2 m to 2 m and developed an empirical relationship between pile diameter and load level for given head deflection. Byrne et al. (2015) recommended a "Numerical-Based Design Method," where *p-y* curves and other resistance components used in a Winkler beam model are calibrated based on in-depth FE analysis and field load tests. The diameter effect in large-diameter drilled shafts arises mainly due to the following two factors: 1) *p-y* lateral resistance models fail to characterize soil-shaft interaction properly during lateral loading; and 2) conventional Winker's *p-y* spring model ignores the contribution of other load transfer mechanisms. A drilled shaft subjected to both axial and lateral loading develops the following lateral resistance components, as identified by Vallabhan and Alikhanlou (1982), Lam and Martin (1986), Ashour and Helal (2014) and others: lateral soil resistance (p), side shear due to vertical settlement (t), resisting moment due to side shear generating from shaft rotation (m_r), end bearing resistance at tip (q), tip shear resistance (v_b), and tip moment resistance (m_b). Some of these resisting mechanisms become more significant for drilled shafts with larger diameters. Representation of different soil lateral resistance components mobilized in large-diameter drilled shafts are shown in Fig 4.1. Proper understanding and formulation of soil-structure interaction during both static and dynamic lateral loading is a major challenge in any form of numerical analysis and has been addressed many times in past research (Nogami et al., 1992; Ashour and Norris, 2000; Lin et al., 2015; Kavand and Yazdi, 2019). As soil characterization (e.g., choice of soil subgrade reaction) is also a crucial part of accurately modeling soil-structure interaction during lateral loading, many site-specific *p-y* models have been proposed recently. For example, Li and Yang

(2017) developed the *p-y* model for frozen silt, which produces 50 to 170 times the amount of soil resistance given for sand by Reese et al. (1974). Lin et al. (2015) examined soil-pile interaction by performing a lateral load test on a hollow steel pile instrumented with advanced sensors and formulated a *p-y* relationship based on measured lateral resistance and displacement at various depths.

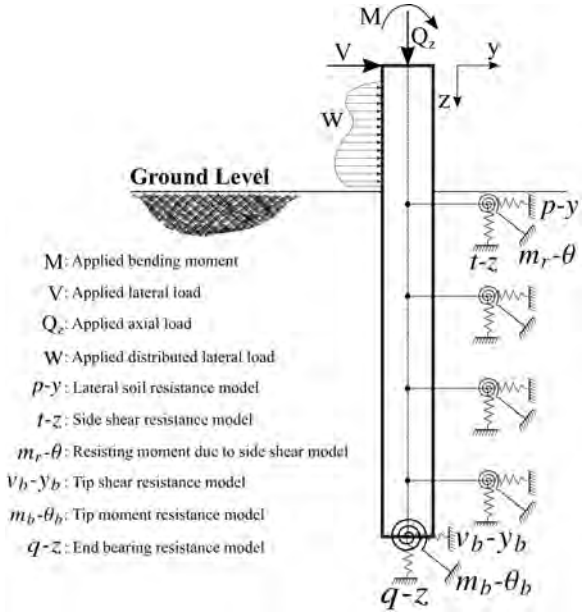

Figure 4.1: Numerical Winkler's spring models of major lateral resistance components in large-diameter drilled shaft.

The focus of this paper is the improvement of numerical lateral load analysis by incorporating additional major lateral resistance components, such as resisting moment due to side shear (m_r) as well as tip shear (v_b) and tip moment resistance (m_b). These lateral resistances are typically absent in conventional *p-y* analysis, resulting in conservative responses for large-diameter drilled shafts. The inclusion of side shear resistance to numerical lateral analysis has been addressed in past research by Ashour and Helal (2014) and Taghavi et al. (2020). Taghavi et al. (2020) proposed an improved, robust procedure to calculate m_r from mobilized side shear due to shaft rotation using the *t-z* model defined at particular depth. In this way,

the axial soil-shaft response can be "coupled" to the lateral load analysis (Taghavi et al., 2020).

This paper builds on the past approaches that include side shear resistance in the form of a modified *p-y* equation for circular shaft, and it is implemented using the finite-difference formulation. The modified equation enables consideration of the non-uniform variation of side shear, resulting from shaft rotation. The applicability of two existing tip shear resistance models in numerical analysis, given by Vallabhan and Alikhanlou (1982) (for soil) and McVay et al. (2008) (for rock) is discussed. A simplified tip moment resistance model for circular shaft is proposed in this study. The improved *p-y* method with all relevant major lateral resistance components is introduced as "unified *p-y* method" in this paper. In order to perform such a unified *p-y* analysis, a MATLAB-based, finite-difference program, NVShaft, has been developed. Two well-characterized load test programs were carefully selected to evaluate the proposed unified *p-y* method using NVShaft. The selected load test programs are: 1) Las Vegas load test program (Rinne et al., 1996) and 2) Pile Soil Analysis (PISA) load test program (Byrne et al., 2015). Two load tests conducted on 0.61 m and 2.44 m diameter drilled shafts in Las Vegas were chosen to study the diameter effect, considering the local cementitious soil conditions in Nevada. Two, 2 m diameter steel piles from the PISA project provide the opportunity to study diameter effects in sandy and clayey site conditions. The rigid shaft-like responses from the PISA project demand consideration of pile tip resistance components in the lateral load tests. Finally, a parametric study to investigate the role of various modifications in the conventional *p-y* approach as a function of increasing shaft diameters was carried out, considering the different site conditions from the mentioned load test programs.

4.2 Introduction to NVShaft and Unified p-y Analysis

NVShaft is a MATLAB-based finite difference program currently under development at the University of Nevada, Reno. The program can perform a comprehensive lateral and axial load analysis for a single deep foundation by employing *p-y* and *t-z* soil resistance characterization. The program provides versatile options to users modeling different soil resistance components and varying soil layering and shaft section properties. In the case of a shaft embedded in a layered soil profile, NVShaft allows the users to perform layering correction, as proposed by Georgiadis (1983). Multiple shaft section properties can be specified in a single analysis, including tapered and nonlinear shaft sections characterized by user-defined moment-curvature curves. Users can perform *p-y* analysis under loading and nodal constraints at the shaft head and can specify tip shear and moment as boundary conditions at the shaft bottom. To date, a total of 19 *p-y* models have been included in the program's library. This includes some recently developed *p-y* models, such as those for weakly-cemented sand (Juirnarongrit and Ashford, 2004), marine clay (Jeong et al., 2011), and Florida Limestone (McVay and Niraula, 2004). NVShaft has several API (2014) recommended *t-z* and *q-z* models for sand and clay, to be used with the unified *p-y* analysis. Additional functionalities include the use of p-multipliers; the flexibility to specify the location of applied lateral load; the option to perform *t-z* analysis prior to *p-y* analysis; the calculation of critical shaft length for lateral stability; the ability to perform buckling analysis of shaft-column; calculation of shaft-head stiffness matrix and the calculation of shaft depth to fixity. The features included in NVShaft were verified by comparing computed responses against those generated by commercially-available programs, whenever modeling parameters were the same (Bhuiyan et al., 2020, 2021).

4.2.1 Mobilization of Side Shear in *p-y* Analysis

Mobilization of side shear resistance plays a vital role when a large-diameter drilled shaft is subjected to lateral loading (Vallabhan and Alikhanlou, 1982; Ashour and Helal, 2014; Taghavi et al., 2020). In the past, drilled shafts had smaller diameters in civil engineering applications, and the contribution of side shear was considered insignificant in performing *p-y* analysis. As shown in Fig. 4.2, rotation of a drilled shaft section laterally loaded from left to right would result in incremental vertical displacements on both sides. Assuming the drilled shaft to have axial load applied at the top prior to the lateral load, one would routinely perform an axial load (*t-z*) analysis before performing *p-y* analysis. After obtaining the vertical displacement profile from the *t-z* analysis, we can account for the incremental vertical displacement during the lateral load analysis. The resulting incremental side shear would generate resisting moment both on passive (m_{rp}) and active side (m_{ra}) as shown in Fig. 4.2.

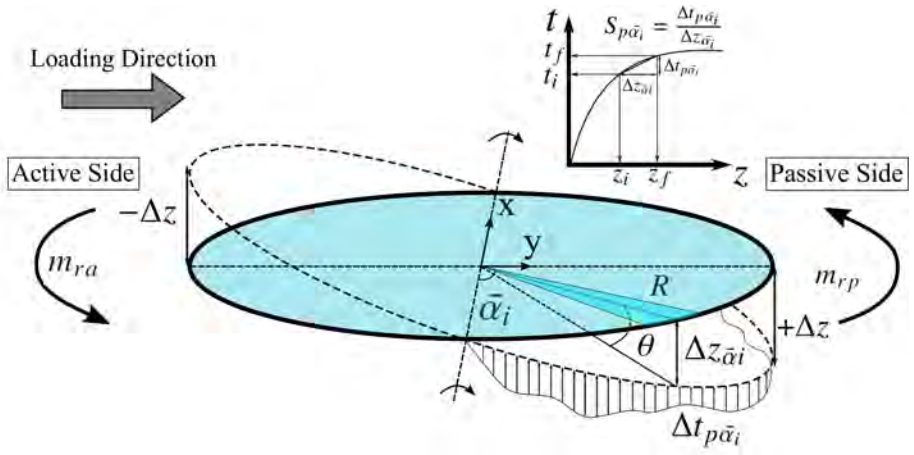

Figure 4.2: Mobilization of incremental side shear ($\Delta t_{\bar{\alpha}_i}$) and resisting moment components per unit length (m_r) due to rotation of a drilled shaft section.

One can divide the quarter of the whole shaft section (considering symmetry) into n radial slices (Taghavi et al., 2020). The incremental vertical displacement due

to shaft rotation at the mid-circumference of the i^{th} slice, where the radius (R) makes the angle $\bar{\alpha}_i$ from the axis of rotation, is given by the following equation,

$$\Delta z_{\bar{\alpha}_i} = (R \sin \bar{\alpha}_i) \frac{dy}{dz} \tag{4.1}$$

where $\frac{dy}{dz}$ can be approximated as the shaft rotation (Taghavi et al., 2020). On the passive side, the incremental vertical shear resistance ($\Delta t_{p\bar{\alpha}_i}$) obtained from the relevant t-z curve can be used in the following equation to calculate the resisting moment per unit shaft length, considering both quarters of the shaft section,

$$m_{rp} = 2R^2 \int_0^{\pi/2} \Delta t_{p\bar{\alpha}_i} \sin \bar{\alpha}_i d\alpha_i \tag{4.2}$$

We can calculate the secant slope of the t-z curve on the passive side ($S_{p\bar{\alpha}_i}$) as shown in Fig. 4.2 to obtain the following equation, incorporating Eq. 4.1,

$$m_{rp} = 2R^3 \frac{dy}{dz} \int_0^{\pi/2} S_{p\bar{\alpha}_i} \sin^2 \bar{\alpha}_i d\alpha_i = 2R^3 C_{mp} \frac{dy}{dz} \tag{4.3}$$

where $C_{mp} = \int_0^{\pi/2} S_{p\bar{\alpha}_i} \sin^2 \bar{\alpha}_i d\alpha_i$. Considering the secant slope of the t-z curve on the active side ($S_{a\bar{\alpha}_i}$), we can assume $C_{ma} = \int_0^{\pi/2} S_{a\bar{\alpha}_i} \sin^2 \bar{\alpha}_i d\alpha_i$, and obtain a similar equation for m_{ra}. The total resisting moment due to side shear can be calculated using the equation, for a given shaft diameter D,

$$m_r = m_{rp} + m_{ra} = \frac{D^3}{4}(C_{ma} + C_{mp}) \frac{dy}{dz} \tag{4.4}$$

During numerical analysis, NVShaft performs trapezoidal integration to calculate m_{rp} (and similarly, m_{ra}) using Eq. 4.2. For a given shaft rotation, both C_{mp} and

C_{ma} can then be calculated. If we consider m_r in the formulation of *p-y* equation, when the axial load term is included, the equation is similar to that proposed by Ashour and Helal (2014),

$$EI\frac{d^4y}{dz^4} + Q_z\frac{d^2y}{dz^2} - \frac{dm_r}{dz} - p - w = 0 \tag{4.5}$$

where E = Elastic section modulus of drilled shaft, I = moment of inertia, Q_z = axial load in the shaft, p = lateral soil reaction, and w = additional applied distributed lateral load (if any). The value of the term $\frac{dm_r}{dz}$ is negligible for smaller-diameter drilled shafts, but becomes more prominent in the case of larger-diameter shafts, especially when embedded in stiff soil or rock (Taghavi et al., 2020). Considering both Eq. 4.4 and Eq. 4.5, we get the modified *p-y* equation for circular shaft section,

$$EI\frac{d^4y}{dz^4} + Q_z\frac{d^2y}{dz^2} - \frac{D^3}{4}(C_{ma} + C_{mp})\frac{d^2y}{dz^2} - p - w = 0 \tag{4.6}$$

The solution for the shear force along the shaft length is given by,

$$V = EI\frac{d^3y}{dz^3} + \left\{Q_z - \frac{D^3}{4}(C_{ma} + C_{mp})\right\}\frac{dy}{dz} \tag{4.7}$$

In a previous study, considering the strain wedge (SW) model, Ashour and Helal (2014) assumed that side shear is mobilized only on the passive (i.e., loading) side, reaching maximum values at the extremities in the loading direction, and the minimum value of zero in the perpendicular direction (Bierschwale et al., 1981). Taghavi et al. (2020) developed m_r-θ curves based on finite-element models. In NVShaft, a finite-difference approach is used, enabling a more simplified analysis. The m_r is calculated internally along the shaft length as a function of user-specified

t-z curves. The variation of incremental side shear around the shaft circumference depends on the selected *t-z* model, and it may have non-uniform distribution. In general, the program uses Eq. 4.7 to check for the tolerance of specified shear force as the boundary condition and solves Eq. 4.6 in the process.

4.2.2 Tip Shear Resistance Models

In conventional *p-y* analysis, two of the four required boundary conditions are often specified as zero shear and moment at shaft tip location (Fig. 4.1). This assumption is reasonable for flexible shaft response, when the displacement at tip location is negligible (Reese and Van Impe, 2011). However, lateral field load tests conducted on rigid, short-drilled shafts in many cases result in a significant amount of tip displacement (y_b) (Zhu et al., 2015; Gupta and Basu, 2016; Byrne et al., 2020; McAdam et al., 2020). In homogeneous soil conditions, Woodward et al. (1972) defined rigid shaft as $L/T \leq 2$, where L = shaft length, T = relative stiffness factor $= \sqrt[4]{EI/\bar{k}}$, and $\bar{k}$ = average coefficient of subgrade reaction of soil. Such cases require that tip shear resistance (v_b) be included in *p-y* analysis. Vallabhan and Alikhanlou (1982) proposed a simple elastic, perfectly plastic v_b-y_b model, where the mobilized ultimate tip shear resistance can be calculated based on the Mohr-Coulomb criterion as,

$$v_{b,max} = c_{ub} + \frac{Q_b}{A_b} \tan \phi_b \tag{4.8}$$

where c_{ub} = cohesion, ϕ_b = angle of friction of soil at shaft tip, Q_b = axial load at shaft tip, and A_b = area of shaft tip cross-section. As in the case of Vallabhan and Alikhanlou (1982), it is assumed that v_b can be estimated based on linear

relationship up to y_b of 3.05 mm, just before $v_{b,max}$ is mobilized. Vallabhan and Alikhanlou (1982) implemented their model in the analyses of a 1.2 m diameter, 4.6 m long straight pier, and observed a significant increase in lateral resistance compared to conventional *p-y* analysis. A similar study was conducted by Li et al. (2017), where the mobilized v_b versus y_b relationship was obtained based on load tests on reduced-scale rigid shafts embedded in overconsolidated sand. The derived v_b-y_b model, when implemented and compared with the conventional p-y analysis (i.e., no tip shear), showed significant differences in shaft response. Recently, Fuentes et al. (2020) proposed a simple, but robust, v_b-y_b model for sand based on Mohr-Coulomb's theory. The model was formulated particularly for monoshafts supporting offshore wind turbines with certain geometric ranges of diameter and embedded length.

In NVShaft, the v_b-y_b model by Vallabhan and Alikhanlou (1982) has been included for its simplicity and can be used for the analysis of shafts with tips located in the soil. As for rock, a somewhat similar v_b-y_b model by McVay et al. (2008) can be used, which requires rock strength as an additional input parameter. The applications of both models have been illustrated in this study, with accompanying field load test simulations using NVShaft.

4.2.3 Simplified Tip Moment Resistance Model

Similar to tip shear resistance, rigid shafts with larger diameters embedded in stiffer soil or rock may also experience significant tip moment resistance (m_b) as a function of shaft tip rotation (θ_b). Applying an m_b-θ_b model as a boundary condition in p-y analysis ensures a more realistic and acceptable representation of soil-shaft

interaction. In the studies mentioned above, Vallabhan and Alikhanlou (1982) and McVay et al. (2008) also proposed m_b-θ_b models. The m_b-θ_b model by Vallabhan and Alikhanlou (1982) is based on an influence factor, I_m equal to 6.0, and is independent of shaft end bearing resistance. Based on centrifuge test results, McVay et al. (2008) suggested a more elaborate m_b-θ_b model for Florida Limestone using the stiffness relationship originally developed by Bell (1991). The model relies on a stiffness matrix to correlate m_b with an assigned v_b-y_b relationship, and it may require multiple numerical analyses if specified tolerance is not met.

A new robust m_b-θ_b model has been proposed in this study for use in any foundation soil. The model features two main input parameters: ultimate bearing stress (q_{ult}) and coefficient of subgrade reaction (k_v). The model, originally proposed by Siddharthan et al. (1992) for a simple rectangular strip foundation resting on Winkler's springs, was modified for a circular drilled shaft section. It is assumed that the rotation θ_b causes a linear variation in vertical deformation at the tip. Considering m_b to be positive in the clockwise direction, the bearing stress will be maximum (q_{max}) in the right and minimum (q_{min}) in the left extremities of the shaft cross-section. At some high value of θ_b, q_{min} can become zero, indicating lift-off condition. On the other hand, yielding may take place when q_{max} equals to or exceeds the q_{ult} of the soil layer, as shown in Fig. 4.3a. As discussed in Siddharthan et al. (1992), both special conditions need to be considered in the m_b-θ_b model. In lift-off condition, a portion of the shaft tip interface losing contact with soil material adds complexity and negates the simplified use of Winkler's spring in the model. Also, both conditions can occur simultaneously at high θ_b, and could invalidate the assumptions about smaller shaft-base rotation in the formulation (Siddharthan et al., 1992). As in the original model, the m_b-θ_b relationship depends on two cases: lift-off occurring before or after the yielding of soil in contact with the drilled shaft

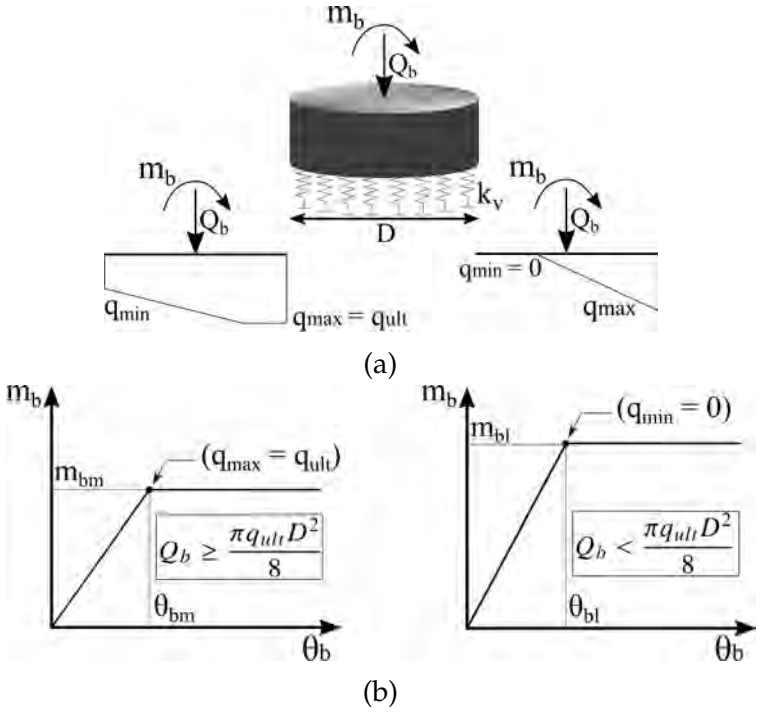

Figure 4.3: Proposed simplified model for tip moment resistance: (a) Winkler's spring characterization of soil beneath a circular shaft and distributed bearing stress for yielding and lift-off conditions, (b) proposed m_b-θ_b model when yielding of soil occurs before and after lift-off.

takes place. For either case, it was assumed that the model would become plastic whenever the lift-off or yielding condition is met. It can be shown that for a given m_b, q, and q_{ult}, lift-off will take place after the yielding of soil if either one of the following conditions is met:

$$m_b \leq \frac{Q_b D}{8} \text{ or, } Q_b \geq \frac{\pi q_{ult} D^2}{8} \tag{4.9}$$

For both cases, the initial linear m_b-θ_b relationship is given by,

$$m_b = \frac{\pi k_v D^4 \theta_b}{64} \tag{4.10}$$

The shaft tip moment and corresponding rotation that would cause cause yielding before lift-off are given by,

$$m_{bm} = \left(q_{ult} - \frac{4Q_b}{\pi D^2} \right) \left(\frac{\pi D^3}{32} \right) \tag{4.11}$$

$$\theta_{bm} = \frac{2}{k_v D} \left(q_{ult} - \frac{4Q_b}{\pi D^2} \right) \left(\right. \tag{4.12}$$

If lift-off takes place prior to soil yielding, the corresponding moment (m_{bl}) can be calculated from Eq. 4.9. The shaft base rotation causing the lift-off would then be,

$$\theta_{bl} = \frac{8Q_b}{\pi k_v D^3} \tag{4.13}$$

The m_b-θ_b model for circular drilled shafts for both cases is shown in Fig. 4.3b. The proposed simplified m_b-θ_b model has been used in the NVShaft simulations of all load test programs mentioned in this study.

4.3 Evaluation of NVShaft Based on Lateral Load Tests

4.3.1 Las Vegas (NV) Load Test Program

An extensive load test program was carried out in Las Vegas, Nevada, as part of the Interstate I-15/US 95 reconstruction project. This load test program was designed to verify the level of axial and lateral load capacity of drilled shafts in local soil conditions (Rinne et al., 1996; Bhuiyan et al., 2020). The cemented soil in

the Las Vegas valley, more commonly known as caliche, is classified as Intermediate Geo-material (IGM) (Brown et al., 2010), and shows extreme heterogeneity in depth, thickness, and strength (Rinne et al., 1996; Stone et al., 2001). The partial cementation in soil and caliche layer in this region had been a great challenge for engineers for years and was the primary focus of the testing program. A total of five lateral and ten axial load tests at four different sites were conducted as a part of this program, and a total of 13 test drilled shafts were constructed. For the purpose of evaluation of NVShaft and to study the diameter effect in the local soil conditions of Nevada, a 0.61 m diameter, 10.88 m long drilled shaft and a 2.44 m diameter, 9.75 m long drilled shaft from site No. 1 were considered. The schematics of these drilled shafts with the choice of *p-y* models based on the subsurface investigation report (Rinne et al., 1996) for different underlying soil layers, are shown in Fig. 4.4.

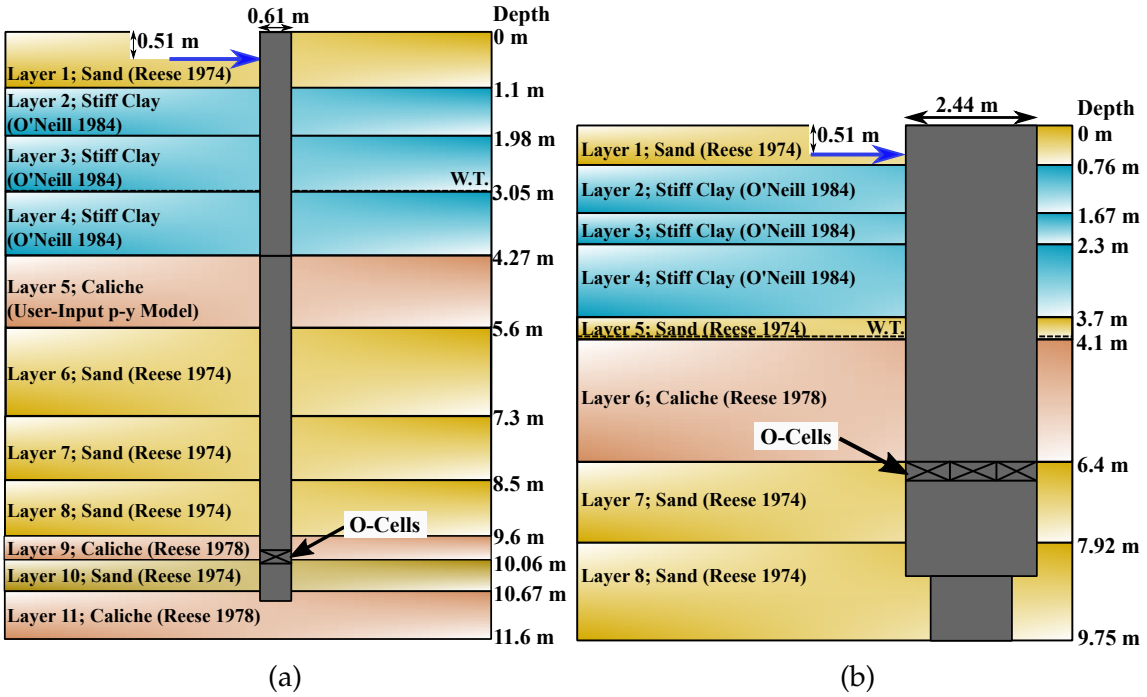

Figure 4.4: Drilled Shaft details and generalized soil profiles for: (a) 0.61 m diameter and (b) 2.44 m diameter test shafts in Las Vegas load test program.

Subsurface and Drilled shaft Properties used in NVShaft Models

The subsurface investigation included standard penetration test (SPT), dilatometer tests, and laboratory tests, such as grain size distribution, Atterberg limits, direct shear strength, unconfined compression strength, and triaxial shear strength tests. Five borings were made in four sites, which included boring B-1 and B-5 in close proximity to site No. 1. Some alluvial and sheet wash soil, probably originating from original interchange construction, were present near the ground surface. The majority of the reported soil profile consisted of partially-cemented dense clayey and silty sand layers in the test site, with hard caliche layers encountered at several depths. Based on soil investigation at site No. 1, the first caliche layer was located between 4.11 m and 4.27 m of depth and stretched from 5.64 m to 6.4 m. Unconfined and triaxial compressive strength tests on core samples resulted in unconfined compressive strength (q_u) of caliche, ranging from 28 MPa to 73 MPa. The soil lateral (p-y) and side shear resistance (t-z) models were chosen accordingly throughout the soil strata based on the relevant soil types. The integrated clay model (O'Neill and Gazioglu, 1984) and sand p-y (Reese et al., 1974) models were used to represent lateral resistance of clay and sand, respectively. The p-y model for the first caliche layer at the 0.61 m diameter shaft location was back-calculated based on the triaxial load test (Rinne et al., 1996). For the remaining caliche layers, the p-y model for vuggy limestone (Reese and Nyman, 1978) was used. As for the side shear resistance, API (2014) recommended t-z curves were chosen for sand and clay layers. For caliche layers, the t-z model for Florida limestone (McVay and Niraula, 2004) was used. The required soil parameters, such as effective unit weight (γ'), angle of friction (ϕ), cohesive strength (c_u), uniaxial compressive strength (q_u), soil modulus (E_s), and strain corresponding to 50% of deviator stress (ϵ_{50}), were obtained from

the site investigation report of Rinne et al. (1996). The missing soil parameters were calculated using several empirical formulas from Brown et al. (2010) and the Caltrans (2021) manual. A summary of the soil characterization and selected *p-y* and *t-z* models to perform unified analysis in NVShaft for 0.61 m and 2.44 m diameter shafts are shown in Table 4.1 and Table 4.2, respectively. The selected *q-z* and v_b-y_b models for these shafts are summarized in Table 4.3. To conduct bi-directional axial load tests, the Osterberg Cells (O-Cells) were placed at the depths of 9.81 m and 6.4 m from grade level for the 0.61 m and the 2.44 m diameter shafts, as shown in Fig. 4.4. The information on rebar details from Rinne et al. (1996) was used in the computer program CSiBridge (Wilson, 2016). The program generated nonlinear moment-curvature relationships, as shown in Fig. 4.5, for use in the NVShaft models as user-inputs to model the nonlinear behavior of shafts.

Table 4.1: Characterized soil profile for 0.61 m diameter drilled shaft in Las Vegas load test program.

Depth (m)	*p-y* Model	*t-z* Model	ϕ (Degree)	c_u (kPa)	q_u (MPa)	E_s (MPa)
0 - 1.1	Sand	API Sand	37	-	-	-
1.1 - 1.98	Integrated Clay	API Clay	-	211*	-	56
1.98 - 3.05	Integrated Clay	API Clay	-	198	-	50
3.05 - 4.27	Integrated Clay	API Clay	-	113	-	44
4.27 - 5.6	User-input *p-y*	Florida Limestone	-	-	-	-
5.6 - 7.3	Sand	API Sand	37	-	-	-
7.3 - 8.5	Sand	API Sand	32*	-	-	-
8.5 - 9.6	Sand	API Sand	37	-	-	-
9.6 - 10.06	Vuggy Limestone	Florida Limestone	-	-	54*	-
10.06 - 10.67	Sand	API Sand	37	-	-	-
10.67 - 11.6	Vuggy Limestone	Florida Limestone	-	-	54*	-

$*$ Measured from in-situ/laboratory

Table 4.2: Characterized soil profile for 2.44 m diameter drilled shaft in Las Vegas load test program.

Depth (m)	p-y Model	t-z Model	ϕ (Degree)	c_u (kPa)	q_u (MPa)	E_s (MPa)
0 - 0.76	Sand	API Sand	37	-	-	-
0.76 - 1.67	Integrated Clay	API Clay	-	106	-	35
1.67 - 2.3	Integrated Clay	API Clay	-	253	-	58
2.3 - 3.7	Integrated Clay	API Clay	-	126	-	28
3.7 - 4.1	Sand	API Sand	33	-	-	-
4.1 - 6.4	Vuggy Limestone	Florida Limestone	-	-	66*	-
6.4 - 7.92	Sand	API Sand	40	-	-	-
7.92 - 9.75	Sand	API Sand	40	-	-	-

$*$ Measured from in-situ/laboratory

Table 4.3: Selected q-z and v_b-y_b models in the predictions of selected load tests in NVShaft.

Load Test Program	Test Shaft	q-z Model	v_b-y_b Model
Las Vegas	0.61 m Diameter Shaft	API Clay	McVay et al. (2008)
	2.44 m Diameter Shaft	API Sand	Vallabhan and Alikhanlou (1982)
PISA	DL2	API Sand	Vallabhan and Alikhanlou (1982)
	CL2	API Clay	Vallabhan and Alikhanlou (1982)

Field Observations and Uncertainties Related to Lateral Load Tests

In both test shafts, lateral loads were applied approximately 0.51 m below ground level using a hydraulic jack. The 0.61 m diameter shaft experienced a maximum horizontal deflection of 0.081 m when subjected to 1014.2 kN maximum lateral load in 53.4 kN increments. The 2.44 m diameter shaft experienced a maximum horizontal deflection of 0.035 m when subjected to 7019.3 kN maximum lateral load in 444.8 kN increments.

Prior to performing the lateral load tests, both test shafts were subjected to axial loads via O-Cells. The maximum axial loads of 1628 kN and 17410.3 kN were

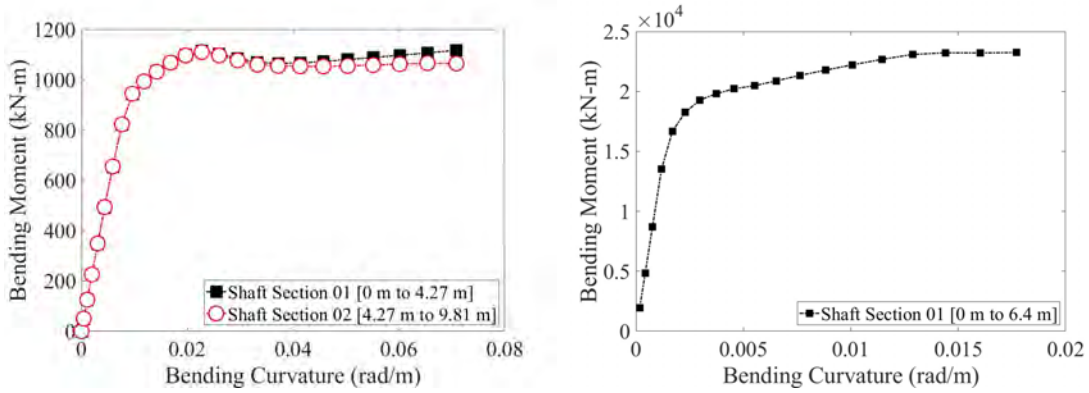

(a) (b)

Figure 4.5: CSiBridge generated moment-curvature plots for: (a) 0.61 m diameter drilled shaft, (b) 2.44 m diameter drilled shaft.

applied to the 0.61 m and 2.44 m diameter shaft, respectively. Axial load tests were conducted on both the partially constructed and completed 0.61 m diameter shaft. Dial gage readings from the 2.44 m diameter shaft indicated 0.034 m of upward movement and 0.0205 m of downward movement at the maximum test load, applied in three cycles. The response from the 2.44 m diameter shaft after the axial load test raised some concerns about the lateral load test being conducted subsequently, since the formation of radial cracks and a radius zone of 4.6 m of upward movement of soil at the nearby ground surface was observed (Z. Zafir, personal communication, September 27, 2019). The upward movement of soil was around 0.013 m at 9910.6 kN of axial load at the radial distance of 1.524 m from the shaft edge. The mobilization of tensile strain near O-Cells location reported in the strain profile diagram (Rinne et al., 1996) and the rigid lateral shaft deflection up to the depth around 4.9 m [Fig. 4.6b] also indicate some crushing of concrete material and damage to the O-Cells (A. Bafghi, personal communication, October 24, 2019). In addition to some reported deficiencies in drilled shaft construction and the presence of cementation in soil, the soil-shaft response due to the prior axial load test adds to the uncertainty of the predicted lateral load response in NVShaft.

Despite these limitations, the fact that lateral load tests were conducted on test shafts with different diameters embedded in the caliche-dominant site is a unique aspect of this project. The Las Vegas load test program is considered one of the most extensive load tests to be performed in the region and hence, was chosen for this study.

Numerical Predictions by NVShaft

The NVShaft predictions of deflection profiles using the proposed unified *p-y* analysis, at three different lateral loads for the 0.61 m and 2.44 m diameter shafts, are shown in Fig. 4.6. By comparing with the measured deflection profiles, it can be said the 0.61 m diameter shaft exhibited flexible responses. As for the 2.44 m diameter shaft, the measured response was inconclusive below the depth of 5 m. Four sets of load-deflection curves are presented in Fig. 4.7 based on: 1) measured data from the field load test, 2) uncoupled *p-y* analysis (including only lateral resistance), 3) coupled *p-y* analysis (including additional side shear resistance), and 4) unified *p-y* analysis (including additional tip shear and tip moment resistances). By analyzing Fig. 4.7, it can be seen that the addition of side shear resistance resulted in an 18.7% and 28.2% reduction in shaft head deflection at corresponding maximum lateral loads for the 0.61 m and 2.44 m diameter shaft, respectively. Reasonable agreement between NVShaft's predicted response and measured data can be observed for both of these shafts at smaller load levels. At higher lateral loads, however, the measured response is softer compared to the numerical prediction, particularly for the 2.44 m diameter shaft. The potential damage to the shaft from the prior axial load tests, including crushing of concrete, crack formation, and the upward heave of soil, are the possible reasons for these deviations. The deviation in response to

higher load levels was investigated from the perspective of measured and predicted maximum curvature comparison plots, as shown in Fig. 4.8. The curvature was back-calculated from field inclinometer data, shown in Fig. 4.6. A smaller measured maximum curvature in comparison, particularly for the 2.44 m diameter shaft, indicates the possibility of rigid movement of the cracked upper portion during the application of higher lateral loads, as indicated in Fig. 4.6.

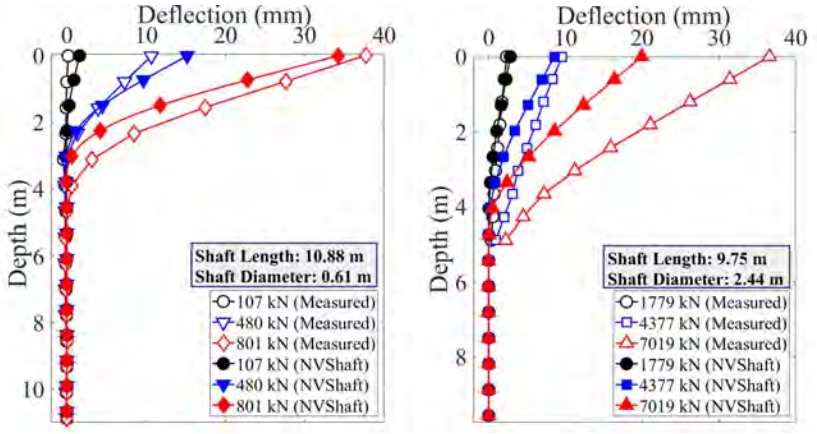

(a) (b)

Figure 4.6: Comparison of measured and NVShaft-predicted deflection profiles for: (a) 0.61 m diameter and (b) 2.44 m diameter drilled shafts using unified *p-y* analysis.

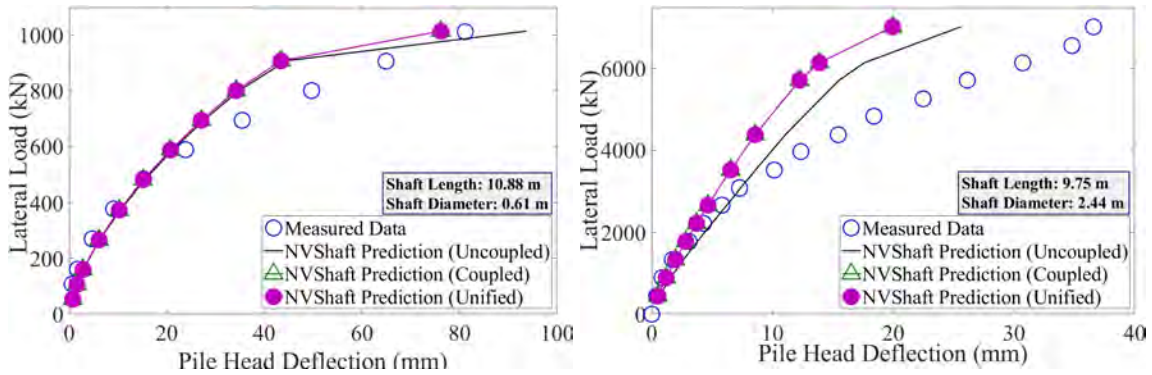

(a) (b)

Figure 4.7: Comparison of measured and NVShaft-predicted load-displacement response, considering the effects of side shear and tip resistance for: (a) 0.61 m diameter and (b) 2.44 m diameter drilled shafts.

As shown in Fig. 4.7, the effect of side shear is more prominent for the 2.44 m

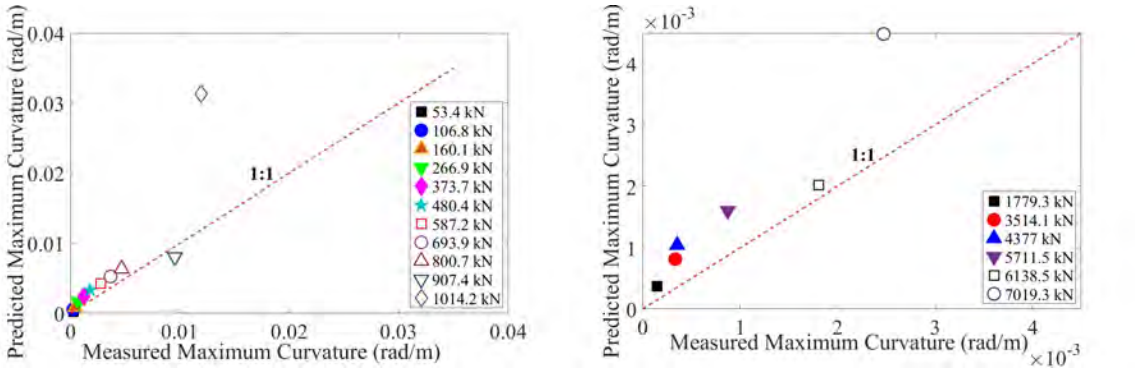

(a) (b)

Figure 4.8: Comparison of measured and NVShaft-predicted maximum curvature for: (a) 0.61 m diameter and (b) 2.44 m diameter drilled shafts.

diameter shaft, resulting in a better prediction at smaller lateral loads. The negligible amount of predicted tip displacement and rotation of both drilled shafts seen in the deflection profiles (Fig. 4.6) explains the small contributions of tip resistances at the applied lateral loads. NVShaft also produces m_r profile diagrams as additional outputs of coupled *p-y* analysis; these are shown in Fig. 4.9 for both test shafts. The profile diagrams reveal sudden increases of m_r at the locations of the caliche layers. Also, relatively higher m_r values for the 2.44 m diameter shaft indicate greater mobilization of side shear in *p-y* analysis.

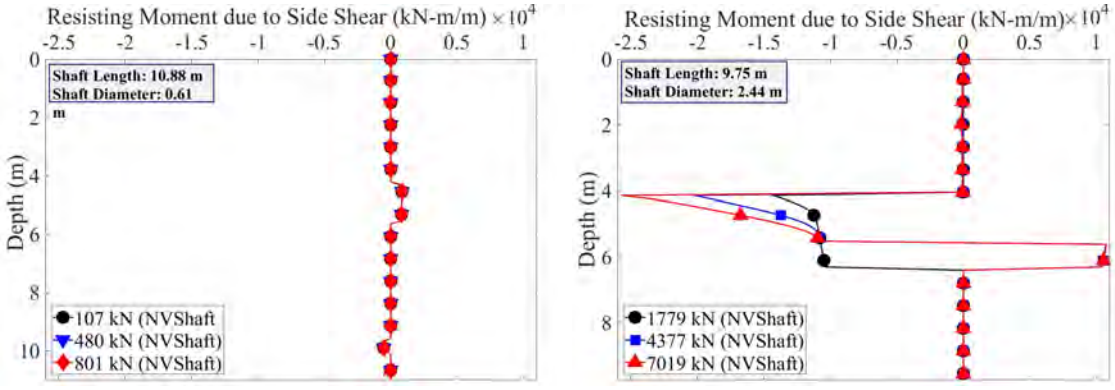

(a) (b)

Figure 4.9: NVShaft-predicted resisting moment due to side shear (m_r) profile for: (a) 0.61 m diameter and (b) 2.44 m diameter drilled shafts.

4.3.2 PISA Load Test Program

A recent numerical-based design method proposed by Byrne et al. (2015) recommends mitigating the major limitations of the conventional *p-y* model based on calibration between 3D finite element model results and field load testing results. This approach was developed and showcased in the Pile Soil Analysis (PISA) project, involving medium-scale field load tests conducted in two sites with different subsurface characteristics. The site locations included: 1) Cowden, in north-east England, with over-consolidated, low plastic glacial clay till; and 2) Dunkirk, in northern France, with normally-consolidated dense sand. These sites are well known for extensive subsurface investigations and field load testings (Jardine, 1985; Sim et al., 2013). The soils at these two sites were extensively characterized to implement in numerical models. As described in Zdravković et al. (2020), in-situ and laboratory tests, such as CPT, SCPT, hand vane shear test, bender element test, triaxial compression test, and triaxial extension tests were carried out. The applied monotonic loads in the load tests were maintained in constant velocity stages, to allow creep displacement at the shaft head (Byrne et al., 2020).

Numerical Modelling in NVShaft

For the evaluation of NVShaft, test piles CL2 (from Cowden site) and DL2 (from Dunkirk site) were chosen. The tubular, steel piles with diameters of 2 m were embedded in respective soil layers. The geometries of these test piles, including pile embedment length (L), diameter (D), installed embedment length to diameter ratio, length above ground surface (h), and wall thickness (t_h), are summarized in Table 4.4. The characterized soil profile in NVShaft numerical models for the

Cowden and Dunkirk sites based on information available in the literature are summarized in Table 4.5 and Table 4.6, respectively. Soil properties such as soil degradability factor (F), relative density (D_r), and initial void ratio (e_0) are also shown. As mentioned in O'Neill and Gazioglu (1984), F is applied to reduce the ultimate soil resistance (p_{ult}) in the integrated clay model based on soil ductility and type of lateral loading (static or cyclic).

Table 4.4: Geometries of test piles from PISA load test program used for evalulation of NVShaft.

Site Location	Test Shaft	L (m)	D (m)	Installed L/D (-)	h (m)	(t_h) (mm)
Cowden	CL2	10.60	2	5.3	10.10	25
Dunkirk	DL2	10.57	2	5.29	9.89	38

Table 4.5: Characterized soil profile for test pile CL2 in PISA load test program.

Depth (m)	p-y Model	t-z Model	γ' (kN/m^3)	c_u (kPa)	E_s (MPa)	ϵ_{50} -	F -
0 - 1	Integrated Clay	API Clay	21.2	50 - 130	7 - 26	0.006	0.75
1 - 2	Integrated Clay	API Clay	11.4	130 - 160	26 - 32	0.005	0.75
2 - 3.75	Integrated Clay	API Clay	11.4	160 - 105	32 - 21	0.005	0.75
3.75 - 12	Integrated Clay	API Clay	11.4	105 - 150	21 - 30	0.005	0.75

Table 4.6: Characterized soil profile for test pile DL2 in PISA load test program.

Depth (m)	p-y Model	t-z Model	γ' (kN/m^3)	ϕ (Degree)	D_r (%)	e_0 -
0 - 3	Sand	API Sand	17.1	43	100	0.57
3 - 4	Sand	API Sand	17.1	37	75	0.628
4 - 30	Sand	API Sand	10.1	37	75	0.628

The lateral and side shear resistances of Cowden soil were simulated in NVShaft using the integrated clay (O'Neill and Gazioglu, 1984) and API clay (API, 2014) models, respectively. The sand p-y model given by Reese et al. (1974) and API sand t-z and q-z models (API, 2014) were implemented for Dunkirk soil for the same

purpose. To model the tip shear resistances of both Cowden and Dunkirk soil, the v_b-y_b model by Vallabhan and Alikhanlou (1982) was chosen. The Cowden soil exhibited ductile behavior during the triaxial compression test when axial strain exceeded 20%. A soil degradability factor (F) of 0.75 was chosen for Cowden clay, which is one of the required inputs in the integrated clay model, following the recommendation of Gazioglu and O'Neill (1984). In both sites, it was reported that gap formation occurred during loading in the active faces of the test piles. The gap extended up to a depth of 6.15 m for test pile CL2 (Byrne et al., 2020). The pile-soil interaction in the lateral analysis of the test piles was properly captured in NVShaft by allowing mobilization of the resisting moment due to side shear only on the passive side.

NVShaft Predictions Based on Additional Lateral Resistance Components

NVShaft-predicted deflection and bending moment diagrams (considering mobilized side shear and tip resistances), along with the measured data for test pile CL2 and DL2, are shown in Fig. 4.10 and Fig. 4.11, respectively. The rigid pile responses from the deflection diagrams in Fig. 4.10a and Fig. 4.11a indicate the possibility of higher mobilization of tip resistances along with side shear during lateral loading. The load-pile head deflection predicted by NVShaft, considering different lateral resistance components and the measured responses of the selected test piles from the PISA load test program, is shown in Fig. 4.12. The contribution of side shear and tip resistances can be seen in the differences in predicted uncoupled, coupled, and unified load-displacement responses, which are significantly greater for the test pile at the clayey Cowden site, compared to the sandy site at Dunkirk. For test pile CL2, coupled and unified *p-y* analysis resulted in 24.4% and 41.5% reductions

in pile head deflection at maximum lateral load, respectively, relative to uncoupled analysis [Fig. 4.12a]. For test pile DL2 in sandy soil, coupled and unified analysis yielded 2.4% and 5.1% reductions in pile head deflection at maximum lateral load, respectively [Fig. 4.12b].

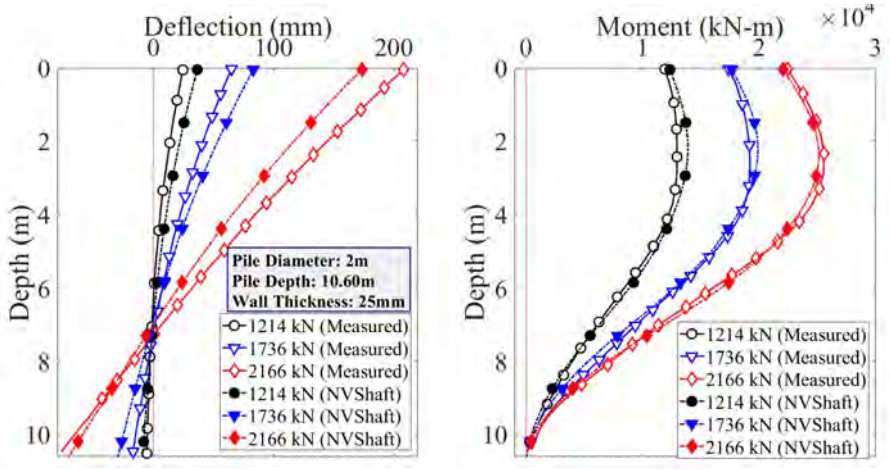

(a) (b)

Figure 4.10: Comparison of measured and NVShaft-predicted (a) deflection and (b) bending moment profiles for test pile CL2 using unified *p-y* analysis.

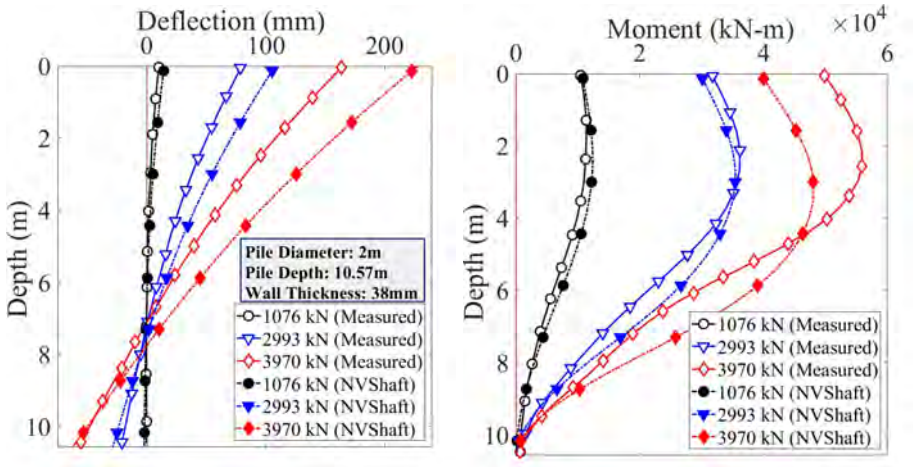

(a) (b)

Figure 4.11: Comparison of measured and NVShaft-predicted (a) deflection and (b) bending moment profiles for test pile DL2 using unified *p-y* analysis.

The mobilized m_r profiles of the test piles from the two different sites are shown

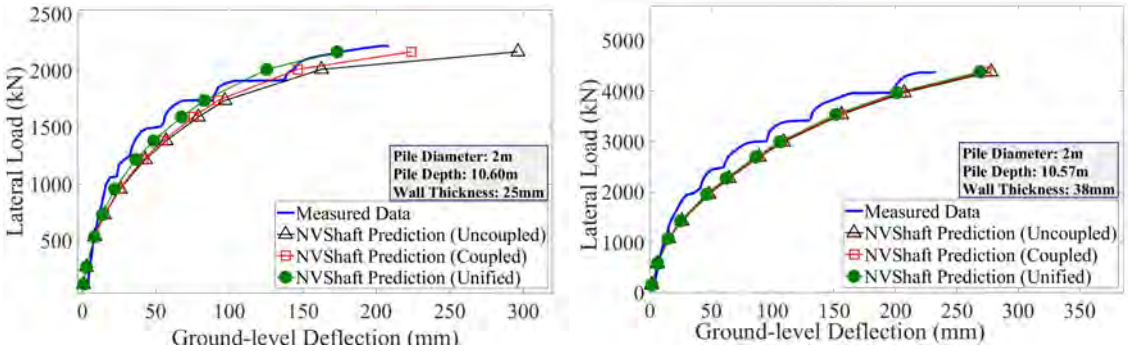

(a) (b)

Figure 4.12: Comparison of measured and NVShaft-predicted load-displacement response, considering the effects of side shear and tip resistance for: (a) test pile CL2 and (b) test pile DL2.

in Fig. 4.13. The mobilization of side shear-generated resisting moment (m_r) seems to be higher at the Cowden clay site, compared to the Dunkirk sand site. As seen in Fig. 4.13, mobilization of m_r occurred at a comparatively shallower depth (2 m) at the clay site, compared to the sandy site. Based on these observations and the fact that the test piles from both load tests were almost identical, with the applied lateral load being significantly higher at the sandy site, it can be construed that over-consolidated glacial clay produced more diameter effects compared to normally-consolidated dense sand. Moreover, the m_r in sand is calculated as a function of mobilized side resistance from the API sand t-z model (API, 2014). The identical m_r profiles at higher load levels in sand [Fig. 4.13b] indicate the side resistance i.e., the m_r to be mobilized at the ultimate value. Based on inspection of the response diagrams, NVShaft made fairly good predictions in deflection, bending moment diagram, and general load-deflection behavior by considering all the lateral resistance components in the PISA load test program.

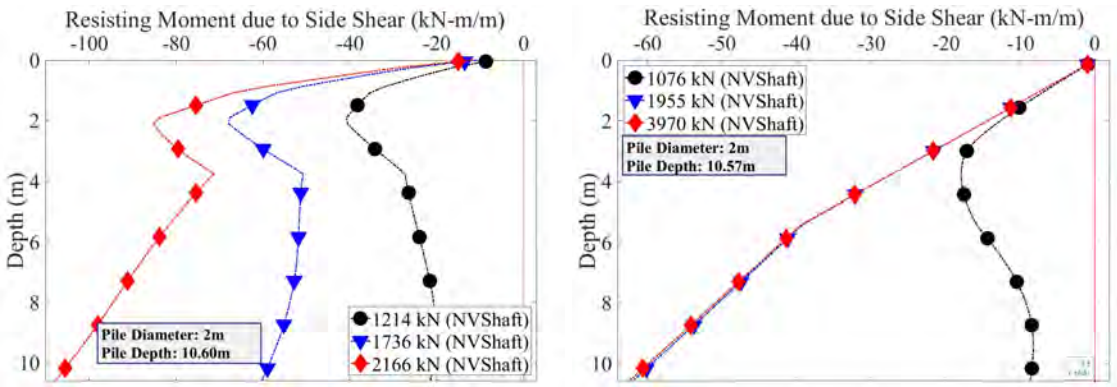

(a) (b)

Figure 4.13: NVShaft-predicted resisting moment due to side shear (m_r) profile for: (a) test pile CL2 and (b) test pile DL2.

4.4 Investigation on Diameter Effects

The effect of side shear, tip shear, and tip moment resistances for a specific applied lateral load with increasing shaft diameter was investigated using the shaft and soil properties from the load test programs mentioned in this study. The percent reduction in shaft head deflections, compared to the responses obtained from conventional *p-y* analysis, was calculated with the inclusion of additional lateral resistance components, in the following cumulative order: 1) addition of tip moment resistance (coupled with tip moment only), 2) addition of tip shear resistance (coupled with tip moment and tip shear), and 3) addition of side-shear induced resistance (unified). For these calculations, the flexural stiffness (EI) values of the test shafts were kept constant, corresponding to the mentioned load test programs. This was done to exclude the effect of stiffness at different shaft diameters during the diameter effects investigation. The contribution from v_b and m_b depends on the mobilized axial load at the shaft tip, according to the described models. Since no axial load was applied in these lateral load tests, to ensure some mobilization of v_b and m_b, shaft self-weights were considered. Fig. 4.14 shows the percent reduction in

shaft head deflection with increasing shaft diameter in the context of the Las Vegas load test (based on the 2.44 m diameter shaft) and PISA load test (both DL2 and CL2 test piles). The effects of tip moment, tip shear, and side shear resistance can be seen in the gradually stiffer response of the shaft (i.e., the higher percent reduction in shaft head deflection) with the subsequent inclusion of the additional resistance components. The addition of side shear resistance in *p-y* analysis causes the most reduction in shaft head deflection, followed by the addition of tip shear resistance. In a study for a short, rigid pier in clay, Vallabhan and Alikhanlou (1982) made a similar observation.

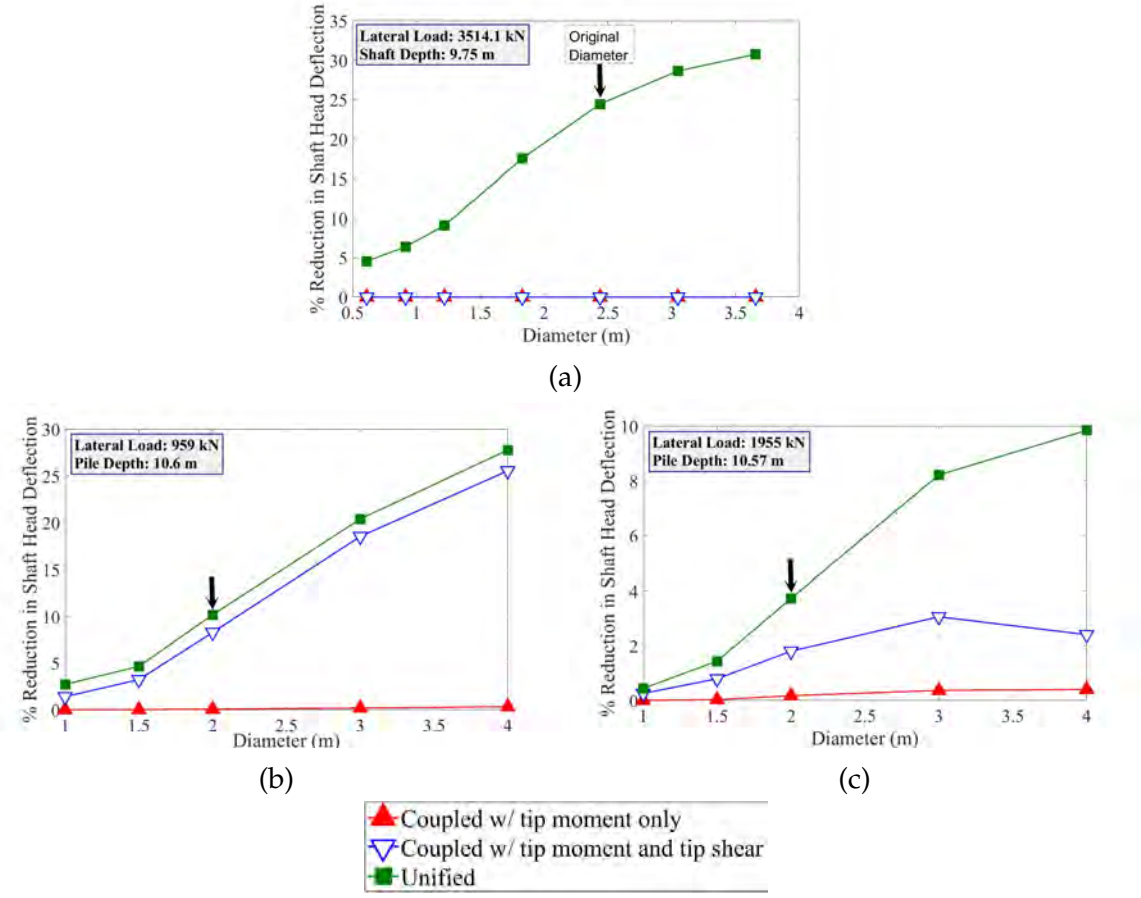

Figure 4.14: Percent reduction in shaft head deflection due to inclusion of different lateral resistance components with increasing diameter, in the context of: (a) the 2.44 m diameter shaft from the Las Vegas load test, (b) test shaft CL2 and (c) DL2 from the PISA load test program.

Although the 2.44 m diameter shaft from the Las Vegas load test was simulated considering multiple types of soil material, the diameter effect due to side shear mostly stems from the caliche layers. This fact can be substantiated by the m_r profile diagrams shown in Fig. 4.9. As seen in Fig. 4.14a, the diameter effect due to m_r causes a maximum 30.7% reduction in shaft head deflection at 3.7 m diameter for 3514.1 kN of lateral load. In this case, contributions from v_b and m_b are almost non-existent due to flexural shaft response [Fig. 4.14a]. Finally, performing unified *p-y* analysis at two different lateral loads on the original 2 m diameter shafts from PISA load tests resulted in 10.2% and 3.7% reduction in shaft head deflection compared to the responses from uncoupled *p-y* analysis, in clayey and sandy sites, respectively. The reduction in shaft head deflection increased to 27.8% and 9.8% in clayey and sandy sites, respectively, at the same lateral loads when the diameter increased to 4 m [Fig. 4.14b and 4.14c]. The diameter effect study reveals stiffer shaft response in the clay layer, compared to the sand layer, after the inclusion of m_r, v_b, and m_b components. This finding is identical to the one from the PISA numerical parametric study discussed in Byrne et al. (2015).

4.5 Conclusions

Due to its simplicity, reliability, and applicability in numerical programs, the *p-y* method based on Winkler's spring model is a widely popular method among engineers. However, as many have noted, the method fails to accurately model the complete soil-shaft interaction for larger diameter and short shafts. Proper characterization of soil layers and inclusion of all the lateral resistance components are important steps to properly study the behavior of laterally-loaded drilled shafts. In this study, the application of a unified *p-y* method is presented, a method that ac-

counts for and includes the resisting moment per unit length (m_r) due to incremental side shear during numerical lateral analysis. Apart from side shear, tip resistances also become significant, especially in the case of short rigid shafts embedded in stiff soil or rock material. This can be properly addressed by implementing suitable tip shear (v_b-y_b) and tip moment resistance (m_b-θ_b) models as boundary conditions in the *p-y* analysis.

The MATLAB-based finite-difference program, NVShaft, is introduced, which is capable of performing the unified *p-y* analysis. Two built-in v_b-y_b models, to simulate tip shear resistance in soil and rock, are included in the NVShaft Library. An m_b-θ_b model, originally proposed for strip footing, was revised for a circular shaft section and was included in NVShaft analysis. NVShaft's capabilities in performing the unified *p-y* analysis were evaluated in the context of two load test programs.

In the context of Nevada's local soil condition, 0.61 m and 2.44 m diameter drilled shafts from the Las Vegas load test program were considered. The presence of cemented layers, excessive soil heave, radial crack formation, and the crushing of concrete and O-cells from the prior axial load tests adversely affected the lateral load response of the test shaft. For the larger, 2.44 m diameter shaft, the addition of m_r resulted in significant improvement in numerical prediction at smaller load levels, indicating diameter effects in play, and resulted in a maximum of 28.2% reduction in shaft head deflection compared to an uncoupled *p-y* prediction. For higher load levels, the measured response is softer, which can be explained by the possibilities of rigid lateral movement of the upper cracked portion of the shaft originating from axial load tests. The m_r profile diagrams from both test shafts indicate lateral resistance due to side shear originating mostly from the caliche layers.

In the PISA load test program, two 2 m diameter rigid steel piles, one embedded in uniform, low plastic over-consolidated clay (in Cowden, England) and another in normally-consolidated, dense sand (in Dunkirk, France) were considered. Compared to uncoupled prediction, performing unified *p-y* analyses resulted in 41.5% and 5.1% reduction in ground-level deflection in clayey and sandy sites, respectively, at maximum lateral loads. Gradual improvement of numerical prediction by NVShaft can be observed with the inclusion of additional lateral resistance components in the *p-y* analysis, especially for the Cowden soil, as also seen from the original study.

The diameter effect in lateral load analysis was further assessed in the context of the selected load test programs. It was found that the diameter effect in large-diameter shafts, for the considered soil materials, comes mostly from the contribution of m_r, followed by the contribution from v_b. This further investigation provides some guidelines to quantify diameter effects as part of the design consideration of large-diameter drilled shaft.

4.6 References

AASHTO (2020). *AASHTO LRFD Bridge Design Specifications*. AASHTO, Washington, D.C.

API (2014). *API Recommended Practice 2A-WSD - Planning, Designing, and Constructing Fixed Offshore Platforms – Working Stress Design*. API.

Ashour, M. and Helal, A. (2014). Contribution of vertical skin friction to the lateral resistance of large-diameter shafts. *Journal of Bridge Engineering*, 19(2):289–302.

Ashour, M. and Norris, G. (2000). Modeling lateral soil-pile response based on

soil-pile interaction. *Journal of Geotechnical and Geoenvironmental Engineering*, 126(5):420–428.

Bell, R. W. (1991). The analysis of offshore foundations subjected to combined loading. Master's thesis, University of Oxford, Oxford, UK.

Bhuiyan, F. M., Siddharthan, R. V., Motamed, R., and Sanders, D. H. (2020). Evaluation of a new *p-y* analysis tool for lateral analysis of drilled shafts using load tests in Nevada. In *DFI 45th Annual Conference on Deep Foundations*, pages 303–312. October 13-16.

Bhuiyan, F. M., Toth, J., Siddharthan, R. V., and Motamed, R. (2021). Evaluation of existing *t-z* models for caliche based on numerical analysis of bi-directional load tests using NVShaft. In *DFI 46th Annual Conference on Deep Foundations*, pages 21–31, Las Vegas, Nevada. October 12-15.

Bhushan, K. and Scheyhing, C. (2002). Lateral load tests on drilled piers in San Diego area residual and formational soils. In *Proceedings 27th annual conference on deep foundations, San Diego, CA*.

Bierschwale, M. W., Coyle, H. M., and Bartoskewitz, R. E. (1981). Lateral load tests on drilled shafts founded in clay. In *Drilled piers and caissons*, pages 98–113. ASCE.

Brown, D. A., Turner, J. P., Castelli, R. J., and Americas, P. (2010). Drilled shafts: Construction procedures and lrfd design methods. Technical Report FHWA-NHI-10-016, United States. Federal Highway Administration.

Byrne, B., McAdam, R., Burd, H., Houlsby, G., Martin, C., Zdravkovic, L., Taborda, D., Potts, D., Jardine, R., Sideri, M., et al. (2015). New design methods for large diameter piles under lateral loading for offshore wind applications. In *3rd*

International Symposium on Frontiers in Offshore Geotechnics, Oslo, Norway, June, pages 10–12.

Byrne, B. W., McAdam, R. A., Burd, H. J., Beuckelaers, W. J., Gavin, K. G., Houlsby, G. T., Igoe, D. J., Jardine, R. J., Martin, C. M., Muir Wood, A., et al. (2020). Monotonic laterally loaded pile testing in a stiff glacial clay till at cowden. *Géotechnique*, 70(11):970–985.

Caltrans (2021). *Caltrans geotechnical manual*.

Finn, W. L. and Dowling, J. (2015). Modelling effects of pile diameter. *Canadian Geotechnical Journal*, 53(1):173–178.

Fuentes, W., Gil, M., and Rivillas, G. (2020). A p–y model for large diameter monopiles in sands subjected to lateral loading under static and long-term cyclic conditions. *Journal of Geotechnical and Geoenvironmental Engineering*, 147(2):04020164.

Gazioglu, S. M. and O'Neill, M. W. (1984). Evaluation of py relationships in cohesive soils. In *Analysis and design of pile foundations*, pages 192–213. ASCE.

Georgiadis, M. (1983). Development of py curves for layered soils. In *Geotechnical practice in offshore engineering*, pages 536–545. ASCE.

Gupta, B. K. and Basu, D. (2016). Analysis of laterally loaded rigid monopiles and poles in multilayered linearly varying soil. *Computers and Geotechnics*, 72:114–125.

Jardine, R. J. (1985). Investigations of pile-soil behaviour with special reference to the foundations of offshore structures. *Ph.D thesis, University of London*.

Jeong, S., Kim, Y., and Kim, J. (2011). Influence on lateral rigidity of offshore piles using proposed p–y curves. *Ocean engineering*, 38(2-3):397–408.

Juirnarongrit, T. and Ashford, S. A. (2004). Lateral load behavior of cast-in-drilled-hole piles in weakly cemented sand. *Transportation research record*, 1868(1):190–198.

Kavand, A. and Yazdi, M. (2019). Kinematic interaction of pile groups with liquefied soil during lateral spreading based on 1g shake table tests. In *Earthquake Geotechnical Engineering for Protection and Development of Environment and Constructions*, pages 3218–3225. CRC Press.

Lam, I. P., Kapuskar, M., and Chaudhuri, D. (1998). Modeling of pile footings and drilled shafts for seismic design. In *Technical Report MCEER*, number 98-0018. US Multidisciplinar Center for Earthquake Engineering Research.

Lam, I. P. and Martin, G. R. (1986). Seismic design for highway bridge foundations. pages 7–21.

Li, Q. and Yang, Z. (2017). P–Y approach for laterally loaded piles in frozen silt. *Journal of geotechnical and geoenvironmental engineering*, 143(5):04017001.

Li, W., Zhu, B., and Yang, M. (2017). Static response of monopile to lateral load in overconsolidated dense sand. *Journal of Geotechnical and Geoenvironmental Engineering*, 143(7).

Lin, H., Ni, L., Suleiman, M. T., and Raich, A. (2015). Interaction between laterally loaded pile and surrounding soil. *Journal of geotechnical and geoenvironmental engineering*, 141(4):04014119.

Matlock, H. (1970). Correlations for design of laterally loaded piles in soft clay. *Offshore technology in civil engineering's hall of fame papers from the early years*, pages 77–94.

McAdam, R. A., Byrne, B. W., Houlsby, G. T., Beuckelaers, W. J., Burd, H. J., Gavin, K. G., Igoe, D. J., Jardine, R. J., Martin, C. M., Muir Wood, A., et al. (2020). Mono-

tonic laterally loaded pile testing in a dense marine sand at Dunkirk. *Géotechnique*, 70(11):986–998.

McVay, M. and Niraula, L. (2004). Development of PY curves for large diameter piles/drilled shafts in limestone for FBPIER. Technical Report Final Report.

McVay, M. C. et al. (2008). Distribution of end bearing, tip shear and rotation on drilled shafts with combined loading in Florida limestone. Technical Report Final Report.

Nogami, T., Otani, J., Konagai, K., and Chen, H.-L. (1992). Nonlinear soil-pile interaction model for dynamic lateral motion. *Journal of Geotechnical Engineering*, 118(1):89–106.

O'Neill, M. and Gazioglu, S. (1984). Integrated formulation of py relationships in clays. *A Report to the American Petroleum Institute, Report PRAC-82-41-2, University of Houston*.

Reese, L. and Nyman, K. (1978). Field load tests of instrumented drilled shafts at Islamorada, Florida. *Report to the Girdler Foundation and Exploration Corporation, Clearwater, FL, February*.

Reese, L. C., Cox, W. R., and Koop, F. D. (1974). Analysis of laterally loaded piles in sand. *Offshore technology in civil engineering hall of fame papers from the early years*, pages pp. 95–105.

Reese, L. C. and Van Impe, W. F. (2011). *Single piles and pile groups under lateral loading*. Milton Park, UK: Taylor & Francis.

Reese, L. C., Wang, S. T., Isenhower, W. M., Arrellaga, J. A., and Hendrix, J. (2000). A program for the analysis of piles and drilled shafts under lateral loads. *Ensoft, Inc., Austin, TX*.

Reese, L. C. and Welch, R. C. (1975). Lateral loading of deep foundations in stiff clay. *Journal of the Geotechnical engineering division*, 101(7):pp. 633–649.

Rinne, E., Thompson, J., and Vanderpool, W. (1996). *I-15/US 95 load test program, Las Vegas, Nevada*. Kleinfelder, Inc., Las Vegas, Nevada.

Siddharthan, R., Ara, S., and Norris, G. M. (1992). Simple rigid plastic model for seismic tilting of rigid walls. *Journal of Structural Engineering*, 118(2):pp. 469–487.

Sim, W. W., Aghakouchak, A., and Jardine, R. J. (2013). Cyclic triaxial tests to aid offshore pile analysis and design. *Proceedings of the Institution of Civil Engineers-Geotechnical Engineering*, 166(2):111–121.

Stone, R., Luke, B., Jacobson, E., and Werle, J. (2001). An overview of engineering with cemented soils in Las Vegas. In *Proc. 36th Ann. Symp. Eng. Geol. Geotech. Eng*, pages 135–144.

Taghavi, A., McVay, M., Niraula, L., Davidson, M., and Patil, A. (2020). Axial and lateral resistance coupling in the analysis of large-diameter drilled shafts. *Engineering Structures*, 206:110160.

Vallabhan, C. and Alikhanlou, F. (1982). Short rigid piers in clays. *Journal of the Geotechnical Engineering Division*, 108(10):1255–1272.

Wilson, E. L. (2016). CSI analysis reference manual for SAP2000, ETABS, SAFE and CSIBridge. *Berkeley: Computer & Structures Inc*.

Woodward, R. J., Gardner, W. S., and Greer, D. M. (1972). *Drilled pier foundations*. McGraw-Hill.

Zdravković, L., Jardine, R. J., Taborda, D. M., Abadias, D., Burd, H. J., Byrne,

B. W., Gavin, K. G., Houlsby, G. T., Igoe, D. J., Liu, T., et al. (2020). Ground characterisation for PISA pile testing and analysis. *Géotechnique*, 70(11):945–960.

Zhu, B., Sun, Y., Chen, R., Guo, W., and Yang, Y. (2015). Experimental and analytical models of laterally loaded rigid monopiles with hardening p–y curves. *Journal of Waterway, Port, Coastal, and Ocean Engineering*, 141(6):04015007.

CHAPTER 5

NUMERICAL INVESTIGATION OF DIAMETER EFFECT ON LATERAL RESPONSE OF DEEP FOUNDATION: PARAMETRIC STUDY BASED ON FIELD LOAD TESTS

Abstract

The numerical *p-y* analysis based on the beam on nonlinear Winkler foundation (BNWF) model is a widely accepted tool to predict the lateral response of drilled shaft using computer programs. The conventional *p-y* method neglects the contributions from additional lateral resistance components such as side shear-induced resisting moment, tip shear, and tip moment resistances for larger diameter shaft, known as the diameter effect. A finite-difference program, NVShaft has been developed to perform a unified *p-y* analysis capable of implementing major lateral resistance springs in the BNWF model. This paper provides the results of a parametric investigation on the diameter effect based on variation in parameters such as soil type, strength characteristics, pile diameter, embedment depth, and applied axial load in both sandy and clayey site conditions. Using the capabilities of NVShaft, the parametric study identifies the key parameters causing diameter effects from different types of lateral resistance components. This was done by considering hypothetical numerical models based on two lateral load tests from the PISA load test program in Europe. Variation in soil strength, embedment depth, and applied axial loads significantly affects the lateral soil-shaft interaction and is captured by the parametric study. Shorter embedment depth and larger applied axial load caused major increases in tip resistances in numerical models. The results indicate a more significant diameter effect in clay material in the context of PISA project, with

a maximum of 73% reduction in pile head displacement relative to the response obtained from the conventional analysis. Two case studies involving numerical simulations of additional lateral load tests in marine clay and weakly cemented sand are presented, to compare diameter effects in these unique site conditions.

5.1 Introduction

The use of drilled shafts as a deep foundation system to support bridge piers, offshore wind turbines, abutments, and other structures offers some advantages compared to using other types of deep foundations. Relatively easier construction method with minimal vibration and noise in site, small footprint, larger capacity, and efficiency in countering seismic load make drilled shaft a more economical choice in many recent projects (Bhushan and Scheyhing, 2002; Rinne et al., 1996). A single drilled shaft can replace several smaller diameter monopiles, and the recent trend is indicating the possible uses of drilled shafts with diameters as large as 10m in near future (Byrne et al., 2015).

The focus of this study is the numerical lateral load analysis of large diameter drilled shaft. The beam on nonlinear Winkler foundation (BNWF) model, otherwise known as *p-y* method is a widely accepted tool recommended by design codes (i.e., (API, 2014; AASHTO, 2020)) to perform lateral analysis of drilled shaft. In this method, the soil lateral resistance is characterized by a series of *p-y* springs, and the shaft is assumed to behave as idealized Euler's beam model. The numerical lateral load analysis is commonly carried out using finite-element (i.e., (BSI, 2019)), finite-difference (i.e., (Isenhower et al., 2017)) or strain wedge (i.e., (Norris, 1986)) model. The conventional *p-y* model neglects the contribution from other lateral

resistance mechanisms such as resisting moment generated due to mobilized side shear (m_r), tip shear (V_b), and tip moment (M_b) resistance. Based on several studies, performing conventional *p-y* analysis of large diameter shaft result in conservative lateral response (Vallabhan and Alikhanlou, 1982; Bhushan and Scheyhing, 2002; McVay and Niraula, 2004; Taghavi et al., 2020). Finn and Dowling (2015) defined the effect of larger pile diameter causing conservative predicted responses in the conventional *p-y* analysis as "pile diameter effect". Finn and Dowling (2015) conducted a parametric investigation using LPILE and continuum-based finite element program VERSAT-P3D (Wu, 2006) for different pile diameters ranging from 0.2 m to 2 m. Finn and Dowling (2015) concluded that the diameter effect based on the response obtained from LPILE analysis becomes significant when pile head lateral displacement exceeds 60 mm.

In order to improve the conventional *p-y* method, Ashour and Helal (2014) integrated mobilized side shear resistance generated from lateral response in BNWF, strain wedge model and observed up to 40% increase in shaft-head lateral stiffness (K_d) compared to conventional response. For clayey material, Ashour and Helal (2014) also performed a parametric study to investigate the increase in K_d with different soil-shaft parameters such as shaft length to diameter ratio (L/D) and the cohesive strength (c_u). In another study, Taghavi et al. (2020) used the numerical tool FB-Multipier (BSI, 2019) to 'couple' the axial and lateral resistance mechanism in the BNWF framework. Taghavi et al. (2020) also conducted parametric investigations on the effects of shaft-head fixity, embedded length, shaft diameter, and strength of rock material on mobilized m_r. These studies helped explain the mechanism of mobilized side shear resistance in numerical models with varying soil shaft parameters. For example, as stated by Taghavi et al. (2020), maximum rotation due to lateral response increases with smaller embedment depth, causing more diameter

effect compared to shafts having larger depth. However, these mentioned studies did not investigate the effects of these parameters on tip moment and tip shear lateral resistance components.

In a more recent study, Wang et al. (2020) proposed a unified, two-spring lateral resistance model applicable for monopiles embedded in soft clay. The model can account for different L/D ratios and assumes pure lateral soil resistance above the rotation point, which is defined as the depth where pure rotation and almost zero displacements occur. Both V_b and M_b are integrated into a proposed moment-rotation spring which is applied at the rotation point. Wang et al. (2020) reported that for flexible piles ($10 < L/D \leq 30$) embedded in normally consolidated clay, m_r may contribute up to 1% of lateral capacity, while for semi-rigid and rigid piles, this contribution may increase up to 6% of lateral capacity. Fu et al. (2020) took a different approach and proposed a multi-spring model for clayey soil conditions in China by scaling the site-specific soil shear stress-strain relationship. In addition to lateral soil resistance, the method can also implement m_r and V_b soil resistances in finite-element analysis.

In this study, a parametric investigation on the effect of soil strength parameters (i.e., angle of friction, ϕ, and cohesive strength, c_u), shaft diameter (D), embedment depth (L), and applied axial load (P_x) on different additional lateral resistance components is presented. A finite-difference program, NVShaft was utilized to perform this investigation. NVhaft was originally developed as part of a research project to improve the numerical lateral analysis in the context of Nevada's local soil condition. In a previous study, the authors proposed a unified *p-y* method implemented in NVShaft which considers additional resisting moment due to side shear (m_r) and tip resistances (V_b and M_b) in BNWF model (Bhuiyan et al., 2022).

The additional lateral resistances discussed as part of the proposed unified *p-y* method were implemented in the parametric investigation performed in this study. The investigation was carried out in the context of two lateral load tests conducted in two different sites from the Pile Soil Analysis (PISA) project (Byrne et al., 2015). The project originally aimed at mitigating the diameter effect by suggesting an advanced, numerical-based design method for laterally loaded large diameter shaft. Hypothetical numerical models based on lateral load tests conducted in a sandy site at Dunkirk, France, and a clayey site at Cowden, England were developed at NVShaft for this study. To further investigate and compare the diameter effect in clay and sand material outside of the scope of the original parametric study, numerical predictions of lateral load tests in marine clay and weakly cemented sand are also presented as case studies.

5.2 Overview of NVShaft

NVShaft is a MATLAB-based, finite difference program capable of performing both axial and lateral load analysis. The program was originally developed to perform a more robust and sophisticated version of numerical lateral load analysis. The improved version of lateral analysis, termed as the unified *p-y* method, can consider side shear, tip shear, and tip moment resistances in the Winkler's soil spring model. A summary of different types of models to simulate different components of lateral resistance is shown in Table 5.1. Apart from the models mentioned in Table 5.1, users have the option to define their own model parameters as user inputs. More details on various features included in NVShaft related to performing numerical lateral analysis along with one validation example can be found in Bhuiyan et al. (2020).

NVShaft can also perform numerical axial load (*t*-*z*) analysis, with a unique feature that lets the user specify the location of the bi-directional cell. Hence, numerical finite-difference simulation of bi-directional static load test can be performed. The capability of NVShaft to perform axial load analysis is described in Bhuiyan et al. (2021), along with a validation example.

Table 5.1: Summary of lateral resistance models included in NVShaft.

Model Type	Lateral Resistance	Axial Side Resistance	Axial Tip Resistance	Tip Shear Resistance	Tip Moment Resistance
Number of Models	20	6	4	2	1

5.3 Overview of Unified *p*-*y* Analysis

5.3.1 Side Shear Resistance

To perform the numerical lateral load analysis, the following *p*-*y* equation, derived from Euler's beam formula, is typically solved by the commercial programs,

$$EI\frac{d^4y}{dz^4} + Q_z\frac{d^2y}{dz^2} - \frac{D^3}{4}(C_{ma} + C_{mp})\frac{d^2y}{dz^2} - p - w = 0 \tag{5.1}$$

where E = elastic modulus of drilled shaft section, I = moment of inertia of drilled shaft section, y = displacement at depth x , Q_z = axial load in the shaft, p = soil reaction per unit length, and w = applied distributed load per unit length.

Although the conventional *p*-*y* equation yields reasonable predicted responses for smaller diameter shafts, numerous studies in the past suggest erroneous, comparatively softer shaft responses than field measured data for shafts having larger

diameters. This discrepancy typically occurs due to the absence of side shear, tip shear, and tip moment resistances in Winkler's spring model, which is illustrated in Fig. 5.1. An additional term in Eq. 5.1, representing resisting moment generating from side shear more prominent in shafts with larger diameters, can result in more realistic soil-shaft interaction in numerical analysis (Ashour and Helal, 2014; Taghavi et al., 2020). The idea is that a laterally loaded shaft with a larger diameter undergoes a significant amount of vertical displacement, compare to the shaft with a smaller diameter, leading to higher mobilization of side resistance (Fig. 5.1).

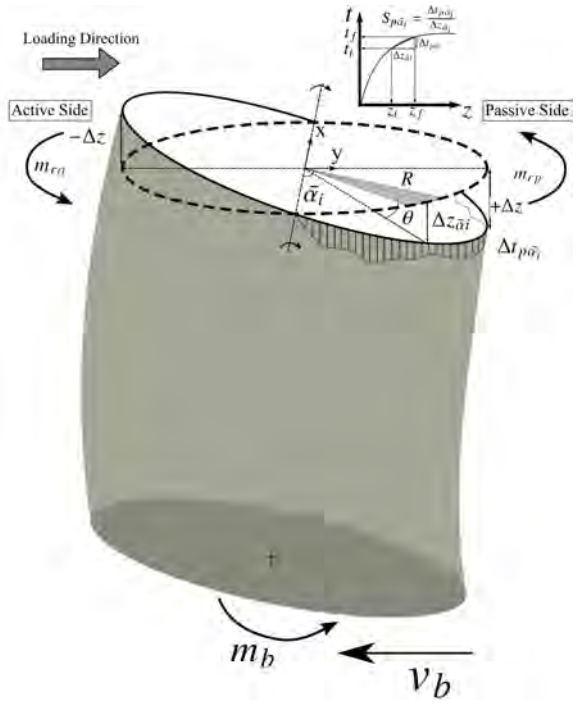

Figure 5.1: Mobilization of side resistance and resulting resisting moment per unit length (m_r) due to rotation of a circular drilled shaft section. Mobilization of tip shear (v_b) and tip moment (m_b) resistances are also illustrated.

For a circular shaft section, to simulate numerical lateral load analysis in finite-difference domain, Bhuiyan et al. (2022) proposed to use the following modified *p-y* equation,

$$EI\frac{d^4y}{dz^4} + Q_z\frac{d^2y}{dz^2} - \frac{D^3}{4}(C_{ma} + C_{mp})\frac{d^2y}{dz^2} - p - w = 0 \tag{5.2}$$

where, C_{mp} and C_{ma}, corresponding to the passive and active side of the shaft, respectively, can be defined as the function of the secant slope of the *t*-*z* curve and the angle ($\bar{\alpha}_i$) as shown in Fig. 5.1. The additional term in Eq. 5.2 can be defined as,

$$m_r = m_{rp} + m_{ra} = \frac{D^3}{4}(C_{ma} + C_{mp})\frac{dy}{dz} \tag{5.3}$$

where, m_{rp} and m_{ra} are resisting moment per unit length on the active and passive side, respectively. While performing the *p*-*y* analysis, NVShaft calculates the incremental side shear using the defined side shear resistance (*t*-*z*) model and solves Eq. 5.2 to obtain predicted lateral responses of the drilled shaft.

5.3.2 Tip Shear Resistance

Based on some past studies, a considerable amount of tip displacement can be observed when lateral load tests have been performed on short, rigid drilled shaft (Zhu et al., 2015; Byrne et al., 2020; McAdam et al., 2020). Introducing tip shear resistance in the *p*-*y* model in such cases enables more realistic soil-shaft interaction, which is typically ignored in the conventional *p*-*y* analysis. In NVShaft, the tip shear resistance model proposed by Vallabhan and Alikhanlou (1982) has been included to be used for any type of soil material. This model is used in the simulation of PISA load tests and the parametric study described in this paper. For rock material, a somewhat similar model proposed by McVay et al. (2008) can be used.

5.3.3 Tip Moment Resistance

To capture the tip moment resistance originating from the tip rotation of a rigid shaft embedment in stiff material, a simplified tip moment resistance model has been included in NVShaft. As described in Bhuiyan et al. (2022), the model depends on two criteria of soil-shaft response: 1) Occurrence of shaft tip lift-off i.e., a portion of shaft tip losing contact with soil or rock material and 2) bearing stress of soil or rock material exceeding ultimate bearing strength. The linear, perfectly plastic tip moment resistance model depends on which of the above two criteria occurs before the other. The model calculates the tip moment resistance by using the coefficient of subgrade reaction (k_v), bearing stress at shaft tip (Q_b), and shaft tip rotation (θ_b). A more elaborate detail on the simplified tip moment model can be found in Bhuiyan et al. (2022).

5.4 Details on PISA Load Test Program

To perform parametric investigations on the diameter effect, two hypothetical models were developed based on two load tests from the PISA project; one from a sandy site at Dunkirk and another from a clayey site at Cowden. The hypothetical models were analyzed in NVShaft to perform the mentioned parametric investigation. A brief overview of the PISA load test program is discussed in the subsequent sections.

5.4.1 Background

An advanced numerical-based design method proposed by Byrne et al. (2015) requires calibration between predicted response obtained from 3D FE analysis and measured response obtained from field load tests. The method is highlighted in the Pile Soil Analysis (PISA) project, involving medium-scaled lateral load tests at two different sites: 1) The normally consolidated sandy site in Dunkirk, France and 2) the low plastic, over-consolidated clayey site in Cowden, England. These sites were deliberately chosen because of extensive subsurface investigation and field load testing conducted in two distinct types of soil materials (Jardine, 1985; Sim et al., 2013). Directed by DONG Energy, and supervised by an Academic Work Group (AWG), the PISA project started in August 2013 and was completed in 2016. The proposed design method made three major improvements in the design of drilled shaft for lateral loading as mentioned in Byrne et al. (2017): 1) Calibration of soil parameters to be used in the soil resistance models. 2) Accurate dynamic lateral load simulation for wind turbines and 3) Additional lateral resistance components significant in larger diameter shafts.

5.4.2 Subsurface Conditions of the Test Sites

Dunkirk Test Site

The Dunkirk test site in northern France consists of normally consolidated marine sand up to 30 m in depth. The naturally deposited sand is overlain by 3 m deep hydraulic fill deposits. As reported by Zdravković et al. (2020), the groundwater table can be found at 5.4 m depth, and the relative density of the hydraulic fill

and the marine sand are approximated as 100% and 75%, respectively. The bulk unit weight of the sand above and below the water table is reported to be 17.1 kN/m3 and 19.9 kN/m3, respectively (Chow, 1997). Apart from the field measured data from previous studies, several new CPT and SCPT conducted in the test pile locations revealed a somewhat uniform sand profile (Zdravković et al., 2020).

Cowden Test Site

The soil characteristics of the Cowden test site is summarized by Powell et al. (2003). The overconsolidated clay till extends up to the depth of 40 m with two, 1 m thick intermitted sand layers located around 12 m and 18 m of depths. The ground water table is reported at 1 m depth from the ground surface (Zdravković et al., 2020).

5.4.3 Description of the Test Piles

In PISA project, tubular, steel pipe pile with specified small (D = 0.273 m), medium (D = 0.762 m) and large (D = 2 m) diameters were subjected to monotonic lateral loads. In the Dunkirk test site, the nominal length to diameter ratios (L/D) of the test piles were set to 3, 5.25, and 8. Similar L/D values were adopted in the Cowden test site, aside from one test pile (CM3) having L/D = 10. The thickness (t) of the steel pipe piles from both test sites ranged between 7 mm to 38 mm, while the shaft length above the ground surface (h) ranged between 5 m to 10.10 m.

To investigate the diameter effect based on NVShaft analysis, the large diameter piles DL2 (from Dunkirk) and CL2 (from Cowden) were considered in this study. A summary of different geometries of these test piles is shown in Table 5.2. The

baseline models showing original soil characteristics and shaft dimensions for both of these test piles are shown in Fig. 5.2.

Table 5.2: Geometries of the considered test piles from PISA load test program.

Site Location	Test Shaft	L (m)	D (m)	Installed L/D (-)	h (m)	t_h (mm)
Dunkirk	DL2	10.57	2	5.29	9.89	38
Cowden	CL2	10.60	2	5.3	10.10	25

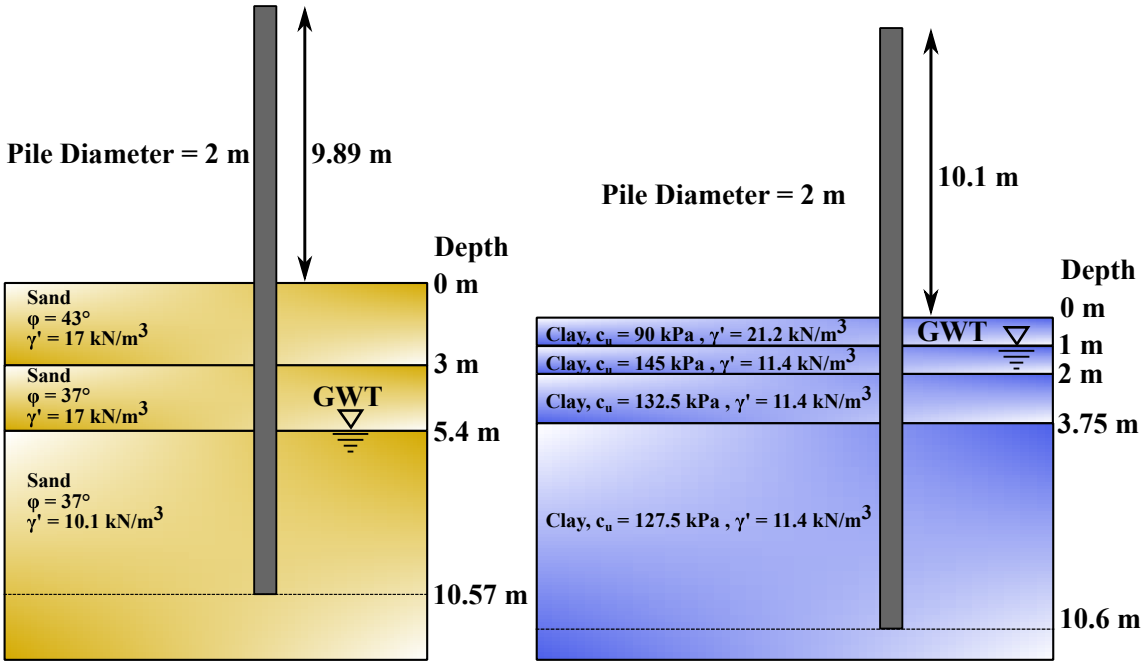

Figure 5.2: Baseline models based on original PISA load tests showing idealized soil profiles and shaft dimensions for test pile (a) DL2 and (b) CL2.

5.4.4 Numerical Modeling in NVShaft

Table 5.3 and 5.4 summarizes the idealized soil profile used in the parametric study for the Dunkirk and Cowden test sites, respectively. Additional soil parameters such as effective unit weight (γ'), cohesive strength (c_u), soil modulus (E_s), strain

factor (ϵ_{50}), soil degradability factor (F) and angle of friction (ϕ) are also shown. The lateral soil resistances at these sites were simulated by using the integrated clay (O'Neill and Gazioglu, 1984) and the sand (Reese et al., 1974) *p-y* models. The API recommended *t-z* and *q-z* models were used for the side and end bearing resistances, respectively (API, 2014). The tip shear resistance proposed by Vallabhan and Alikhanlou (1982) and tip moment resistance by Bhuiyan et al. (2022) were implemented in the unified *p-y* analysis. Following the recommendation by O'Neill and Gazioglu (1984), the soil degradability factor (F) was set as 0.75 for the Cowden clay site, as the reported axial strain at failure during triaxial test was 20% (Zdravković et al., 2020).

Table 5.3: Idealized soil profile for test pile DL2 used in parametric study.

Depth (m)	*p-y* Model	*t-z* Model	γ' (kN/m^3)	ϕ (Degree)
0-30	Sand	API Sand	11	37.6

Table 5.4: Idealized soil profile for test pile CL2 used in parametric study.

Depth (m)	*p-y* Model	*t-z* Model	γ' (kN/m^3)	c_u (kPa)	E_s (MPa)	ϵ_{50}
0-12	Integrated Clay	API Clay	12.2	126.6	25.3	0.005

5.5 Overview of Parametric Study to Investigate Diameter Effect

A parametric study was conducted to investigate diameter effect in the context of two test sites from the PISA load test program. The diameter effect was quantified in terms of percent reduction in pile head displacements after incorporating different additional lateral resistance components. The inclusion of additional lateral resistance models was done in the following order: 1) Tip moment resistance (coupled with tip moment only); 2) Tip shear resistance (coupled with tip moment and tip

shear) and 3) Side shear resistance (unified). Table 5.5 summarizes ranges of key soil and pile properties implemented in the diameter effect study. The effect of individual parameters was analyzed for different pile diameters up to 10 m. The influence from increasing value of soil angle of friction and cohesive strength, in the context of the Dunkirk and Cowden sites, respectively, was investigated. The effect of increasing embedment depth and applied axial load on lateral load responses of piles with increasing diameters was also included in the parametric study.

Table 5.5: Ranges of soil and shaft properties used to investigate diameter effect in the context of PISA load test program.

Site Location	Test Pile	Pile Diameter (m)	ϕ (Degree)	c_u (kPa)	Embedment Depth (m)	Axial Load (kN)	Lateral Load (kN)
Dunkirk	DL2	2-10	35-42	-	9-14	376-7000	1955
Cowden	CL2	1.5-10	-	80-200	8-13	252-3000	959

5.5.1 Effect of Soil Strength Parameters

The pile diameter ranging from 2 m to 4 m, and the increasing ϕ value were assigned in the numerical models characterized for test pile DL2. A similar investigation on the increasing c_u value was carried out for test pile CL2. Fig. 5.3 and Fig. 5.4 show the diameter effect due to increasing ϕ and c_u values, respectively for 2 m and 4 m pile diameters. In both cases, higher values of soil strength and pile diameters resulted in stiffer lateral responses, which in turn produced minimal diameter effect. Similar to our previous findings (Bhuiyan et al., 2022), the diameter effect stems mostly from side shear-induced resisting moment, followed by tip shear resistance in both cases. By comparing both Fig. 5.3 and 5.4, it can be said that the diameter effect is subtler for increasing soil strength in sandy soil, compared to clayey soil. For sandy soil, the softest lateral response resulting from 35 degree of ϕ and 2 m

pile diameter yielded a 27.7% reduction in head displacement after performing the unified *p-y* analysis. Increasing pile diameter to 4 m resulted in a stiffer response at the corresponding 1955 kN lateral load [Fig. 5.3b] and a lesser diameter effect (19.6% reduction at ϕ = 35 degree) compared to the plots shown in Fig. 5.3a. In contrast, clayey soil appeared to exhibit more diameter effect (Fig. 5.4), with a clear increase in percent reduction in pile head displacement from 16.2% to 46.5% at c_u = 80 kPa when diameter increased from 1.5 m to 4 m, at a constant 959 kN of lateral load. Similar to the observation made for sandy soil, a decreasing trend in diameter effect can be observed in clayey soil with increasing c_u (soil strength) parameter values at all considered pile diameters.

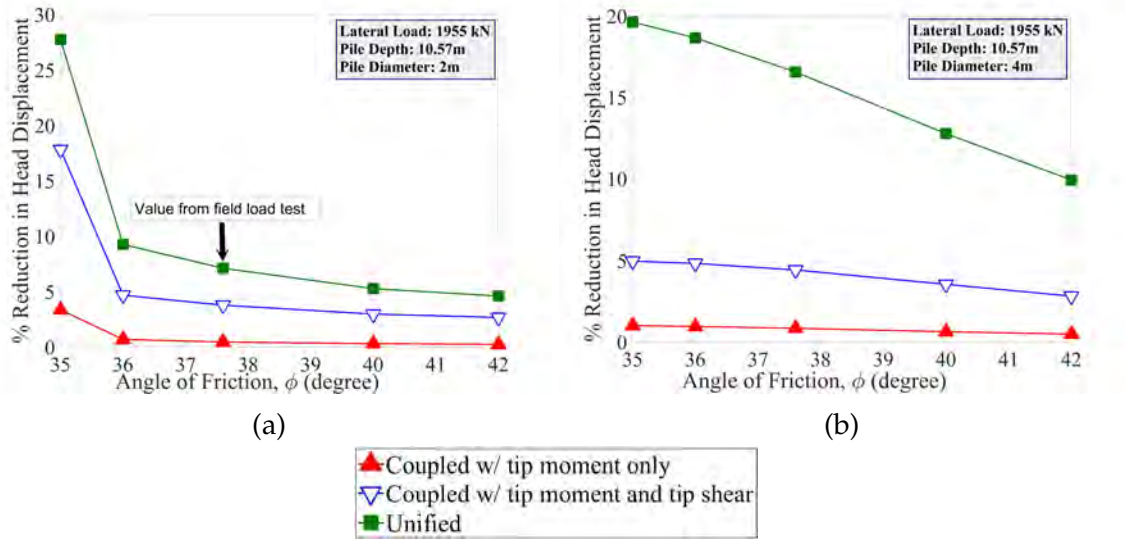

Figure 5.3: Percent reduction in shaft head displacement due to inclusion of different lateral resistance components with increasing angle of friction for (a) 2 m and (b) 4 m diameter of test pile DL2.

5.5.2 Effect of Pile Embedment Length

The diameter effect study in terms of increasing pile embedment length was carried out in the context of test piles DL2 and CL2. The results obtained from the

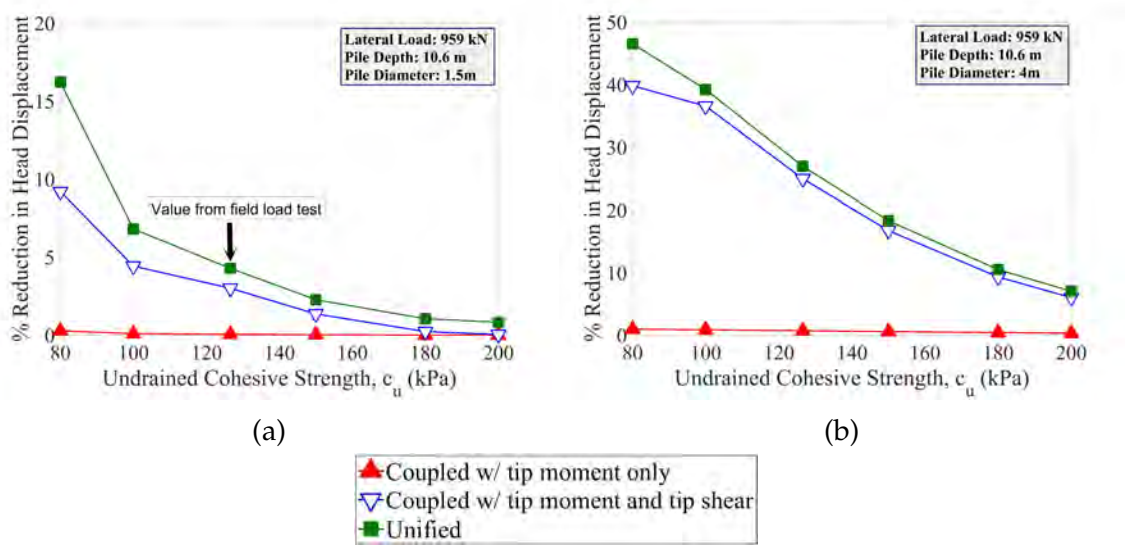

Figure 5.4: Percent reduction in shaft head displacement due to inclusion of different lateral resistance components with increasing cohesive strength for (a) 1.5 m and (b) 4 m diameter of test pile CL2.

parametric investigation are shown in Fig. 5.5 and 5.6 for sandy and clayey sites, respectively. The percent reductions in pile head displacement after including lateral resistance components, corresponding to 2 m, 6 m, and 10 m pile diameters are shown. Fig. 5.5a indicates the softest lateral response in the sand when performing a unified *p-y* analysis on the pile with 2 m diameter and 10 m embedment length, leading to a 13.1% reduction in pile head displacement. Increasing the embedment length in each pile diameter and lateral load resulted in stiffer responses, which were observed for up to 6 m pile diameter. The effect of increasing embedment length in sand diminished at higher pile diameter, as Fig. 5.5c shows a somewhat constant percent reduction value for 10 m pile diameter.

The diameter effect in clay is relatively more significant as shown in Fig. 5.6, where increasing diameter led to larger reductions in head displacements. For the considered minimum of 8 m of embedment length, pile diameters of 1.5 m and 10 m resulted in 28.8% and 73% reduction in pile head displacement in clay, respectively

[Fig. 5.6a and 5.6c].

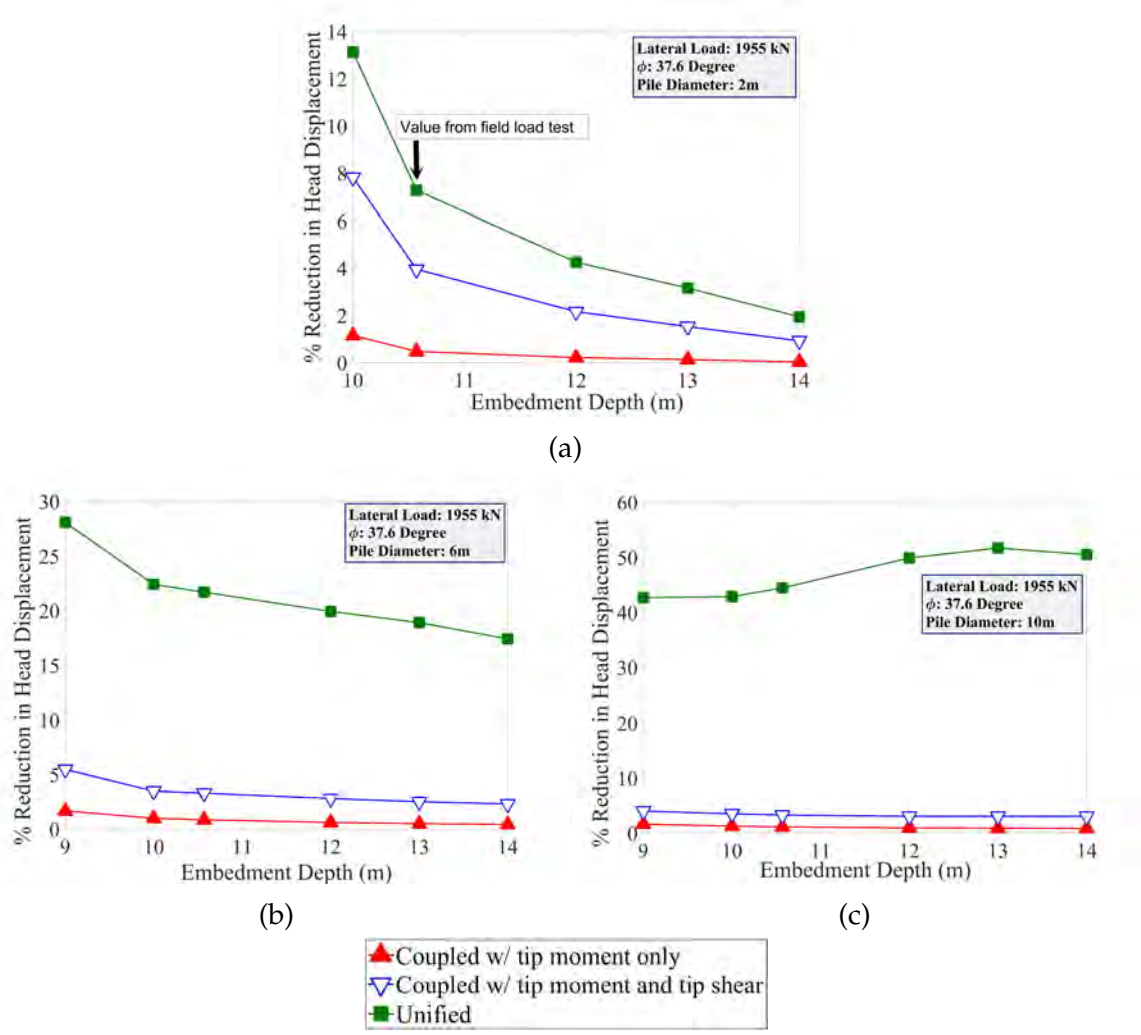

Figure 5.5: Percent reduction in shaft head displacement due to inclusion of different lateral resistance components with increasing embedment depths for (a) 2 m, (b) 6 m and (c) 10 m diameter of test pile DL2.

Shaft with $L/T \leq 2$ is typically expected to behave in a rigid manner, where L = shaft length; $T = \sqrt[4]{EI/\bar{k}}$; $\bar{k}$ = average coefficient of subgrade reaction of soil (Woodward et al., 1972). Measured response from lateral field load tests on the rigid shaft is known to produce a larger maximum rotation near the application of lateral load and failure initiates in soil material (Taghavi et al., 2020). A considerable amount of tip displacement and tip rotation is also very common based on observed responses

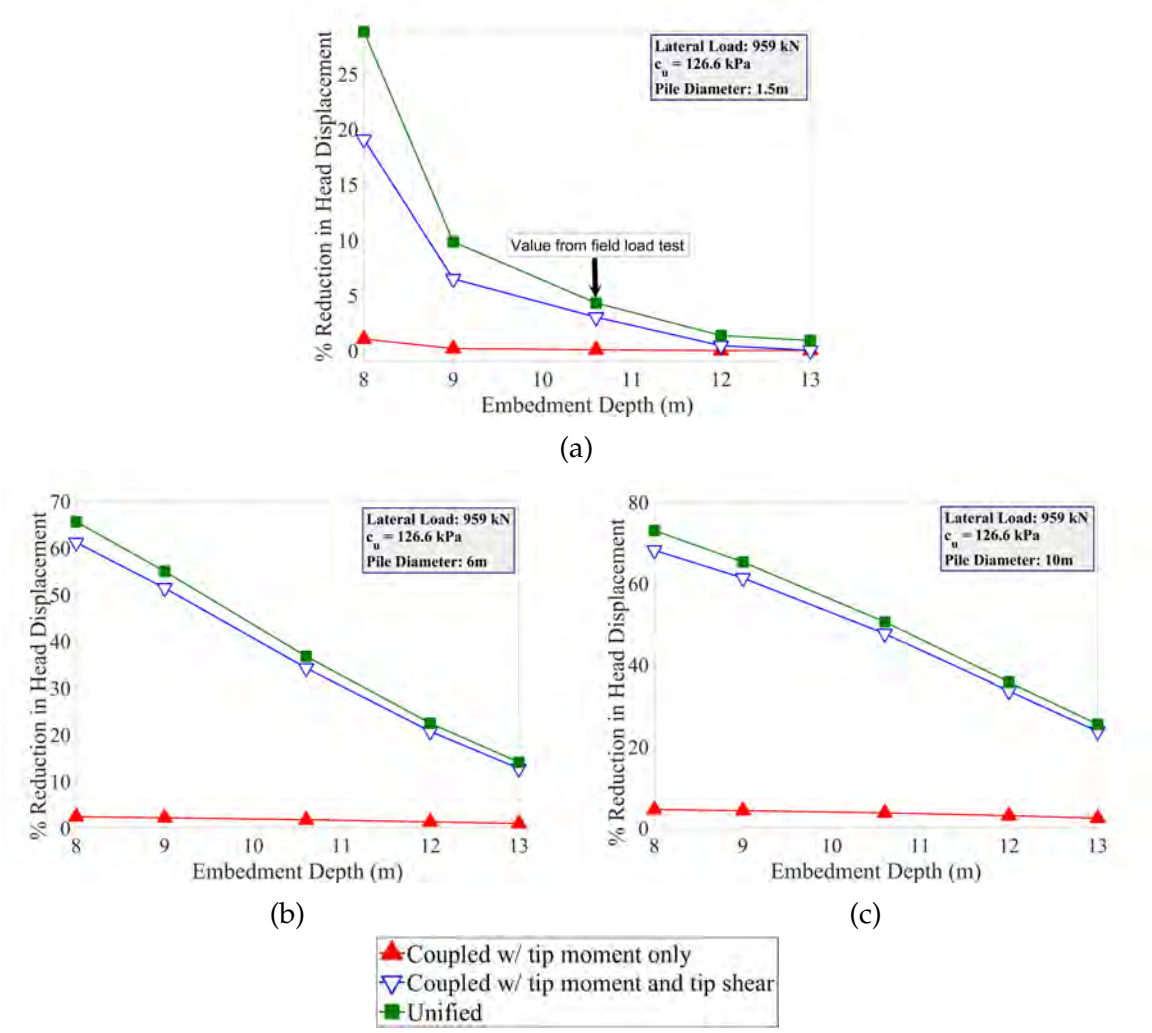

Figure 5.6: Percent reduction in shaft head displacement due to inclusion of different lateral resistance components with increasing embedment depths for (a) 1.5 m, (b) 6 m and (c) 10 m diameter of test pile CL2.

from field load tests conducted on rigid shaft (Vallabhan and Alikhanlou, 1982; Zhu et al., 2015; Gupta and Basu, 2016; Byrne et al., 2020). The profiles for deflection and resisting moment due to side shear at different embedment lengths for sandy and clayey sites are shown in Fig. 5.7 and Fig. 5.8, respectively. The transition from rigid to flexural shaft response shown in these plots also substantiates the mobilization of the larger resisting moment and tip displacement typically observed in rigid shaft responses. The flexible response of the pile causing smaller tip displacement at both

materials generates smaller m_r near the pile tip locations. For sandy material, the m_r profiles at 9 m and 10.57 m embedment depth for a 3 m diameter pile appear to be identical [Fig. 5.7b]. This indicates the m_r to be mobilized at the ultimate resistance value, which is given by the linear, perfectly plastic API Sand t-z model. The m_r profile diagram in clayey soil in Fig. 5.8b shows higher mobilization of m_r near the ground surface and along the overall pile length compared to the diagram for sandy material. In summary, these results suggest that the diameter effect tends to be more significant in clayey soil, compared to sandy soil.

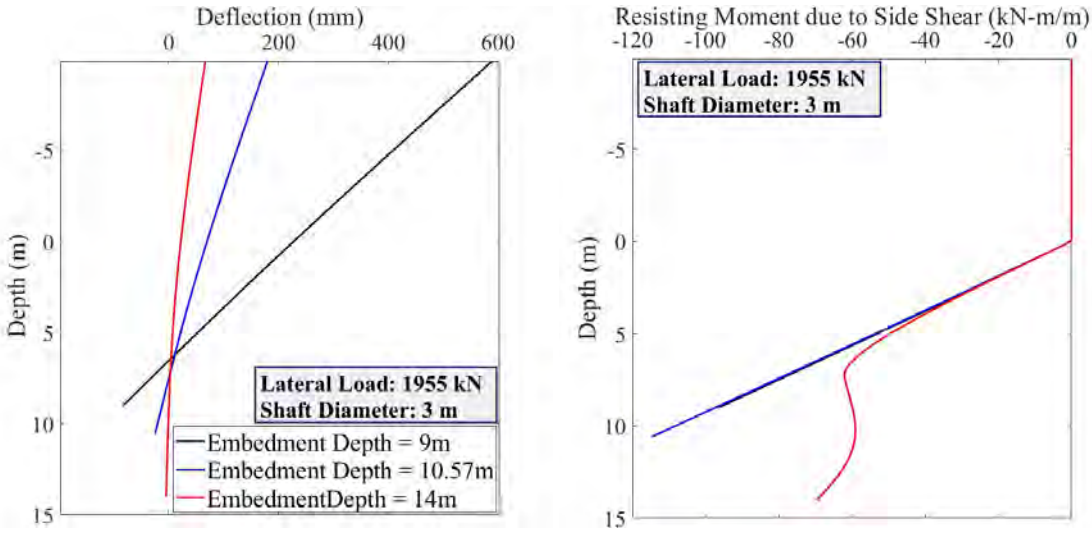

Figure 5.7: Transition from rigid to flexible lateral responses shown in the (a) deflection profiles and (b) resisting moment due to side shear profiles with increasing embedment depth of test pile DL2.

5.5.3 Effect of Axial Load

The effect of increasing the axial load on different additional lateral resistance components was investigated, and the results are shown in Fig. 5.9 and Fig. 5.10 for sandy and clayey sites, respectively. The percent reduction plots are shown

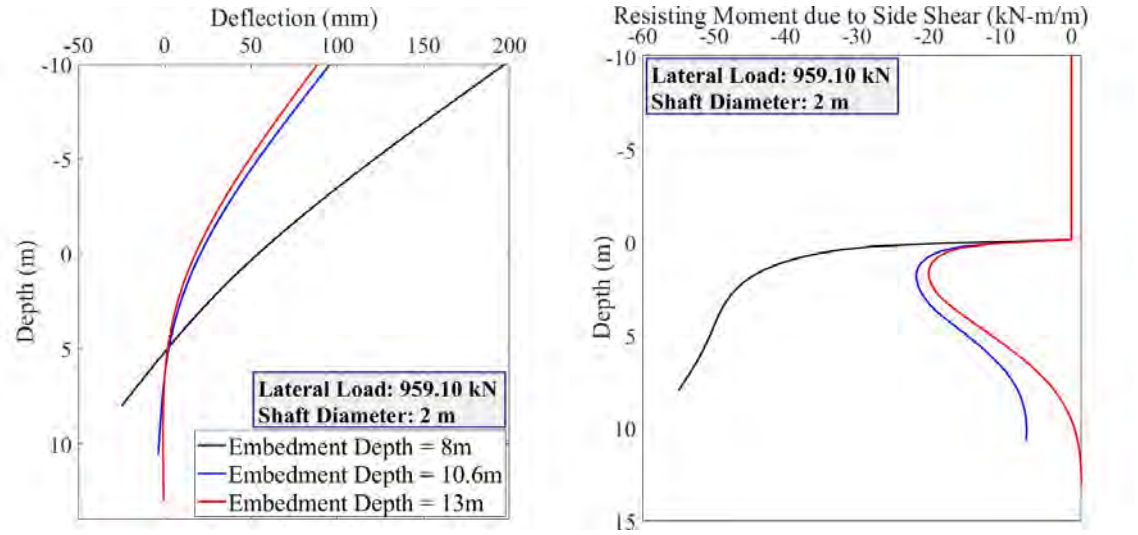

(a) (b)

Figure 5.8: Transition from rigid to flexible lateral responses shown in the (a) deflection profiles and (b) resisting moment due to side shear profiles with increasing embedment depth of test pile CL2.

for 2 m and 10 m pile diameters at both sites. In contrast to the observation for other parameters, the results show that higher axial load causes larger percent reductions in head displacement for the addition of tip moment resistance. In sandy material, the addition of side shear resistance did not cause significant reductions in head displacement beyond 3320 kN of axial load for 2 m pile diameter [Fig. 5.9a]. Increasing the pile diameter along with axial load in sandy material resulted in a reasonable amount of diameter effect compared to conventional *p-y* analysis. For 10 m pile diameter, 19.3%, 53.6%, and 65.4% reduction in head displacement were obtained at 7000 kN axial load after the inclusion of tip moment, tip shear, and side shear resistance, respectively [Fig. 5.9b].

The similar results shown in Fig. 5.10 for clay material indicate larger impacts from the axial load on diameter effect compared to sandy material. A significant percent reduction in displacement coming from the tip moment resistance with increasing pile diameter can be seen. As shown in Fig. 5.10, including tip moment

resistance to the conventional *p-y* model at 3000 kN axial load resulted in 1.4% and 35.7% reduction in head displacement for 2 m and 10 m diameter, respectively. At the same axial load, the subsequent inclusion of tip shear resistance resulted in additional 7.2% and 23.7% reduction in head displacement for 2m and 10m diameter, respectively.

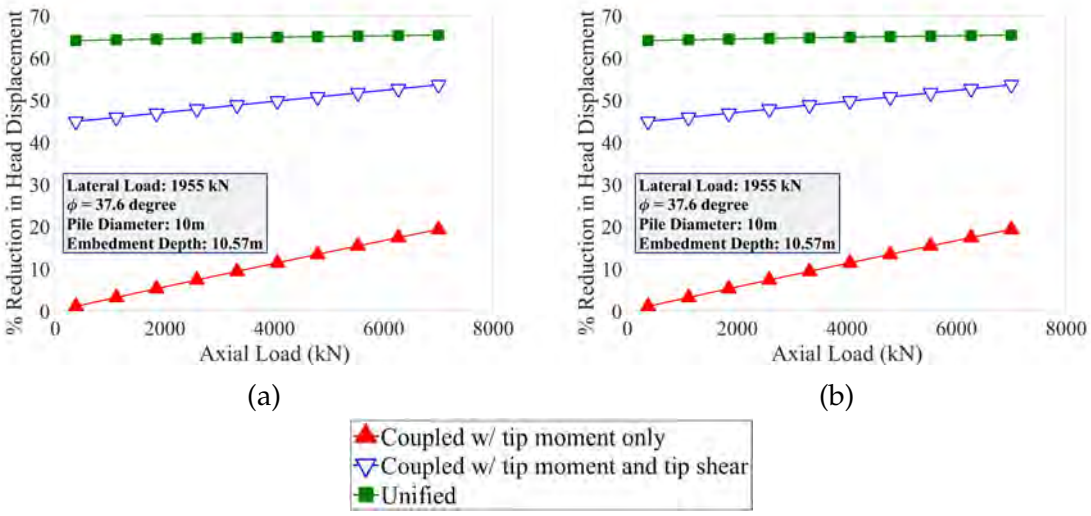

Figure 5.9: Percent reduction in shaft head displacement due to inclusion of different lateral resistance components with increasing applied axial load for (a) 2 m and (b) 10 m diameter of test pile DL2.

5.5.4 Comparison of Lateral Resistance Models for Sand and Clay

To understand the mechanism of added lateral resistance models in sand and clay, comparisons of *t-z* and tip shear resistance models for sand and clay material along with their variation with different parameters are shown in Fig. 5.11 and Fig. 5.12. The API sand *t-z* model shown in Fig. 5.11a is diameter independent and varies slightly with increasing angle of friction (ϕ) values. Based on previous studies on early *t-z* model formulation for sand, vertical displacement to cause maximum mobilization of side shear resistance is independent of pile diameter, particularly

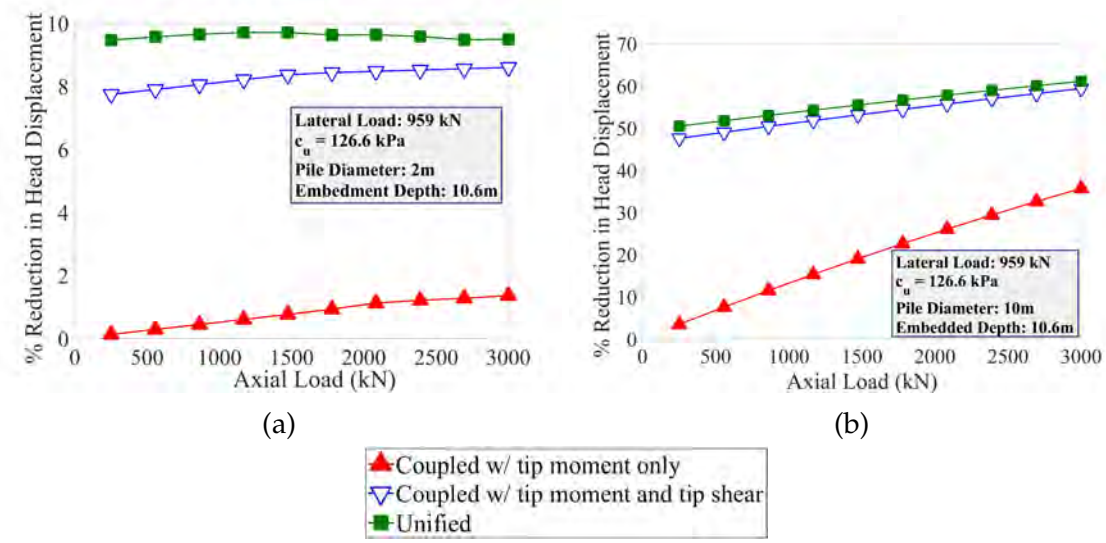

Figure 5.10: Percent reduction in shaft head displacement due to inclusion of different lateral resistance components with increasing applied axial load for (a) 2 m and (b) 10 m diameter of test pile CL2.

when the diameter is larger than 0.305 m (12 inches) (Vijivergiya, 1977; Mosher, 1984). On the other hand, API clay *t*-*z* model shows significant variation with cohesive strength (c_u) and pile diameter [Fig. 5.11b]. A similar observation can be made when comparing the tip shear resistance model given by Vallabhan and Alikhanlou (1982) for sand and clay material (Fig. 5.12).

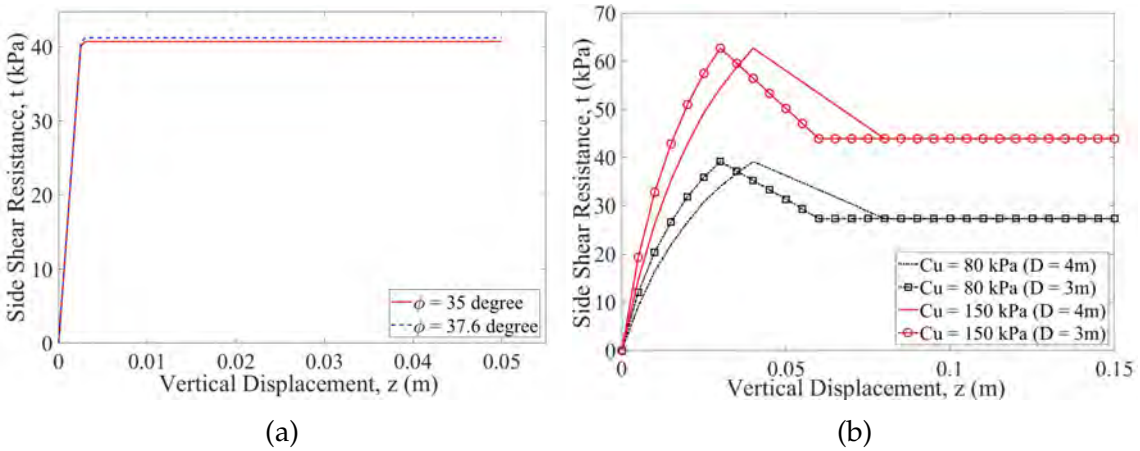

Figure 5.11: Comparison between API *t*-*z* models for (a) sand and (b) clay material.

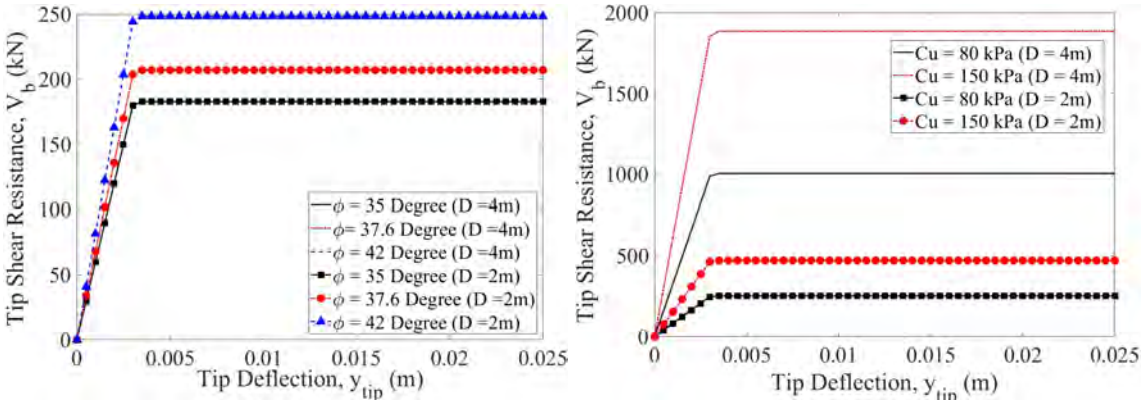

(a) (b)

Figure 5.12: Comparison between tip shear resistance models by Vallabhan and Alikhanlou (1982) for (a) sand and (b) clay material.

5.6 Simulations of lateral load tests in clayey and sandy sites: Case studies

In this section, lateral load test simulations in sandy and clayey soil conditions in the context of two different load test programs are presented. The lateral load analyses in similar soil conditions are discussed in an attempt to complement the major findings from this study. The selected load test programs are: 1) the University of California, San Diego (UCSD) lateral load tests in weakly cemented sand (Juirnarongrit and Ashford, 2004) and 2) Incheon Bridge cyclic lateral load tests in marine clay (Jeong et al., 2007).

5.6.1 UCSD lateral load tests

As part of a research project to derive a *p-y* model for weakly cemented sand commonly encountered in site locations along the southern California coast, instrumented full-scale lateral load tests were performed on cast-in-drilled-hole (CIDH)

piles with diameters ranging from 0.4 to 1.2 m (Juirnarongrit and Ashford, 2004). The lateral load tests were carried out at the University of California, San Diego (UCSD) test site. As obtaining undisturbed samples was problematic due to the weakly cemented nature of the soil, performing laboratory tests were not possible. The common soil properties such as unit weight and angle of friction were obtained by using correlations from the SPT-N values. Two boreholes were drilled to the depths of 20 m and 24 m as part of the site investigation, and no groundwater table was reported. The sandy soil in the test site was reported to be medium dense to very dense, and the average unit weight was approximated as 20 kN/m^3. The angle of friction was approximated as 42°in the first 6 m depth, and 45°in the underlying bottom layers. Based on direct shear test results from past investigations, Juirnarongrit and Ashford (2004) assumed cohesive strength (c_u) to be 20 kPa in the test site location. (Juirnarongrit, 2002).

The 0.6 m diameter and 1.2 m diameter CIDH piles from the UCSD load test program were considered for this study. Both test piles had an embedment depth of 12 m. The CIDH piles were subjected to both static and cyclic lateral loading. The back-calculated *p-y* relations reported by Juirnarongrit and Ashford (2004) were used to define lateral soil resistance of weakly cemented sand layers. As for the axial side resistance, API recommended (API, 2014) *t-z* model was used. The tip shear resistance model by Vallabhan and Alikhanlou (1982) and tip moment resistance model by (Bhuiyan et al., 2022) were implemented to simulate tip resistances in the numerical analyses. The measured and predicted load-displacement plots after performing both uncoupled and unified *p-y* analyses are presented in Fig. 5.13. The predicted load-displacement responses from the original study by Juirnarongrit and Ashford (2004) are also shown. While all the predicted responses presented in Fig. 5.13 show good agreement with measured data for both lateral load tests,

performing unified *p-y* analyses resulted in almost identical responses in both cases. Including additional lateral resistance components in unified *p-y* analyses caused 0.37% and 0.72% maximum reduction in pile head displacements relative to the prediction from uncoupled analyses, for the 0.6 m and 1.2 m diameter pile, respectively. In the original lateral load tests, the yielding of steel pile section took place before the mobilization to ultimate lateral soil resistance, causing the back-calculated *p-y* curves for the weakly cemented sand to appear to be independent of the pile diameter (Juirnarongrit and Ashford, 2004). The extensive numerical prediction of UCSD lateral load tests presented in this study also indicate less diameter effect of sand material in terms of missing lateral resistance components in the original test condition.

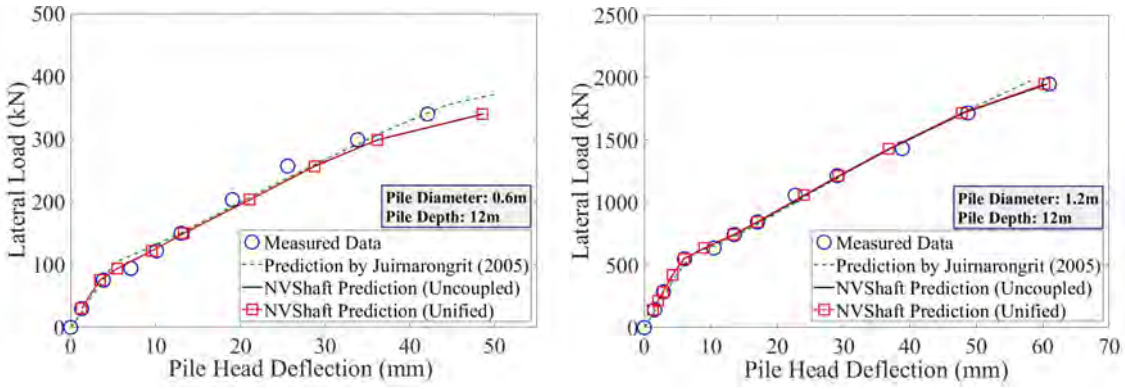

(a) (b)

Figure 5.13: Comparison of measured and NVShaft-predicted load-displacement response, for: (a) 0.6 m diameter and (b) 1.2 m diameter CIDH piles from the UCSD lateral load tests.

5.6.2 Incheon Bridge cyclic lateral load tests

To quantify the lateral soil resistance of marine clay, lateral load tests were performed on three small-scale driven piles (LTP-1, LTP-2, LTP-3) and a full-scale

drilled shaft (LTP-4) (Jeong et al., 2007). The load test program was carried out as part of the 11.66 km long Incheon bridge construction project, to connect Songdo city to Incheon International Airport in South Korea. The driven steel pile had 1.016 m of outer diameter, 25.6 m of embedment depth, 16 mm of wall thickness, and pile heads located 1 m above the ground surface. The drilled shaft was constructed with 2.4 m diameter, 44.3 m of embedment depth, and the shaft head located 9.1 m above the ground surface. Subsurface exploration included sampling from three borings near the test locations, recording standard penetration test (SPT) blow counts, and many other in-site tests. The soil profiles in the site locations revealed the formation of marine clay with thicknesses between 16 m to 19 m near the ground surface. The clay layers are underlain with silt, sand, weathered soil, weathered rock, and soft rock material. To characterize the soil and rock material properties at the test locations, triaxial tests, consolidation tests, unconfined compression tests, and basic soil classification tests were carried out. Summary of characterized soil profiles along with the chosen *p-y* and *t-z* models used in numerical modeling for test pile LTP-1, and test shaft LTP-4 are shown in Table 5.6 and Table 5.7, respectively. A site-specified, experimental *p-y* model for marine clay (Jeong et al., 2011) has been developed based on lateral load test results, which is also implemented in NVShaft analyses in this study. For the underlying sand and silt material, the API (API, 2014) recommended *p-y* model given by O'Neill and Murchison (1983) was implemented. The axial side resistances of the soil layers were modeled using the API sand and clay *t-z* models (API, 2014). For the weathered soft rock material located near the pile and shaft tip locations, the *p-y* model for weak rock given by Reese (1997), and the *t-z* model for Florida limestone proposed by McVay and Niraula (2004) were used in the numerical models. The tip shear and tip moment lateral resistances were simulated by adopting the models proposed by McVay et al. (2008) and Bhuiyan

et al. (2022), respectively.

Table 5.6: Characterized soil profile for test pile LTP-1 from Incheon Bridge project.

Depth (m)	*p-y* Model	*t-z* Model	ϕ (Degree)	c_u (kPa)	q_u (MPa)	E_s (MPa)
0 - 3.5	Marine Clay	API Clay	-	18	-	10.17
3.5 - 16.5	Marine Clay	API Clay	-	40	-	22.6
16.5 - 20.9	Marine Clay	API Clay	-	60	-	27
20.9 - 25.5	API Sand	API Sand	34	-	-	-
25.5 - 25.6	Weak Rock	Florida Limestone	-	-	25	-

Table 5.7: Characterized soil profile for test shaft LTP-4 from Incheon Bridge project.

Depth (m)	*p-y* Model	*t-z* Model	ϕ (Degree)	c_u (kPa)	q_u (MPa)	E_s (MPa)
0 - 3.5	Marine Clay	API Clay	-	18	10.17	-
3.5 - 18.4	Marine Clay	API Clay	-	40	22.6	-
18.4 - 30.3	API Sand	API Sand	34	-	-	-
30.3 - 37.9	Weak Rock	Florida Limestone	-	-	6	-
37.9 - 44.3	Weak Rock	Florida Limestone	-	-	25	-

The lateral load tests were performed following the ASTM D-3966 standard testing procedure (on Soil and Rock, 2007). Cyclic loads were applied in increments from reaction piles using the oil pressure jack as the loading device. As reported in Jeong et al. (2007), the maximum applied lateral loads for test pile LTP-1, and test shaft LTP-4 were 900 kN and 1000 kN, respectively. It was mentioned that the drilled shaft LTP-4 was subjected to a smaller lateral load compared to its design capacity, as it was intended to serve as one of the bridge foundations. The lateral responses were measured by using strain gauges, inclinometers, and LVDTs. The measured and the NVShaft predicted load-displacement responses for LTP-1 and LTP-4, highlighting both the conventional and the unified *p-y* analyses are shown in Fig. 5.14. A good match between predicted and measured responses can be observed for both lateral load tests. Performing unified *p-y* analysis caused slight improvement to numerical

predictions compared to uncoupled (conventional) *p-y* analyses. For test pile LTP-1, performing unified *p-y* analysis caused 2.95% reduction in pile head displacement compared to conventional predicted response at maximum applied lateral load [Fig. 5.14a]. The linear nature of load-displacement response for LTP-4, shown in Fig. 5.14b indicates the elastic lateral response of the shaft. This explains the relatively smaller 1.06% reduction in shaft head displacement after performing the unified *p-y* analysis, despite the shaft having a larger diameter (2.4 m) compared to test pile LTP-1.

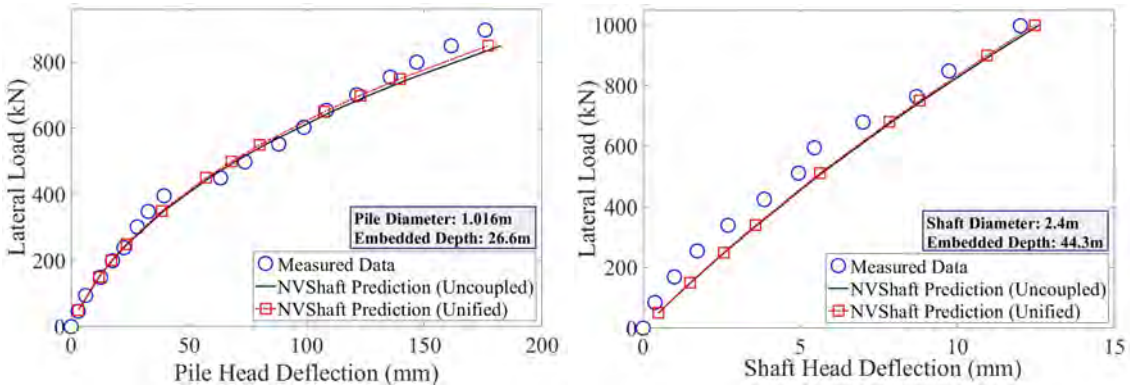

(a) (b)

Figure 5.14: Comparison of measured and NVShaft-predicted load-displacement response, for: (a) test pile LTP-1 and (b) test shaft LTP-4 from the Incheon Bridge cyclic lateral load tests.

5.6.3 Diameter effects in marine clay and weakly cemented sand

The 1.2 m diameter CIDH pile from the UCSD lateral load tests and test shaft LTP-4 from the Incheon Bridge cyclic lateral load tests were considered for numerical simulations to conduct a more in-depth investigation on diameter effects in these test conditions. In both cases, 500 kN of the lateral load was applied in the numerical models as boundary conditions. Contributions from side shear, tip

shear, and tip moment resistances in terms of increasing diameter, as shown as percent reductions in ground line displacements, in weakly cemented sand and marine clay are presented in Fig. 5.15 and Fig. 5.16, respectively. Corresponding ground line displacements at different diameters and considered lateral resistance components are also shown in these figures. Since the test pile and shaft both had small tip displacements and tip rotations and exhibited flexible lateral responses, the effects of tip shear and tip moment resistances on the overall lateral responses were negligible. By observing Fig. 5.15b and Fig. 5.16b, it can be concluded that the inclusion of side shear-induced resistance caused the majority of reductions in ground line displacements in both soil conditions. Performing unified *p-y* analysis considering the site condition from Incheon Bridge cyclic lateral load tests in marine clay appear to cause softer lateral response and higher percent reduction in ground line displacement at the minimum considered diameter of 1.2 m, compared to similar analyses in weakly cemented sand based on UCSD lateral load tests. Considering all the additional lateral resistances in *p-y* analysis of 1.2 m of pile diameter in weakly cemented sand resulted in 3.8 mm of ground line displacement and 0.36% reduction in ground line displacement (Fig. 5.15). At the same shaft diameter and lateral loading, performing unified *p-y* analysis at marine clay soil condition resulted in a relatively softer response, with 30.4 mm of ground line displacement and 1.9% reduction in ground line displacement (Fig. 5.16). At the 8 m of diameter, obtained ground line displacements after performing unified *p-y* analyses in weakly cemented sand and marine clay are 0.21 mm [Fig. 5.15a] and 0.52 mm [Fig. 5.16a], respectively. In this regard, the diameter effect is more significant in weakly cemented sand compared to marine clay, with 24.7% and 4.9% reduction in ground line displacement, as seen in Fig. 5.15b and Fig. 5.16b, respectively.

The difference in diameter effect originating from the inclusion of mobilized

side shear-induced resistance in weakly cemented sand and marine clay can be further explained by the resisting moment due to side shear (m_r) profile diagrams, as shown in Fig. 5.17. The variation in m_r profile diagrams, obtained from unified *p-y* simulations, at 2.4 m, 6 m, and 8 m diameters in weakly cemented sand and marine clay is presented. The characterized soil profile summarized in Table 5.7 indicates the presence of weathered soft rock material at 30.3 m to 44.3 m depth locations, which explains the corresponding high m_r values as seen in Fig. 5.17b. Based on past studies, a wedge-type soil flow mechanism is typically observed at shallower depths for laterally loaded flexible piles, which causes a significant impact on the overall lateral pile response (Hong et al., 2017; Wang et al., 2020). In accordance with the past observations, the lateral responses in the site condition from the Incheon Bridge project are mostly affected by the overlying marine clay material, where little variation in m_r is observed with a subsequent increase in shaft diameter from 2.4 m to 8 m. On the contrary, the dense weakly cemented sand material caused a significant increase in m_r along the pile embedded depth, when pile diameter is increased in the same manner [Fig. 5.17a]. Although performing unified *p-y* analysis resulted in more diameter effects in marine clay considering the original test conditions, the effect of further mobilization of side shear resistance becomes more prominent in weakly cemented sand at larger pile diameters (Fig. 5.17). As reported in the original study, the weakly cemented sand had a unit weight of 20 kN/m^3 and the angle of friction varied between 42°and 45°(Juirnarongrit and Ashford, 2004). As the weakly cemented sand was stiffer and denser compared to marine clay, a more diameter effect is observed beyond the scope of the test conditions.

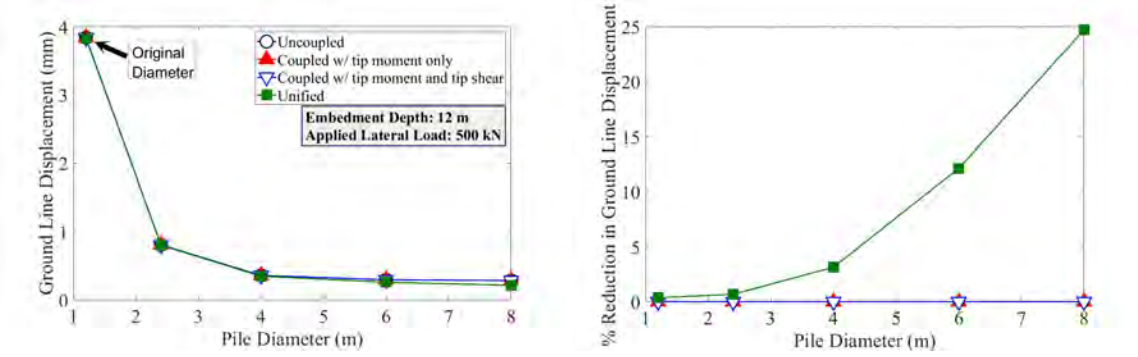

(a) (b)

Figure 5.15: Investigation of diameter effect in weakly cemented sand based on site condition of 1.2 m diameter CIDH pile from the UCSD lateral load tests, as represented by variation of: (a) ground line displacement and (b) percent reduction in ground line displacement with increasing pile diameter.

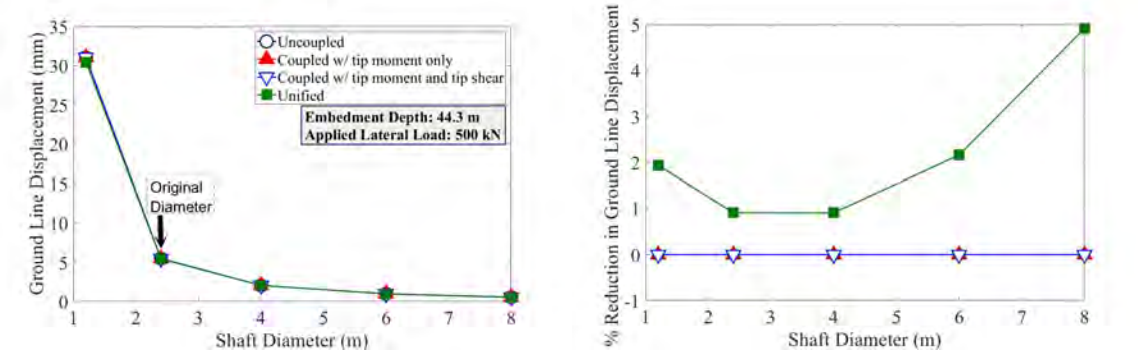

(a) (b)

Figure 5.16: Investigation of diameter effect in marine clay based on site condition of test shaft LTP-4 from the Incheon Bridge cyclic lateral load tests, as represented by variation of: (a) ground line displacement and (b) percent reduction in ground line displacement with increasing shaft diameter.

5.7 Conclusions

The goal of this study was to perform a parametric investigation on diameter effect which is commonly observed in the conventional numerical *p-y* model of laterally loaded large diameter drilled shafts. Variation in common soil and shaft properties such as pile diameter, embedment depth, soil strength parameters (angle of friction and cohesive strength) and applied axial load influences the added lateral resistance

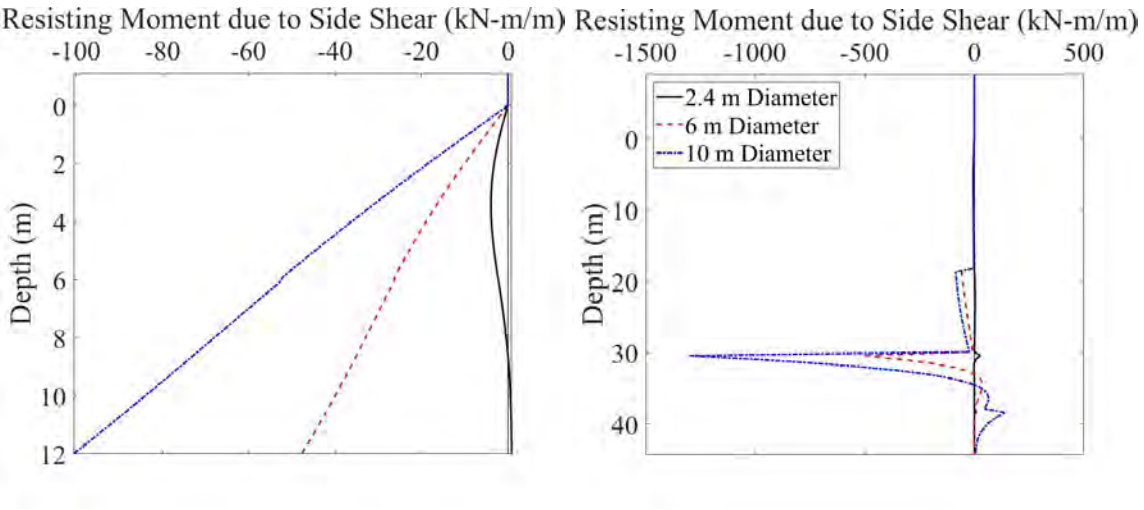

(a) (b)

Figure 5.17: Variation in the resisting moment due to side shear (m_r) profiles with increasing diameter for: (a) 1.2 m diameter CIDH pile from the UCSD lateral load tests and (b) test shaft LTP-4 from the Incheon Bridge cyclic lateral load tests.

mechanisms in the numerical model, which was observed in the parametric study. The investigation was done in the context of two baseline lateral load test program performed as part of Pile Soil Analysis (PISA) project in Europe. The soil and shaft properties from the test pile DL2, from the sandy site at Dunkirk, and CL2 from the clayey site at Cowden were utilized to form two reference numerical models.

In general, it was observed that increasing soil strength parameters and embedment depth at the constant lateral load and pile diameter resulted in stiffer response and less diameter effect. The transition from rigid to flexural pile response was observed at both sites when embedment depth was increased in the parametric study. It was observed that larger mobilized m_r, tip displacement and tip rotation at rigid lateral response caused significant diameter effect. Increasing both embedment depth and pile diameter beyond 6 m did not cause significant decrease in percent reduction in head displacement in sandy soil. In clayey soil, increasing pile diameter from 2 m to 10 m resulted in significant increase in percent reduction from

28.8% to 73% at considered minimum 8 m of embedment depth. Increasing applied axial load caused significant increase in tip shear and tip moment resistances in numerical model, resulting in more diameter effect in both soil conditions. In sandy soil, 19.3% and 53.6% reduction in pile head displacement was obtained at 7000 kN axial load and 10 m diameter when tip moment and tip shear resistances were included in the *p-y* model, respectively. In clayey soil, inclusion of tip moment resistance at 3000 kN axial load caused 1.4% and 35.7% reduction in head displacement for 2 m and 10 m diameter, respectively.

Based on the results from the parametric study, it can be concluded that clayey soil produced more diameter effect compared to sandy soil when additional lateral resistances were added to the conventional *p-y* model, in the context of the PISA load test program. This observation was substantiated by the comparison of both *t-z* and tip shear resistance models for sand and clay. These observations indicate that clayey soil requires more sophistication in lateral numerical modeling compared to sandy soil, and the lateral response relies heavily on the proper representation of soil-pile interactions.

Two additional case studies involving NVShaft simulations of UCSD lateral load tests in weakly cemented sand and Incheon Bridge lateral load tests in marine clay resulted in 0.72% and 2.95% maximum reductions in head displacements, respectively when unified *p-y* analyses were performed. Although the marine clay material exhibited a more diameter effect in the original test conditions, further investigation revealed a relatively more diameter effect in weakly cemented sand at larger diameters, as the sand material at the UCSD test site was stiffer and denser in comparison.

5.8 References

AASHTO (2020). *AASHTO LRFD Bridge Design Specifications*. AASHTO, Washington, D.C.

API (2014). *API Recommended Practice 2A-WSD - Planning, Designing, and Constructing Fixed Offshore Platforms – Working Stress Design*. API.

Ashour, M. and Helal, A. (2014). Contribution of vertical skin friction to the lateral resistance of large-diameter shafts. *Journal of Bridge Engineering*, 19(2):289–302.

Bhuiyan, F. M., Motamed, R., Siddharthan, R. V., and Sanders, D. H. (2022). Evaluation of a unified *p-y* method for lateral analysis of large-diameter drilled shafts using NVShaft. *Transportation Geotechnics*. Accepted.

Bhuiyan, F. M., Siddharthan, R. V., Motamed, R., and Sanders, D. H. (2020). Evaluation of a new *p-y* analysis tool for lateral analysis of drilled shafts using load tests in Nevada. In *DFI 45th Annual Conference on Deep Foundations*, pages 303–312. October 13-16.

Bhuiyan, F. M., Toth, J., Siddharthan, R. V., and Motamed, R. (2021). Evaluation of existing *t-z* models for caliche based on numerical analysis of bi-directional load tests using NVShaft. In *DFI 46th Annual Conference on Deep Foundations*, pages 21–31, Las Vegas, Nevada. October 12-15.

Bhushan, K. and Scheyhing, C. (2002). Lateral load tests on drilled piers in San Diego area residual and formational soils. In *Proceedings 27th annual conference on deep foundations, San Diego, CA*.

BSI (2019). *FB-MultiPier user's manual, v. 5.5*. Bridge Software Institute, University of Florida, Gainesville, FL.

Byrne, B., McAdam, R., Burd, H., Houlsby, G., Martin, C., Zdravkovic, L., Taborda, D., Potts, D., Jardine, R., Sideri, M., et al. (2015). New design methods for large diameter piles under lateral loading for offshore wind applications. In *3rd International Symposium on Frontiers in Offshore Geotechnics (ISFOG 2015), Oslo, Norway, June*, pages 10–12.

Byrne, B. W., McAdam, R. A., Burd, H. J., Beuckelaers, W. J., Gavin, K. G., Houlsby, G. T., Igoe, D. J., Jardine, R. J., Martin, C. M., Muir Wood, A., et al. (2020). Monotonic laterally loaded pile testing in a stiff glacial clay till at cowden. *Géotechnique*, 70(11):970–985.

Byrne, B. W., McAdam, R. A., Burd, H. J., Houlsby, G. T., Martin, C. M., Beuckelaers, W. J. P., Zdravkovic, L., Taborda, D., Potts, D., Jardine, R., et al. (2017). Pisa: new design methods for offshore wind turbine monopiles. In *Offshore Site Investigation Geotechnics 8th International Conference Proceeding*, volume 142, pages 142–161. Society for Underwater Technology.

Chow, F. (1997). Investigations into displacement pile behaviour for offshore foundations. *Ph. D Thesis, Univ. of London (Imperial College)*.

Finn, W. L. and Dowling, J. (2015). Modelling effects of pile diameter. *Canadian Geotechnical Journal*, 53(1):173–178.

Fu, D., Zhang, Y., Aamodt, K. K., and Yan, Y. (2020). A multi-spring model for monopile analysis in soft clays. *Marine Structures*, 72:102768.

Gupta, B. K. and Basu, D. (2016). Analysis of laterally loaded rigid monopiles and poles in multilayered linearly varying soil. *Computers and Geotechnics*, 72:114–125.

Hong, Y., He, B., Wang, L., Wang, Z., Ng, C. W. W., and Mašín, D. (2017). Cyclic

lateral response and failure mechanisms of semi-rigid pile in soft clay: centrifuge tests and numerical modelling. *Canadian Geotechnical Journal*, 54(6):806–824.

Isenhower, W. M., Wang, S.-T., and Vasquez, L. G. (2017). *User's manual for LPile 2018*. Ensoft, Austin, TX.

Jardine, R. (1985). *Investigations of pile-soil behaviour, with special reference to the foundations of offshore structures*. PhD thesis, Imperial College London (University of London).

Jeong, S., Kim, Y., and Kim, J. (2011). Influence on lateral rigidity of offshore piles using proposed p–y curves. *Ocean engineering*, 38(2-3):397–408.

Jeong, S., Kim, Y., Kim, J., and Shin, S. (2007). Cyclic lateral load tests of offshore large diameter piles of incheon bridge in marine clay. In *The Seventeenth International Offshore and Polar Engineering Conference*. OnePetro.

Juirnarongrit, T. (2002). *Effect of diameter on the behavior of laterally loaded piles in weakly cemented sand*. PhD thesis, University of California, San Diego.

Juirnarongrit, T. and Ashford, S. A. (2004). Lateral load behavior of cast-in-drilled-hole piles in weakly cemented sand. *Transportation research record*, 1868(1):190–198.

McAdam, R. A., Byrne, B. W., Houlsby, G. T., Beuckelaers, W. J., Burd, H. J., Gavin, K. G., Igoe, D. J., Jardine, R. J., Martin, C. M., Muir Wood, A., et al. (2020). Monotonic laterally loaded pile testing in a dense marine sand at Dunkirk. *Géotechnique*, 70(11):986–998.

McVay, M. and Niraula, L. (2004). Development of PY curves for large diameter piles/drilled shafts in limestone for FBPIER. Technical Report Final Report, University of Florida.

McVay, M. C. et al. (2008). Distribution of end bearing, tip shear and rotation on drilled shafts with combined loading in Florida limestone. Technical Report Final Report.

Mosher, R. L. (1984). Load-transfer criteria for numerical analysis of axially loaded piles in sand. part 1. load-transfer criteria. Technical report, Army Engineer Waterways Experiment Station Vicksburg MS.

Norris, G. (1986). Theoretically based bef laterally loaded pile analysis. In *Proceedings of the 3rd international conference on numerical methods in offshore piling*, pages 361–386. Navtes.

on Soil, A. C. D.-. and Rock (2007). *Standard test methods for deep foundations under lateral load*. ASTM International.

O'Neill, M. and Gazioglu, S. (1984). Integrated formulation of py relationships in clays. *A Report to the American Petroleum Institute, Report PRAC-82-41-2, University of Houston*.

O'Neill, M. W. and Murchison, J. M. (1983). *An evaluation of py relationships in sands*. University of Houston.

Powell, J., Butcher, A., et al. (2003). Characterisation of a glacial clay till at cowden, humberside. *Characterisation and engineering properties of natural soils, AA Balkema, Lisse, the Netherlands*, pages 983–1020.

Reese, L. C. (1997). Analysis of laterally loaded piles in weak rock. *Journal of Geotechnical and Geoenvironmental engineering*, 123(11):1010–1017.

Reese, L. C., Cox, W. R., and Koop, F. D. (1974). Analysis of laterally loaded piles in sand. *Offshore technology in civil engineering hall of fame papers from the early years*, pages pp. 95–105.

Rinne, E., Thompson, J., and Vanderpool, W. (1996). *I-15/US 95 load test program, Las Vegas, Nevada*. Kleinfelder, Inc., Las Vegas, Nevada.

Sim, W. W., Aghakouchak, A., and Jardine, R. J. (2013). Cyclic triaxial tests to aid offshore pile analysis and design. *Proceedings of the Institution of Civil Engineers-Geotechnical Engineering*, 166(2):111–121.

Taghavi, A., McVay, M., Niraula, L., Davidson, M., and Patil, A. (2020). Axial and lateral resistance coupling in the analysis of large-diameter drilled shafts. *Engineering Structures*, 206:110160.

Vallabhan, C. and Alikhanlou, F. (1982). Short rigid piers in clays. *Journal of the Geotechnical Engineering Division*, 108(10):1255–1272.

Vijivergiya, V. (1977). Load-movement characteristics of piles. In *4th Symp. of Waterway, Port, Coastal and Occean Div., ASCE*, volume 2, pages 269–284.

Wang, L., Lai, Y., Hong, Y., and Mašín, D. (2020). A unified lateral soil reaction model for monopiles in soft clay considering various length-to-diameter (l/d) ratios. *Ocean Engineering*, 212:107492.

Woodward, R. J., Gardner, W. S., and Greer, D. M. (1972). *Drilled pier foundations*. McGraw-Hill.

Wu, G. (2006). VERSAT-P3D: A computer program for dynamic 3-dimensional finite element analysis of single piles and pile groups. *Wutec Geotechnical International, Vancouver, Canada*.

Zdravković, L., Jardine, R. J., Taborda, D. M., Abadias, D., Burd, H. J., Byrne, B. W., Gavin, K. G., Houlsby, G. T., Igoe, D. J., Liu, T., et al. (2020). Ground characterisation for PISA pile testing and analysis. *Géotechnique*, 70(11):945–960.

Zhu, B., Sun, Y., Chen, R., Guo, W., and Yang, Y. (2015). Experimental and analytical models of laterally loaded rigid monopiles with hardening p–y curves. *Journal of Waterway, Port, Coastal, and Ocean Engineering*, 141(6):04015007.

CHAPTER 6
SUMMARY AND CONCLUSIONS

6.1 Concluding Remarks

This study introduces a MATLAB-based, finite-difference program, NVShaft, which is capable of performing numerical axial and lateral load analyses. The program was developed as a verified and validated tool to evaluate a unified *p-y* method proposed in this study. Although *p-y* method has been widely implemented in engineering projects since the early development of modern computer programs, recent studies suggest the method typically yields unreliable lateral responses for larger diameter drilled shafts (Bhushan and Scheyhing, 2002; McVay and Niraula, 2004; Ashour and Helal, 2014; Taghavi et al., 2020). The limitation of *p-y* analysis due to larger shaft diameter is more popularly known as the 'pile diameter effect' (Finn and Dowling, 2015). The proposed unified *p-y* method can consider the resisting moment due to mobilized side shear (m_r), tip shear (v_b), and tip moment (m_b) resistances, which are typically ignored in the conventional Winkler's spring model. A simplified tip moment resistance model for the circular shaft section is also proposed in this study, to be implemented in NVShaft as part of the unified *p-y* analysis.

The verification of NVShaft in terms of performing conventional *p-y* and *t-z* analysis was done by comparing the outputs obtained from similar analyses using commercially available programs. To validate the numerical capabilities of NVShaft, lateral load test data were collected and compiled from past studies. Special focus was given to lateral load tests conducted on larger diameter shafts in Nevada's local cemented soil condition. Performing lateral load analysis on both smaller and

larger diameter shafts in a variety of subsurface conditions using the capability of NVShaft presented an opportunity to understand more about the diameter effect, and to validate the proposed unified *p-y* method. A more in-depth parametric investigation of the diameter effect in clayey and sandy soil is also presented, by analyzing the lateral load test program from the PISA project in Europe (Byrne et al., 2015). The soil strength parameters such as cohesive strength and angle of friction, shaft embedment depth and applied axial load along with variation in pile diameter influencing various lateral resistance mechanisms were investigated.

As the inclusion of mobilized side shear resistance in the unified *p-y* analysis requires calculation from the defined *t-z* models, the ability to perform axial load (*t-z*) analysis has been made available in NVShaft as a complimentary feature. Apart from conventional axial load tests, NVShaft can also perform bi-directional static load test simulations. Axial load tests simulations based on I-15/US 95 reconstruction project (Rinne et al., 1996) and the Las Vegas City Center project (LOADTEST, 2005) in caliche-dominant sites are presented as validation examples to assess the capability of NVShaft to perform numerical *t-z* analysis. The evaluation of the soft rock (Asem and Gardoni, 2019) and Florida limestone (McVay and Niraula, 2004) *t-z* models to simulate side shear resistance of caliche is also presented in this regard.

The major outcomes of this research as presented in the previous chapters are summarized below:

- The validation example related to the conventional *p-y* simulations of the 2 ft and 8 ft diameter drilled shafts presented a good example of the complexity of lateral load response in Las Vegas subsurface condition. As reported in the original study by Rinne et al. (1996), the axial load tests were conducted

prior to lateral load tests, which caused instability in the surrounding soil near the ground surface and crushing of drilled shaft concrete near the O-cell locations, particularly for the 8 ft diameter shaft. The crushing of concrete can be clearly interpreted from the reported tensile strain development near the O-cell location for the 8 ft diameter shaft. Some deficiency in drilled shaft construction and monolithic behavior at the shaft-caliche interface (Sinnreich, 2012; Karakouzian et al., 2015) are some of the probable reasons behind these extreme measured responses. Predicted responses from numerical *p-y* simulations in NVShaft for both of the considered test shafts were in good agreement with the measured data at smaller load levels. At larger load levels, the predicted lateral responses were much stiffer compared to the measured data, particularly for the 8 ft diameter drilled shaft. The deviations from the measured data at larger load levels can be explained by the complexity related to axial load tests. A comparison of the maximum measured and predicted bending curvature for the 8 ft diameter shaft also indicates the cracked response of concrete during the lateral load test. For the 2 ft diameter shaft, the maximum predicted curvatures were in good agreement with the measured response at small to medium load levels. Since both of the test shafts were modeled based on nonlinear stiffness properties, this particular observation indicates that NVShaft is well capable of capturing the nonlinear drilled shaft response during *p-y* analysis.

- Evaluation of the soft rock and Florida limestone *t-z* models to simulate side shear resistance of caliche was done based on numerical simulations of axial load tests from the I-15/US 95 and the Las Vegas City Center projects. Both conventional top-loaded and bi-directional static load test simulations were carried out using NVShaft. The aforementioned severe observed responses

during axial loading for the 8 ft diameter shaft can explain the stiffer predicted response compared to the measured data, for both types of axial load test simulations. Good agreement compared to measured data was observed for the 2 ft diameter shaft from the I-15/US 95 load test program. In this case, the applied bi-directional load was too small to properly interpret the axial load capacity of the shaft. Assigning larger axial loads in the numerical *t-z* model enabled to approximate the axial load carrying capacity of the 2 ft diameter shaft. It was observed that the implementation of the *t-z* model for Florida limestone in the context of this load test generated a stiffer axial response, and higher axial load capacity, compared to the *t-z* model for soft rock material. For the 4 ft diameter shaft from the Las Vegas City Center project, using both of the considered *t-z* models also resulted in good agreement with respect to the measured response. For this particular test shaft, the equivalent top load-settlement curve obtained from measured bi-directional test data was softer compared to the predicted response. This observation can be explained by the location of the bi-directional cells relative to the nearby caliche layers, as reported in a study by Afsharhasani et al. (2020).

- Evaluation of unified *p-y* analysis was done by simulating lateral load tests from the I-15/US 95 and the PISA load test program. Inclusion of resisting moment due to side shear (m_r) in the Winkler's spring model for the 2.44 m (8 ft) diameter shaft caused significant improvement in the predicted response and 28.2% reduction in shaft head deflection compared to response obtained from uncoupled (conventional) *p-y* analysis. At a larger lateral load level, unified *p-y* analysis caused further deviation from the measured response for the same 8 ft diameter shaft, which can be attributed to the deficiency in drilled shaft response and extreme soil-shaft response during the prior

axial load testing. As for the two, 2 m diameter piles from the PISA load tests, performing unified *p-y* analyses resulted in 41.5% and 5.1% reduction in ground-level deflection in clayey and sandy soil conditions, respectively. Reasonable agreement with the measured data could be observed in both cases when unified *p-y* analyses were performed. Similar to the observations in the past studies, it was observed that the diameter effect in the considered subsurface conditions stems mostly from the resisting moment due to side shear, followed by the contribution from tip shear resistance.

- The parametric study performed in the context of the PISA load test program, and load test simulations based on two other projects indicate more diameter effect in rigid deep foundation embedded in stiffer soil material. The diameter effect due to changing soil and shaft parameters revealed that the contribution of additional lateral resistance mechanisms is less when the lateral response of the pile is stiffer. In clayey soil percent reduction in head displacement increased from 28.8% to 73% at 8 m of embedment depth, when diameter increased from 2 m to 10 m. A relatively less diameter effect is seen for sandy soil, as the percent reduction in head displacement remains almost constant when pile diameter is increased beyond 6 m along with increasing embedment depth. Increasing applied axial load appears to increase the contributions from tip shear and tip moment resistances. For example, considering tip shear and tip moment resistances in sandy soil in the context of the PISA load test program resulted in a 53.6% reduction in pile head displacement at 7000 kN of axial load and 10 m pile diameter. Numerical lateral analysis in clayey site condition resulted in 35.7% reduction in pile head displacement when only tip moment resistance is included in the conventional BNWF model, considering 3000 kN of axial load and 10 m diameter pile. Two case

studies based on Incheon Bridge and UCSD lateral load tests in this context also indicate more diameter effect in clay compared to sand material, in the original test conditions.

6.2 Research Impact

This research presents some key features and recommendations to improve the numerical axial and lateral load analysis, particularly in Nevada's cemented soil conditions. The proposed unified *p-y* method can be easily implemented in the developed finite-difference program, NVShaft. The program has the ability to assist in the design of drilled shafts with a modest collection of lateral and axial resistance models and features similar to other commercial programs. The unique features in NVShaft such as the capability of performing the unified *p-y* analysis and bi-directional static load test simulation are expected to improve the overall design of deep foundation in a variety of subsurface conditions. The program also has the option to perform lateral stability analysis, which involves the calculation of critical shaft length based on a series of *p-y* simulations. The lateral stability analysis has been included in NVShaft as a design aid and can be implemented using factored loading conditions based on the LRFD concept. The parametric investigation presented in this study based on the PISA load test program suggests considerable diameter effects in terms of different soil and shaft parameters, particularly for cohesive soil material. NVShaft was developed originally as a research tool to perform an in-depth investigation on the diameter effect and can be used in future research to improve the design and analysis of drilled shaft foundations.

6.3 Recommendations for Future Research

This study aims to improve the numerical axial and lateral load analysis, particularly in the context of larger diameter shafts and cemented soil conditions. The observation made in this research calls for further investigation and validation. Some recommendations to substantiate the major findings of this study in the form of prospective future research are outlined below,

- The added features and capabilities of the finite-difference program, NVShaft needs to be further verified and validated. Special focus should be given to validating the proposed unified *p-y* analysis, and the ability to perform bi-directional static load test simulation, as these are the two major unique features of the program. This can be done by comparing the predicted response obtained from other reliable finite-difference and finite-element programs, and measured field and centrifuge load test data. Some of the recently proposed *p-y* and *t-z* models (Juirnarongrit and Ashford, 2004; McVay and Niraula, 2004; McVay et al., 2008; Jeong et al., 2011; Asem and Gardoni, 2019) have been included in the program. The capabilities of these models in different site conditions should be validated based on numerical simulations of high-quality axial and lateral load tests.
- Parametric investigation on diameter effect relating to different test conditions should be performed. The diameter effect study presented in this paper focuses on sand, clay, and cemented soil prevalent in Las Vegas Valley. This has been done based on some limited numbers of considered load test programs. The recent increase in the use of larger shaft diameter in different site conditions presents the opportunity to further investigate the diameter effect, by exploiting numerical features available in NVShaft.

6.4 References

Afsharhasani, R., Karakouzian, M., and Farhangi, V. (2020). Effect of competent caliche layers on measuring the capacity of axially loaded drilled shafts using the osterberg test. *Applied Sciences*, 10(18):6169.

Asem, P. and Gardoni, P. (2019). A load-transfer function for the side resistance of drilled shafts in soft rock. *Soils and Foundations*, 59(5):1241–1259.

Ashour, M. and Helal, A. (2014). Contribution of vertical skin friction to the lateral resistance of large-diameter shafts. *Journal of Bridge Engineering*, 19(2):289–302.

Bhushan, K. and Scheyhing, C. (2002). Lateral load tests on drilled piers in San Diego area residual and formational soils. In *Proceedings 27th annual conference on deep foundations, San Diego, CA*.

Byrne, B., McAdam, R., Burd, H., Houlsby, G., Martin, C., Zdravkovic, L., Taborda, D., Potts, D., Jardine, R., Sideri, M., et al. (2015). New design methods for large diameter piles under lateral loading for offshore wind applications. In *3rd International Symposium on Frontiers in Offshore Geotechnics (ISFOG 2015), Oslo, Norway, June*, pages 10–12.

Finn, W. L. and Dowling, J. (2015). Modelling effects of pile diameter. *Canadian Geotechnical Journal*, 53(1):173–178.

Jeong, S., Kim, Y., and Kim, J. (2011). Influence on lateral rigidity of offshore piles using proposed p–y curves. *Ocean engineering*, 38(2-3):397–408.

Juirnarongrit, T. and Ashford, S. A. (2004). Lateral load behavior of cast-in-drilled-hole piles in weakly cemented sand. *Transportation research record*, 1868(1):190–198.

Karakouzian, M., Afsharhasani, R., and Kluzniak, B. (2015). Elastic analysis of drilled shaft foundations in soil profiles with intermediate caliche layers. In *IFCEE 2015*, pages 922–928.

LOADTEST (2005). Report on drilled shaft load testing (Osterberg method), City Center - test shaft 1, Las Vegas, NV. Project No. LT-9160-1, LOADTEST, Inc.

McVay, M. and Niraula, L. (2004). Development of PY curves for large diameter piles/drilled shafts in limestone for FBPIER. Technical Report Final Report.

McVay, M. C. et al. (2008). Distribution of end bearing, tip shear and rotation on drilled shafts with combined loading in Florida limestone. Technical Report Final Report.

Rinne, E., Thompson, J., and Vanderpool, W. (1996). *I-15/US 95 load test program, Las Vegas, Nevada*. Kleinfelder, Inc., Las Vegas, Nevada.

Sinnreich, J. (2012). Strain gage analysis for nonlinear pile stiffness. *Geotechnical Testing Journal*, 35(2):367–374.

Taghavi, A., McVay, M., Niraula, L., Davidson, M., and Patil, A. (2020). Axial and lateral resistance coupling in the analysis of large-diameter drilled shafts. *Engineering Structures*, 206:110160.

Appendices

APPENDIX A

USER'S MANUAL FOR NVSHAFT VERSION 1.0

A.1 Introduction

NVShaft is a MATLAB-based, finite-difference program developed to perform both numerical axial (*t-z*) and lateral (*p-y*) load analysis for a single pile or drilled shaft foundation. The major feature of the program is its capability to perform a proposed unified *p-y* analysis, considering the additional mobilized side shear-induced resisting moment (m_r), tip shear (v_b), and tip moment (m_b) resistances in the Winkler's spring model. These additional resistance mechanisms become more apparent for larger diameter rigid shafts with a small length to diameter ratio (L/D). The program can also perform numerical *t-z* analysis, including the capability to simulate bi-directional static load tests where the user can specify the location of the bi-direction cell or O-cell below pile/shaft head location. The finite-difference spring models for *p-y* and *t-z* analysis, representing different lateral and axial resistance springs is shown in Fig. A.1a and Fig. A.1b, respectively.

While performing the unified *p-y* and the *t-z* analysis, NVShaft tries to solve the Eq. 1.4 and Eq. 1.2, respectively. After a successful analysis, the program can generate graphical features for the presentation of results, and also offers additional features for special analyses related to lateral loading. The users can generate output files containing raw data in Microsoft Excel (.xlsx) format and also in pdf report format.

In total, the program features 19 *p-y*, 7 *t-z*, 5 end bearing (*q-z*), 2 tip shear (v_b-y_b), and 1 tip moment (m_b-θ_b) resistance models, and also allows the users to define their own models as user-input models. The built-in models can be used to simulate axial and lateral resistances for a wide range of soil and rock materials. In the

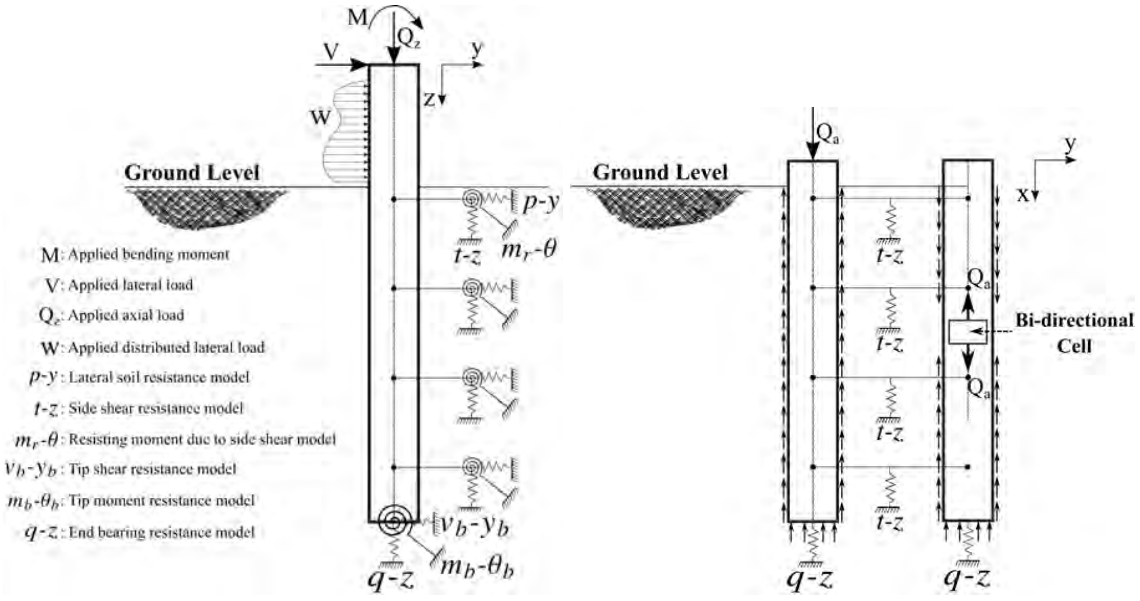

Figure A.1: Major resistance components in the finite-difference model for an (a) laterally loaded and (b) axially loaded drilled shaft for conventional top-down and bi-directional static load test.

case of performing *p-y* analysis for a pile/drilled shaft embedded in a layered soil profile, NVShaft also has the option to perform layering correction following the procedure given by Georgiadis (1983). For both *p-y* and *t-z* analysis, several types of boundary conditions may be selected, and the variation in the structural properties of the shaft/pile can be defined. NVShaft can also capture the nonlinear stiffness properties of pile/shaft sections, which should be defined by the user-input moment-curvature or stiffness-moment relationships.

In the subsequent sections, different features of the NVShaft Graphical Users Interface (GUI) are explained for the users' convenience.

A.2 Overview of the NVShaft GUI

NVShaft GUI features the following major tabs to define parameters related to *p-y* and *t-z* analysis.

1. **Home Tab:** To specify general options related to *p-y* and *t-z* analysis.
2. **Boundary Condition Tab:** To specify boundary conditions related to axial and lateral loading.
3. **Shaft Properties Tab:** To define pile or shaft section properties.
4. **Soil Properties Tab:** To define major axial and lateral resistance models as outlined in Fig. A.1. This tab contains the following sub-tabs,
   (a) **Lateral Resistance Tab:** To define lateral (*p-y*) resistance models of the soil/rock materials.
   (b) **Vertical Side Resistance Tab:** To define axial (*t-z*) resistance models of the soil/rock materials.
   (c) **Tip Resistance Tab:** To define end bearing, tip shear, and tip moment resistance models of the soil/rock materials.

The GUI also features the following buttons in the toolbar.

1. **New Button:** To create a blank project.
2. **Open Button:** To open an existing project from a directory.
3. **Save Button:** To save the current project in the current directory. In NVShaft, projects are saved in .mat format.
4. **Save As Button:** To save the current project in a user-specified directory.
5. **Run Analysis Button:** To start numerical analysis based on the input parameters defined in the current state of the program. If the program encounters

no error after clicking on the Run Analysis Button, the analysis is initiated. A progress bar is shown with a "Stop Analysis" button, which lets the users stop the analysis after the current iteration. If NVShaft fails to complete an analysis, an error dialog box is shown with the relevant error messages.

6. **Generate Output File Button:** To create output file, either in Excel spreadsheet (.xlsx) or report (.pdf) format. This button only becomes active after a successful analysis. After the successful generation of the output file, a dialog box is shown indicating the path where the output file is saved. If the program fails to generate an output file, an error dialog box is shown instead. Sample output files in Excel spreadsheet and report format are presented in Fig. A.2.

7. **Plot Available Outputs Button:** To regenerate the output plots from the previous calculations. This button only becomes active after a successful analysis.

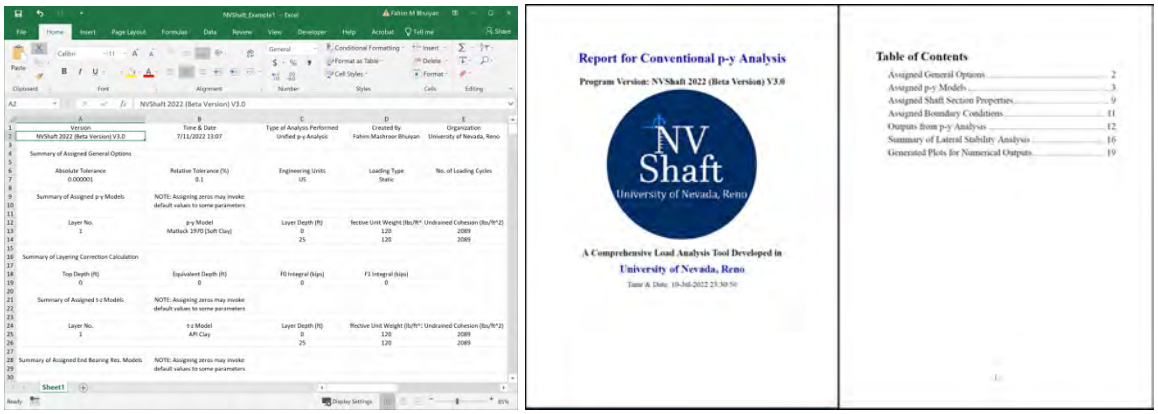

(a) (b)

Figure A.2: Sample outputs generated in NVShaft in (a) Excel spreadsheet (.xlsx) and (b) report (.pdf) format.

A.3 Defining General Properties

In NVShaft, the general properties can be specified from the **Home** tab, which appears as shown in Fig. A.3 and Fig. A.4, depending on the type of analysis the users choose to perform. Various features available in the Home tab are discussed in the following sections.

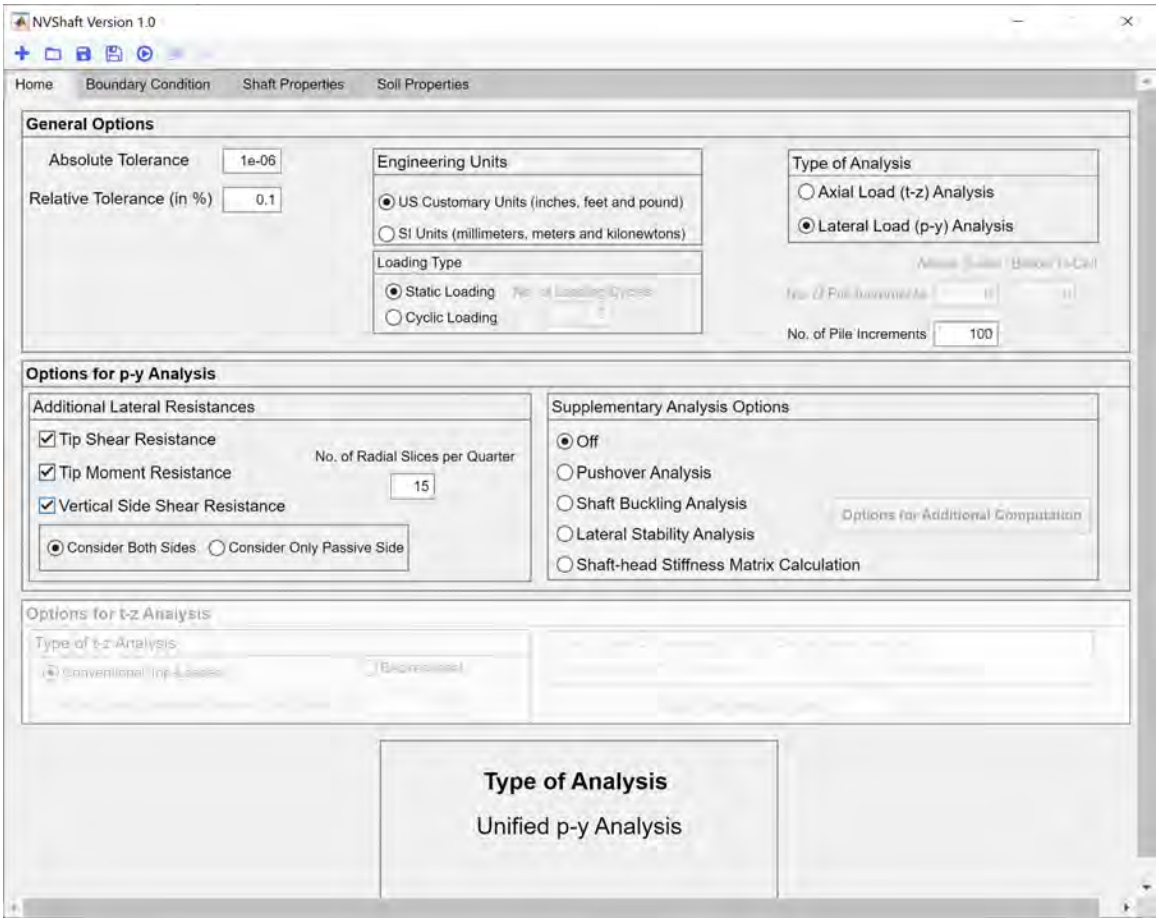

Figure A.3: The appearances of the Home tab when the lateral load (*p-y*) analysis radio button is selected.

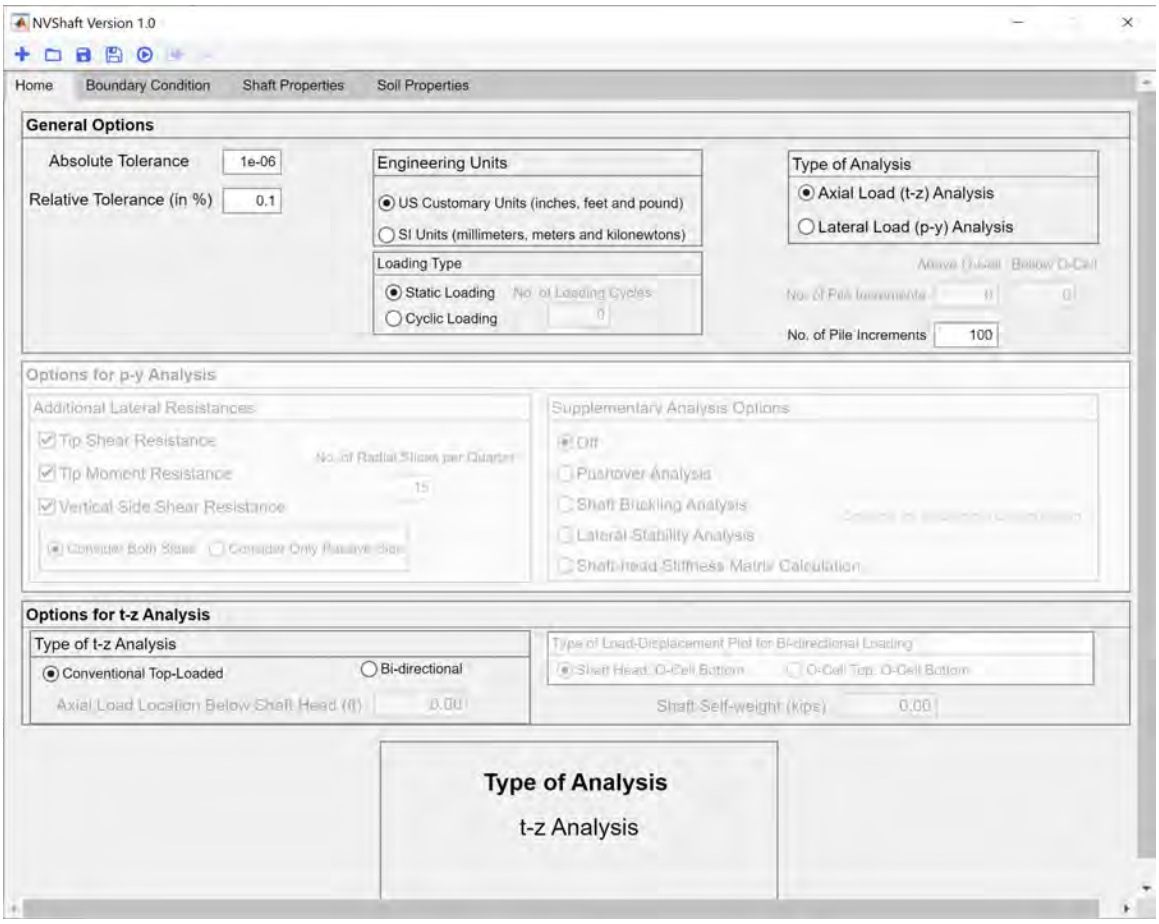

Figure A.4: The appearances of the Home tab when the axial load (*t-z*) analysis radio button is selected.

A.3.1 General Options

1. **Absolute Tolerance:** Controls the absolute error tolerance during the finite-difference analysis by the built-in MATLAB differential equation solver (**bvp4c**). Uses **1e-06** as the default value.

2. **Relative Tolerance (in %):** Controls the relative error tolerance during the finite-difference analysis by the built-in MATLAB differential equation solver (**bvp4c**). Uses **0.1** as the default value.

3. **Engineering Units:** Sets the engineering system of units as either **US Customary Units (inches, feet and pound)** or **SI Units (millimeters, meters and**

kilonewtons). The complete list of units for different parameters in NVShaft is summarized in Table A.1.

4. **Type of Analysis:** Sets the analysis type as either **axial load (*t-z*)** or **lateral load (*p-y*)** analysis. Depending on this selection, additional options get enabled as shown in Fig. A.3 and Fig. A.4.

5. **No. of Pile Increments:** Sets the number of increments to discretize the finite-difference model. If the user chooses to simulate the bi-directional static load test, then the number of pile increments for the segments both above and below the O-cell location needs to be defined.

6. **Loading Type:** Sets either **static** or **cyclic** type of loading to perform the *p-y* analysis. If cyclic loading type is chosen, the number of loading cycles also has to be assigned to modify the corresponding *p-y* models. The list of *p-y* models to support cyclic loading is highlighted in Table A.2.

A.3.2 Options for *p-y* Analysis

The panel allows the users to enable additional **tip shear**, **tip moment** and **vertical side shear resistance** in the numerical model (Fig.A.3). Disabling these additional resistances prompts NVShaft to perform conventional *p-y* analysis similar to other commercial finite-difference programs. The proposed unified *p-y* analysis is performed if all of the additional lateral resistances are selected in the check boxes. The user can also specify the **number of radial slices per quarter of shaft section**, to calculate the resisting moment (m_r) as shown in Fig. 4.2. The users also have the option to consider both sides or only the passive side of the shaft while calculating the m_r.

Table A.1: List of units for different input/output parameters in NVShaft.

Input/Output Parameters	SI Units	US Customary Units
Length/ Depth	m	ft
Diameter/ Wall Thickness/ Lateral Deflection/ Width/ Depth	mm	in
Section Stiffness	$kN.m^2$	$kips.in^2$
Section Elastic Modulus	kN/m^2	$kips/in^2$
Bending Moment	$kN.m$	$kips.ft$
Curvature	rad/m	rad/in
Shear/ Axial Force	kN	$kips$
Mobilized Soil Reaction/ Lateral Soil Resistance	kN/m	lbs/in
Resisting Moment per Length	$kN.m/m$	$kips.ft/ft$
Rotational Stiffness	$kN.m/rad$	$kips.ft/rad$
Effective Unit Weight	kN/m^3	lbs/ft^3
Friction Angle	$Degree$	$Degree$
Subgrade Modulus	kN/m^3	lbs/in^3
Cohesive Strength	kN/m^2	lbs/ft^2
Strain Factor	-	-
Uniaxial Compressive Strength	kN/m^2	lbs/in^2
Initial Elastic/ Intact Rock/ Mass Rock Modulus	kN/m^2	lbs/in^2
RQD	%	%
SPT Blow Count	$blows/ft$	$blows/ft$
Dilatometer/ Pressuremeter Modulus/ Cone Tip Resistance	kN/m^2	lbs/in^2
Ultimate Side Resistance	kN/m^2	lbs/ft^2

The following supplementary analysis options are available in the NVShaft Version 1.0, which can be performed after a successful *p-y* analysis.

1. **Pushover Analysis**
2. **Shaft Buckling Analysis**
3. **Lateral Stability Analysis**
4. **Shaft-head Stiffness Matrix Calculation**

Selecting the **Options for Additional Computation** button allows the users to define additional parameters for these options. More detail on the supplementary analysis options can be found in Section A.7.

A.3.3 Options for *t-z* Analysis

In NVShaft, the users can perform two different types of axial load test simulations, as shown in Fig. A.4.

1. **Conventional Top-Loaded Axial Load Test**
2. **Bi-directional Static Load Test**

For the bi-directional static load test simulation, the users need to define the **location of the axial load (i.e., bi-directional cell) below shaft head** (Fig. A.1b) and also the **self-weight of the shaft portion above bi-directional cell or O-cell**. The users may choose two different types of load-displacement plots for bi-directional loading.

1. **Plot corresponding to shaft head and O-cell bottom locations**
2. **Plot corresponding to O-cell top and O-cell bottom locations**

A.4 Defining Boundary Condition

The boundary conditions for both lateral and axial load analysis can be specified from the **Boundary Condition** tab, which contains the features as shown in Fig. A.5. The tab provides the following features in the GUI.

1. **Select Loading Case Drop Down Menu:** Allows the users to select from different loading cases. The loading cases can be added, inserted and deleted by selecting the **Add**, **Insert** and **Delete** buttons, respectively.

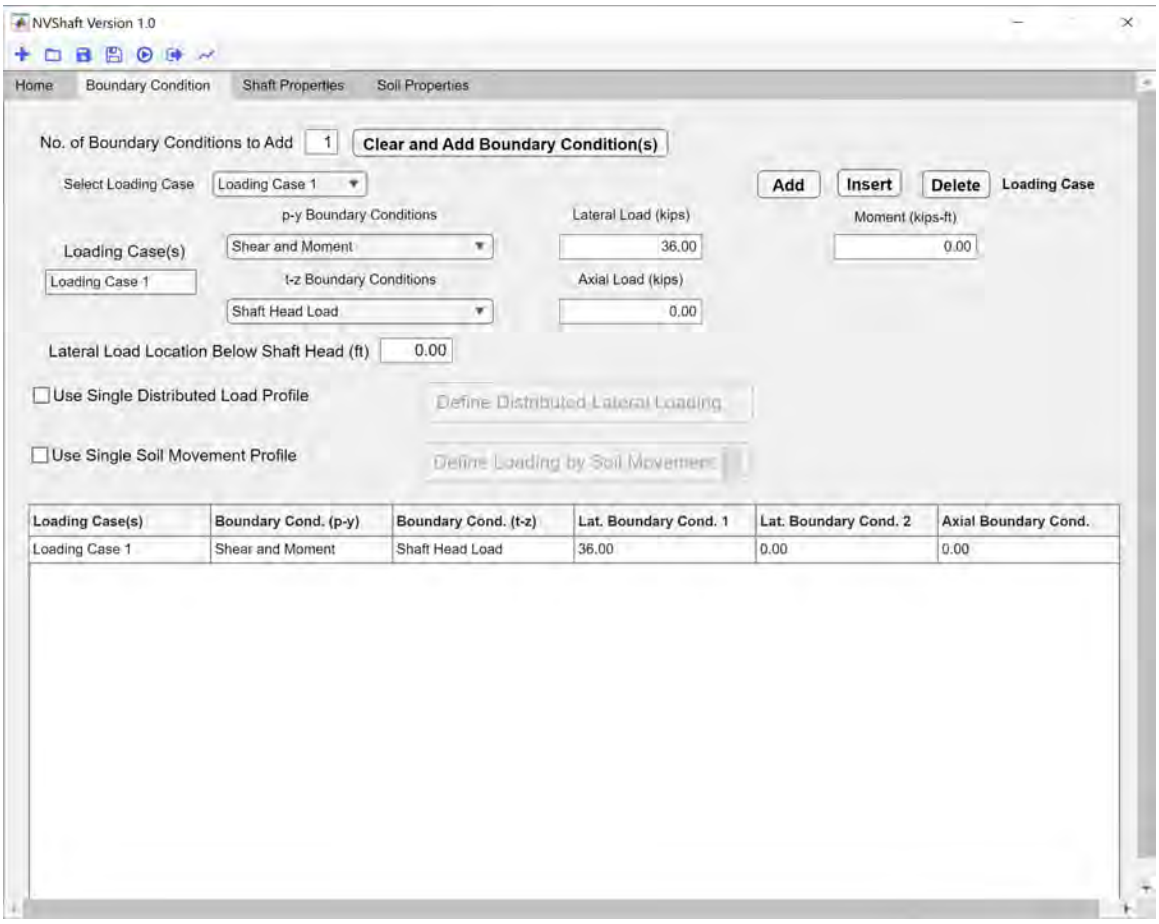

Figure A.5: The Boundary Condition tab in NVShaft GUI.

2. ***p-y* Boundary Conditions Drop Down Menu:** In NVShaft, the following options are available to define the boundary conditions for the lateral loading.

   (a) **Shear and Moment**

   (b) **Shear and Slope**

   (c) **Shear and Rotational Stiffness**

   (d) **Displacement and Moment**

   (e) **Displacement and Slope**

3. ***t-z* Boundary Conditions Drop Down Menu:** The boundary conditions for the axial loading can be selected from the following options.

(a) **Shaft Head Load**

(b) **Tip Displacement**

The boundary condition for *t-z* analysis only becomes available when the users either choose to include **vertical side shear resistance** in the *p-y* analysis, or selects ***t-z* analysis** as the type of analysis in the **Home** tab. The **tip displacement** as the boundary condition can only be selected for the **conventional top-loaded** axial load test simulations.

4. **Clear and Add Boundary Condition(s) Button:** Allows the definition of any number of null boundary conditions for both *p-y* and *t-z* analysis. By default, **Shear and Moment** and **Shaft Head Load** are chosen for *p-y* and *t-z* boundary condition, respectively.
5. **Location of Applied Lateral Load:** Can be specified only when the **shear force** is selected as one of the *p-y* boundary conditions in all loading cases.
6. **Single Distributed Load Profile:** This feature is only available when the users choose to perform *p-y* analysis. Selecting the **Define Distributed Lateral Loading** button opens the **Define Distributed Lateral Loads** input window as shown in Fig. A.6a, which allows the users to define the depth (below shaft head) and the corresponding lateral load intensity values. The window also allows pasting values copied to the clipboard.
7. **Single Soil Movement Profile:** This feature becomes available when the *p-y* analysis is chosen as the type of analysis. Selecting the **Define Loading by Soil Movement** button opens the **Define Lateral Soil Movement Profile** input window as shown in Fig. A.6b, which allows the users to define the depth (below GL) and the corresponding lateral soil movement values.

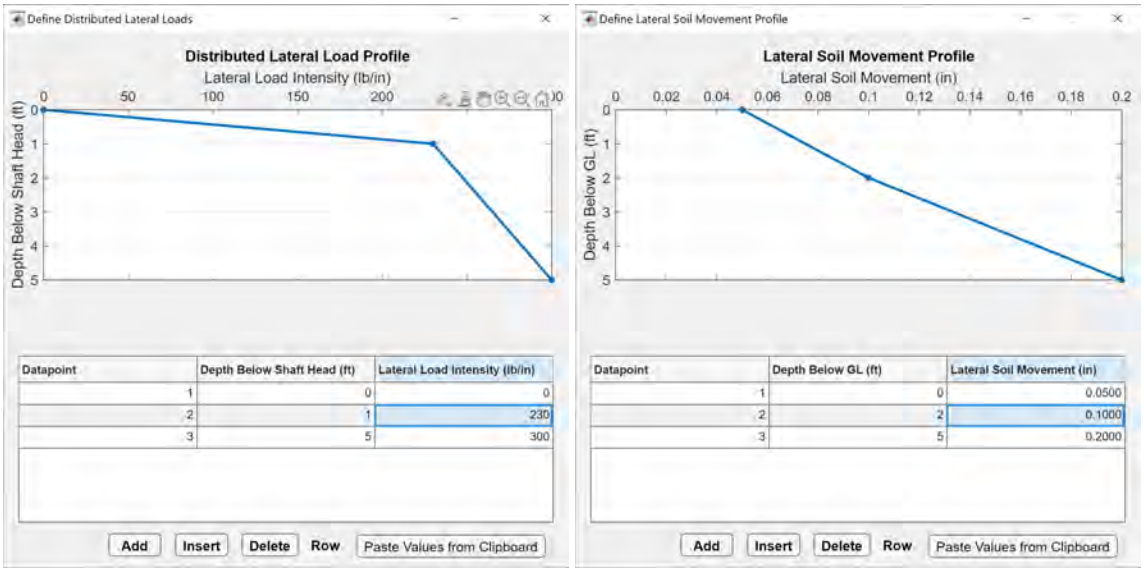

(a) (b)

Figure A.6: Input windows to define (a) distributed lateral loads and (b) lateral soil movement profile.

A.4.1 Sign Conventions in NVShaft

The sign conventions used in NVShaft for different boundary conditions are summarized below.

- Lateral load (as *p-y* boundary condition) is positive (+ve) when applied from left to right.
- Axial load (as *t-z* boundary condition) is positive (+ve) when applied in downward direction.
- Tip displacement (as *t-z* boundary condition) is positive (+ve) in downward direction.
- Bending moment and rotational stiffness (as *p-y* boundary conditions) are positive (+ve) when assigned in clockwise direction.
- Mobilized axial load is positive (+ve) in downward direction.
- Slope is positive (+ve) in anticlockwise direction.

- Lateral displacement is positive (+ve) toward right.
- Vertical displacement is positive (+ve) in upward direction.
- Resisting moment per length due to side shear is positive (+ve) in clockwise direction.

The sign conventions used in NVShaft for *p-y* analysis is illustrated in Fig. A.7, which is similar to the commercial *p-y* analysis program LPILE (Isenhower and Wang, 2011). For *t-z* analysis, NVShaft uses the sign convention for vertical displacement and axial load, as shown in Fig. A.8.

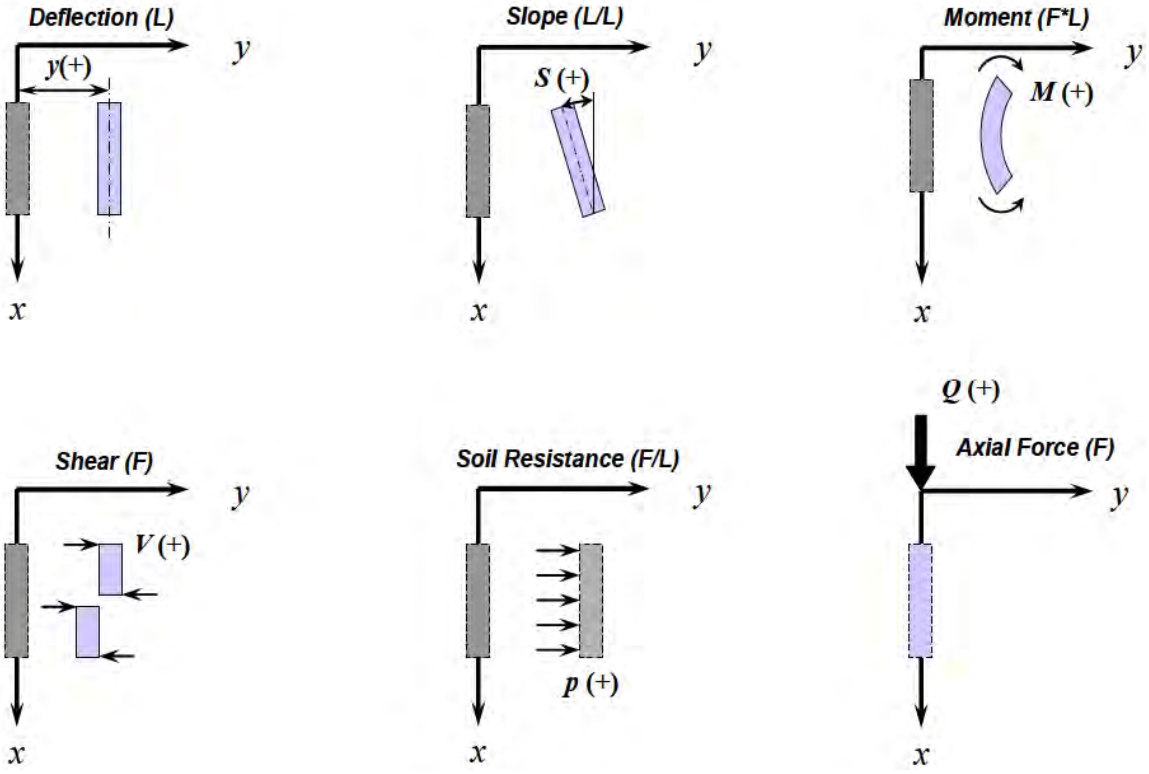

Figure A.7: Sign conventions used in NVShaft for *p-y* analysis. (Source: Isenhower and Wang 2011)

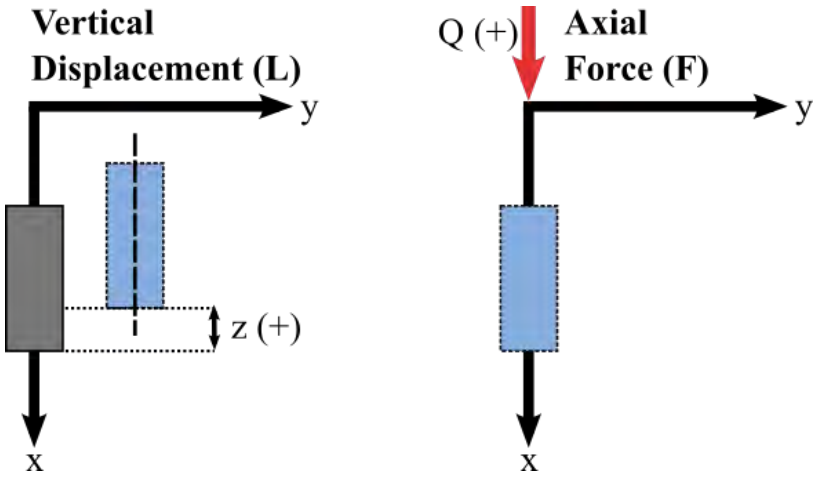

Figure A.8: Sign conventions used in NVShaft for *t-z* analysis.

A.5 Defining Shaft Properties

The properties of the shaft sections can be defined from the **Shaft Properties** tab, which contains the features as shown in Fig. A.9. The tab provides the following features to the users.

1. **Select Section Drop Down Menu:** To select from different shaft sections specified by the users. The sections can be added, inserted and deleted by selecting the **Add**, **Insert** and **Delete** buttons, respectively. Checking the **Copy Current Section Properties for New Section** check box allows to copy the current section properties when a new section is added or inserted.
2. **Shaft Head Location:** Specifies the shaft head location with respect to the GL. The positive value, in this case, indicates the shaft head to be located below GL, while the negative value assigns the shaft head location above GL.
3. **Section Length:** Assigns the length of the selected shaft section. NVShaft throws an error if the new length of the shaft exceeds the depth of the bottom-most soil layer.

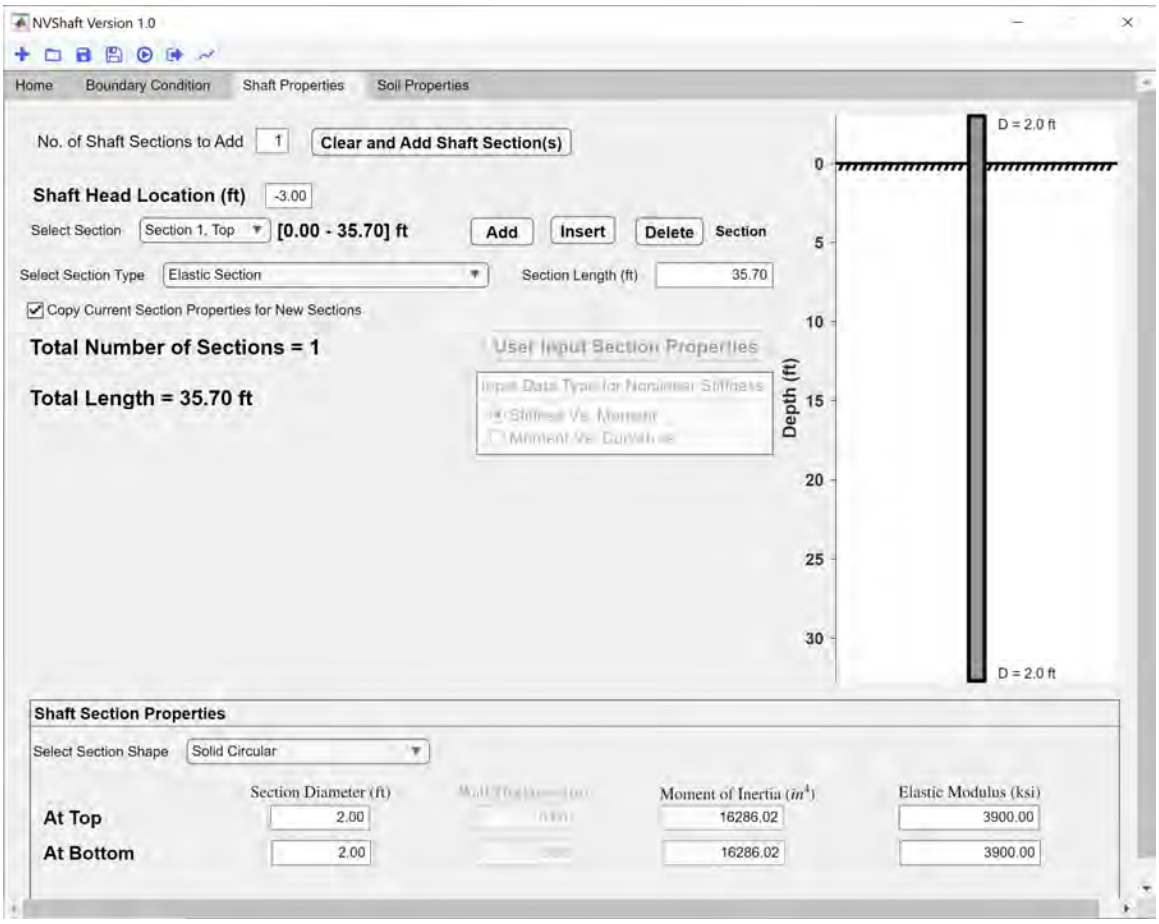

Figure A.9: The Shaft Properties tab in NVShaft GUI.

4. **Section Type Drop Down Menu:** Three different shaft section types are available to be implemented in the *p*-*y* analysis.

   (a) **Elastic Section:** Assumes uniform elastic section property for the whole shaft section.

   (b) **User-defined Elastic Section:** In this case, the elastic stiffness of the shaft section is assigned by the users as a function of depth. Selecting the **User Input Section Properties** button opens the **Define Elastic Section Properties** input window (Fig. A.10a), in which the users can assign the bending stiffness values at corresponding depths below the shaft head.

   (c) **User-defined Nonlinear Bending Section**: For this option, the nonlinear

stiffness property of the section is defined by selecting either **Stiffness Vs. Moment** or **Moment Vs. Curvature** relationship. Selecting the **User Input Section Properties** button opens the **Define Nonlinear Section Properties** input window (Fig. A.10b), in which the users can assign the nonlinear stiffness properties of the selected shaft section at various axial thrust values.

Regardless of the selection, NVShaft assumes elastic properties in all shaft sections while performing the *t-z* analysis.

5. **Clear and Add Shaft Section(s) Button:** Allows the definition of any number of **elastic** shaft sections with zero length, diameter and elastic modulus values.
6. **Shaft Section Properties:** The panel allows the users to define section properties of the selected shaft section, including section **diameter**, **wall thickness**, **width**, **depth** and **elastic modulus**. The panel features a drop down menu to select from three different section shapes, which is only available for **elastic section** type.
   (a) **Solid Circular**
   (b) **Pipe**
   (c) **Rectangular**

   For both **user-define elastic section** and **user-defined nonlinear bending section**, NVShaft assumes the shaft section shape to be **solid circular**.

A.6 Defining Soil Properties

Different lateral and axial resistance models can be defined from the **Soil Properties** tab. The tab includes three sub-tabs to characterize the soil resistance in numerical

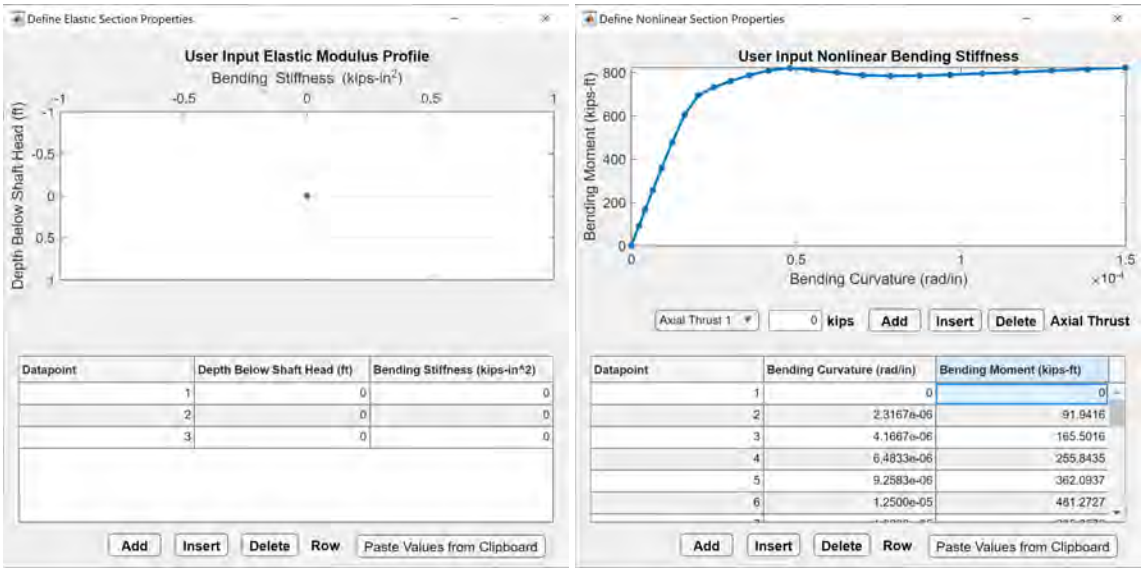

(a) (b)

Figure A.10: Input windows to define (a) distributed lateral loads and (b) lateral soil movement profile.

analysis.

1. **Lateral Resistance Tab:** Allows the users to define the lateral resistance (p-y) models.
2. **Vertical Side Resistance Tab:** Allows the users to define the vertical side resistance (t-z) models.
3. **Tip Resistance Tab:** Allows the users to define the end bearing (q-z), tip shear (v_b-y_b) and tip moment (m_b-θ_b) resistance models.

The available features of these tabs are more elaborately discussed in the following sections.

A.6.1 Lateral Resistance

The characterization of soil/rock lateral resistance (p-y) models can be done in the **Lateral Resistance** tab, which contains the features as shown in Fig A.11. The tab

provides the following features to the users.

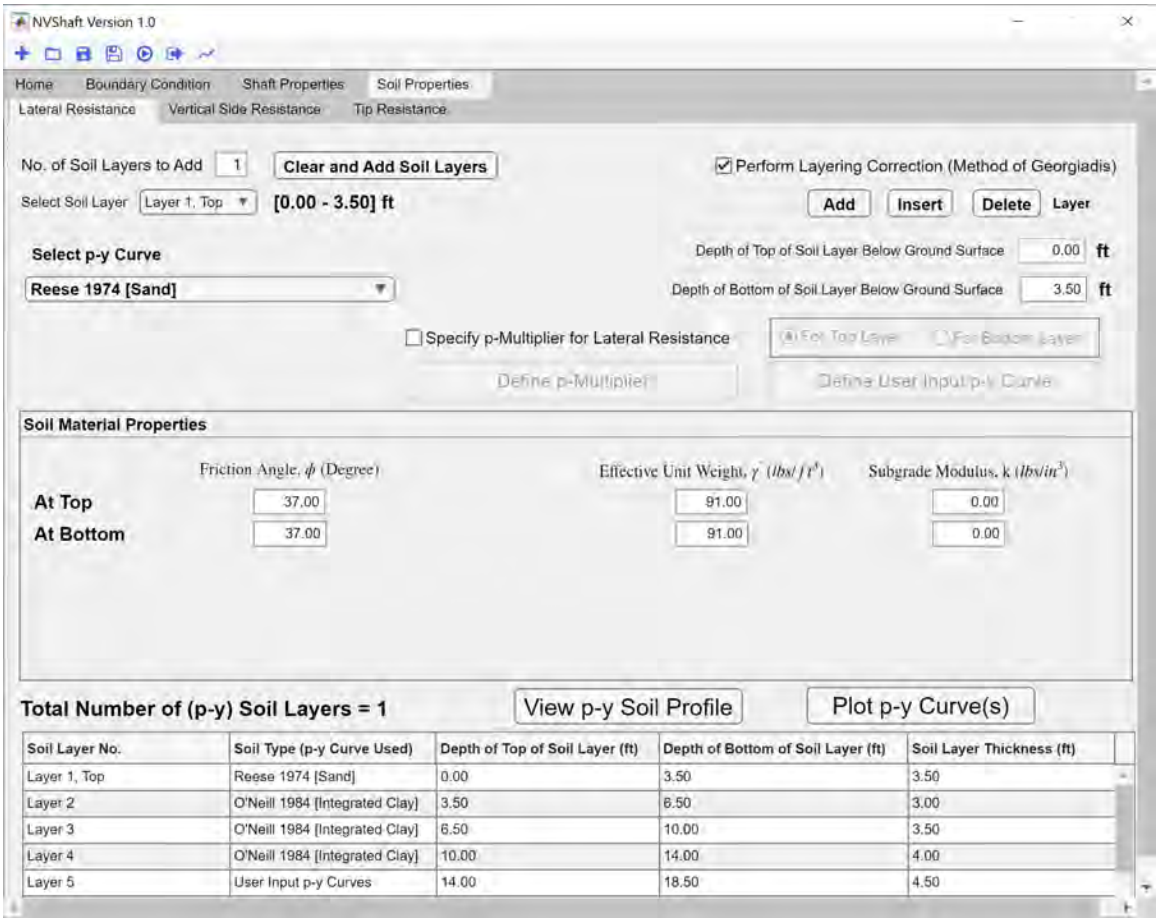

Figure A.11: The Lateral Resistance tab in NVShaft GUI.

1. **Select Soil Layer Drop Down Menu:** To select from different *p-y* soil layers specified by the users. The *p-y* layers can be added, inserted and deleted by selecting the **Add**, **Insert** and **Delete** buttons, respectively.

2. **Top and Bottom Depths of *p-y* Soil Layer below GL:** Allows the users to define the *p-y* layers thicknesses.

3. ***p-y* Curve Drop Down Menu:** To select from a total of 19 built-in *p-y* models, and the user-input *p-y* model to define lateral soil resistance of the selected soil layer. The list of available built-in *p-y* models in NVShaft, and their

applicability for static and cyclic types of loading is summarized in Table A.2. Selecting the **Define User Input *p-y* Curve** button opens the **Define User Input *p-y* Curve** input window as shown in Fig A.12a, which allows the users to define the user-input *p-y* model for the top or bottom depth of the selected soil layer.

4. **Clear and Add Soil Layer(s) Button:** Allows the definition of any number of soil layers characterized by the Matlock (1970) *p-y* models.
5. **Soil Material Properties Panel:** Contains different soil/rock material properties to be defined by the users depending on the assigned *p-y* model of the selected soil layer.
6. **Define *p*-Multiplier Button:** Users can click on the **Define *p*-Multiplier** button after selecting the **Specify *p*-Multiplier for Lateral Resistance** check box, to define the ***p*-Multiplier** values at top and bottom depths of soil layers. This can be done in the **Define *p*-Multiplier** input window as shown in Fig A.12b.
7. **Plot *p-y* Curve(s) Button:** Allows the users to specify the depths in the **Specify Depths to Plot *p-y* Curve(s)** input window (Fig. A.12c) where the generated *p-y* plots are desired.
8. **View *p-y* Soil Profile Button:** Opens a window containing the schematics of the defined *p-y* soil models along with the shaft/pile cross sections. A sample soil profile diagram generated by NVShaft is shown in Fig. A.15a.

A.6.2 Vertical Side Resistance

The axial resistance (*t-z*) models of the soil/rock material can be defined in the **Vertical Side Resistance** tab, which contains the features as shown in Fig A.13. The tab provides the following features to the users.

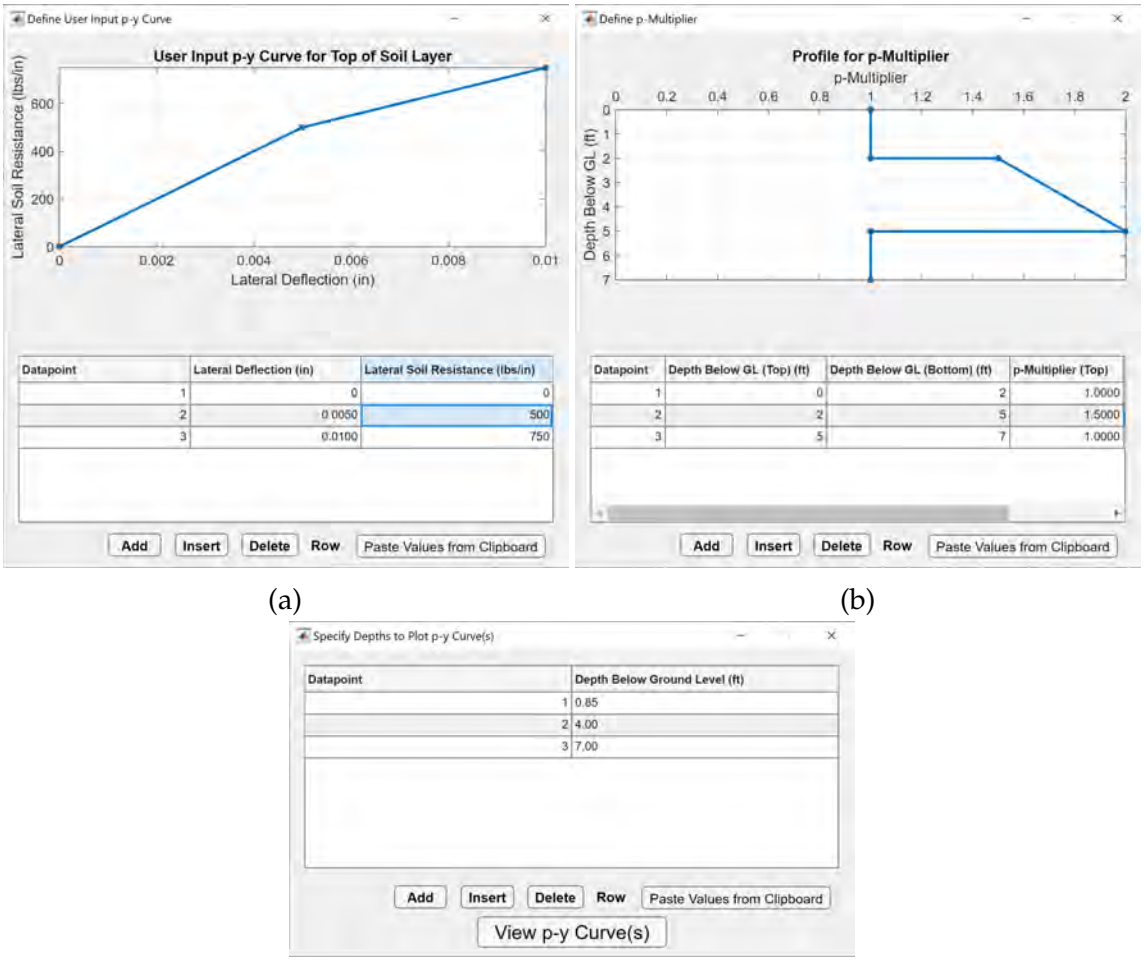

Figure A.12: Input windows to assign (a) user-input *p-y* values at top and bottom depths of soil layers, (b) *p*-multiplier values at specified depths and (c) depth values below GL to plot *p-y* curve(s).

1. **Select Soil Layer Drop Down Menu:** To select from different *t-z* soil layers specified by the users. The *t-z* layers can be added, inserted and deleted by selecting the **Add**, **Insert** and **Delete** buttons, respectively.

2. **Top and Bottom Depths of *t-z* Soil Layer below GL:** Allows the users to define the *t-z* layers thicknesses.

3. ***t-z* Curve Drop Down Menu:** To select from a total of 7 built-in *t-z* models, and the user-input *t-z* model to define vertical side resistance of the selected

Table A.2: List of available built-in *p-y* models in NVShaft.

Soil/Rock Type	*p-y* Model Citation	Loading Type
Modified Stiff Clay w/o Free Water	Brown (2002)	Static/Cyclic
Elastic Subgrade	-	Static
Cemented c-ϕ Soil	Evans and Duncan (1982)	Static/Cyclic
Marine Clay	Jeong et al. (2011)	Static
Loess Soil	Johnson (2006)	Static/Cyclic
Weakly Cemented Sand	Juirnarongrit and Ashford (2004)	Static
Massive Rock	Liang et al. (2009)	Static
Soft Clay	Matlock (1970)	Static/Cyclic
Soft Clay w User-Defined J	Matlock (1970)	Static/Cyclic
Florida Limestone	McVay and Niraula (2004)	Static
API Sand	O'Neill and Murchison (1983)	Static/Cyclic
Integrated Clay	O'Neill and Gazioglu (1984)	Static/Cyclic
Sand	Reese et al. (1974)	Static/Cyclic
Stiff Clay w Free Water	Reese and Welch (1975)	Static/Cyclic
Strong Rock/ Vuggy Limestone	Reese and Nyman (1978)	Static
Weak Rock	Reese (1997)	Static
Liquefied Sand	Rollins et al. (2005)	Static
Piedmont Residual Soil	Simpson and Brown (2006)	Static
Stiff Clay w/o Free Water	Welch and Reese (1972)	Static/Cyclic

soil layer. The list of available built-in *t-z* models in NVShaft is summarized in Table A.3. Selecting the **Define User Input *t-z* Curve** button opens the **Define User Input *t-z* Curve** input window as shown in Fig A.14a, which allows the users to define the user-input *t-z* model for the top or bottom depth of the

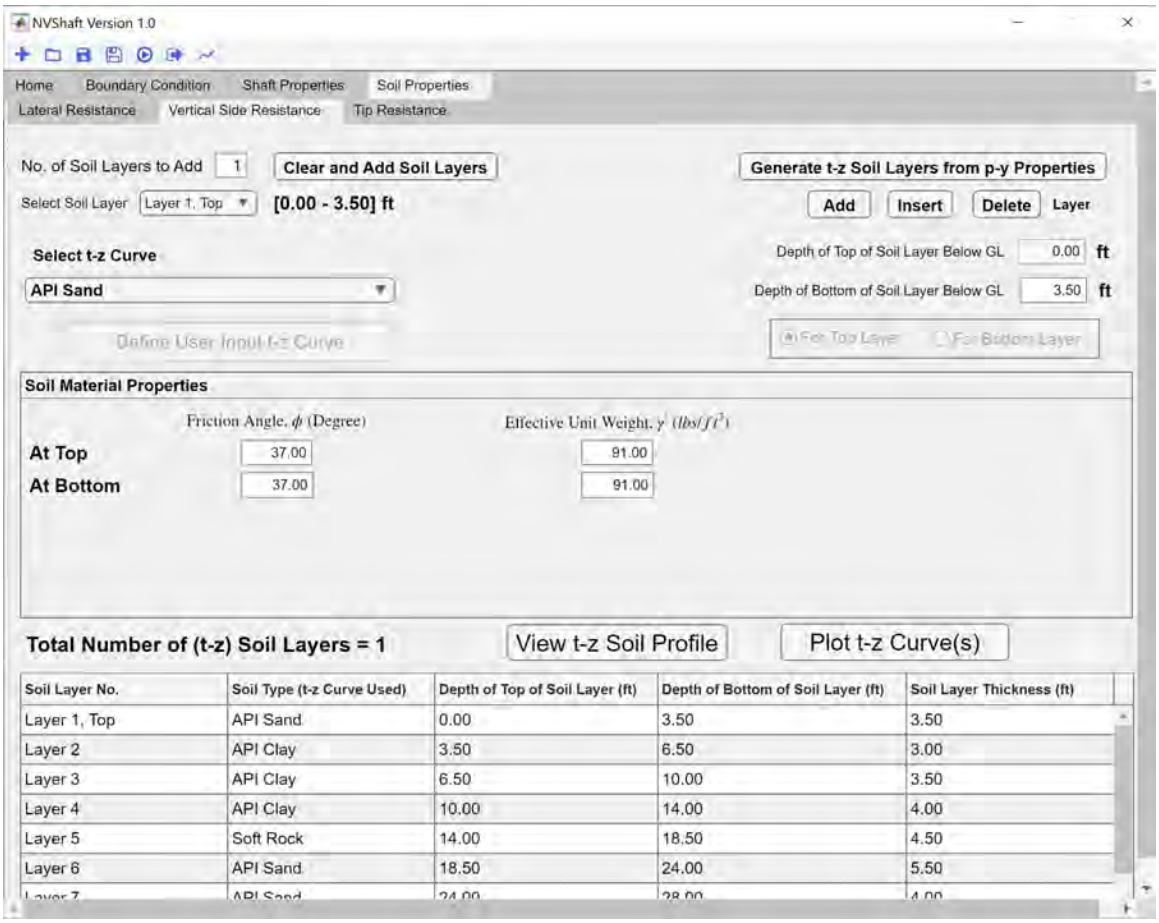

Figure A.13: The Vertical Side Resistance tab in NVShaft GUI.

selected soil layer.

4. **Clear and Add Soil Layer(s) Button:** Allows the definition of any number of soil layers characterized by the API Clay (API, 2014) *t-z* models.

5. **Soil Material Properties Panel:** Contains different soil/rock material properties to be defined by the users depending on the assigned *t-z* model of the selected soil layer.

6. **Plot *t-z* Curve(s) Button:** Allows the users to specify the depths in the **Specify Depths to Plot *t-z* Curve(s)** input window (Fig. A.14b) where the generated *t-z* plots are desired.

7. **View *t-z* Soil Profile Button:** Opens a window containing the schematics of

the defined *t-z* soil models along with the shaft/pile cross sections. A sample soil profile diagram generated by NVShaft is shown in Fig. A.15b.

8. **Generate *t-z* Soil Layers from *p-y* Properties Button:** Selecting this button allows NVShaft to roughly construct the *t-z* models, along with the relevant material properties based on the *p-y* models defined in the **Lateral Resistance** tab. This feature can be used to quickly construct the *t-z* soil layers, which are recommended to be adjusted based on site-specific soil/rock properties. By default, the rock layers are assigned with the soft rock *t-z* model (Asem and Gardoni, 2019) with the relevant uniaxial compressive strength values (q_u). In case NVShaft is unable to assign a specific *t-z* model for any soil layer, the API clay (API, 2014) model is assigned as the default model.

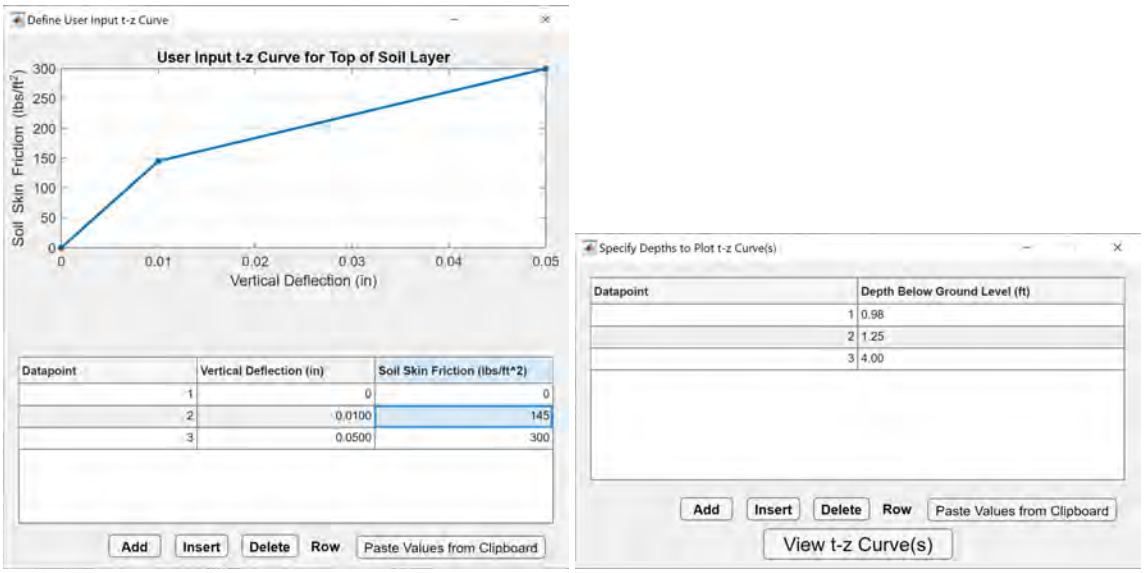

(a) (b)

Figure A.14: Input windows to assign (a) user-input *t-z* values at top and bottom depths of soil layers and (b) depth values below GL to plot *t-z* curve(s).

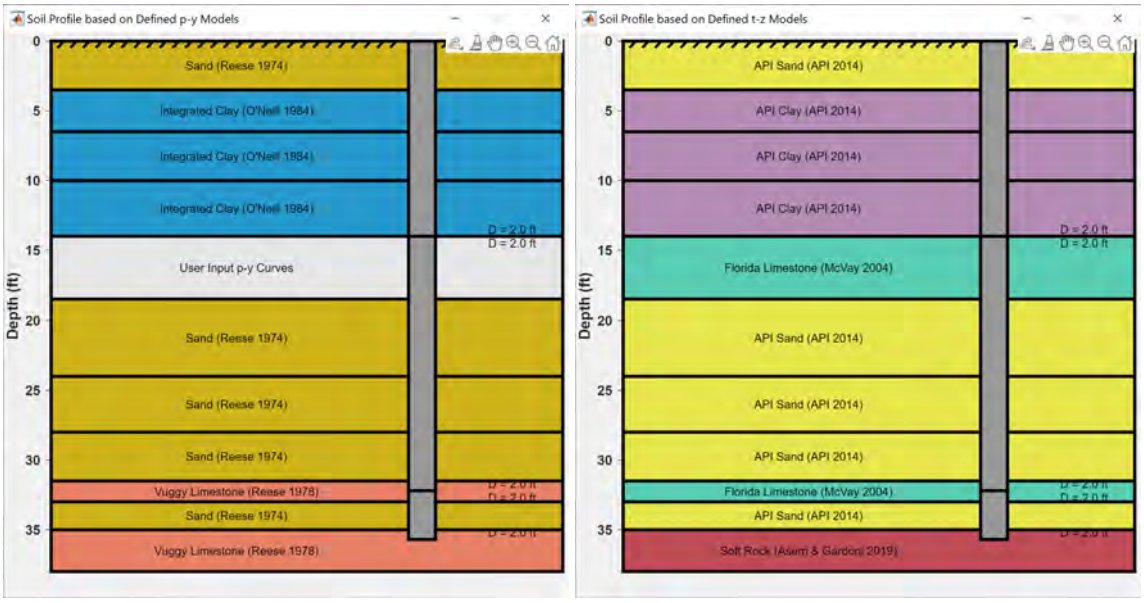

(a) (b)

Figure A.15: Soil profiles based on defined (a) *p*-*y* and (b) *t*-*z* models along with shaft sections generated in NVShaft.

Table A.3: List of available built-in axial resistance models in NVShaft.

Soil/Rock Type	Model Citation	Type of Model
API Clay	API (2014)	*t*-*z* and *q*-*z*
API Residual Clay	API (2014)	*t*-*z* and *q*-*z*
API Sand	API (2014)	*t*-*z* and *q*-*z*
Coyle Reese Clay	Coyle and Reese (1966)	*t*-*z* and *q*-*z*
Florida Limestone	McVay and Niraula (2004)	*t*-*z*
Mosher Sand	Mosher (1984)	*t*-*z* and *q*-*z*
Soft Rock	Asem and Gardoni (2019)	*t*-*z*

A.6.3 Tip Resistance

Different tip resistance models of the soil/rock material can be defined in the **Tip Resistance** tab, which contains the features as shown in Fig A.16. The tab allows the options to define end bearing (q-z), tip shear (v_b-y_b), and tip moment (m_b-θ_b)

resistance models for numerical analysis. A summary of available q-z models for different soil and rock materials is shown in Table A.3. The built-in v_b-y_b and m_b-θ_b models available in NVShaft are summarized in Table A.4. Features related to defining different types of tip resistance models are discussed in the following sections.

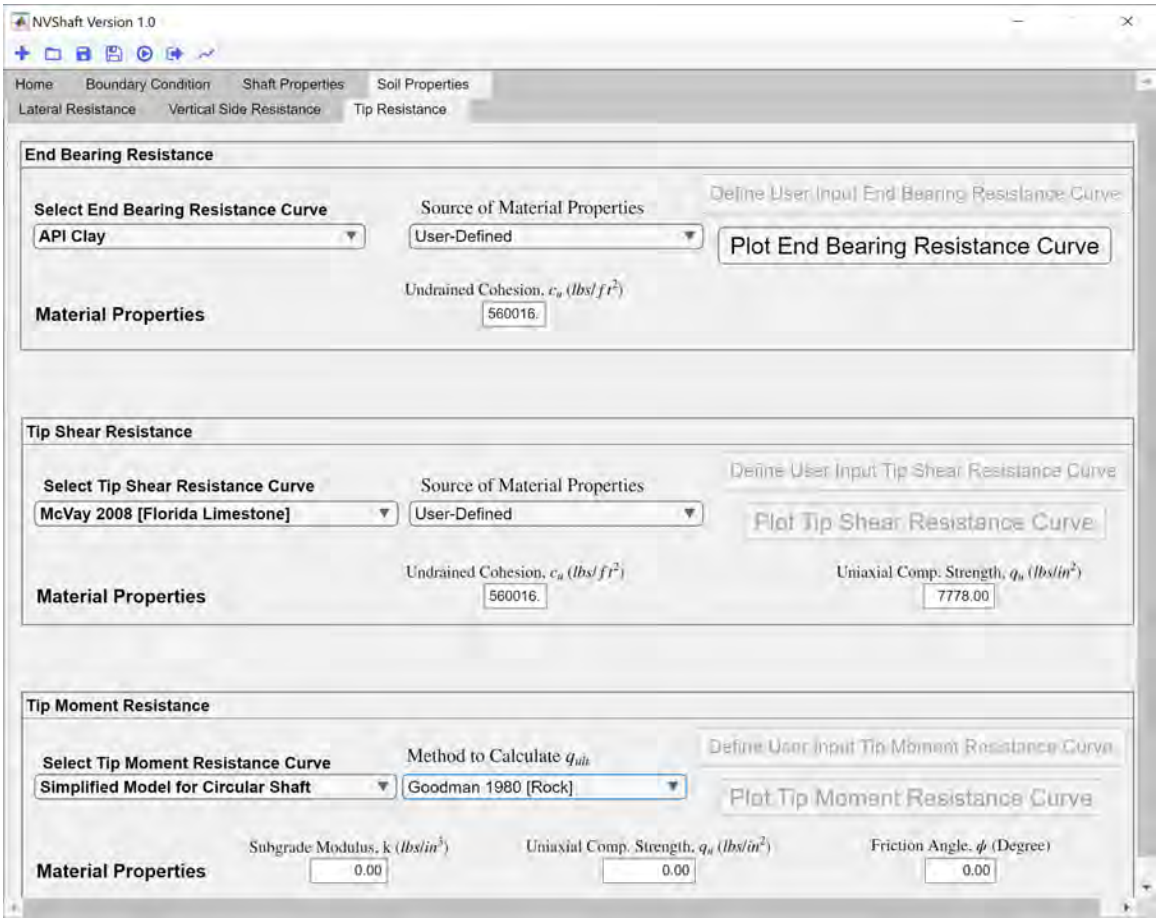

Figure A.16: The Tip Resistance tab in NVShaft GUI.

End Bearing Resistance

1. **Tip Shear Resistance Curve Drop Down Menu:** To select from a total of 2 built-in q-z models, and the user-input q-z model to define end bearing resistance of the soil layer at tip location. The list of available built-in q-z models

Table A.4: List of available built-in axial resistance models in NVShaft.

Type of Model	Soil/Rock Type	Model Citation
v_b-y_b	Florida Limestone	McVay et al. (2008)
	Soil Material	Vallabhan and Alikhanlou (1982)
m_b-θ_b	Soil/Rock Material	Bhuiyan et al. (2022)

in NVShaft is summarized in Table A.3. Selecting the **Define User Input End Bearing Resistance Curve** button opens the **Define User Input *q*-*z* Curve** input window as shown in Fig A.17a, which allows the users to define the user-input *q*-*z* model for soil layer at pile/shaft tip location.

2. **Source of Material Properties Drop Down Menu:** Used to determine the source of material properties to calculate the relevant end bearing resistance model. If the **User-Defined** option is selected, then the material properties need to be defined manually by the users. On the other hand, if the **Obtain from Soil Model at Shaft Tip** option is selected, material properties are obtained from the defined *p*-*y* and *t*-*z* soil characteristics.
3. **Plot End Bearing Resistance Curve Button:** To plot the end bearing resistance curve based on the defined model and material properties.

Tip Shear Resistance

1. **Tip Shear Resistance Curve Drop Down Menu:** To select from a total of 2 built-in v_b-y_b models, and the user-input v_b-y_b model to define tip shear resistance of the soil layer at tip location. The list of available built-in v_b-y_b models in NVShaft is summarized in Table A.4. Selecting the **Define User Input Tip Shear Resistance Curve** button opens the **Define User Input Tip Shear Resistance** input window as shown in Fig A.17b, which allows the users to

define the user-input v_b-y_b model for soil layer at pile/shaft tip location.

2. **Source of Material Properties Drop Down Menu:** Used to determine the source of material properties to calculate the relevant tip shear resistance model. The drop down menu is similar to the one in the **End Bearing Resistance** tab. If the **Obtain from Soil Model at Shaft Tip** option is selected, material properties are obtained from the defined p-y and t-z soil characteristics.
3. **Plot Tip Shear Resistance Curve Button:** To plot the tip shear resistance curve based on the defined model and material properties.

Tip Moment Resistance

1. **Tip Moment Resistance Curve Drop Down Menu:** To choose from a built-in simplified m_b-θ_b model for circular shaft section (Table A.4), and the user-input m_b-θ_b model to define tip moment resistance of the soil/rock layer at tip location. Selecting the **Define User Input Tip Moment Resistance Curve** button opens the **Define User Input Tip Moment Resistance** input window as shown in Fig A.17c, which allows the users to define their own user-input m_b-θ_b model for soil/rock layer at pile/shaft tip location.
2. **Method to Calculate q_{ult} Drop Down Menu:** Used to select the appropriate method to calculate the ultimate bearing capacity (q_{ult}) of soil/rock material, when the simplified m_b-θ_b model is chosen. The drop down menu offers the following options to the users.

   (a) **From Defined End Bearing Model:** The q_{ult} is calculated based on the defined q-z model in the **End Bearing Resistance** panel.

   (b) **Brown et al. 2010 [Rock]:** The q_{ult} is calculated following an empirical formula given by Brown et al. (2010).

(c) **Goodman 1980 [Rock]:** In this case, an empirical formula given by Goodman (1980) is used to calculate the q_{ult}.

(d) **Zhang 2004 [Weak Rock]:** The q_{ult} is calculated using the correlation given by Zhang (2004).

3. **Plot Tip Moment Resistance Curve Button:** To plot the tip moment resistance curve based on the defined model and material properties.

A.6.4 Default Soil Properties used in Resistance Models

In NVShaft, some of the lateral and axial resistance models allow the use of default values of some material properties based on empirical formulas and past recommendations. Users can assign zero values, which prompts NVShaft to assign the default values for these parameters. The default parameters used in different models are summarized in this section.

Default Values in Clay *p-y* Models

The default parameters (e.g., subgrade modulus, soil modulus and strain factor) used in various clay *p-y* models are summarized in Table A.5 to Table A.8.

Table A.5: Default Subgrade Modulus (k) used in Reese and Welch (1975) and Brown (2002) *p-y* models.

Cohesive Strength, c_u (kN/m^2)	Subgrade Modulus, k (kN/m^3) [Static Loading]	Subgrade Modulus, k (kN/m^3) [Cyclic Loading]
0 - 95.8	135.7e3	542.9e2
95.8 - 191.6	271.4e3	108.6e3
>191.6	542.9e3	217.2e3

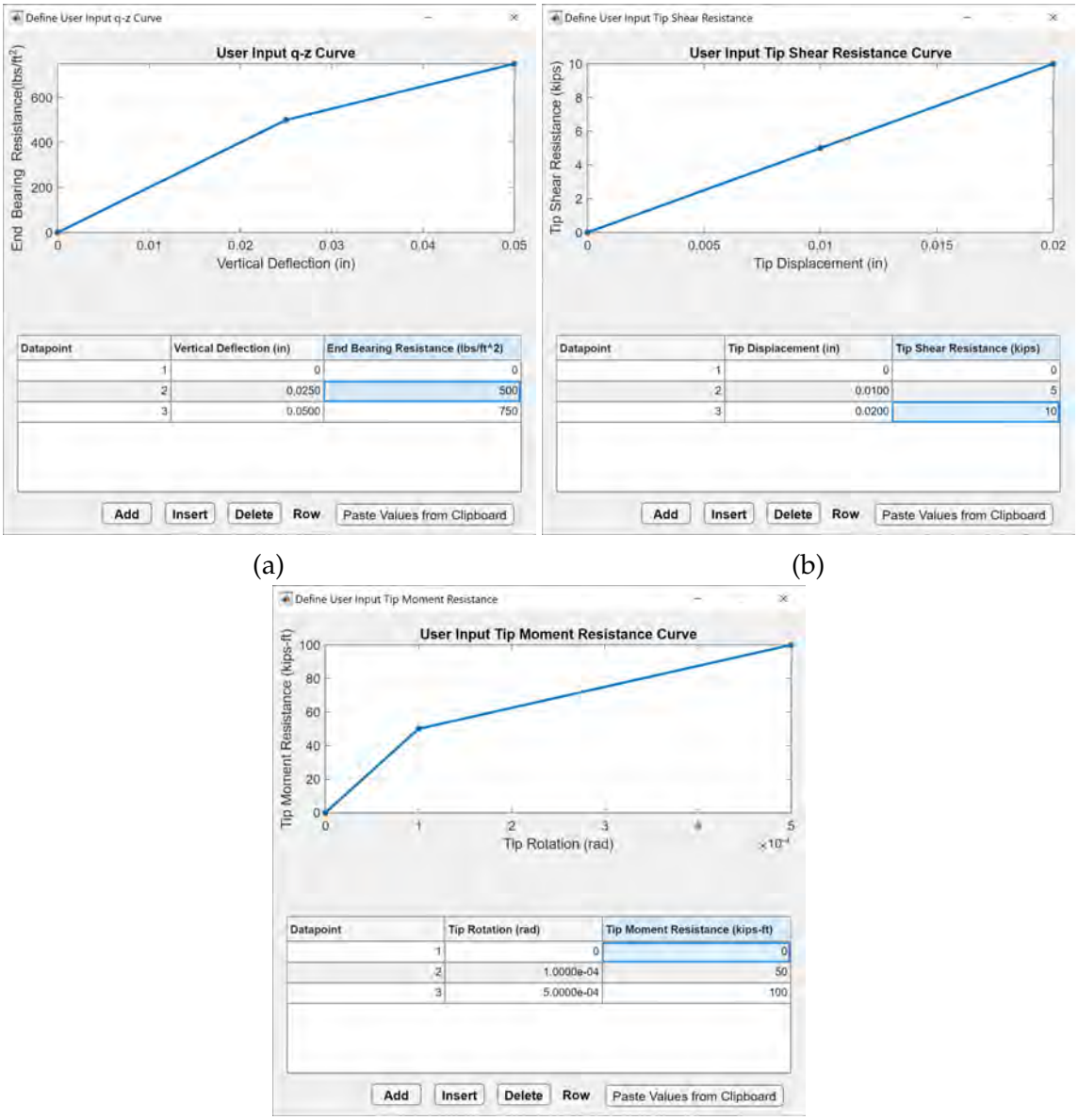

Figure A.17: Input windows to assign user-input (a) end bearing (q-z), (b) tip shear (v_b-y_b) and (c) tip moment (m_b-θ_b) resistance models at pile/shaft tip location.

Default Values in Sand and Cemented c-ϕ Soil p-y Models

In NVShaft, the sand p-y models given by Reese et al. (1974) and O'Neill and Murchison (1983) uses the correlation shown in Fig. A.18 to obtain the default values of modulus of subgrade reaction (k). For the p-y model for c-ϕ soil by Evans

Table A.6: Default strain factor (ϵ_{50}) used in Welch and Reese (1972), Reese and Welch (1975), O'Neill and Gazioglu (1984) and Brown (2002) *p-y* models.

Cohesive Strength, c_u (kN/m^2)	Strain Factor, ϵ_{50}
0 - 47.9	0.011
47.9 - 95.8	0.007
95.8 - 191.5	0.005
>191.5	0.004

Table A.7: Default strain factor (ϵ_{50}) used in Matlock (1970) *p-y* model.

Cohesive Strength, c_u (kN/m^2)	Strain Factor, ϵ_{50}
0 - 24	0.02
24 - 48	0.01
>48	0.005

and Duncan (1982), the correlation shown in Fig. A.19 is used instead.

Default Values in Soft Rock *t-z* model

In the soft rock *t-z* model proposed by Asem and Gardoni (2019), the following equation is used to calculate the default value of mass rock modulus (E_m).

$$E_m = 150 \times q_u^{1.1} \tag{A.1}$$

Where q_u is the unconfined compressive strength of rock material. In Eq. A.1, both E_m and q_u are in units of MPa.

Table A.8: Default Soil Modulus (E_s) used in O'Neill and Gazioglu (1984) and Jeong et al. (2011) *p-y* models.

Cohesive Strength, c_u (kN/m^2)	Soil Modulus, E_s (kN/m^2)
0 - 23.9	344.7
23.9 - 47.9	344.7 - 1034.2
47.9 - 95.8	1034.2 - 3102.6
95.8 - 191.5	3102.6 - 10342.1
191.5 - 383	10342.1 - 34473.8
>383	34473.8

Default Values in Simplified Tip Moment Resistance Model

In the proposed simplified tip moment resistance model, the modulus of subgrade reaction is utilized as one of the required input parameters. The users can input zero for the subgrade modulus, which prompts NVShaft to calculate the default k value depending on the type of *p-y* model defined previously in the **Lateral Resistance** tab. For clay, sand, and c-ϕ soil *p-y* models, NVShaft follows the above-mentioned empirical correlations to calculate the default k values. If the *p-y* model at shaft tip location corresponds to rock material, then NVShaft first calculates the elastic modulus of rock (E_t) using the following equation given by Sachpazis (1990).

$$E_t = q_u \times 0.3752 + 4.4279 \tag{A.2}$$

Where E_t is in GPa and q_u is in MPa. After calculating E_t, the following equation given by Selvadurai (1985) is used to compute the default k value of rock.

$$k = \frac{0.65}{D} \times \frac{E_t}{(1 - \nu^2)} \tag{A.3}$$

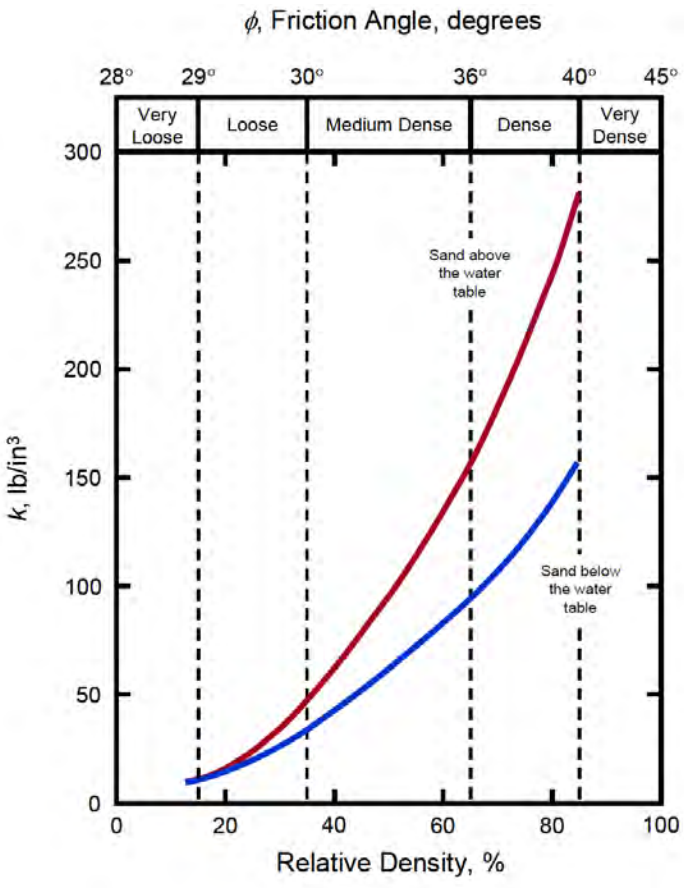

Figure A.18: Representative values of modulus of subgrade reaction (k) for sand p-y models. (Source: Isenhower and Wang 2011)

Where D is the pile/shaft diameter and ν is the Poisson's ratio of rock, which is assumed to be 0.3 for simplicity.

A.7 Supplementary Analysis Options

NVShaft offers different supplementary p-y analysis options to the users, to be carried out after performing the p-y analyses based on the defined loading cases. These options can be selected in the **Supplementary Analysis Options** panel in the **Home** tab, and the specific input parameters can be defined in the corresponding input window after clicking on the **Options for Additional Computation** button

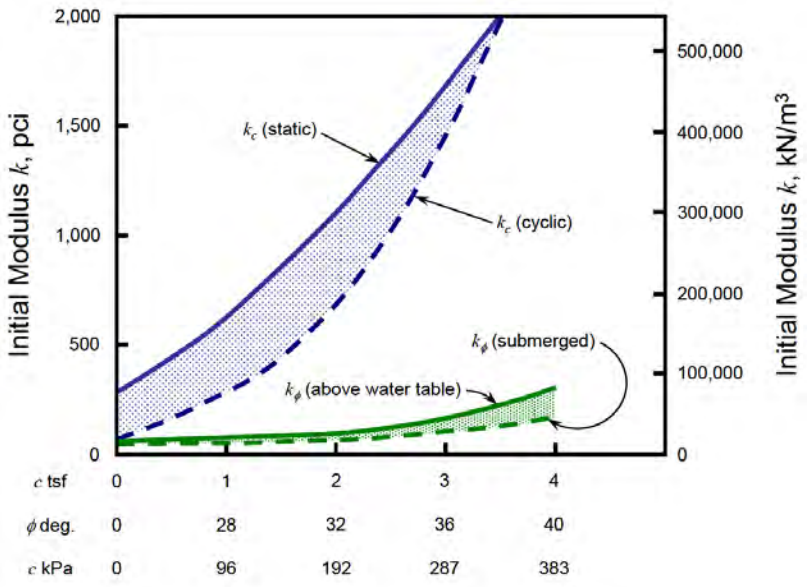

Figure A.19: Representative values of modulus of subgrade reaction (k) for p-y model of c-ϕ soil. (Source: Isenhower and Wang 2011)

located in the same panel (Fig. A.3). The available features of the additional p-y analysis options are discussed in the following sections.

A.7.1 Pushover Analysis

The parameters to perform pushover analysis in NVShaft can be defined in the input window as shown in Fig. A.20. The parameters to perform the analysis can be defined in the input window using the features described below.

1. **Shaft-head Fixity Conditions:** Defines the fixity condition at the shaft-head location to perform the pushover analysis. The radio button group has the following three options.

   (a) **Pinned Head (assume zero moment):** Applies zero moment as one of the boundary conditions.

   (b) **Fixed Head (assume zero rotation):** Applies zero rotation as one of the

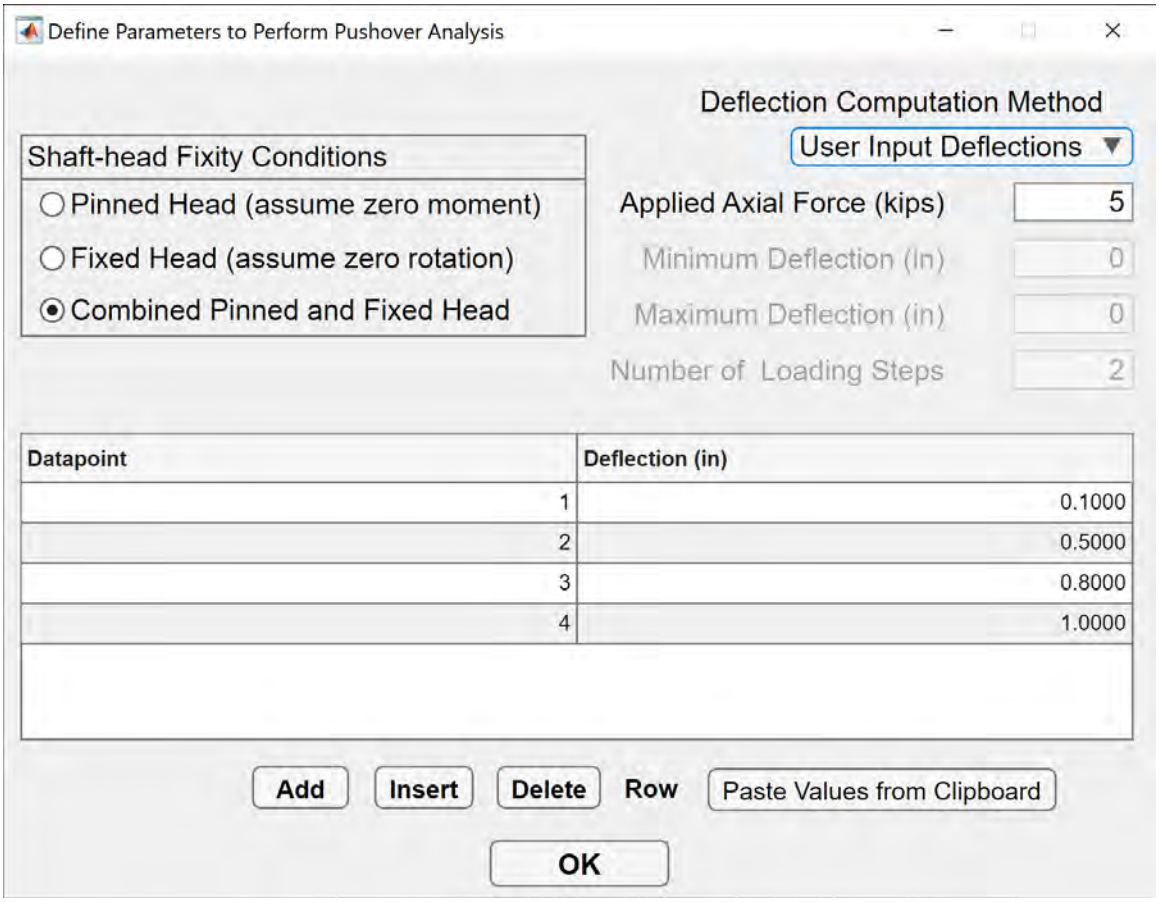

Figure A.20: Input window to define parameters to perform pushover analysis.

boundary conditions.

(c) **Combined Pinned and Fixed Head:** Applies both of the options mentioned above and performs two sets of pushover analyses.

Deflection Computation Method Drop Down Menu: Defines the calculation method to obtain the input deflection values to perform the pushover analysis. The drop down menu provides three different options.

(a) **Arithmetic:** Evenly distributes the input deflection values based on **Minimum Deflection**, **Maximum Deflection** and **Number of Loading Steps** numeric edit field inputs.

(b) **Logarithmic:** Calculates the input deflection values in logarithmic dis-

tribution based on **Minimum Deflection**, **Maximum Deflection** and **Number of Loading Steps** numeric edit field inputs.

(c) **User Input Deflections:** The deflection values can be defined by the users in the input entry table.

2. **Applied Axial Force:** Axial force to be applied in the *p-y* spring model can be defined in the numeric edit field.

A.7.2 Shaft Buckling Analysis

The shaft buckling analysis can be carried out in NVShaft after defining the parameters in the input window as shown in Fig. A.21. The input window has the following features to control different options related to the shaft buckling analysis.

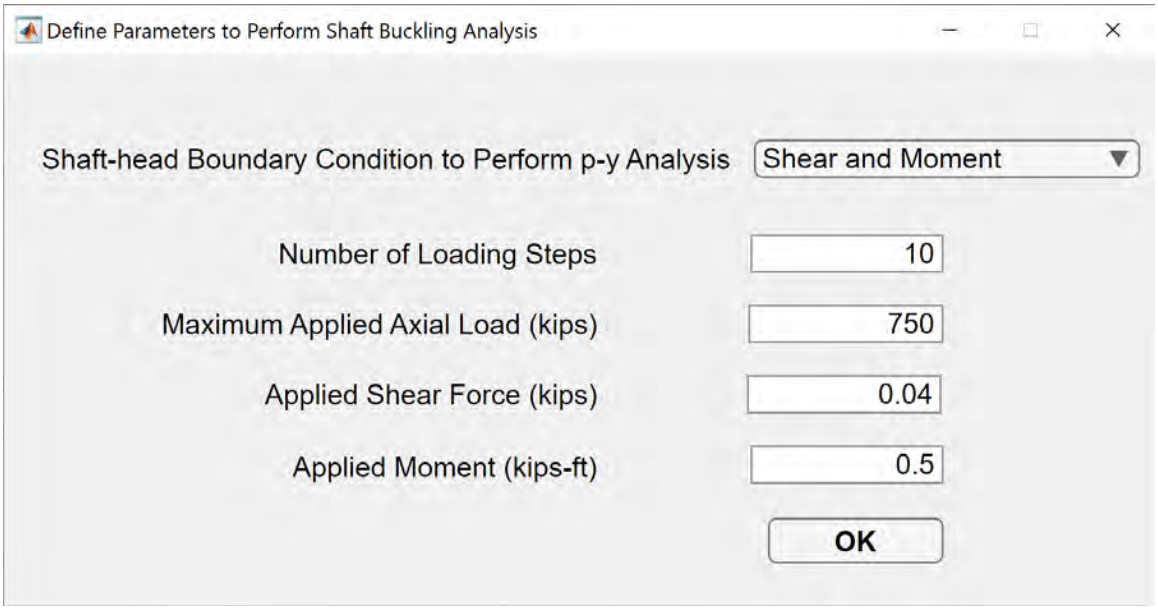

Figure A.21: Input window to define parameters to perform shaft buckling analysis.

1. ***p-y* Boundary Condition Drop Down Menu:** Defines the boundary condition for lateral load analysis and provides the following three options.

(a) **Shear and Moment:** Applies shear and moment type *p-y* boundary condition.

(b) **Shear and slope:** Applies shear and slope type *p-y* boundary condition.

(c) **Shear and Rot. Stiffness:** Applies shear and rotational stiffness type *p-y* boundary condition.

In all of the options, the shear force is applied as the first boundary condition, which can be specified in the **Applied Shear Force** numeric edit field, and the second boundary condition (e.g., moment, slope, or rotational stiffness) can be defined in the numeric edit field located below.

2. **Number of Loading Steps:** Defines the number of loading steps based on evenly distributed increasing axial load from zero to the maximum value.

3. **Maximum Applied Axial Load:** Allows the definition of the maximum applied axial load to be considered in the shaft buckling analysis.

A.7.3 Lateral Stability Analysis

The input parameters for the lateral stability analysis in NVShaft can be defined in the input window as shown in Fig. A.22. The input window has the following features to control different options related to the lateral stability analysis.

1. **Lateral Stability Analysis Method Drop Down Menu:** Assigns the lateral stability analysis method. The users can choose from the following methods available in the program.

   (a) **Methods by ADOT:** Performs stability analysis following the method given by ADOT (2010).

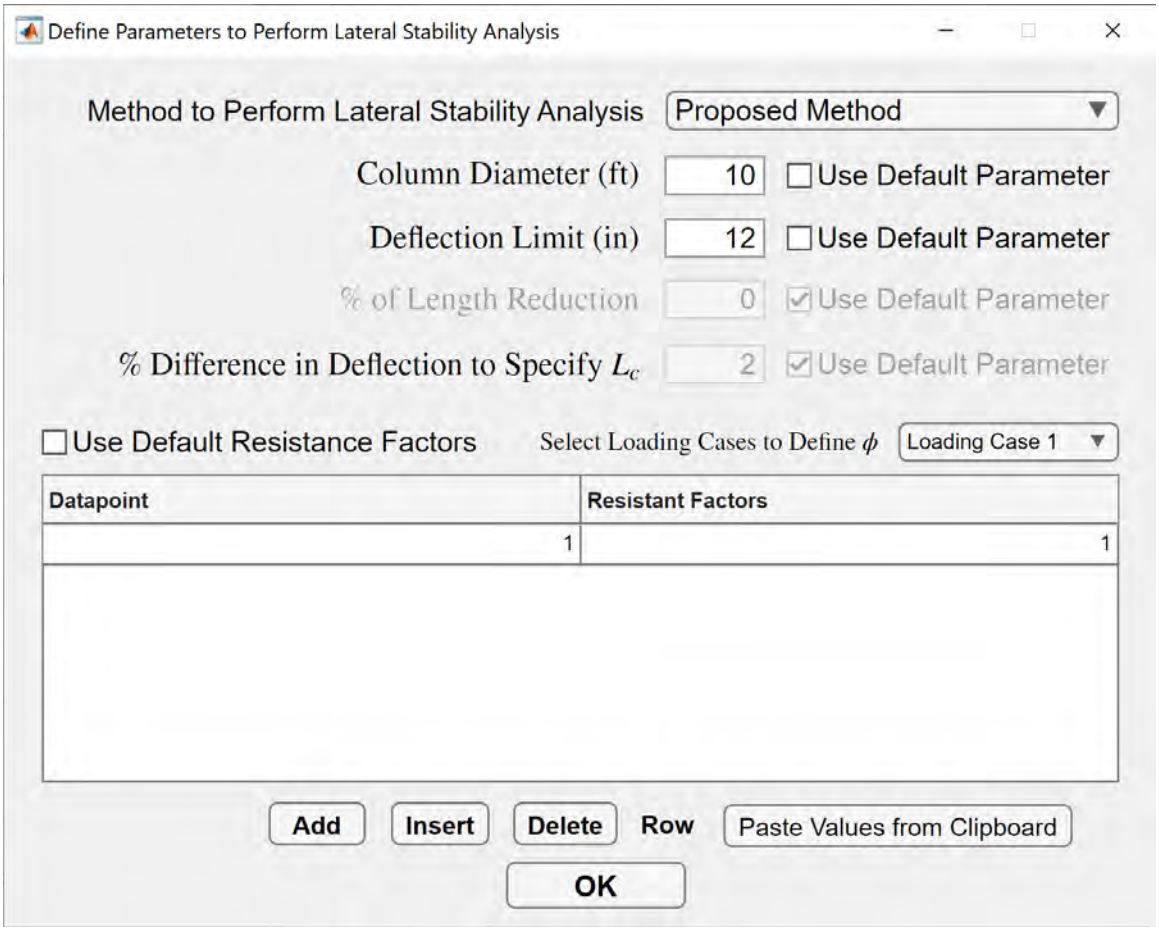

Figure A.22: Input window to define parameters to perform lateral stability analysis.

(b) **Methods by NDOT:** Performs stability analysis following the method outlined in NDOT (2019).

(c) **Proposed Method:** Performs lateral stability analysis following a method proposed by the authors.

(d) **Specify User Input Parameters:** Lateral stability analysis can be performed using the user input parameters.

More details about the methods to perform lateral stability analysis can be found in Appendix B.

2. **Input Parameters to Control Lateral Stability Analysis:** Depending on the

selection of the method, the following input parameters are available to carry out the lateral stability analysis.

(a) $\boldsymbol{L_{initial}/D_{mean}}$ **Ratio:** Defines the initial length to mean diameter ratio to initiate the lateral stability analysis. This parameter is not available in the proposed method, as in that case the initial length is calculated either from shaft overhead length or shaft diameter.

(b) **Column Diameter:** Defines the column diameter to be used in the proposed lateral stability analysis method. The input value is used to calculate the initial shaft length (L_{init}) to start the analysis.

(c) **Deflection Limit:** Specifies the deflection limit for the stability analysis. In the proposed method, the length of the shaft is increased in the subsequent *p-y* analysis, while for the other three methods shaft length is decreased. For the proposed method, the calculated deflection values are ignored in calculating L_c if they exceed the specified deflection limit. For the other three methods, NVShaft terminates the stability analysis for a specific loading case, if the deflection values exceed the specified limit.

(d) **% of Length Reduction:** Only available for the ADOT and NDOT method and specify user input parameters options. Should be defined to control the percent reduction of shaft length in the subsequent *p-y* analysis.

(e) **% Difference in Deflection to Specify $\boldsymbol{L_c}$:** This parameter is used to calculate the critical shaft length (L_c) from the lateral stability plot (Fig. B.1b).

(f) **Resistance Factors:** Resistance factors can be used to increase the loads to be applied as boundary conditions. The loading cases defined in the **Boundary Condition** tab can be selected from the **Select Loading Cases to Define $\boldsymbol{\phi}$** drop down menu, and the corresponding resistance factor

values can be given as inputs. The user input values of the resistance factors can be specified in the input entry table as shown in Fig. A.22. The default values of the resistance factor for the ADOT and NDOT methods are 1.0 and 0.8, respectively.

The allowable ranges of these input parameters and the default values used in the lateral stability analysis for different methods are summarized in Table A.9.

Table A.9: Default values and allowable ranges of input parameters to perform lateral stability analysis.

Method	$L_{initial}/D_{mean}$ Ratio		Deflection Limit	% of Length Reduction		% Difference in Defl. to Specify L_c
-	Default Value	Allowable Range	Default Value	Default Value	Allowable Range	Default Value
Method by ADOT	15	10-15	4 in/ 101.6 mm	10	10-15	5%
Method by NDOT	10	-	4 in/ 101.6 mm	1*Mean Diameter	-	2%
Proposed Method	-	-	24 in/ 609.6 mm	-	-	2%
Specify User Input Parameters	-	-	4 in/ 101.6 mm	-	-	-

A.7.4 Shaft-head Stiffness Matrix Calculation

The options for the shaft-head stiffness matrix calculation in NVShaft can be defined from the input window as shown in Fig. A.23. The following options are available in this case, as discussed below.

1. **Boundary Conditions for p-y Analysis:** Defines the boundary conditions to perform *p-y* analysis as part of the shaft-head stiffness matrix calculation. The radio button group has the following options.

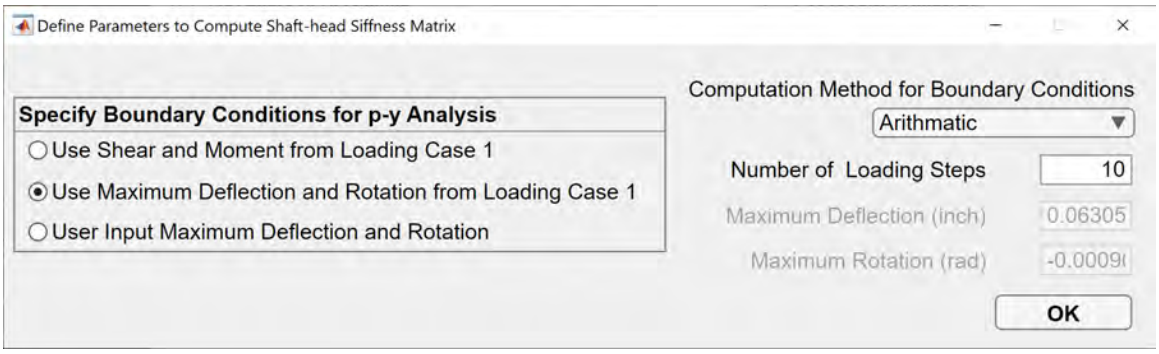

Figure A.23: Input window to define parameters to compute shaft-head stiffness matrix.

(a) **Use Shear and Moment from Loading Case 1**

(b) **Use Maximum Deflection and Rotation from Loading Case 1**

(c) **User Input Maximum Deflection and Rotation**

The **Maximum Deflection** and **Maximum Rotation** numeric edit fields can be used to specify the boundary conditions for the third option mentioned above.

2. **Computation Method for Boundary Conditions Drop Down Menu:** Defines the calculation method to obtain the input boundary condition to perform the analysis. Depending on the selection, the boundary condition values are calculated based on the **Number of Loading Steps** numeric edit field inputs. The drop down menu provides two different options.

   (a) **Arithmetic:** The boundary condition values are evenly distributed.

   (b) **Logarithmic:** The boundary condition values are logarithmically distributed.

A.8 Example Problems

Two sets of examples are presented in this section to highlight the numerical capabilities of NVShaft. In the first two examples, a simple elastic pile embedded in a single clayey soil layer is considered to perform both conventional and unified *p-y* analyses. In the third and fourth examples, the 4 ft diameter shaft from the Las Vegas City Center Project (LOADTEST, 2005) is considered, to perform the simulations of the conventional top-loaded and the bi-directional axial load tests. The example problems are presented to familiarize the basic features of NVShaft to the users.

A.9 Example 1.1: Conventional *p-y* Analysis of Elastic Pile Embedded in Soft Clay

A.9.1 Defining General Options

After starting the application or clicking the **New** button, navigate to the **Home** tab, and follow these steps:

- **Step 1.1:** On the **General Options** panel, keep the default values of **Absolute** and **Relative Tolerances** *[1e-6 and 0.1]*.
- **Step 1.2:** Keep the default value of **Engineering Units** *[US Customary Units (inches, feet and pound]*.
- **Step 1.3:** Keep the default value of **Loading Type** *[Static Loading]*.
- **Step 1.4:** To perform *p-y* analysis, select **Type of Analysis** as *Lateral Load (p-y) Analysis*.
- **Step 1.5:** Keep the default value of **No. of Pile Increments** *[100]*.

- **Step 1.6:** Keep the default value of **Supplementary Analysis Options** *[off]*.

At this point, the **Home** tab should look like as presented in Fig. A.24.

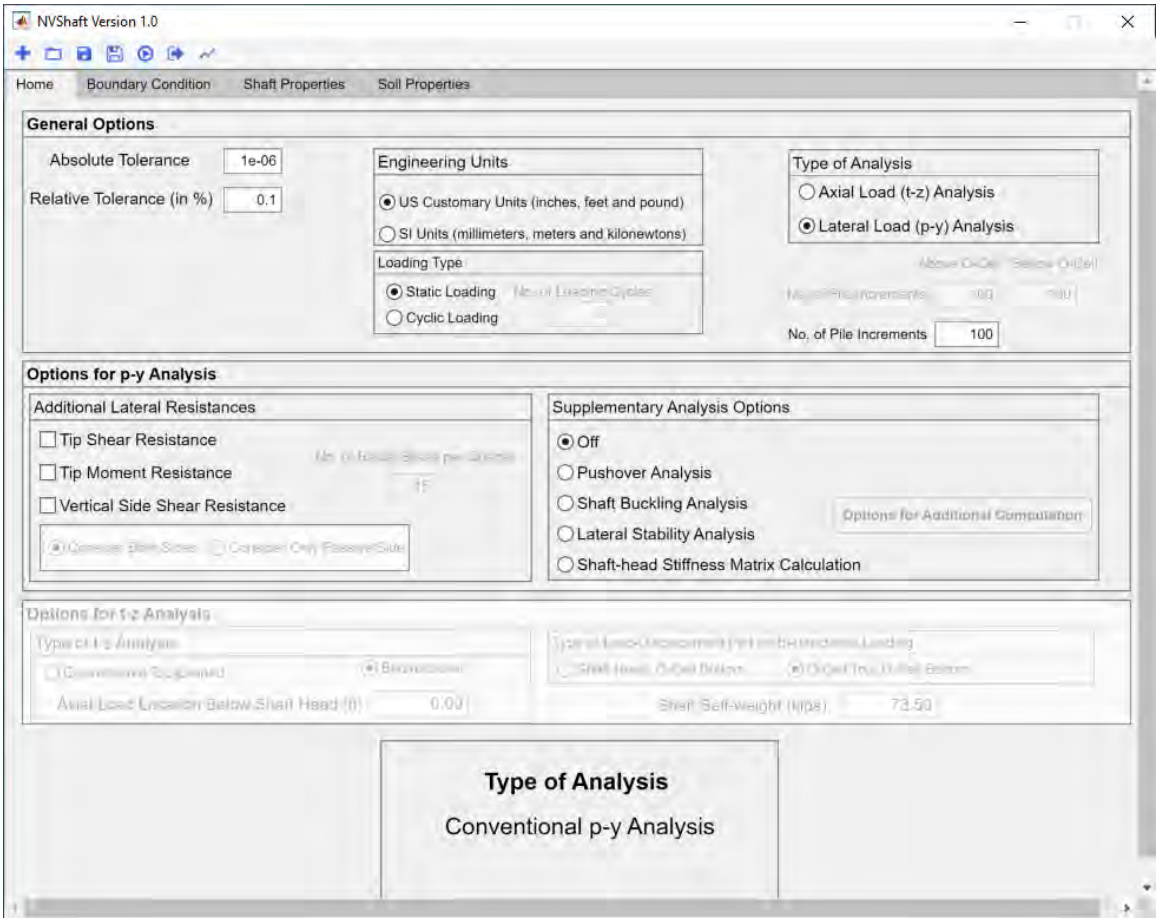

Figure A.24: The Home tab in Example 1.1.

A.9.2 Defining Boundary Conditions

Navigate to the **Boundary Condition** tab, and follow these steps:

- **Step 2.1:** On the **No. of Boundary Conditions to Add** edit field, input *3* and click on **Clear and Add Boundary Condition(s)** button. This will define three zero boundary conditions.

- **Step 2.2:** In all loading cases, keep ***p-y* Boundary Conditions** as *Shear and Moment* and ***t-z* Boundary Conditions** as *Shaft Head Load*.
- **Step 2.3:** Change loading cases from **Select Loading Case** drop down menu. Input the values as shown in Table A.10 to define the boundary conditions in three loading cases.
- **Step 2.4:** Keep the default value of **Lateral Load Location Below Shaft Head (ft)** *[0.00]*.
- **Step 2.5:** Keep the **Use Single Distributed Load Profile** and **Use Single Soil Movement Profile** *unchecked*.

At this point, the **Boundary Condition** tab should look like as shown in Fig. A.25.

Table A.10: Boundary conditions used in Example 1.1 and Example 1.2.

Loading Case	*p-y* Boundary Conditions	*t-z* Boundary Conditions	Lateral Load (kips)	Bending Moment (kips-ft)	Axial Load (kips)
Loading Case 1	Shear and Moment	Shaft Head Load	50	0	25
Loading Case 1	Shear and Moment	Shaft Head Load	75	0	50
Loading Case 1	Shear and Moment	Shaft Head Load	100	0	75

A.9.3 Defining Shaft Properties

Navigate to the **Shaft Properties** tab, and follow these steps:

- **Step 3.1:** Input *25* in **Section Length (ft)** numeric edit field.
- **Step 3.2:** Keep the selection for **Select Section Type** as *Elastic Section*.
- **Step 3.3:** Keep the default value *0.0* in **Shaft Head Location (ft)** numeric edit field.

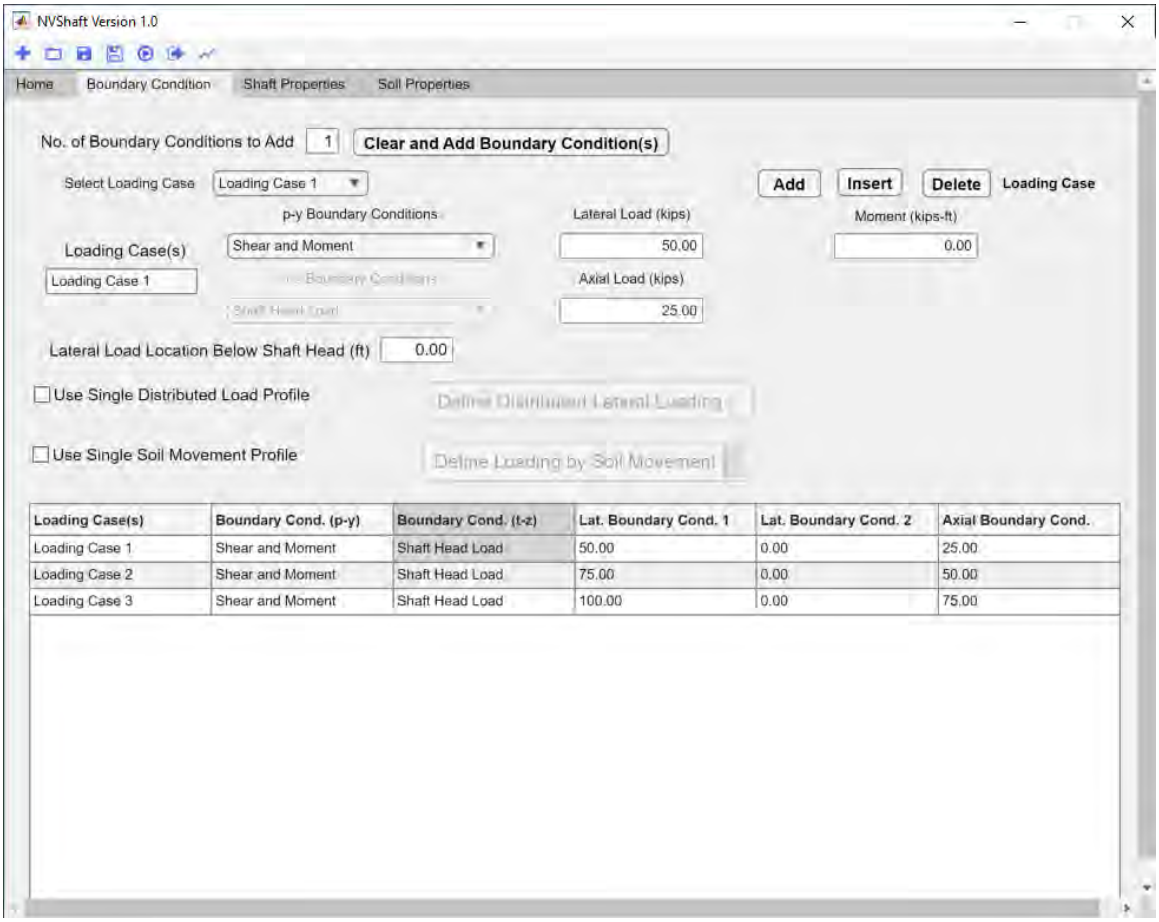

Figure A.25: The Boundary Condition tab in Example 1.1 and 1.2.

- **Step 3.4:** On the **Shaft Section Properties** panel, keep the selection for **Select Section Shape** as *Solid Circular*.
- **Step 3.5:** On the **Shaft Section Properties** panel, input the section properties as summarized in Table A.11.

After following these steps, the **Shaft Properties** tab should look similar to Fig. A.26.

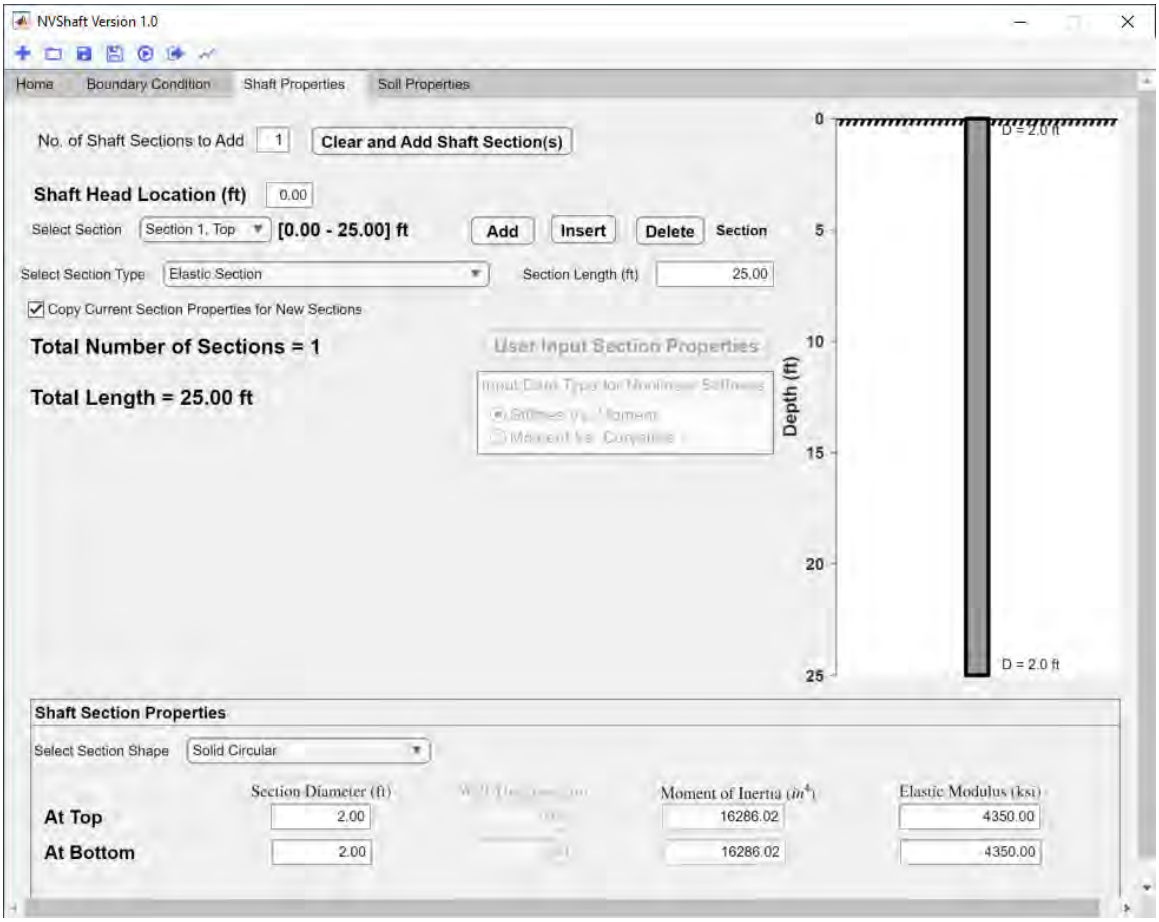

Figure A.26: The Shaft Properties tab in Example 1.1 and 1.2.

Table A.11: Shaft section properties used in Example 1.1 and Example 1.2.

	Section Diameter (ft)	Elastic Modulus (ksi)
At Top	2	4.35e3
At Bottom	2	4.35e3

A.9.4 Defining Lateral Soil Resistance

Navigate to the **Soil Properties** tab. Then go to **Lateral Resistance** tab and follow these steps:

- **Step 4.1:** Input *25* in **Depth of Bottom of Soil Layer Below Ground Surface (ft)** numeric edit field.

- **Step 4.2:** Keep **Specify p-Multiplier for Lateral Resistance** *unchecked*.
- **Step 4.3:** Select *Matlock 1970 [Soft Clay]* from the **Select p-y Curve** drop down menu.
- **Step 4.4:** On the **Soil Material Properties** panel, input the soil properties as shown in Table A.12.

After following these steps, the **Lateral Resistance** tab should be similar to Fig A.27. The schematic of the *p-y* soil layer for Example 1.1 and 1.2 is shown in Fig. A.33a.

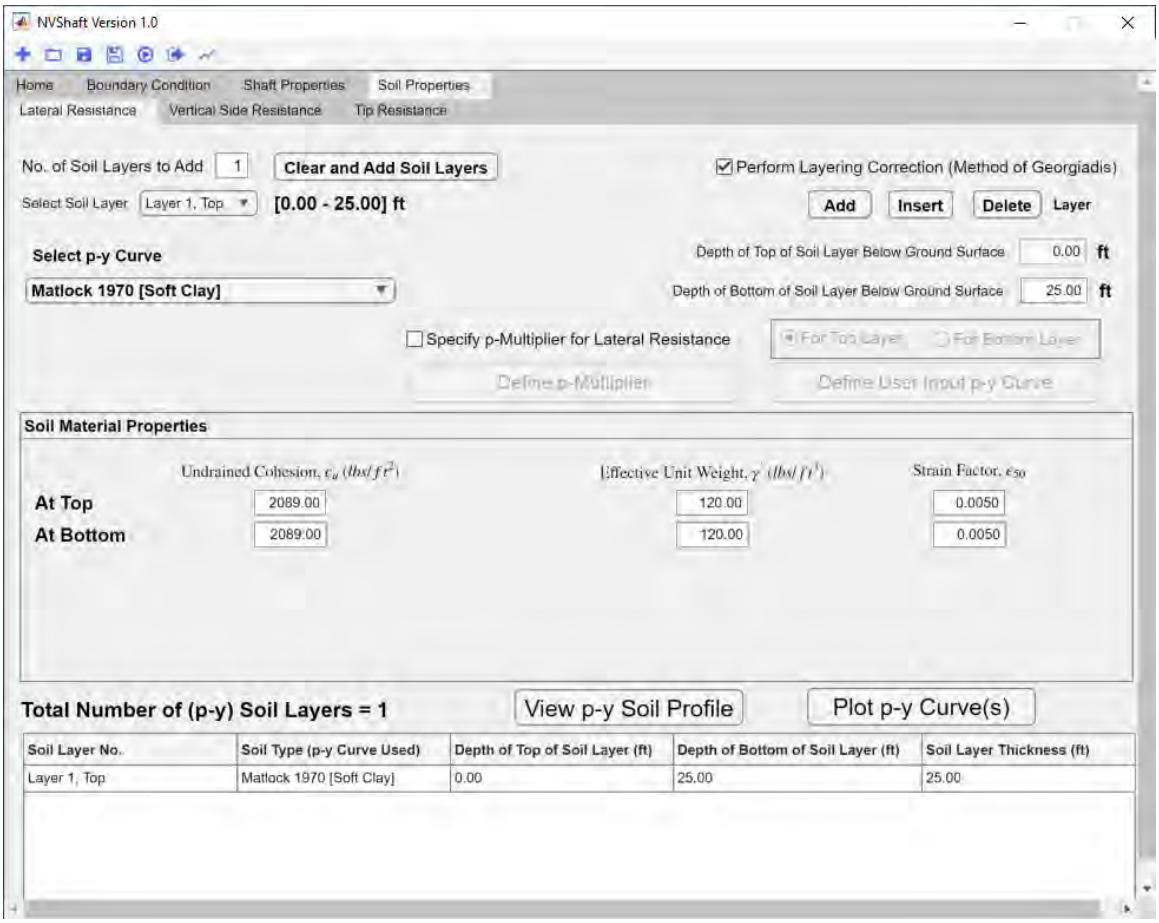

Figure A.27: The Lateral Resistance tab in Example 1.1 and 1.2.

Table A.12: Characterization of soil lateral (*p-y*) resistance in the Example 1.1 and Example 1.2.

	Undrained Cohesion, c_u (lbs/ft^2)	Effective Unit Weight, γ' (lbs/ft^3)	Strain Factor, ϵ_{50}
At Top	2089	120	0.005
At Bottom	2089	120	0.005

A.9.5 Running Analysis and Obtaining Outputs

- **Step 5.1:** Navigate back to the **Home** tab. To run the conventional p-y analysis, click on the **Run** button.
- **Step 5.2:** To generate the output as either Excel spreadsheet (.xlsx) or report (.pdf) format, click on the **Generate Output File** button, which should get enabled after a successful analysis.
- **Step 5.3:** To redo the plots, click on the **Plot Available Outputs** button.

The outputs after a successful analysis of Example 1.1 are shown in Fig A.28 to Fig A.30.

A.10 Example 1.2: Unified *p-y* Analysis of Elastic Pile Embedded in Soft Clay

Example 1.2 uses all the soil and shaft material properties defined to perform the conventional *p-y* analysis in Example 1.1. The additional input parameters required to perform the unified *p-y* analysis of the same problem can be specified by following the steps mentioned below.

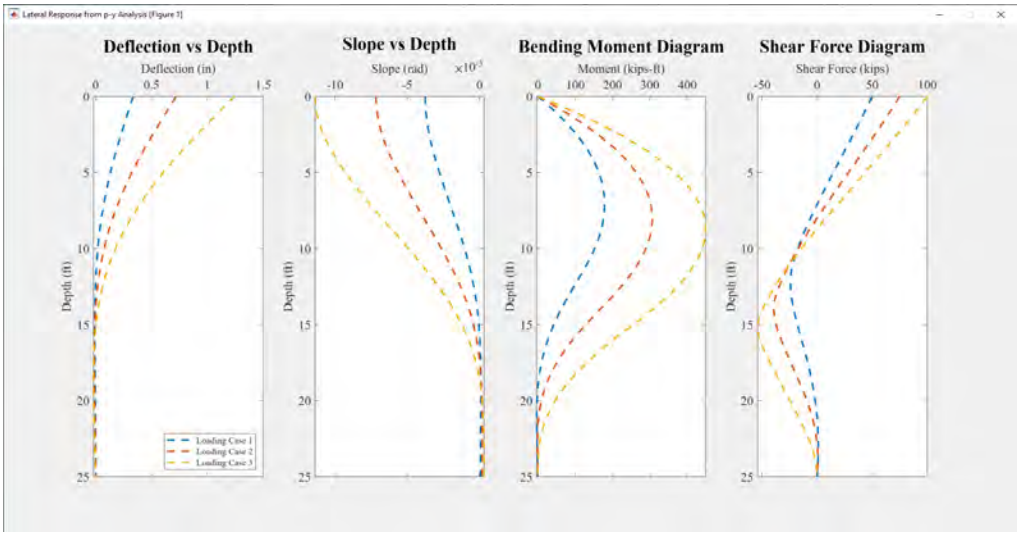

Figure A.28: The deflection, slope, bending moment, and shear force diagram obtained from Example 1.1.

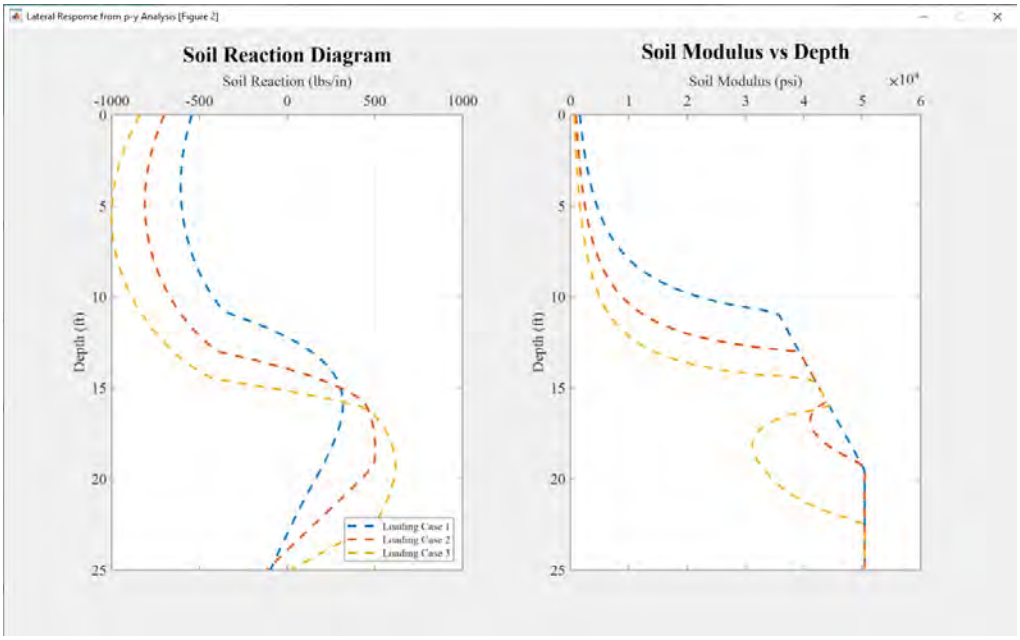

Figure A.29: The soil reaction and soil modulus diagram obtained from Example 1.1.

A.10.1 Defining General Options

Navigate to the **Home** tab, and follow these steps:

- **Step 1.1:** On the **Additional Lateral Resistances** panel, *check* **Tip Shear Resis-**

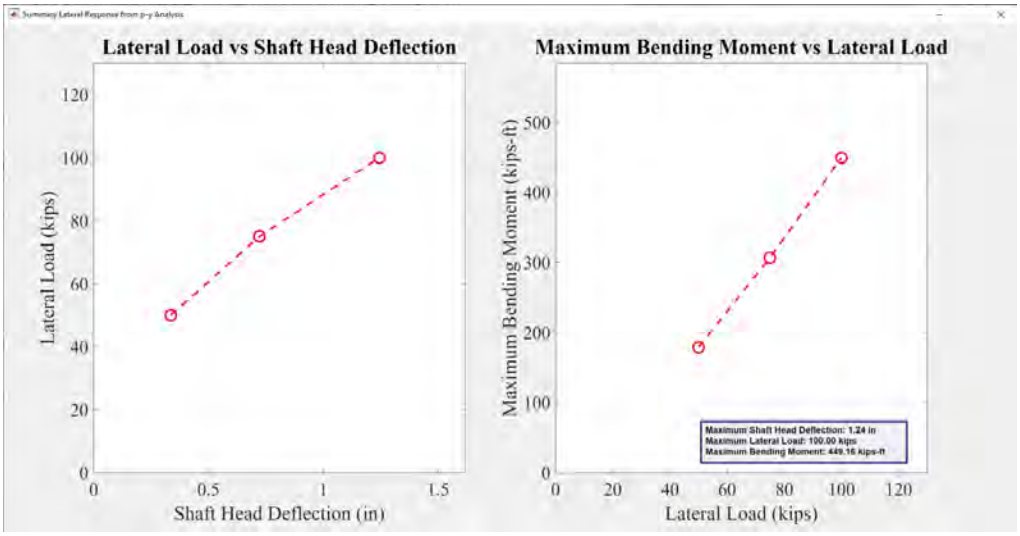

Figure A.30: The lateral load vs head deflection plot and bending moment vs lateral load plot from Example 1.1.

tance, **Tip Moment Resistance** and **Vertical Side Shear Resistance**. This will prompt NVShaft to perform the unified *p-y* analysis.

- **Step 1.2:** Keep the default value of **No. of Radial Slices per Quarter** *[15]*.
- **Step 1.3:** Select **Consider Both Sides** to use both active and passive sides in mobilized side shear calculations.
- **Step 1.4:** Keep the default value of **Supplementary Analysis Options** *[off]*.

After following these steps, the **Home** tab should look similar to Fig. A.31.

A.10.2 Defining Vertical Side Resistance

- **Step 2:** Navigate to **Vertical Side Resistance** tab. To copy the soil properties already defined in the **Lateral Resistance** tab, simply click on **Generate *t-z* Soil Layers from *p-y* Properties**. Click **OK** to the dialogue box with the title **Warning in Defining Soil Properties**.

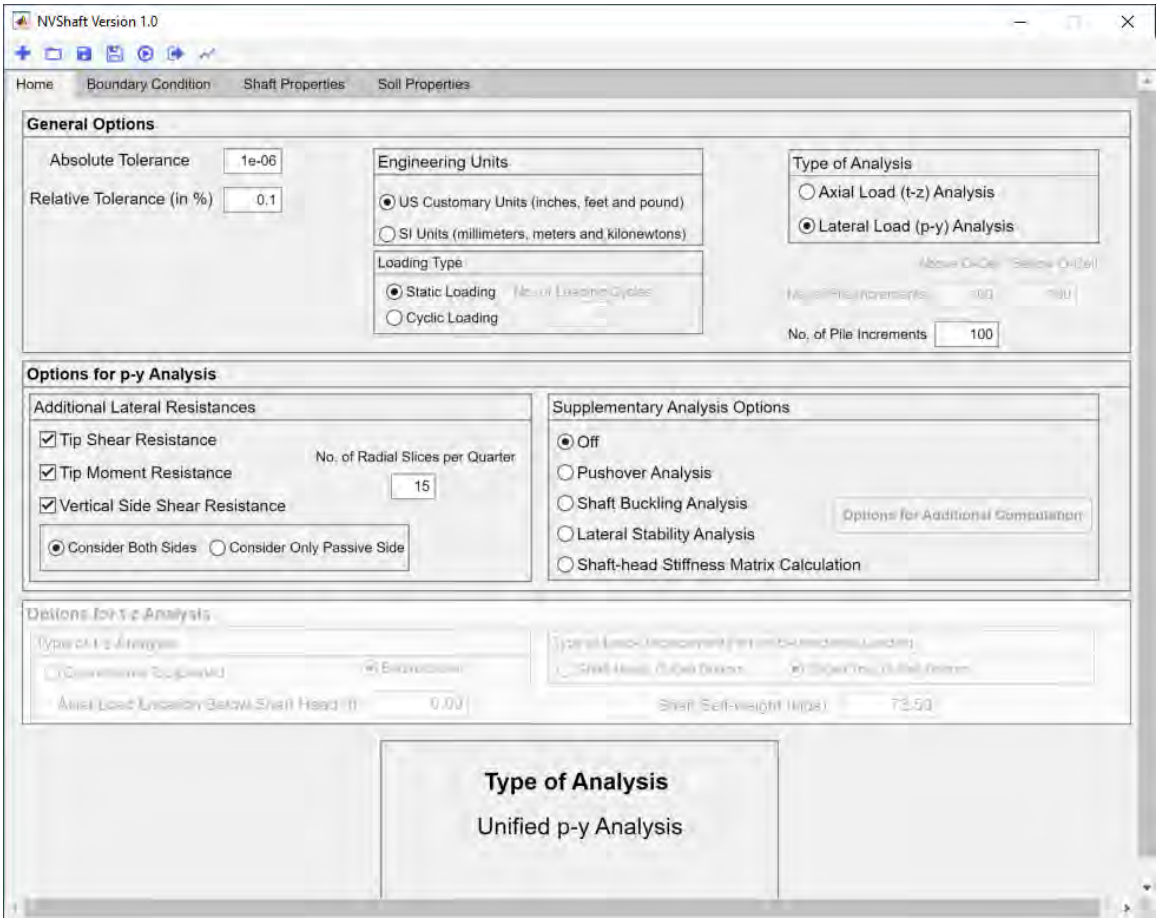

Figure A.31: The Home tab in Example 1.2.

At this point, the **Vertical Side Resistance** tab should look like as shown in Fig. A.32. The schematic of the *t-z* soil layer for Example 1.2 is shown in Fig. A.33b.

A.10.3 Defining Tip Resistances

Navigate to the **Tip Resistance** tab, and follow the steps mentioned below:

- **Step 3.1:** On the **End Bearing Resistance** panel, select *API Clay* from the **Select End Bearing Resistance Curve** drop down menu.
- **Step 3.2:** On the **End Bearing Resistance** panel, from the **Source of Material Properties** drop down menu, select the option *User-Defined*.

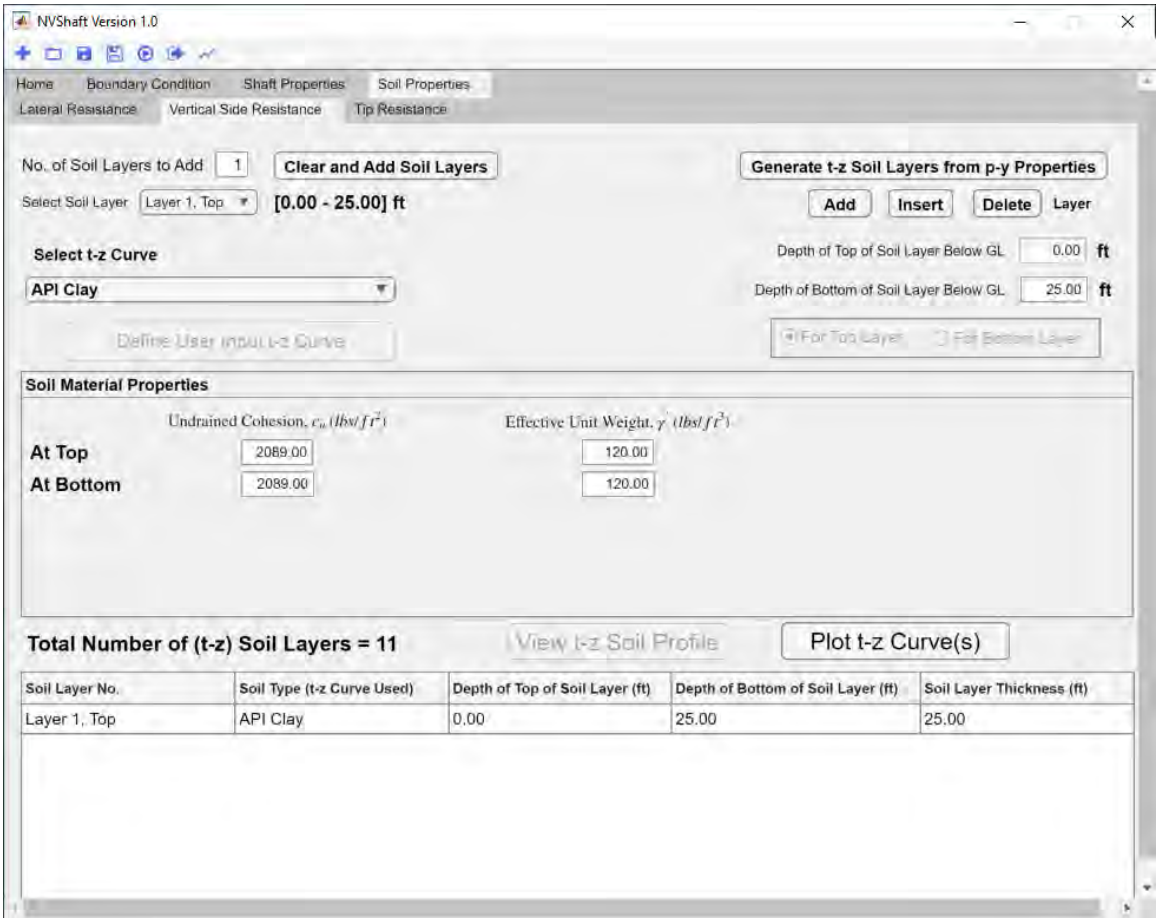

Figure A.32: The Vertical Side Resistance tab in Example 1.2.

- **Step 3.3:** On the **End Bearing Resistance** panel, input *2089* in **Undrained Cohesion, c_u(lbs/ft^2)** edit field.
- **Step 3.4:** On the **Tip Shear Resistance** panel, select *Vallabhan 1982* from the **Select Tip Shear Resistance Curve** drop down menu.
- **Step 3.5:** On the **Tip Shear Resistance** panel, from the **Source of Material Properties** drop down menu, select the option *User-Defined*.
- **Step 3.6:** On the **Tip Shear Resistance** panel, input *2089* in **Undrained Cohesion, c_u(lbs/ft^2)** edit field, and *0* in **Friction Angle, ϕ (Degree)** edit field.
- **Step 3.7:** On the **Tip Moment Resistance** panel, select *Simplified Model for Circular Shaft* from the **Select Tip Moment Resistance Curve** drop down

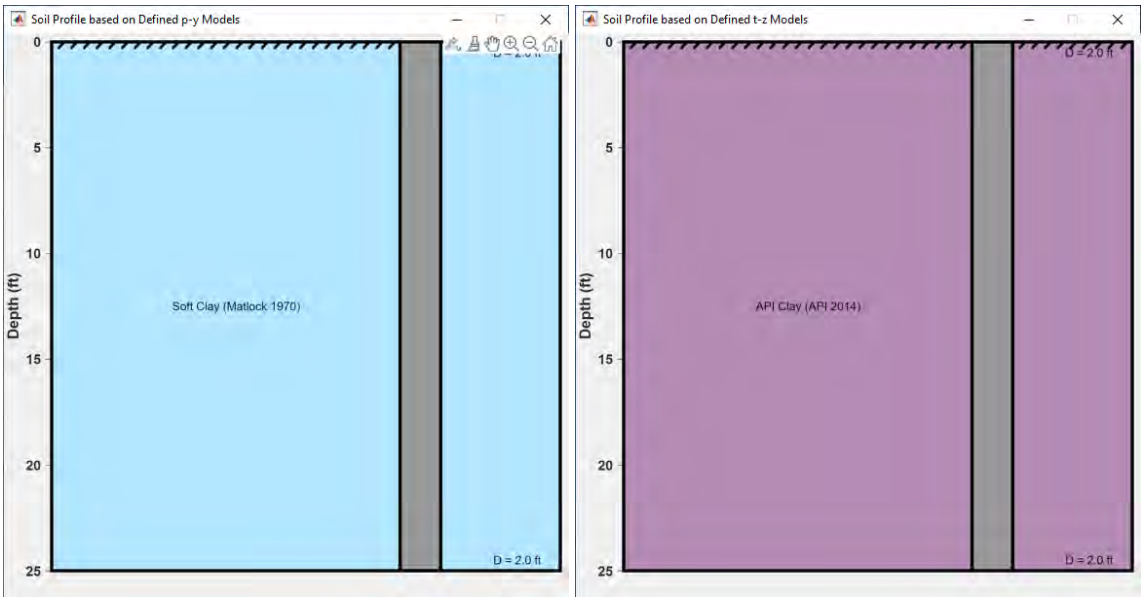

(a) (b)

Figure A.33: The schematics of the (a) *p-y* and (b) *t-z* soil layers along with the pile section profile for Example 1.1 and 1.2.

menu.

- **Step 3.8:** On the **Tip Moment Resistance** panel, select *From Defined End Bearing Model* from the **Method to Calculate q_{ult}** drop down menu.
- **Step 3.9:** On the **Tip Moment Resistance** panel, input *0* in **Subgrade Modulus, k (lbs/in^3)** edit field. This will prompt NVShaft to obtain the default value of subgrade modulus for clay material.

At this point, the **Tip Resistance** tab should look like as shown in Fig. A.34.

A.10.4 Running Analysis and Obtaining Outputs

Follow the steps as described in Section A.9.5. The outputs after a successful analysis of Example 1.2 are shown in Fig A.35 to Fig A.39.

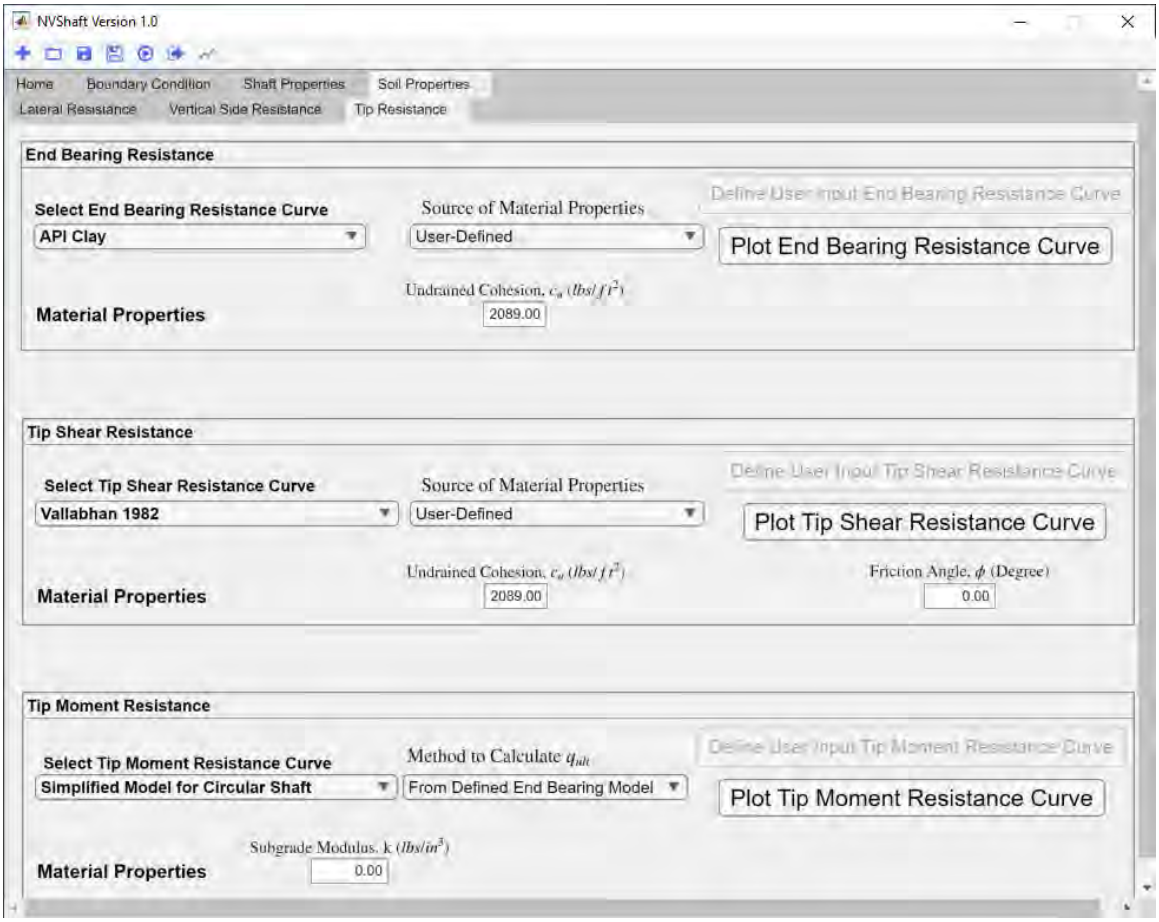

Figure A.34: The Tip Resistance tab in Example 1.2.

A.11 Example 2.1: Conventional Top-loaded Axial Load Test Simulation of Test Shaft from the Las Vegas City Center Project

A.11.1 Defining General Options

After starting the application or clicking the **New** button, navigate to the **Home** tab, and follow these steps:

- **Step 1.1:** On the **General Options** panel, keep the default values of **Absolute** and **Relative Tolerances** *[1e-6 and 0.1]*.
- **Step 1.2:** Keep the default value of **Engineering Units** *[US Customary Units*

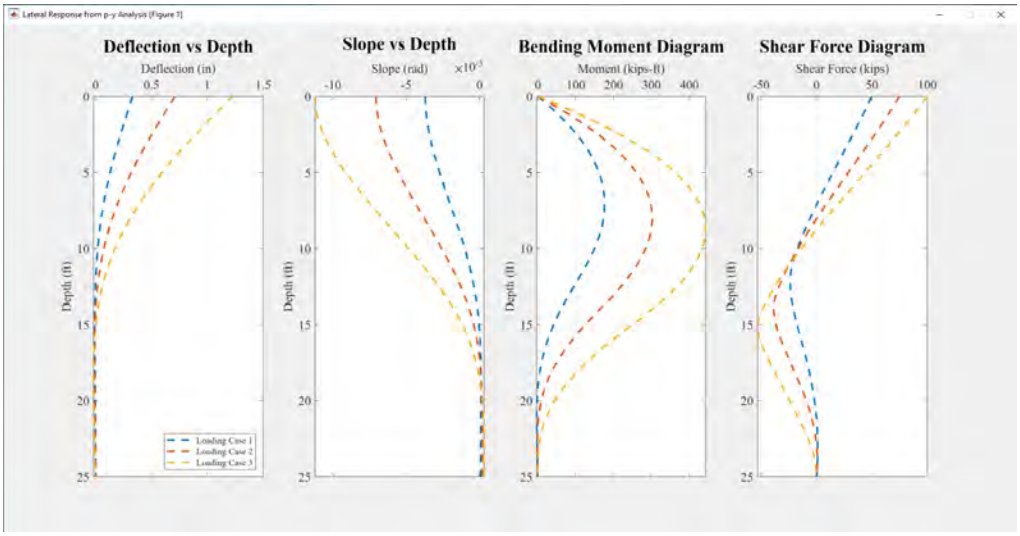

Figure A.35: The deflection, slope, bending moment, and shear force diagram obtained from Example 1.2.

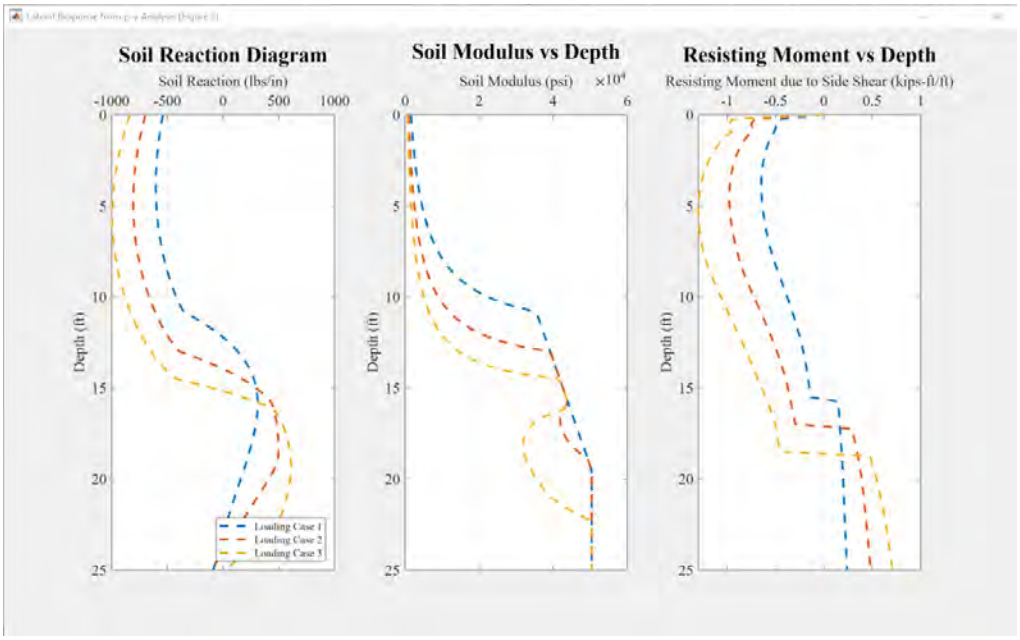

Figure A.36: The soil reaction, soil modulus and resisting moment due to side shear diagram obtained from Example 1.2.

(inches, feet and pound].

- **Step 1.3:** To perform *t-z* analysis, select **Type of Analysis** as *Axial Load (t-z) Analysis*.

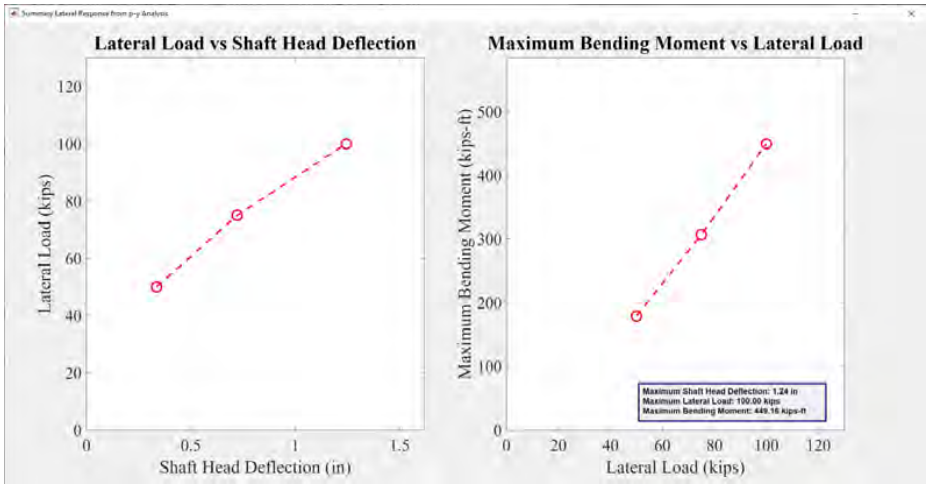

Figure A.37: The lateral load vs head deflection plot and bending moment vs lateral load plot from Example 1.2.

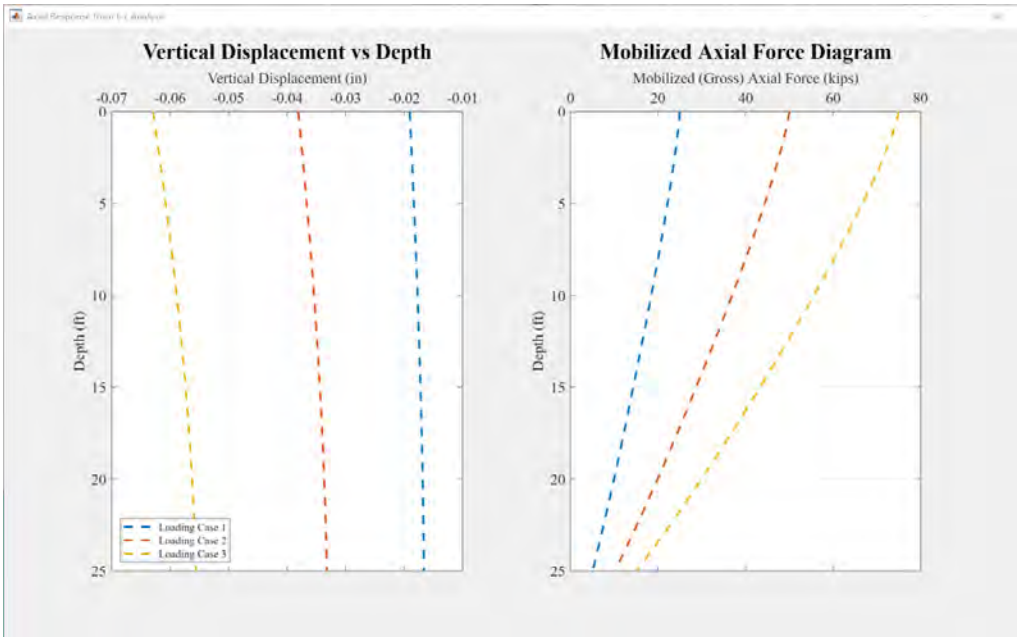

Figure A.38: The vertical displacement and mobilized axial force diagram from Example 1.2.

- **Step 1.4:** Keep the default value of **No. of Pile Increments** *[100]*.
- **Step 1.5:** On the **Type of *t-z* Analysis** panel, select *Conventional Top-Loaded* radio button option. This will prompt NVShaft to apply the axial load at the shaft head in the *t-z* model.

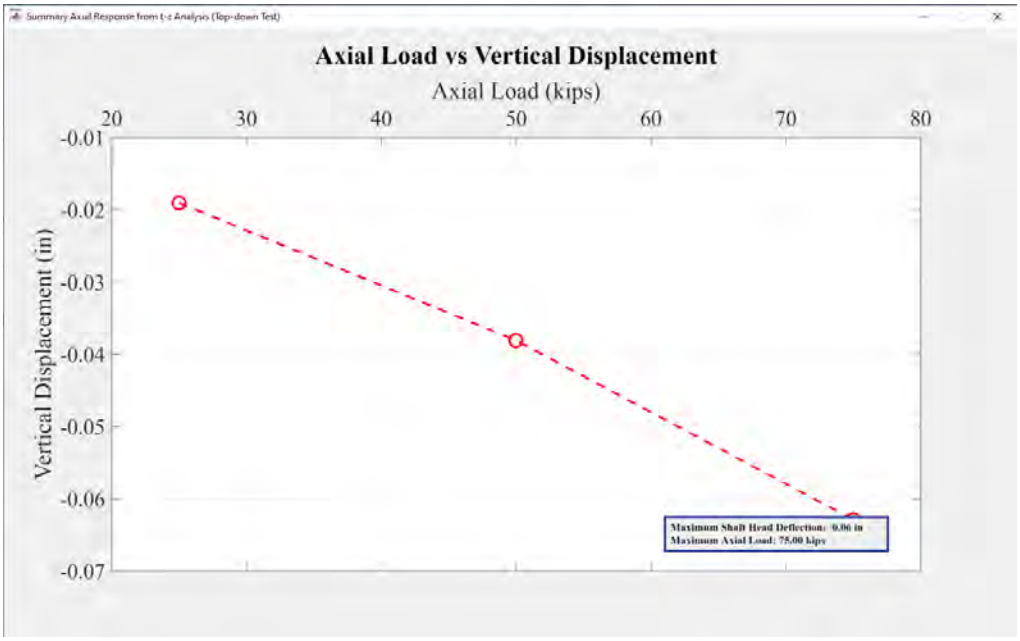

Figure A.39: The axial load vs vertical displacement plot from Example 1.2.

At this point, the **Home** tab should look like as presented in Fig. A.40.

A.11.2 Defining Boundary Conditions

Navigate to the **Boundary Condition** tab, and follow these steps:

- **Step 2.1:** On the **No. of Boundary Conditions to Add** edit field, input *11* and click on **Clear and Add Boundary Condition(s)** button. This will define eleven zero boundary conditions for the *t-z* analysis.
- **Step 2.2:** In all loading cases, keep the ***t-z* Boundary Conditions** as *Shaft Head Load*.
- **Step 2.3:** Change loading cases from **Select Loading Case** drop down menu. Input the values as shown in Table A.13 to define the boundary conditions in all eleven loading cases.

At this point, the **Boundary Condition** tab should look like as shown in Fig. A.41.

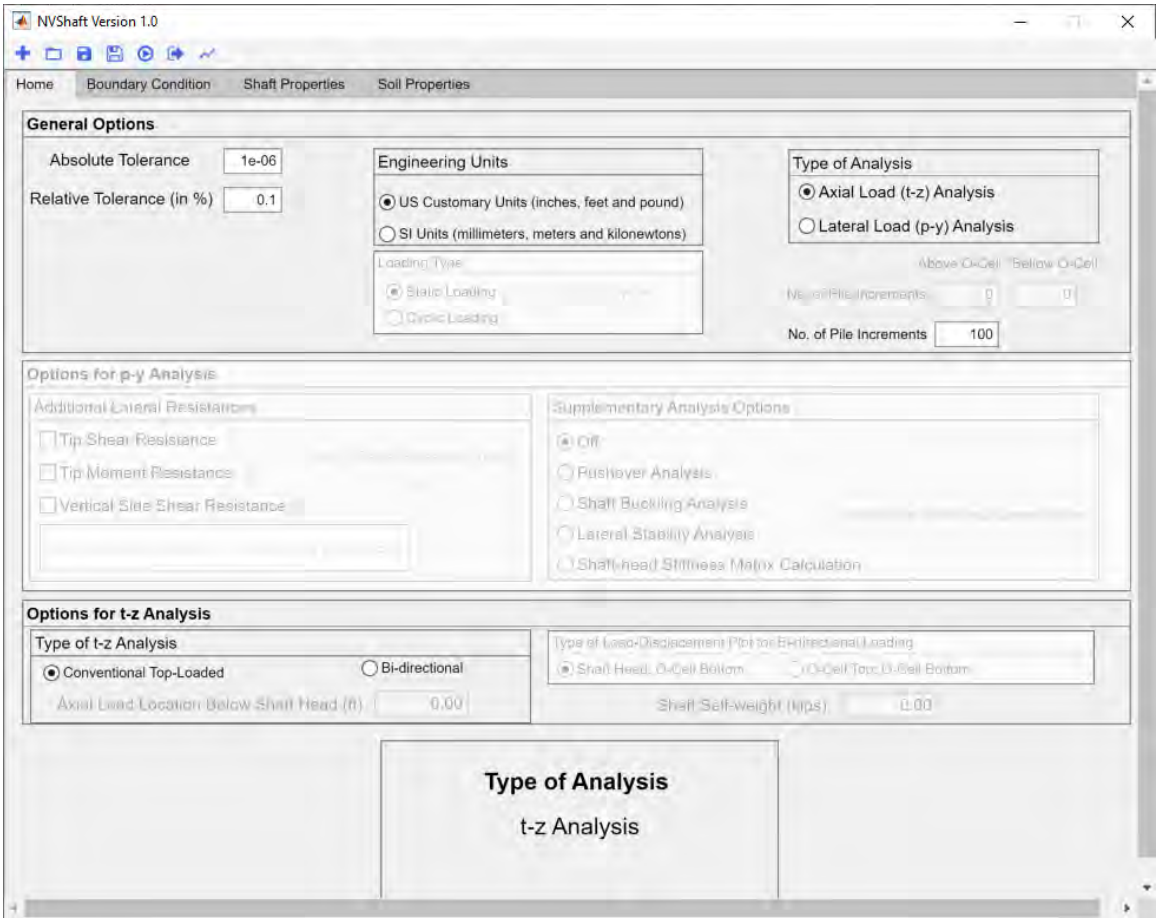

Figure A.40: The Home tab in Example 2.1.

A.11.3 Defining Vertical Side Resistance

Navigate to the **Soil Properties** tab. Then go to **Vertical Side Resistance** tab and follow these steps:

- **Step 3.1:** Input *11* in **No. of Soil Layers to Add** numeric edit field, and then click on **Clear and Add Soil Layers** button. This will cause a total of 11 *API Clay t-z* layers to be added in the numerical model.
- **Step 3.2:** Change the soil layers using the **Select Soil Layer** drop down menu. Input the soil properties and the relevant *t-z* models as shown in Table A.14.

After following these steps, the **Vertical Side Resistance** tab should be similar

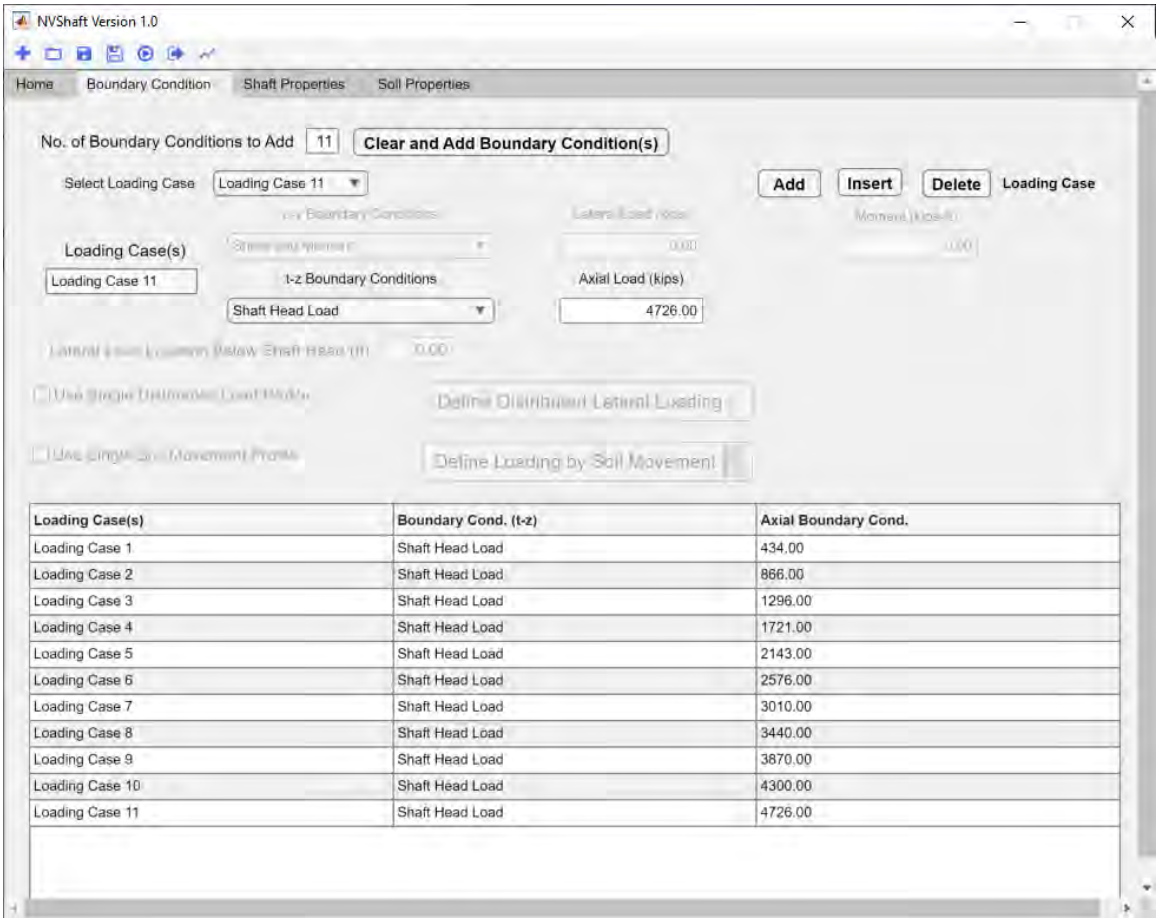

Figure A.41: The Boundary Condition tab in Example 2.1 and 2.2.

to Fig A.42. The schematic of the *t-z* soil layers for Example 2.1 and 2.2 is shown in Fig. A.43.

A.11.4 Defining Tip Resistances

Navigate to the **Tip Resistance** tab, and follow the steps described below:

- **Step 4.1:** On the **End Bearing Resistance** panel, select *API Sand* from the **Select End Bearing Resistance Curve** drop down menu.
- **Step 4.2:** On the **End Bearing Resistance** panel, from the **Source of Material Properties** drop down menu, select the option *User-Defined*.

Table A.13: Boundary conditions used in Example 2.1 and Example 2.2.

Loading Case	*t-z* Boundary Condition	Axial Load (kips)
Loading Case 1	Shaft Head Load	434
Loading Case 2	Shaft Head Load	866
Loading Case 3	Shaft Head Load	1296
Loading Case 4	Shaft Head Load	1721
Loading Case 5	Shaft Head Load	2143
Loading Case 6	Shaft Head Load	2576
Loading Case 7	Shaft Head Load	3010
Loading Case 8	Shaft Head Load	3440
Loading Case 9	Shaft Head Load	3870
Loading Case 10	Shaft Head Load	4300
Loading Case 11	Shaft Head Load	4726

- **Step 4.3:** On the **End Bearing Resistance** panel, input *36* in **Friction Angle, ϕ (Degree)** edit field. Also, input *0* in **Bearing Capacity Factor, N_q** edit field. This will prompt NVShaft to obtain the default value of bearing capacity factor for sand material.

At this point, the **Tip Resistance** tab should look like as shown in Fig. A.44.

A.11.5 Defining Shaft Properties

Navigate to the **Shaft Properties** tab, and follow these steps:

- **Step 5.1:** Input *116.8* in **Section Length (ft)** numeric edit field.
- **Step 5.2:** Keep the selection for **Select Section Type** as *Elastic Section*.
- **Step 5.3:** Input *5.2* in **Shaft Head Location (ft)** numeric edit field.

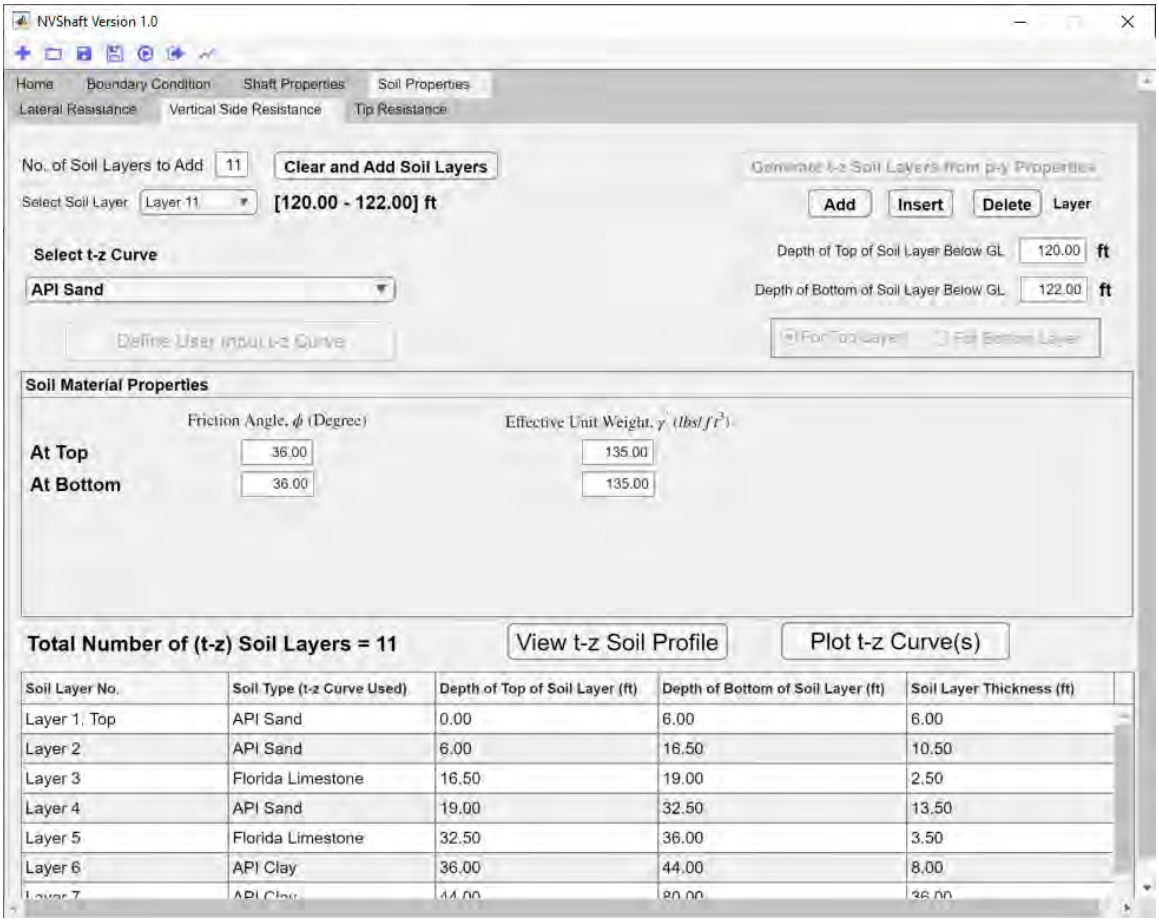

Figure A.42: The Vertical Side Resistance tab in Example 2.1 and 2.2.

- **Step 5.4:** On the **Shaft Section Properties** panel, keep the selection for **Select Section Shape** as *Solid Circular*.
- **Step 5.5:** On the **Shaft Section Properties** panel, input the section properties as summarized in Table A.15.

After following these steps, the **Shaft Properties** tab should look similar to Fig. A.45.

Table A.14: Characterization of vertical side (t-z) resistance in the Example 2.1 and Example 2.2.

Depth (ft)	t-z Model	Effective Unit Weight, γ' (lbs/ft^3)	Friction Angle, ϕ	Undrained Cohesion, c_u (lbs/ft^2)	Ultimate Side Resistance t_u (lbs/ft^2)
0-6	API Sand	126	35	-	-
6-16.5	API Sand	123	39	-	-
16.5-19	Florida Limestone	140	-	-	67085
19-32.5	API Sand	123	35	-	-
32.5-36	Florida Limestone	140	-	-	67085
36-44	API lay	126	-	2750	-
44-80	API Clay	126	-	6178	-
80-90	API Sand	120	37	-	-
90-98	API Clay	130	-	6400	-
98-120	API Clay	122	-	2457	-
120-122	API Sand	135	36	-	-

Table A.15: Shaft section properties used in Example 2.1 and Example 2.2.

	Section Diameter (ft)	Elastic Modulus (ksi)
At Top	4	5007
At Bottom	4	5007

A.11.6 Running Analysis and Obtaining Outputs

Follow the steps as described in Section A.9.5. The outputs after a successful analysis of Example 2.1 are shown in Fig A.46 and Fig A.47.

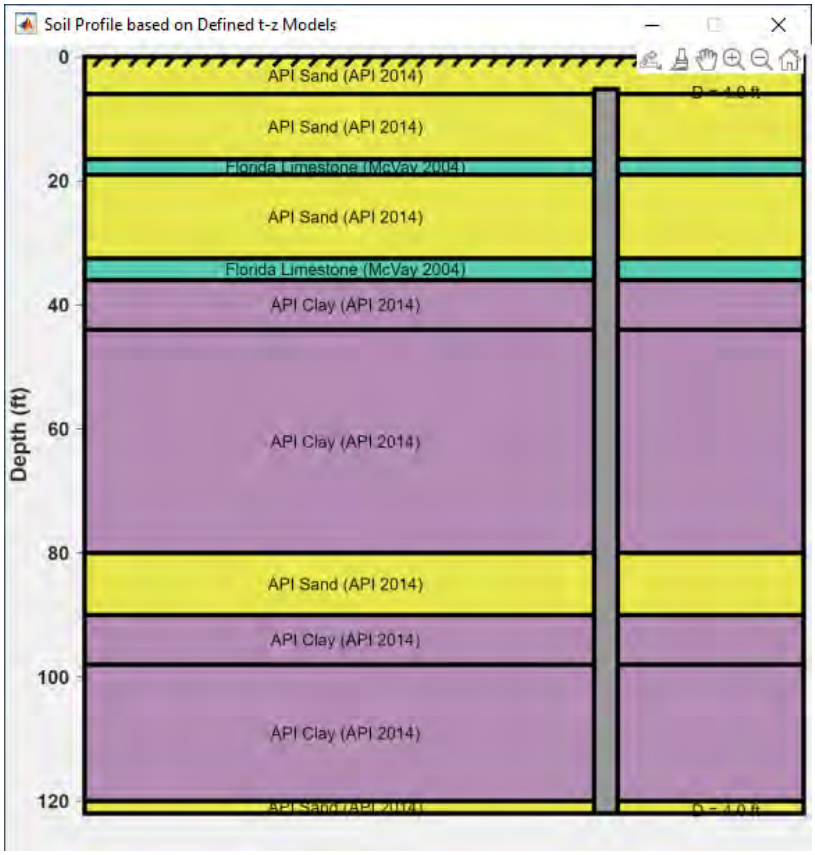

Figure A.43: The schematic of the *t-z* soil layers along with the pile section profile for Example 2.1 and 2.2.

A.12 Example 2.2: Bi-directional Static Axial Load Test Simulation of Test Shaft from the Las Vegas City Center Project

Example 2.2 uses all the soil and shaft material properties defined in Example 2.1. Slight adjustments need to be made in order to change the *t-z* simulation type to that of bi-directional static axial load test, which are described in the following steps.

A.12.1 Defining General Options

Navigate to the **Home** tab, and follow these steps:

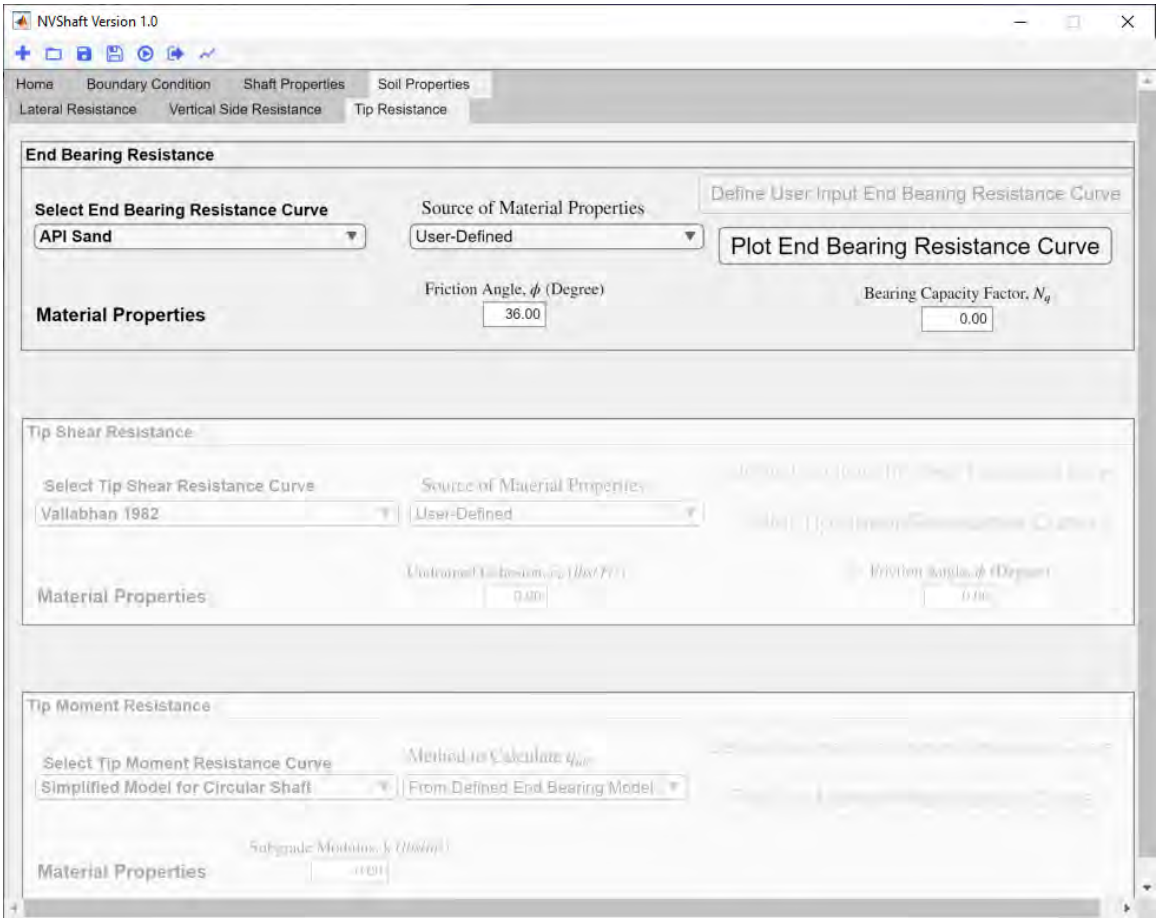

Figure A.44: The Tip Resistance tab in Example 2.1 and 2.2.

- **Step 1.1:** On the **Type of *t-z* Analysis** panel, select *Bi-directional* radio button option. This will prompt NVShaft to apply the axial load at the specified location below shaft head in the *t-z* model.
- **Step 1.2:** Input *60* in the **Axial Load Location Below Shaft Head** numeric edit field, which specifies the location of the bi-directional cell.
- **Step 1.3:** Select *O-Cell Top: O-Cell Bottom* radio button option in the **Type of Load-Displacement Plot for Bi-directional Loading** panel.
- **Step 1.4:** Input *73.5* in the **Shaft Self-weight** numeric edit field.
- **Step 1.5:** Input *100* as the **No. of Pile Increments** for the shaft segments both above and below the O-Cell location.

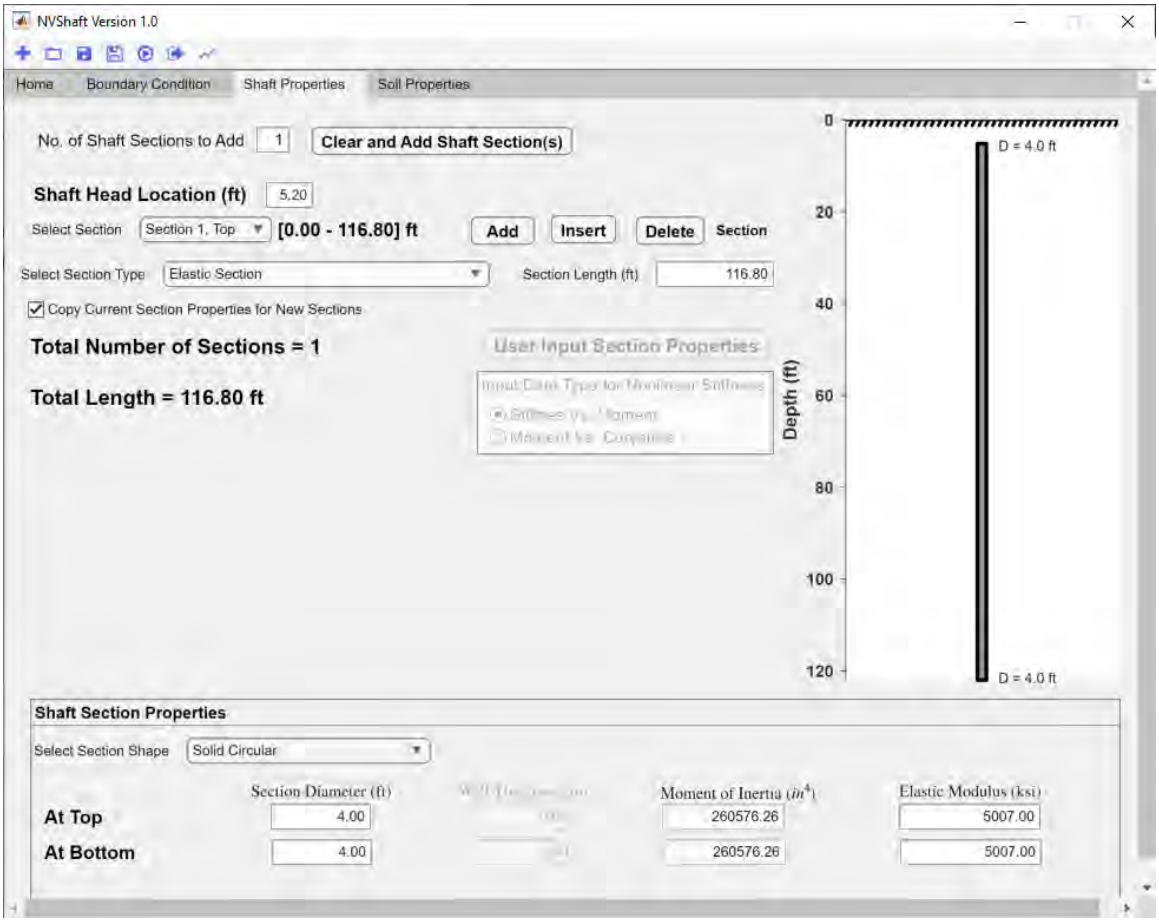

Figure A.45: The Shaft Properties tab in Example 2.1 and 2.2.

After following these steps, the **Home** tab should look similar to Fig. A.48.

A.12.2 Defining Boundary Conditions

Navigate to the **Boundary Condition** tab, and follow the steps described in Section A.11.2.

A.12.3 Running Analysis and Obtaining Outputs

Follow the steps as described in Section A.9.5. The outputs after a successful analysis of Example 2.2 are shown in Fig A.49 and Fig A.50.

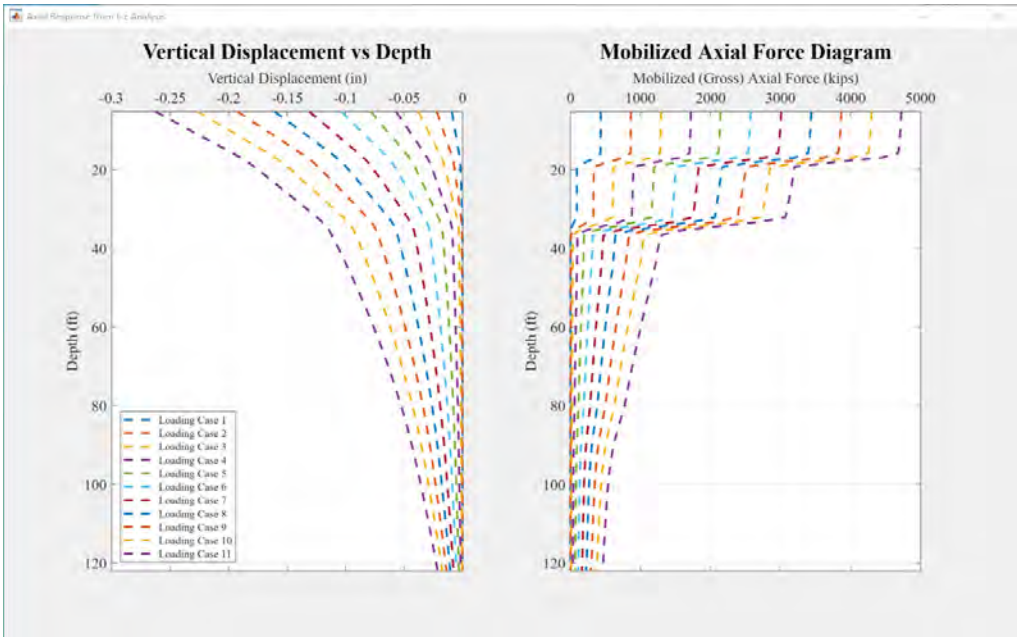

Figure A.46: The vertical displacement and mobilized axial force profile diagram obtained from Example 2.1.

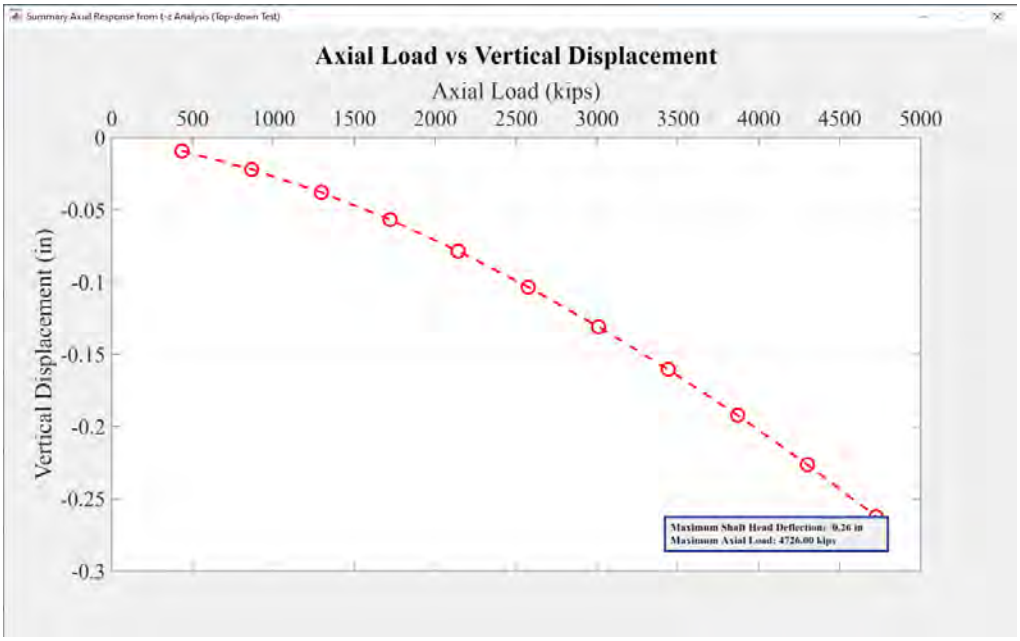

Figure A.47: The axial load vs vertical displacement plot obtained from Example 2.1.

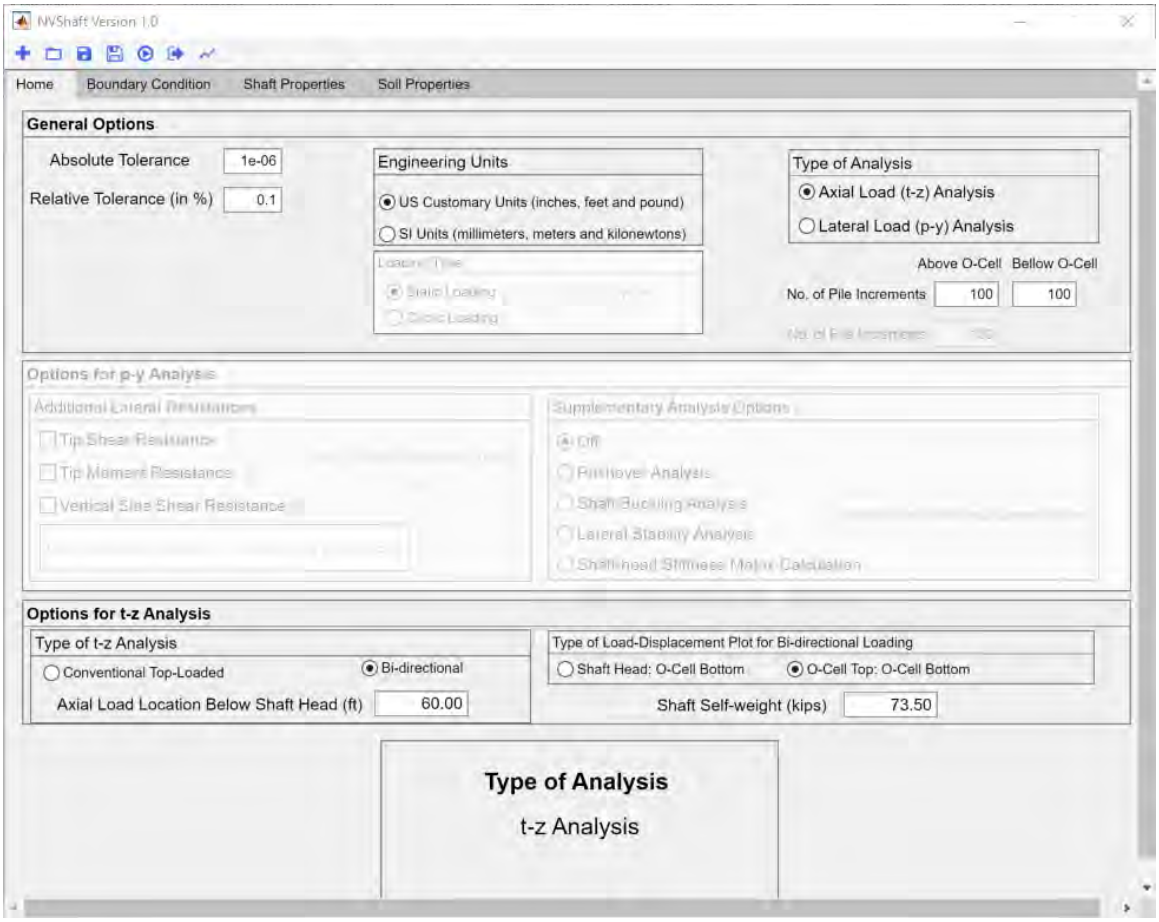

Figure A.48: The Home tab in Example 2.2.

A.13 References

ADOT (2010). *ADOT policy memorandum: ADOT DS-3*. Arizona Department of Transportation. Accessed 4-21-22.

API (2014). *API Recommended Practice 2A-WSD - Planning, Designing, and Constructing Fixed Offshore Platforms – Working Stress Design*. API.

Asem, P. and Gardoni, P. (2019). A load-transfer function for the side resistance of drilled shafts in soft rock. *Soils and Foundations*, 59(5):1241–1259.

Bhuiyan, F. M., Motamed, R., Siddharthan, R. V., and Sanders, D. H. (2022). Evalua-

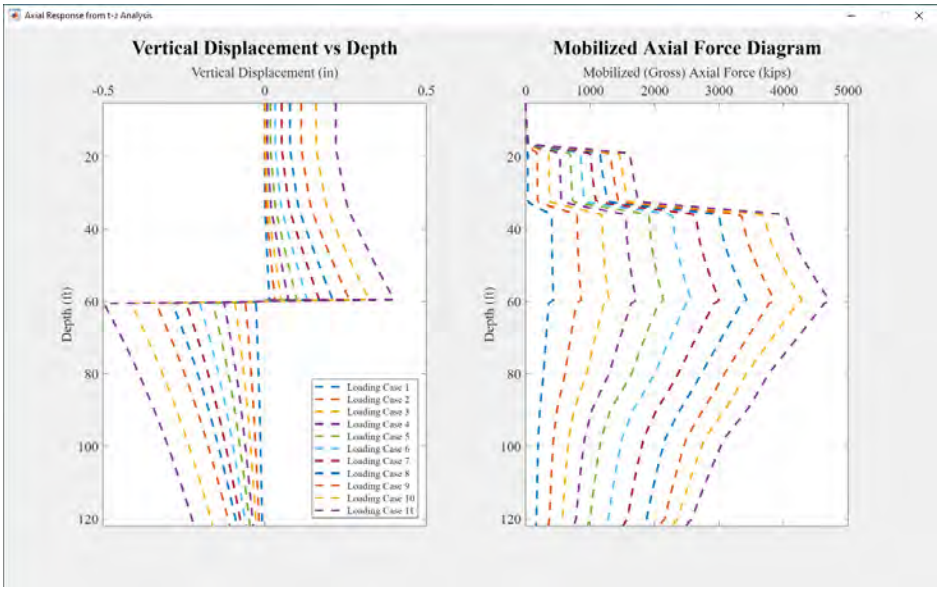

Figure A.49: The vertical displacement and mobilized axial force profile diagram obtained from Example 2.2.

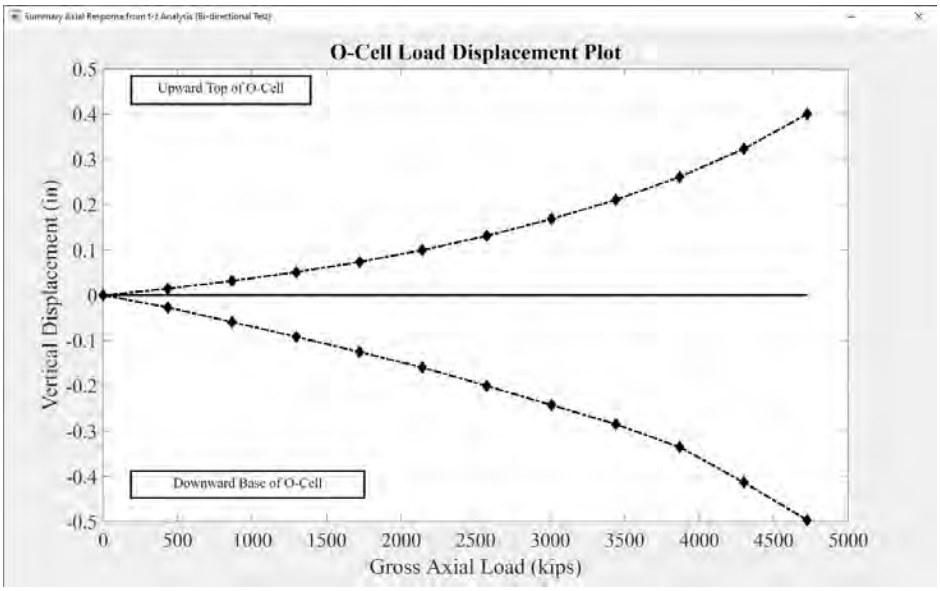

Figure A.50: The O-Cell load displacement plot, corresponding to the upward and downward O-Cell movements obtained from Example 2.2.

tion of a unified *p-y* method for lateral analysis of large-diameter drilled shafts using NVShaft. *Transportation Geotechnics*. Accepted.

Brown, D. A. (2002). Personal communication about "specifying initial k for stiff

clay with no free water". Technical report.

Brown, D. A., Turner, J. P., Castelli, R. J., and Americas, P. (2010). Drilled shafts: Construction procedures and lrfd design methods. Technical Report FHWA-NHI-10-016, United States. Federal Highway Administration.

Coyle, H. M. and Reese, L. C. (1966). Load transfer for axially loaded piles in clay. *Journal of the soil mechanics and foundations division*, 92(2):1–26.

Evans, L. and Duncan, J. (1982). Simplified analysis of laterally loaded piles. Report No. UCB/GT/82-04, University of California, Berkeley.

Georgiadis, M. (1983). Development of py curves for layered soils. In *Geotechnical practice in offshore engineering*, pages 536–545. ASCE.

Goodman, R. (1980). Introduction to rock mechanics.

Isenhower, W. M. and Wang, S.-T. (2011). *Technical manual for LPile, Version 6*. Ensoft, Austin, TX.

Jeong, S., Kim, Y., and Kim, J. (2011). Influence on lateral rigidity of offshore piles using proposed p–y curves. *Ocean engineering*, 38(2-3):397–408.

Johnson, R. (2006). *Soil characterization and py curve development for loess*. PhD thesis, University of Kansas.

Juirnarongrit, T. and Ashford, S. A. (2004). Lateral load behavior of cast-in-drilled-hole piles in weakly cemented sand. *Transportation research record*, 1868(1):190–198.

Liang, R., Yang, K., and Nusairat, J. (2009). p-y criterion for rock mass. *Journal of geotechnical and geoenvironmental engineering*, 135(1):26–36.

LOADTEST (2005). Report on drilled shaft load testing (Osterberg method), City Center - test shaft 1, Las Vegas, NV. Project No. LT-9160-1, LOADTEST, Inc.

Matlock, H. (1970). Correlations for design of laterally loaded piles in soft clay. *Offshore technology in civil engineering's hall of fame papers from the early years*, pages 77–94.

McVay, M. and Niraula, L. (2004). Development of PY curves for large diameter piles/drilled shafts in limestone for FBPIER. Technical Report Final Report.

McVay, M. C. et al. (2008). Distribution of end bearing, tip shear and rotation on drilled shafts with combined loading in Florida limestone. Technical Report Final Report.

Mosher, R. L. (1984). Load transfer criteria for numerical analysis of axially loaded piles in sand. Technical report, U. S. Army Waterways Experiment Station, Automatic Data Processing Center, Vicksburg, Mississippi.

NDOT (2019). *NDOT structures manual: revision 2019-2*. Nevada Department of Transportation.

O'Neill, M. and Gazioglu, S. (1984). Integrated formulation of py relationships in clays. *A Report to the American Petroleum Institute, Report PRAC-82-41-2, University of Houston*.

O'Neill, M. W. and Murchison, J. M. (1983). *An evaluation of p-y relationships in sands*. University of Houston.

Reese, L. and Nyman, K. (1978). Field load tests of instrumented drilled shafts at Islamorada, Florida. *Report to the Girdler Foundation and Exploration Corporation, Clearwater, FL, February*.

Reese, L. C. (1997). Analysis of laterally loaded piles in weak rock. *Journal of Geotechnical and Geoenvironmental engineering*, 123(11):1010–1017.

Reese, L. C., Cox, W. R., and Koop, F. D. (1974). Analysis of laterally loaded piles in sand. *Offshore technology in civil engineering hall of fame papers from the early years*, pages pp. 95–105.

Reese, L. C. and Welch, R. C. (1975). Lateral loading of deep foundations in stiff clay. *Journal of the Geotechnical engineering division*, 101(7):pp. 633–649.

Rollins, K. M., Gerber, T. M., Lane, J. D., and Ashford, S. A. (2005). Lateral resistance of a full-scale pile group in liquefied sand. *Journal of Geotechnical and Geoenvironmental Engineering*, 131(1):115–125.

Sachpazis, C. (1990). Correlating schmidt hardness with compressive strength and young's modulus of carbonate rocks. *Bulletin of the International Association of Engineering Geology-Bulletin de l'Association Internationale de Géologie de l'Ingénieur*, 42(1):75–83.

Selvadurai, A. (1985). Soil-pipeline interaction during ground movement. In *Civil engineering in the arctic offshore*, pages 763–773. ASCE.

Simpson, M. and Brown, D. A. (2006). Personal communication about "method for computing *p-y* curves in piedmont residual soils". Technical report.

Vallabhan, C. G. and Alikhanlou, F. (1982). Short rigid piers in clays. *Journal of the Geotechnical Engineering Division*, 108(10):1255–1272.

Welch, R. C. and Reese, L. C. (1972). Laterally loaded behavior of drilled shafts. Research Report 3-5-65-89, Center for Highway Research, The University of Texas at Austin.

Zhang, L. (2004). *Drilled shafts in rock: analysis and design*. CRC press.

APPENDIX B

LATERAL STABILITY ANALYSIS IN NVSHAFT

In NVShaft, the following methods are available to perform the lateral stability analysis:

1. Method outlined in Nevada Department of Transportation (NDOT) structures manual (NDOT, 2019)
2. Method outlined in Arizona Department of Transportation (ADOT) policy memo (ADOT, 2010)
3. A method proposed by the authors

Among these three methods, only the proposed method allows the shaft head location to be defined above or below the ground level (GL). When the shaft head is located below GL, the predicted deflection at the shaft head is considered to compute the critical shaft length (L_c). Otherwise, when the shaft head is located at or above GL, deflection at GL is used to generate the stability plot. The lateral stability analysis based on different methods is briefly discussed in the following sections.

B.1 Method by NDOT

1. Increase the pile maximum factored loads, Q (i.e. column overstrength moment and shear), by dividing by a *p-y* resistance factor of 0.8. This provides the lateral stability analysis loads, Q_{Lat}.
2. Iterate the soil structure interaction analysis varying the length of the pile in one diameter increments and determine the displacement at the top of the pile due to Q_{Lat}. The minimum displacement, δ_{min}, is reached when the

change in displacement is less than 2% different than the previous iteration (with a one diameter shorter length). The maximum displacement, δ_{max}, is reached at the shortest length of pile that will converge in the analysis and provide a displacement. The minimum displacement, indicating the highest lateral stiffness, is commonly achieved by a pile length of approximately ten diameters. The maximum displacement indicates the shortest length of the pile before failure.

3. Determine the 75% stiffness length, L_{75}. If δ_{max} is more than $1.33\delta_{min}$, then L_{75} is the length of pile that has a displacement equal to $1.33\delta_{min}$. Otherwise, L_{75} is taken as the length of pile at δ_{max}.

4. Determine the critical length, L_c. If δ_{max} is more than $2\delta_{min}$, then L_c is L_{75} plus one pile diameter. Otherwise, L_c is L_{75} plus two pile diameters.

Additionally, the pile with length L_c must have a displacement at the top of pile due to Q_{Lat} less than 10% of the pile diameter. The displacement at the tip of pile due to Q_{Lat} must also be less than 1% of the diameter.

B.2 Method by ADOT

1. Select a shaft diameter. Perform lateral load analysis using applicable strength limit state factored loads, nominal lateral geotechnical resistances (i.e., resistance factor = 1.0) computed in accordance with Article 10.7.3.12 of AASHTO (2010) and bending stiffness computed as $E_C I_G$, where E_C is the elastic modulus of concrete and I_G is the gross (uncracked) moment of inertia for the selected shaft diameter. Since the analysis is iterative, select an initial shaft length, L_{LONG}, that is obviously long, e.g., a shaft length corresponding to 10 to 15 times the shaft diameter.

2. Repeat computations with the length L_{LONG} reduced in 10 to 15% increments and prepare a graph of ground line deflection versus shaft length (i.e., lateral stability plot). Smaller length increments may be warranted as the ground line deflection starts to increase.
3. Identify the critical length, L_c, based on overturning as the length at which the slope of the lateral stability curve is approximately zero as identified by change in ground line deflection less than 5% between two consecutive increments of lengths.
4. Use the length L_c as an initial value for the evaluation of lateral structural stability based on applicable strength and service limit states.

B.3 Proposed Method

The proposed method uses the following terminologies, which are also highlighted in Fig. B.1.

- y_{GL}**:** Deflection of the shaft at GL (taken as shaft head deflection when the head is located below GL).
- D_{col}**:** Diameter of the column or drilled shaft section above GL.
- D_{shaft}**:** Diameter of the drilled shaft.
- L_{init}**:** Shaft embedment length considered to generate the stability plot.
- L_{col}**:** Length of the column or drilled shaft section above GL.
- L_{shaft}**:** Embedment length of the shaft for lateral stability.

The proposed method for lateral stability analysis is summarized in Fig. B.2 to Fig. B.4. The embedment factor to calculate L_{shaft} as given in Caltrans (2019) is shown in Table B.1 below.

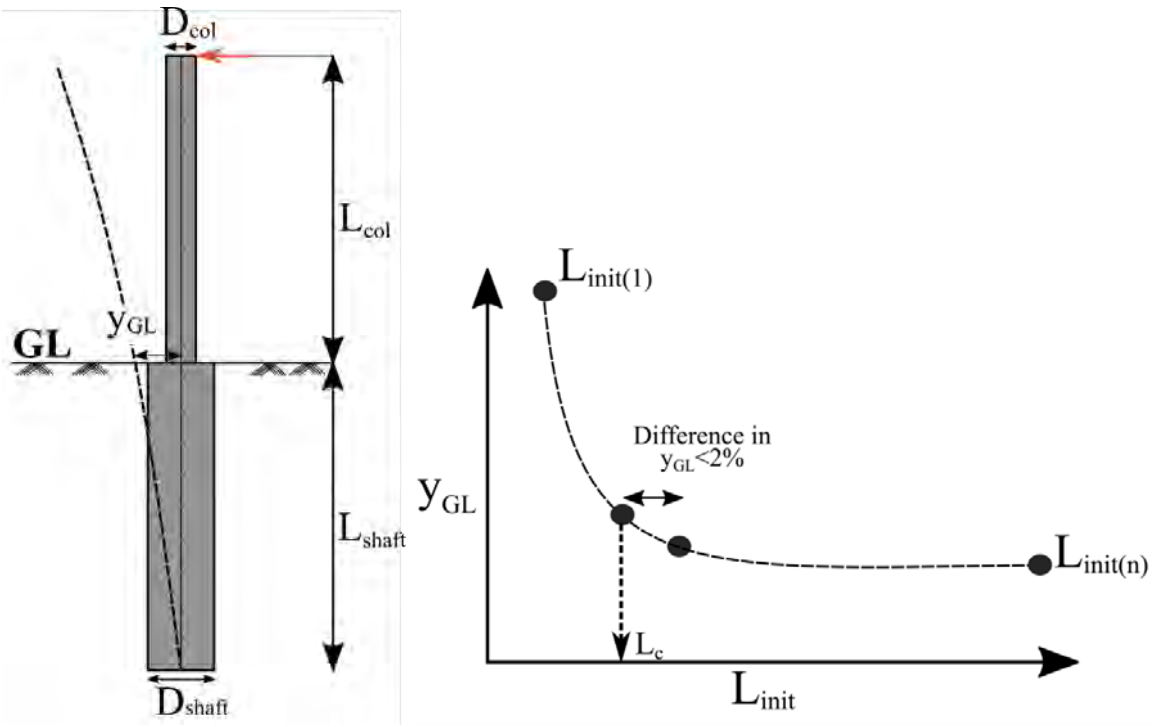

(a) (b)

Figure B.1: (a) Profile diagram showing different terminologies used in the proposed lateral stability analysis and (b) lateral stability plot to calculate shaft critical length.

Table B.1: Embedment factor for pile tip elevation (Caltrans, 2019).

Pile/Shaft	Embedment Factor
Pile/shaft groups in Class S2 soil	1.0
Shafts (Types I and II) in multi-column bents	1.0
Shafts without rock sockets in single-column bents	1.2
Shafts with rock sockets in single-column bents	1.0 (for = CIDH portion) 1.2 (for rock socket portion)

B.4 Validation Examples of the Proposed Method

Two example problems of lateral stability analysis are presented in this section, where the outputs obtained from the three different methods made available in NVShaft are compared. This was done to validate the proposed method relative to the other methods already practiced in the Nevada and Arizona DOTs. The common input parameters related to the lateral stability analysis to perform both

validation examples are summarized in Table B.2. Brief descriptions of the problems and the results are presented in the subsequent sections below.

Table B.2: Input parameters implemented in the validation examples related to the lateral stability analyses.

Input Parameters	Values
Resistance Factor, ϕ	0.8
$L_{initial}/D_{mean}$ Ratio	10 (used in NDOT and ADOT methods)
Deflection Limit	24 in
% of Length Reduction	1*Mean Diameter (in NDOT method) 10% (in ADOT method)
% Difference in y_{GL} to calculate L_c	2% (in NDOT method) 5% (in ADOT method) 2% (in proposed method)

B.4.1 Example 1: Lateral Stability Analysis of an Elastic Pile Embedded in Sand

In this example, a 3 ft diameter elastic pile with the elastic modulus of 3900 ksi and 30 ft of embedment depth is considered. The lateral resistance characteristic of the soil was modeled by the sand *p-y* model given by Reese et al. (1974). The angle of friction (ϕ) and the effective unit weight (γ') of the soil were assumed to be 37°and 130 lbs/ft^3, respectively. Conventional *p-y* analysis option was selected in NVShaft to perform the lateral stability analysis, with the unfactored lateral load of 100 kips applied as the boundary condition.

The soil and shaft section profile diagram and the results of the lateral stability

analyses using three different approaches are shown in Fig. B.5a and Fig. B.6a, respectively. The comparison of the shaft critical length (L_c) obtained from the method by NDOT, ADOT, and the proposed method is presented in Table B.3.

B.4.2 Example 2: Lateral Stability Analysis of 2 ft Diameter Shaft from the I-15/US 95 Load Test Program

The 2 ft diameter shaft from the I-15/US 95 load test program located in site no. 1 was considered to validate the proposed method for lateral stability analysis. For simplicity, the shaft was assumed to have elastic section property and conventional *p-y* analyses were performed. The details about the soil and shaft properties for this example have been elaborately discussed in Section 2.2 of this report. The unfactored lateral load of 36 kips was applied at the shaft head location in the numerical model for this example. The profile diagram showing the shaft section and the *p-y* soil layers are shown in Fig. B.5b. The results of the lateral stability analyses using three different methods are presented Fig. B.6b and Table B.3.

By comparing the results of the two validation examples as presented in Fig. B.6 and Table B.3, it can be concluded that the proposed method is capable of producing comparable, and sometimes conservative values of L_c compared to the other two methods.

Table B.3: Shaft critical lengths (L_c) in ft obtained from different methods of lateral stability analysis.

Method	Example 1	Example 2
NDOT	23.02 ft	13.65 ft
ADOT	24 ft	14 ft
Proposed Method	24 ft	15 ft

B.5 References

AASHTO (2010). *AASHTO LRFD Bridge Design Specifications*. AASHTO, Washington, D.C.

ADOT (2010). *ADOT policy memorandum: ADOT DS-3*. Arizona Department of Transportation. Accessed 4-21-22.

Caltrans (2019). *Caltrans Seismic Design Criteria Version 2.0*. California Department of Transportation. Accessed 7-23-22.

NDOT (2019). *NDOT structures manual: revision 2019-2*. Nevada Department of Transportation.

Reese, L. C., Cox, W. R., and Koop, F. D. (1974). Analysis of laterally loaded piles in sand. *Offshore technology in civil engineering hall of fame papers from the early years*, pages pp. 95–105.

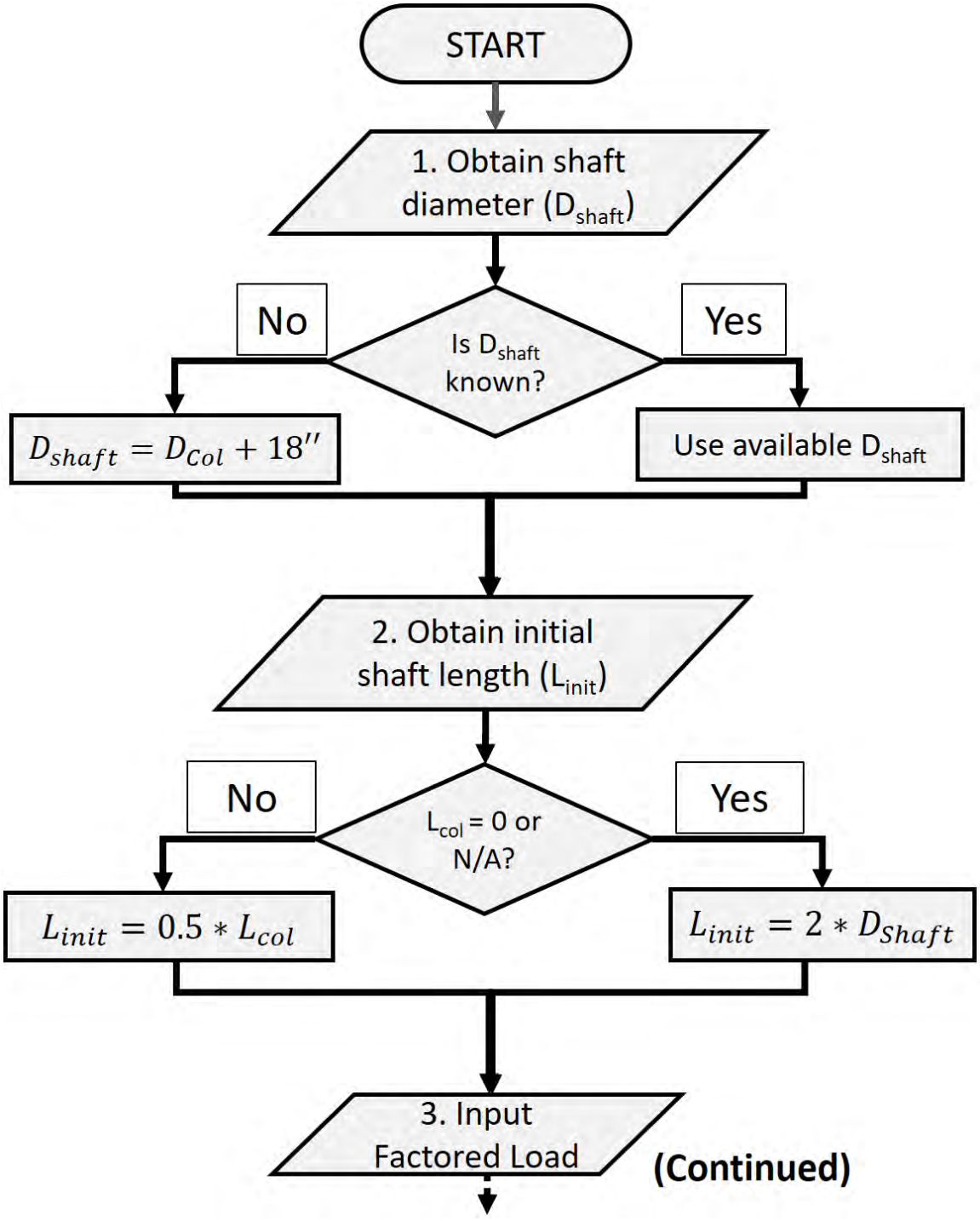

Figure B.2: Flow chart summarizing the proposed lateral stability analysis (1)

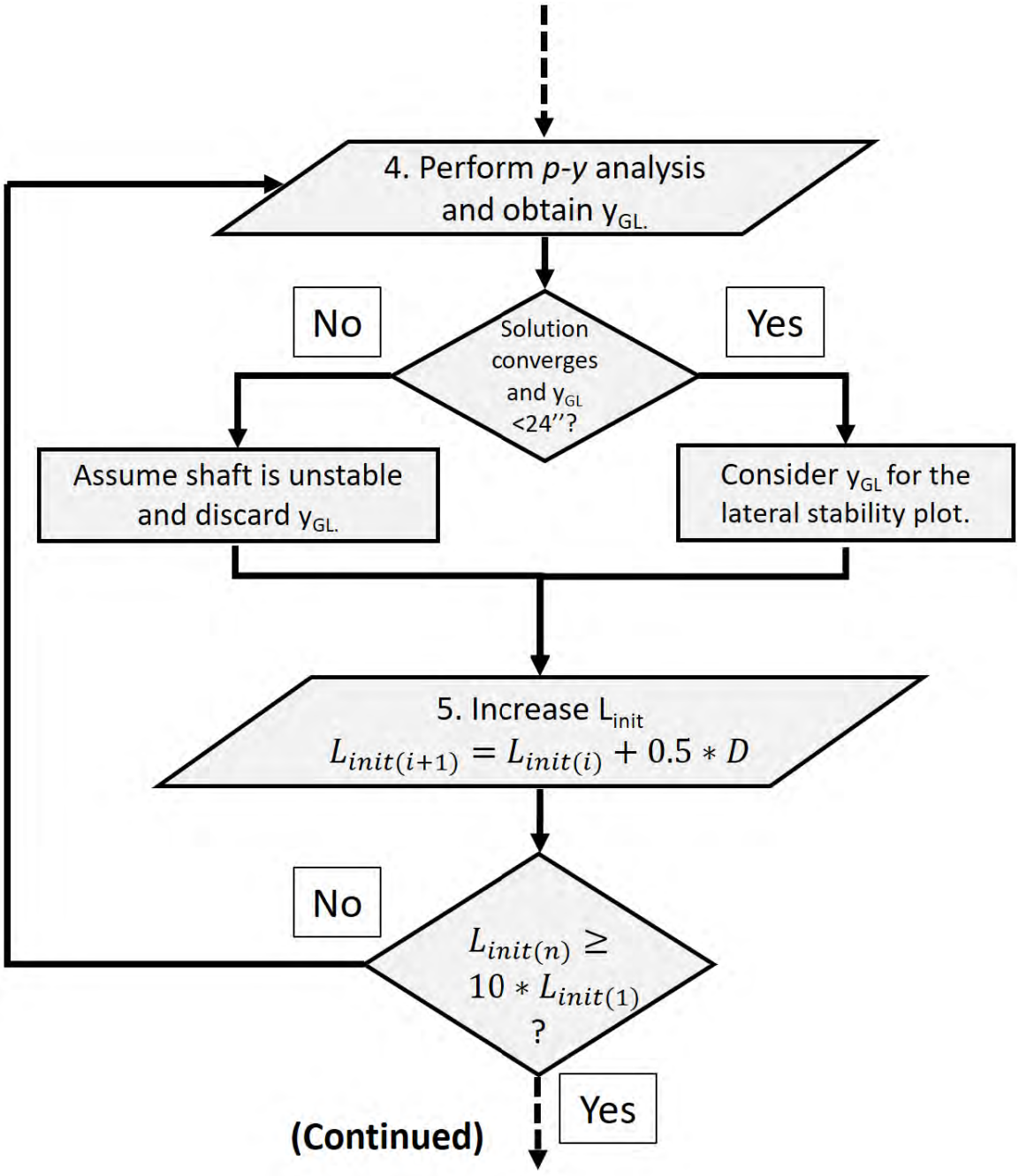

Figure B.3: Flow chart summarizing the proposed lateral stability analysis (2)

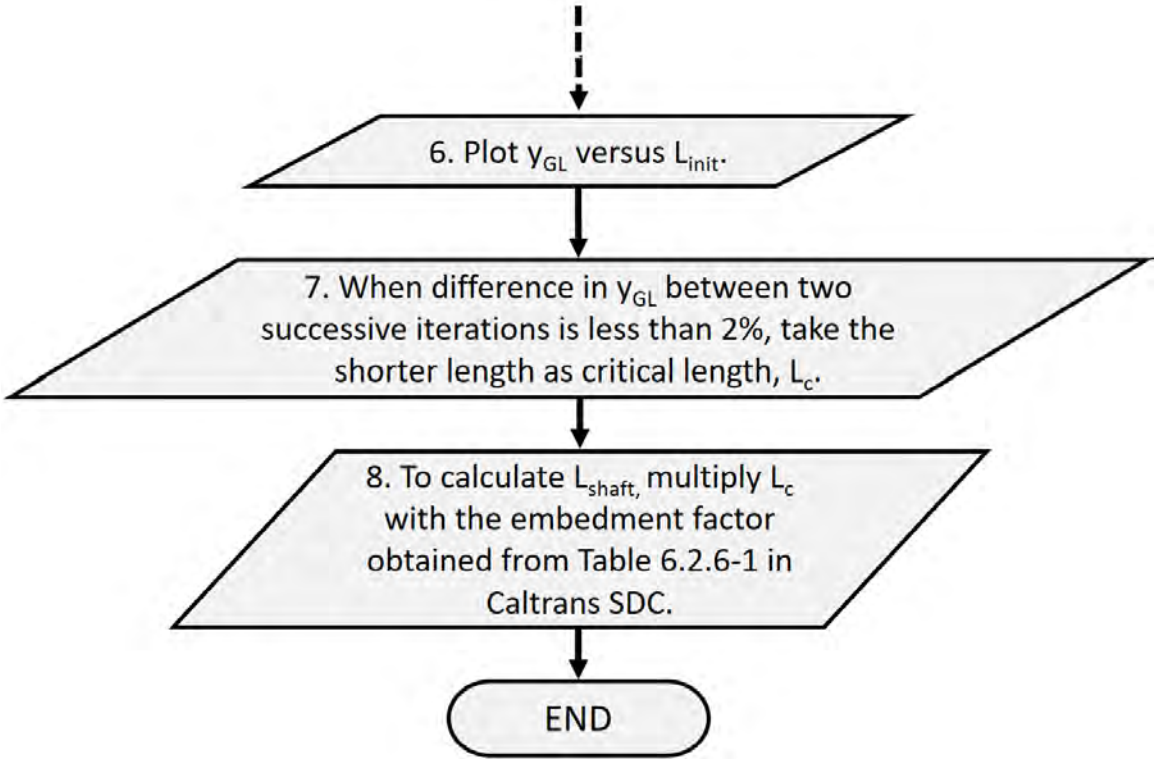

Figure B.4: Flow chart summarizing the proposed lateral stability analysis (3)

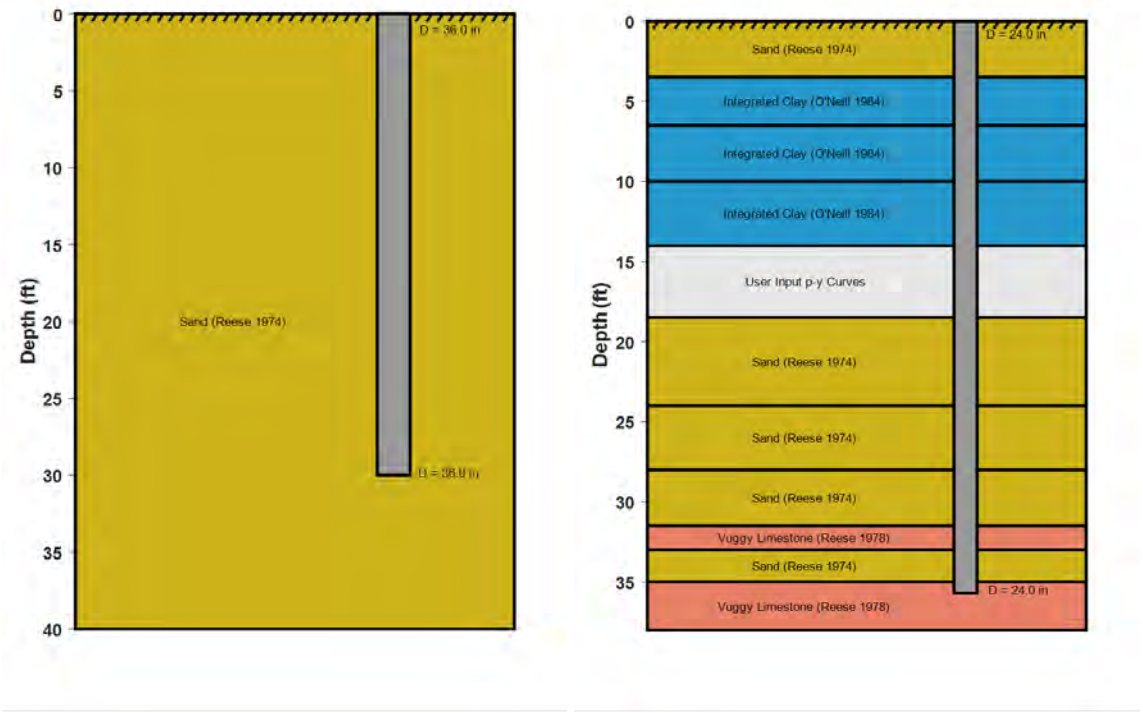

(a) (b)

Figure B.5: Soil and shaft profile diagrams corresponding to (a) Example 1 and (b) Example 2 to validate the proposed method for lateral stability analysis.

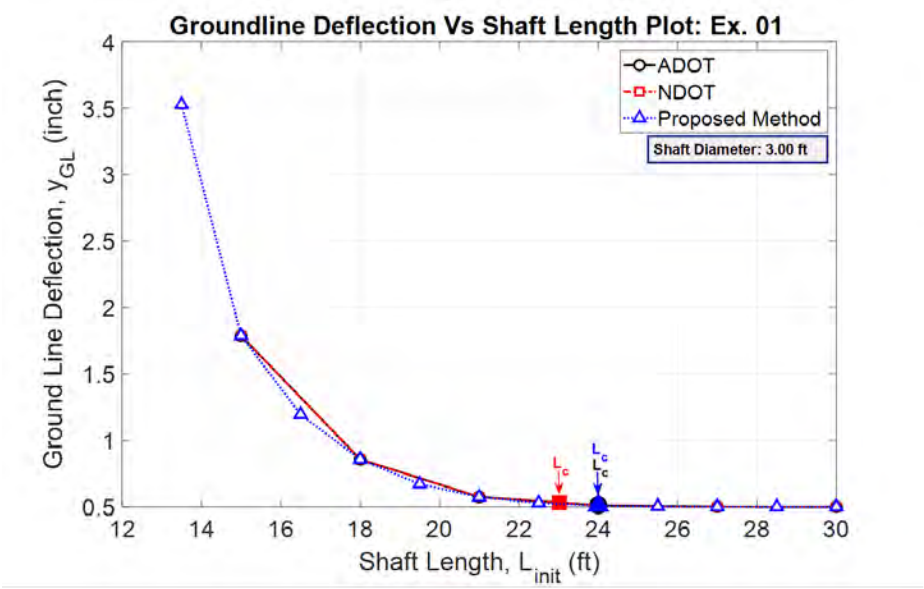

(a)

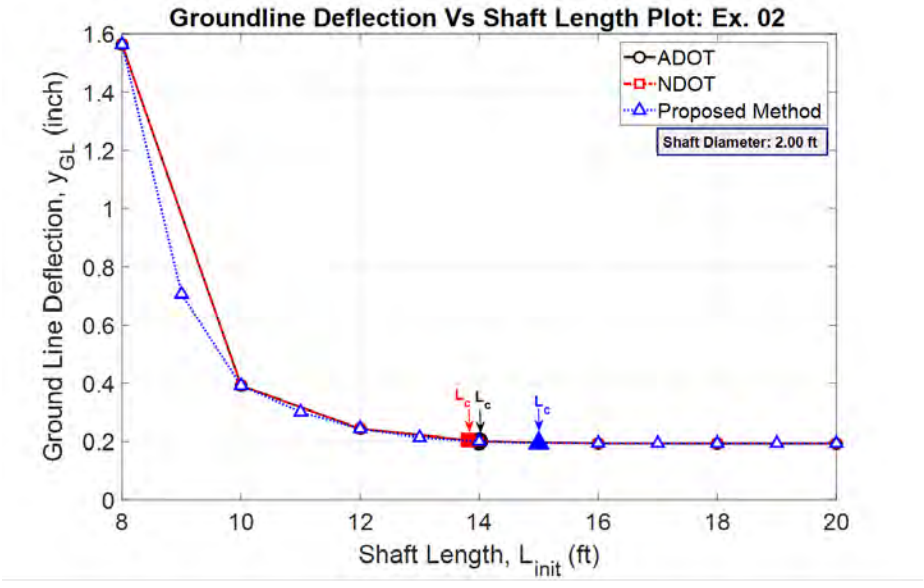

(b)

Figure B.6: Lateral stability plots obtained from the ADOT, NDOT and the proposed method corresponding to (a) Example 1 and (b) Example 2.

Nevada Department of Transportation

Tracy Larkin-Thomason, P.E. Director

Ken Chambers, Research Division Chief

(775) 888-7220

kchambers@dot.nv.gov

1263 South Stewart Street

Carson City, Nevada 89712